Searching for *P-* and *CP-* odd effects
in heavy ion collisions

Xumeu Planells Noguera

Searching for $P-$ and $CP-$ odd effects in heavy ion collisions

Xumeu Planells Noguera

Departament d'Estructura i Constituents de la Matèria
&
Institut de Ciències del Cosmos

Universitat de Barcelona

Advisors:

Domènec Espriu Climent

Alexander A. Andrianov

A thesis submitted for the degree of

PhilosophiæDoctor (PhD) in Physics
(Programa de Doctorado en Física)

November 2014

UNIVERSITAT DE BARCELONA

Institut de Ciències del Cosmos

Abstract

In this thesis we study the possibility that QCD breaks parity at high temperatures and densities, a scenario that may be tested in heavy ion collisions. We present two different approaches to this problem. On the one hand, analytical studies with effective models suggest that QCD may break parity in dense systems due to condensation of pseudoscalar mesons in the isotriplet channel. On the other hand, $P-$ and $CP-$ odd bubbles may appear in a finite volume due to local large topological fluctuations in a hot medium. The presence of a large magnetic field or angular momentum may lead to the so-called Chiral Magnetic Effect. We assume topological fluctuations as the source of parity violation in heavy ion collisions throughout. This effect may be treated in a quasi-equilibrium description by means of a non-trivial axial chemical potential.

We consider the 'two flavour' Nambu–Jona-Lasinio model in the presence of a vector and an axial external chemical potentials and study the phase structure of the model at zero temperature. The Nambu–Jona-Lasinio model is often used as a toy replica of QCD and it is therefore interesting to explore the consequences of adding external vector and axial chemical potentials in this model, mostly motivated by claims that such external drivers could trigger a phase where parity could be broken in QCD. We are also motivated by some lattice analysis that attempt to understand the nature of the so-called Aoki phase using this simplified model. Analogies and differences with the expected behaviour in QCD are discussed and the limitations of the model are pointed out.

We also consider the low energy realization of QCD in terms of mesons when an axial chemical potential is present; a situation that may be relevant in heavy ion collisions. We shall demonstrate that the presence of an axial charge has profound consequences on scalar/pseudoscalar meson physics. The most notorious effect is the appearance of an explicit source of parity breaking. The eigenstates of strong interactions do not have a definite parity and interactions that would otherwise be forbidden compete with the familiar ones. We focus on scalars and pseudoscalars that are described by a generalized linear sigma model. We comment briefly on the screening role of axial vectors in formation of effective axial charge and on the possible experimental relevance of our results, whose consequences may have been already seen at RHIC.

Finally, we investigate how local parity breaking may affect vector physics. A modified dispersion relation is derived for the lightest vector mesons ρ and ω. They are characterised by a mass splitting depending on their polarization. This effect predicts a natural overproduction of lepton pairs in the vicinity of the $\rho - \omega$ resonance peak as well as a polarization asymmetry around this peak. The dilepton excess seems relevant to explain the anomalous dielectron yield quoted by PHENIX/STAR. We present a detailed analysis of the angular distribution associated to the lepton pairs created from these mesons searching for polarization dependencies. Two angular variables are found to carry the main information related to the parity-breaking effect. Possible signatures for experimental detection of local parity breaking are discussed.

A Jennifer Mesa, por haber sido una parte esencial de mi vida durante esta tesis.

Y a mis padres, por darme la oportunidad de aprender y formarme como persona.

To Jennifer Mesa, for being an essential part of my life during this thesis.

And to my parents, for giving me the chance to learn and grow as a person.

Agradecimientos

Quiero agradecer al Prof. Domènec Espriu la oportunidad que me brindó para iniciar este viaje, en el que hemos colaborado en un ambiente muy ameno y distendido. Han sido unos años de trabajo constante pero agradable y enriquecedor tanto a nivel profesional como personal. También me gustaría agradecer al Prof. Alexander Andrianov su hospitalidad y su eterna sonrisa. No sé qué habría sido de mí en San Petersburgo sin él. Quiero expresar mi gratitud también a David d'Enterria por su infinita paciencia conmigo. Nunca pensé que dos meses pudiesen ser tan productivos en tantos aspectos.

No puedo olvidar a toda aquella gente que ha hecho que esta experiencia haya sido una aventura inolvidable. Gracias a mis compañeros de doctorado del departamento de ECM Albert Renau, Vicente Rives y Juan González. Siempre nos quedarán esas partidas de mus. Y a mis colegas durante la carrera José Daniel Madrigal, Héctor García, y en especial Santi Roca y Enrique Pinto, por aquellos momentos en el buffet en que todo se veía mejor mientras nos hartábamos de pizza.

Quiero agradecer también la hospitalidad que recibí en Rusia por parte no sólo del Prof. Alexander Andrianov y su esposa, sino también de su hermano Vladimir, su estudiante Sergey Kolevatov, y Vladimir Zherebchevsky y la gente del Ciclotrón de la Universidad Estatal de San Petersburgo.

A pesar del tiempo que ha pasado, quiero agradecer el papel que han jugado en mi vida algunos profesores durante mi etapa formativa como Gabi Vidagany y Amparo Fuster, extraordinarios profesores y modelos de persona. Y también a Conrad Pérez, sin cuyos consejos mi experiencia en la universidad habría sido mucho más tortuosa.

Quiero dar las gracias a todos aquellos que han estado junto a mí desde hace años y me han apoyado para lo bueno y para lo malo. Gracias a toda mi familia y en especial a mi madre, porque su presencia y su apoyo incondicional no pueden pasarse por alto. Y a mi gente de Ibiza ya sea en Barcelona o en la 'quinta China'. Me refiero a Santi Marí, Christian Marín, Adrián Baena, Laura Tur, María Ramón y muchos más.

Acknowledgements

I want to thank Prof. Domènec Espriu for the opportunity he provided me to start this journey, in which we collaborated in a very friendly and relaxed atmosphere. It has been a time of constant but pleasant work that was enriching for me both on the professional and personal level. I also want to thank Prof. Alexander Andrianov for his hospitality and his eternal smile. I don't know what I would have done without him in Saint Petersburg. I also want to express my gratitude to David d'Enterria for his infinite patience with me. I had never thought that two months could be so productive in so many aspects.

I can't forget all the people who have made this experience an unforgettable adventure. Thanks to my fellow PhD students from the ECM department Albert Renau, Vicente Rives, Juan González. We'll always have those 'mus' games. And to my degree mates José Daniel Madrigal, Héctor García, and specially Santi Roca and Enrique Pinto, for those moments at the buffet in which everything looked better while we were eating pizza to burst.

I also want to thank the hospitality that I received in Russia, not only from Prof. Alexander Andrianov and his wife, but also from his brother Vladimir, his student Sergey Kolevatov, and Vladimir Zherebchevsky and the people from the Cyclotron at the Saint Petersburg State University.

Despite the time that has passed, I want to thank some of the teachers I had during my education for the role they played in my life like Gabi Vidagany and Amparo Fuster, extraordinary teachers and role models. And also Conrad Pérez, because my experience at the university would have been much more tortuous without his advice.

I want to acknowledge all the people who have been with me for years and have supported me through thick and thin. Thanks to my family and specially to my mother, because her presence and unconditional support cannot be missed. And to my people from Ibiza either in Barcelona or thousands of miles away. I am talking about Santi Marí, Christian Marín, Adrián Baena, Laura Tur, María Ramón and many others.

Contents

Chapter 1

Introduction

The nuclear strong force is known to be the responsible for binding the atomic nuclei despite the electromagnetic repulsion between protons. This interaction is one of the four fundamental forces of Nature, like gravity and the electromagnetic and weak forces. The last two interactions can be treated together by means of the unified theory of electro-weak interaction. Electro-weak and strong interactions, but not gravity, can be formulated in terms of a quantum field theory that is known as the Standard Model (SM) of elementary particles. The behaviour of elementary particles is ruled by this successful theory that has been contrasted many times with experiments.

The firsts attempts to deal with strong interactions can be found in the middle of the last century. In 1961 Gell-Mann proposed a phenomenological model [1] to structure the large amount of new hadrons that were being found in accelerator experiments at that time. Over the next decade, the nuclear strong force was formulated at the quantum level by Quantum Chromodynamics (QCD) [2], a non-abelian $SU(3)$ Yang-Mills theory that describes the fundamental interactions between quarks and gluons [3], called partons. Quarks and gluons were introduced as the basic components of hadrons and have an associated colour quantum number due to the symmetry group of QCD. The QCD Lagrangian reads

$$\mathcal{L}_{\text{QCD}} = -\frac{1}{4} G^{\mu\nu,a} G^a_{\mu\nu} + \bar{q}(i\gamma^\mu D_\mu - m)q,$$
$$D_\mu = \partial_\mu - ig G^a_\mu \lambda^a, \quad G^a_{\mu\nu} = \partial_\mu G^a_\nu - \partial_\nu G^a_\mu + g f^{abc} G^b_\mu G^c_\nu, \tag{1.1}$$

where q is the quark field with two implicit indices in colour and flavour spaces and the colour-dependent gluon field is G^a_μ. The strong coupling constant g and the Gell-Mann matrices λ^a in the adjoint representation of $SU(3)$ are also used. There are 3 colours and 6 flavours of quarks. Quarks are massive fermionic states lying in the fundamental representation of the QCD symmetry group while gluons are the massless force carriers, equivalently to photons in electromagnetism, and they belong to the adjoint representation of $SU(3)$.

The strong attraction between a quark-antiquark pair requires a large amount of energy to separate them. Such energy excites the vacuum state up to the point where

1. INTRODUCTION

the creation of a new quark pair becomes energetically favourable and the new particles quickly screen the original charge. This is the qualitative description of quark confinement, which is responsible for the fact that coloured states are never observed alone in Nature. This phenomenon is only known to occur in QCD and believed to be linked to its non-abelian structure. The lack of a rigorous proof of confinement still constitutes a remarkable challenge for theoretical physicists nowadays.

It was experimentally observed that there are only two main structures formed by quarks. Hadrons are separated into baryons and mesons. Baryons are 3-quark states while mesons are composed by a quark-antiquark pair. In order to preserve the Pauli exclusion principle in the formation of baryons a new quantum number, the colour charge, was introduced. Assuming that every quark is associated to one colour, both structures can be arranged to be colourless. This is the reason why it is commonly stated that only colourless (or white) states are observable in Nature.

In addition to the gauge symmetry, the QCD Lagrangian (1.1) shows an invariance under three global discrete symmetries [4, 5]. Parity P reverses the handedness of space that corresponds to reverting the momentum of a particle without flipping its spin. The parity transformation is given by

$$q(\vec{x},t) \to \eta_P \gamma^0 q(-\vec{x},t), \qquad G_0(\vec{x},t) \to G_0(-\vec{x},t), \qquad G_i(\vec{x},t) \to -G_i(-\vec{x},t), \quad (1.2)$$

where η_P is a possible generic phase that is normally taken to be 1 for quarks and leptons without any loss of generality. For antiparticles, η_P is chosen to be -1. Charge conjugation C interchanges particles and antiparticles without any modification of momentum or spin through the transformation

$$q(\vec{x},t) \to -i\eta_C C\bar{q}^T(\vec{x},t), \qquad G_\mu(\vec{x},t) \to -G_\mu^T(\vec{x},t), \qquad (1.3)$$

where η_C is another phase and C is the charge conjugation matrix that obeys the following relations

$$C\gamma_\mu C^{-1} = -\gamma_\mu^T, \qquad C\gamma_5 C^{-1} = \gamma_5^T, C^\dagger = C^{-1} = -C \qquad (1.4)$$

and in the Dirac representation is given by $C = i\gamma^0\gamma^2$. Finally, time reversal T corresponds to an interchange of the forward and backward light-cones, corresponding to reversing the momentum and the spin of a particle via

$$q(\vec{x},t) \to -i\eta_T \gamma_5 C q(\vec{x},-t), \qquad G_0(\vec{x},t) \to -G_0(\vec{x},-t), \qquad G_i(\vec{x},t) \to G_i(\vec{x},-t),$$
$$(1.5)$$

where η_T is again an arbitrary phase. QCD, as any other Lorentz-invariant local quantum field theory with a Hermitian Hamiltonian is also invariant under a simultaneous CPT symmetry.

The quark spectrum is spread over a wide range of masses from $m_{u,d} \sim 5$ MeV up to $m_t \sim 175$ GeV, leading to a clear energy/mass hierarchy. At a given energy scale Λ, the quarks can be separated into light quarks with masses m_q and heavy quarks with m_Q in

such way that the relation $m_q \lesssim \Lambda \ll m_Q$ holds. In this framework at low energies, the effects of heavy quarks amount to redefinitions of the light quark masses m_q and the coupling constants involving the light quarks up to Λ/m_Q corrections. This is known as the decoupling theorem [6]. Low energy theories [7, 8] are usually formulated to describe the physics of strong interactions below the chiral symmetry breaking scale $\Lambda \sim 1$ GeV and hence the number of quark flavours is normally taken to be $N_f = 2, 3$ always including u and d quarks, and sometimes the s quark. For analyses at higher energy scales, other techniques like Heavy Quark Effective Theory are used [9].

In the limit of massless quarks, QCD exhibits an exact $U(N_f)_L \times U(N_f)_R$ global symmetry at the classical level, where N_f is the number of quark flavours that are considered. Under such transformation the quark fields are modified in the following way:

$$q_{L,R}(x) \rightarrow \exp\left(\frac{i}{2}\theta^a_{L,R}T^a\right)q_{L,R}(x), \qquad q_{L,R}(x) \rightarrow \exp\left(\frac{i}{2}\tilde{\theta}_{L,R}\right)q_{L,R}(x), \qquad (1.6)$$

where T^a belong to the adjoint representation of $SU(N_f)$ and $\theta^a_{L,R}, \tilde{\theta}_{L,R}$ are some arbitrary constants that parametrize the transformation. Gluon fields are unaffected by this global symmetry. Any $U(N)$ transformation can be decomposed into $SU(N) \times U(1)$ and thus, the previous global symmetry can be rewritten as $SU(N_f)_L \times SU(N_f)_R \times U(1)_V \times U(1)_A$, where the vector part V is the sum of the left- and right-handed quark numbers and the axial component A corresponds to the subtraction of the previous quantities.

Quantum corrections reveal that the singlet axial-vector current associated to the symmetry under $U(1)_A$, which is conserved at the classical level, develops an anomaly and thus, the true symmetry of the quantum theory reduces to $SU(N_f)_L \times SU(N_f)_R \times U(1)_V$. In Chapter 2 we will address a more detailed explanation of the axial anomaly. The $U(1)_V$ symmetry is related to the baryon number conservation while the rest is usually referred to as the chiral symmetry. If the chiral symmetry were a true symmetry of QCD, one would expect a spectrum of degenerate states with opposite parity. However, this is not observed in Nature implying that the symmetry is broken. In fact, the symmetry is broken spontaneously as the generators of the $SU(N_f)_L \times SU(N_f)_R/SU(N_f)_V$ quotient space do not annihilate the ground state and therefore each of them is associated to a massless Goldstone boson. The physical states corresponding to these Goldstone bosons are the lightest mesons π, η and K, the latter being important only if $N_f = 3$. The finite masses of these particles are understood as a consequence of the explicit symmetry breaking due to the finite quark masses in the QCD Lagrangian. Although exact chiral symmetry is not actually realized in QCD, this treatment may be used as an approximation to work in QCD at low energies developing the so-called Chiral Perturbation Theory (χPT), which is discussed below.

The QCD coupling g determines the strength of the interactions between quarks and gluons and the gluon self-interaction. Gluon self-interactions are allowed due to the non-abelian nature of QCD, unlike the case of electromagnetism where photons can

only interact with other particles. The renormalization of a quantum theory leads to the running of its coupling constant, which is not actually a real constant but depends on the energy scale μ at which a process takes place. A $SU(N_c)$ gauge theory with N_f quark flavours shows [10] that the β function at one loop

$$\beta(g)_{\text{1-loop}} = \frac{\partial g}{\partial \log \mu} = -\frac{g^3}{16\pi^2} \left(\frac{11}{3} N_c - \frac{2}{3} N_f \right) \tag{1.7}$$

is negative for $N_f < \frac{11}{2} N_c$. In particular, the fact that QCD with $N_c = 3$ and $N_f = 6$ quarks is characterised by a negative β function leads to a coupling constant decreasing with rising energy. At high energies QCD is not a strongly interacting theory any more and approaches the free limit. This effect is called asymptotic freedom and in a way it corresponds to the opposite behaviour of the confinement described at low energies.

This picture of QCD allows to use perturbative techniques for the calculations of processes at high energies. The perturbative short-distance parton cross sections and the non-perturbative long-distance quantities may be combined due to QCD factorization theorems [11]. The long-distance contribution includes the parton distribution functions, fragmentation functions, different kinds of form factors, etc. Indeed this method becomes more accurate as energies are further increased due to QCD asymptotic freedom.

At low energies, perturbative calculations are meaningless due to the large coupling among quarks and gluons. Non-perturbative effects cannot be avoided in this regime and therefore many difficulties appear making QCD hard to analytically or numerically solve. Several approaches have been addressed to overcome these problems such as numerical simulations on the lattice [12], effective field theories [7, 8] or $1/N_c$ expansions [13].

One possibility to rigorously define a quantum field theory consists in discretizing it. Lattice calculations are a non-perturbative mechanism where QCD is formulated on a grid of points in Euclidian space-time. A fixed and finite spacing between the points of the grid represents a UV regulator. If the lattice size is taken to be infinitely large and the separation of its sites infinitesimally small, continuum QCD is recovered [12]. The Feynman path integral approach is used to compute correlation functions of hadronic operators and matrix elements of any operator between hadronic states in terms of the fundamental quark and gluon degrees of freedom. The pion mass m_π is normally used to test the reliability of lattice calculations since it is the lightest hadron state and therefore its corresponding wave length is the largest one. If the lattice is not large enough, the pion wave function does not fit in the lattice. This is why large quark masses are normally used in this description leading to a non-physical value for the pion mass. Nevertheless, large lattices with small spacing correspond to a huge number of grid sites leading to computational simulations that need much more time to be performed. In addition, the corrections to finite-volume effects have to be calculated for a realistic comparison with experiments.

A different approach for low energy QCD consists in using effective field theories (EFT). Since they are anyway not visible at large distances, quarks or gluons are integrated out of the model while hadrons become the relevant low-energy degrees of freedom. Imposing the symmetries of QCD to the theory, any observable can be calculated by means of a sort of perturbative expansion in which a power-counting scheme determines the importance of the quantum amplitudes. In the same way the increasing powers of a small coupling constant are used in perturbation theory, EFT usually take advantage of the ratio of a small parameter such as mass, momentum/energy. These theories correspond to the low-energy realization of QCD and therefore they are only valid up to some maximum cut-off scale, making them non-renormalizable. χPT has proven to be a highly successful effective theory where the interactions among the lightest meson states are described (for a review see [7, 8]). Due to the large s quark mass, the convergence of the expansion in the $SU(3)$ sector is somewhat slower as compared with the $SU(2)$ version. A generalisation may be done by accommodating baryon states to the theory leading to additional baryon-baryon and baryon-meson interactions. It is important to note that χPT uses as only ingredients the symmetries of QCD and it is therefore not a model but a low energy realization.

In this thesis we shall use two low energy models: the Nambu–Jona-Lasinio model (NJL) and the sigma model. NJL is a microscopic model including four-fermion vertices that replace the interactions of gluons in QCD. Due to the presence of these terms, the model is not renormalizable but the absence of gluons allows the theory to be bosonised. After this process, one obtains a meson theory including scalar and pseudoscalar fields that can be associated to a sigma model with concrete values for its parameters. In turn the sigma model corresponds to a particular theory that derives from EFT based on χPT assuming scalar dominance of the interaction at low energies. In both NJL and the sigma model chiral symmetry is spontaneously broken due to the formation of a dynamical chiral quark condensate. This condensate provides a constituent mass for the quarks. In the u, d sector, it is expected to be of the order of 300 MeV (based in the mass of nucleons) in contrast with the light mass of current quarks, of order 5 MeV. More details of these two models will be given in Chapters 3 and 4.

When no other method works, the only way to investigate the behaviour of QCD at low energies consists in performing an expansion in terms of the small parameter $1/N_c$. The large N_c limit of a $SU(N_c)$ gauge theory might lead to think that a larger gauge group complicates the theory since it involves an increase of the number of dynamical degrees of freedom. However, this limit can be shown to be a reasonable approximation even for the case of QCD where $N_c = 3$ [13]. In the large-N_c limit the number of gluon species grows as N_c^2 while the number of quarks is of order N_c. QCD becomes a theory of an infinite number of non-interacting zero-width resonances [14], which are mesons and glueballs since baryon masses grow with N_c and can be decoupled and safely ignored. The $1/N_c$ expansion is normally formulated by assigning to each Feynman diagram a power of N_c [15], which is determined by the topology of the diagram. The leading contributions are 'planar' and do not contain quark loops while subleading terms are suppressed by a factor $1/N_c$ due to quark loops and each

non-planar gluon exchange is suppressed by $1/N_c^2$. The qualitatively important point of this approach is the N_c-scaling behaviour of the different diagrams that allows to classify them depending on their relevance. Since $1/N_c$ is not a very small parameter, a perturbative expansion in $1/N_c$ may require the inclusion of a large number of higher order terms if an accurate result is searched.

1.1 The QCD phase diagram

The fact that highly energetic partons could interact almost freely suggests the possibility that confined matter may eventually undergo a phase transition. The system is led to a deconfined regime where the main degrees of freedom of QCD are quarks and gluons instead of hadrons and therefore colourless states do not exist any more.

The study of deconfinement has been addressed by many different collaborations and techniques. QCD lattice calculations can give reliable results on thermodynamic properties of strongly interacting matter only for very small baryon chemical potentials. In this case a crossover type of the deconfinement transition is predicted [16]. Lattice QCD also suggests a phase transition from hadronic phase to quark gluon plasma at $T_c \sim 140 - 190$ MeV [17] (for reviews, see [18]).

This new phase, the so-called quark-gluon plasma (QGP), could be reached at high temperatures and densities, conditions that are reachable in heavy ion collisions (HIC). In fact, recent results from Relativistic Heavy Ion Collider (RHIC) show strong evidence that QGP has been created in the Au+Au collisions at $\sqrt{s_{NN}} = 200$ GeV[19].

By modifying the experimental conditions such as the collision energy or impact parameter, it is possible to explore a broad range of temperatures and densities unravelling the different phases of QCD. While the system is heated and compressed, hadrons are expected to occupy more and more space leading to a ultimate overlapping that triggers a parton 'percolation' between hadrons thus being released. In addition, light quarks lose their constituent mass inside hadrons and acquire their genuine mass triggering a restoration of chiral symmetry. One of the scientific goals of the current high energy heavy ion program is to quantify properties of this QGP matter, such as the equation of state.

In a HIC experiment, heavy nuclei are accelerated to ultra-relativistic speeds before they impact. Immediately after the collision the highly boosted nuclei create a strongly interacting media that reaches extremely high temperatures of the order of several hundreds of MeV, and the density of nuclear matter may be widely exceeded. Understanding the behaviour of the hot and dense fireball constitutes one of the most notorious challenges in QCD. These extreme thermodynamic conditions are believed to exist in two astrophysical contexts: a few microseconds after the 'Big Bang' a transitory stage of strongly interacting matter survived with a temperature ~ 200 MeV (around 10^{12} K) and a small net baryon excess; in the core of neutron stars densities are expected to be a few times the nuclear density. New regions of the QCD phase diagram can be explored by means of current accelerator experiments [20, 21].

The first collisions were performed at the Alternating Grading Synchrotron (AGS) in Brookhaven (BNL) with center-of-mass energies around $\sqrt{s} \sim 5$ GeV per nucleon and later, the CERN Super-proton-Synchrotron (SPS) achieved $\sqrt{s} \sim$20 GeV per nucleon among many other accelerator experiments. Currently RHIC at BNL and the LHC at CERN reach energies as high as $\sqrt{s} \sim 200$ GeV and 5 TeV per nucleon, respectively.
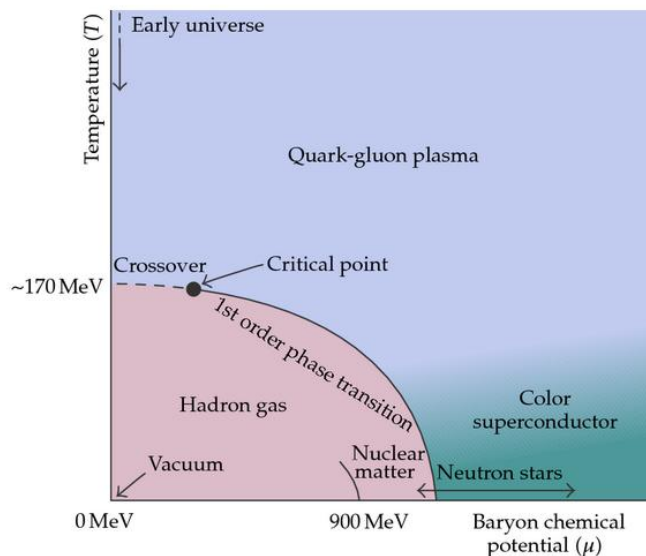
Figure 1.1: QCD phase diagram depending on the temperature and density extracted from [22]. Realistic and speculative phases are indicated.

The phenomenon of deconfinement has also been investigated in accelerator experiments. The crossover transition to the deconfined phase that predicts lattice QCD seems to be confirmed by recent RHIC experiments [23]. In the regime of moderate densities, different approximations predict a possible first order phase transition to the deconfined phase suggesting the existence of a critical point that has been intensively searched at RHIC. One of the main goals of the RHIC low-energy program is to find this critical point by scanning different regions of the phase space colliding gold nuclei at various energies. In order to search for a possible critical point, higher moments of the net-proton distributions are measured in Au+Au collisions over a wide range of chemical potentials. Deviations of several moments with respect to theoretical expectations have been observed at beam energies below $\sqrt{s_{NN}} = 27$ GeV per nucleon [24]. However, higher statistics are needed to obtain definite conclusions. From the theoretical point of view, many different approaches have posed and investigated this critical point.

Dealing with strongly coupled matter complicates the theoretical understanding of the properties and dynamics of the medium. In the last years an increasing interest in strongly coupled techniques led to the study of the liquid plasmas that arise as hot deconfined phases of non-abelian gauge theories which have holographically dual

descriptions as gravitational theories in 4+1 dimensions containing a black hole horizon. A simple example of this gauge/gravity duality has been applied in a strongly coupled $\mathcal{N} = 4$ supersymmetric Yang-Mills theory in the limit of a large number of colours. These sort of analyses have provided plenty of qualitatives insights into the properties of the QGP [25]. In particular, in the limit where the QCD coupling is large at all relevant energy scales the gauge/gravity duality allowed to use holographic calculations in order to obtain detailed dynamical information on the energy loss processes.

Theoretical studies of the QGP thermodynamics revealed that it behaves as a near-ideal Fermi liquid, although research on flow characteristics is ongoing. An important development in recent years has been the conjecture that for any thermal fluid, a fundamental bound on the value of the viscosity may exist [26]. The uncertainty principle requires a non-zero viscosity. More precisely, the conjecture states that the ratio of viscosity to entropy density must satisfy the relation $\eta/s \geq 1/4\pi$ and different investigations have been developed in order to experimentally measure this ratio [27]. The combination of the different results seems to conclude that the produced matter is within a factor of 2-3 of the conjectured bound and therefore, it should correspond to the most ideal fluid that has been ever measured. However, there is evidence that the matter does not behave as a quasi-ideal state of free quarks and gluons, but rather as an almost perfect dense fluid with a nearly complete absorption of high momentum probes [28].

In addition to the QGP and the hadronic phase, other thermodynamical phases have been under discussion together with their corresponding phase transitions. In Fig. 2.4 a tentative phase diagram of QCD is shown depending on the temperature and density. For example, the liquid-gas transition from the nuclear matter to the hadron gas is believed to occur for temperatures of the order of $T \lesssim 10$ MeV and chemical potentials $\mu \simeq 900$ MeV. Another phase is the so-called colour-flavour locked phase (CFL) [29]. At very high densities the 3 lightest quarks u, s, d may form Cooper pairs that correlate their colour and flavour properties leading to a colour superconducting behaviour. The CFL would break the QCD symmetries and exhibit a very different spectrum and transport properties. No experimental evidences of this phase have been found so far but it is conjectured that this form of matter may exist in the core of neutron stars. All in all the structure of the phase diagram at high baryon densities remains rather uncertain.

1.2   Exploring the phase diagram with heavy ion collisions

The dynamics of the nuclear fireball created from a HIC is not trivial. In Fig. 1.2 we present a sketch of a HIC evolving in time and the corresponding phase where the system is found at each moment. At the initial stage, the fireball is compressed for a short period of time between 0.5 and 1 fm. During this time, the system is thought to reach temperatures as high as ~600-700 MeV depending on the model and the experiment (see [30] and references therein) and enter the QGP. In the next stage, all the

phenomenology associated to a deconfined phase takes place while the system starts to thermalize due to strong interactions among the fireball components. The temperature slowly drops down to ~ 200 MeV, a situation where it is still unclear if a mixed phase exists. After an expansion that lasts for 5 to 10 fm, conventional hydrodynamic models and lattice calculations suggest that around $T_c \sim 140 - 190$ MeV, a phase transition leads the system to the hadronic phase, where quarks and gluons regroup again to form hadrons. The experimental probes from hadron interactions may thus provide a valuable insight into the QGP and the deconfinement phase transition. Finally, when the system is cold enough, say $T \sim 100$ MeV, collisions among hadrons cease leading to the freezout of the fireball components, which survive as the final particle states.
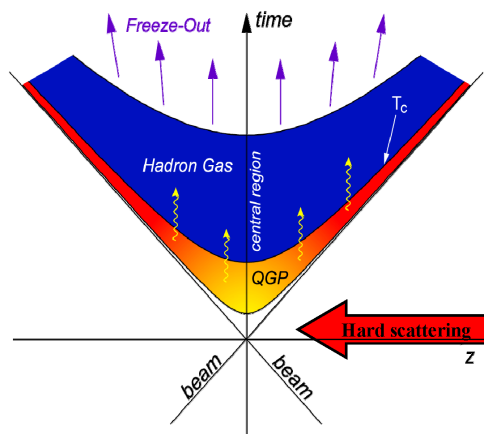
Figure 1.2: Evolution of the nuclear medium created from a HIC depending on time. After the collision the system heats up and reaches the QGP where quarks and gluons become deconfined. Next, a slow cooling process takes place pushing the system to the hadron phase where partons are arranged into baryons and mesons. Finally, when the freezout temperature is met, hadrons do not interact any more.

At high energies, or equivalently, at small values of Bjorken x, gluon densities are very large. Under these circumstances QCD may be described by a many-body theory of weakly coupled partons, the so-called colour Glass Condensate (CGC) [31]. Two highly boosted nuclei in the first stages of a HIC can be considered as two pancakes of CGC. The gluons in the nuclear wavefunctions are disordered and evolve very slowly relative to the time scale of a HIC similar to the behaviour of glasses. Their high density is the responsible for the term condensate. This picture of nuclear matter consists in a coherent classical field which decays into nearly on-shell partons and eventually thermalize to form the QGP. This approach allows to study the initial conditions and equilibration in HIC. In fact, the CGC has to be considered as the non-equilibrium stage preceding the QGP. For this reason, this matter is often called Glasma [32, 33].

One way to analyse the properties of QCD matter in HIC is via the study of the azimuthal anisotropy induced in non-central collisions (for reviews see [34, 35]). Anisotropic collective flow, i.e. anisotropies in particle momentum distributions with

respect to the reaction plane, is highly sensitive to the system properties in the first stages of its evolution (see Fig. 1.3). This is due to the initial asymmetries in the geometry of the system that rapidly wipe out while the system cools down. Early probes are normally characterised by weak interactions but the analysis of collective flow corresponds to a unique hadronic observable. The particle azimuthal distribution measured with respect to the reaction plane is conveniently expanded as a Fourier series [36]. The different harmonics, generically referred to as n-th order flow, of this expansion depend on the rapidity, the transverse momentum and the impact parameter of the collision and are measured at different experiments [37]. Many different hydrodynamical calculations have been addressed to provide qualitative descriptions of collective flows (see [25] and references therein).
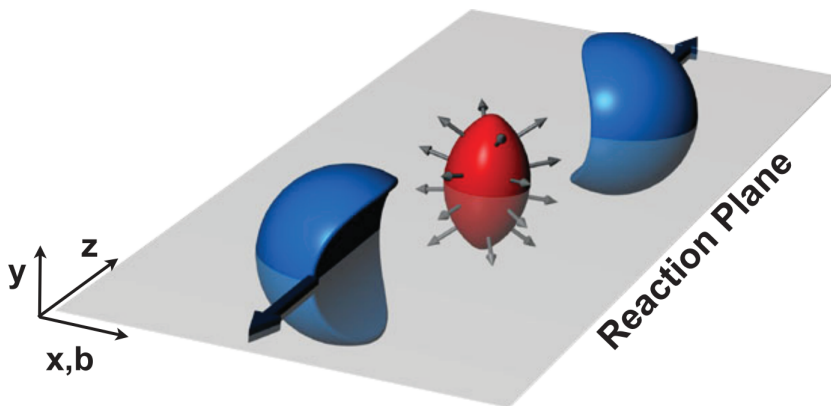
Figure 1.3: In non-central collisions the central region where the two nuclei overlap shows an almond-like shape (graphic extracted from [35]) leading to an initial anisotropy with respect to the reaction plane. This is translated into anisotropies in particle momentum distributions.

When the HIC fireball cools down and enters the hadronic phase, quarks and gluons rearrange to form hadrons. Matter becomes colourless again creating a gas of hadrons. Thermal equilibrium within the gas has been argued to be reached in RHIC and LHC unlike other previous machines like SPS. Many different particles may conform this medium but the partition function is dominated by the lightest degrees of freedom. Thus the fireball can be approximated by gas of pions. Other light meson states may be present in small amounts but baryons are certainly too heavy to play a significant role in this context.

The dynamical evolution of the hadron gas needs to be well understood as it corresponds to the intermediate step between the QGP and the final states that are measured in experiment detectors. The ρ meson is a key player of the hadron gas thermalization. First, ρ mesons strongly interact with pions and their short mean free path allows for multiple scattering processes leading to a regeneration of these particles from pions, i.e., the effective number of ρ mesons is enhanced with respect to the direct production from the hadronization process. And second, studies based on effective hadronic the-

ories seem to agree that the ρ meson spectral function is severely modified in-medium leading to a strong broadening of the resonance [38, 39, 40] with only a little mass shift [41].

On the one hand, a broadening of the ρ meson spectral function may result from its scattering off the baryons in the dense hadronic medium [38]. An extended many-body hadronic model of the ρ in hot meson matter that includes resonance excitations and pion Bose enhancement in the ρ self-energy leads to a broadening of around $\Delta\Gamma_\rho \sim 80$ MeV at a temperature $T = 150$ MeV and a pion density $\varrho_\pi \simeq 0.75\varrho_0$ [42], where ϱ_0 is the nuclear density. In cold nuclear matter, other investigations have been developed in ρN resonance models including the in-medium pion cloud [43] showing a stronger broadening of ~ 300 MeV at $\varrho_N \simeq \varrho_0$ and a comparable mass shift of ~ 40 MeV. On the other hand, the 'dropping' vector meson mass scenario in the dense fireball [44] establishes a link between hadron masses and the quark condensate, the order parameter of the chiral symmetry restoration. The ρ mass scales [41] with the quark condensate and the latter drops due to the high baryon density rather than high temperature. Note that both approaches rely on having a high baryon density. The relative merits of these two different approaches have attracted much debate trying to explain the low invariant mass dilepton excess that has been measured in different experiments [45, 46, 47].

1.3   Hard probes in heavy ion collisions

A variety of signals of the strongly interacting nuclear medium and its dynamics have been proposed. Hard probes, i.e. processes involving large momentum exchanges, may explore small distance physics provided that constituents quarks are heavy enough, a regime that can be well described with perturbative QCD leading to a good theoretical control of the subject.

An important hard probe is the different heavy quarkonia states and their in-medium modifications [48]. The presence of QGP screens the attractive force between a quark-antiquark pair. The maximum distance which allows the formation of quarkonium decreases with the medium temperature. The interaction of these states with a hot medium leads to the modification of their properties and to their complete dissociation at sufficiently high temperatures. Gauge/string duality has shown that heavy quarkonium mesons remain bound in the plasma and the fact that their dissociation temperature drops with increasing meson velocity [25]. Such fracture entails a suppression of quarkonium production in nuclear collisions as compared to their proton-proton equivalent. Most studies of quarkonium have focused on charmonia states such as the J/ψ due to the small b-quark production cross section at low energies. Nevertheless, charm quarks are not sufficiently heavy for a reliable theoretical description and thus, their interactions with the QGP and their production mechanism in HIC are somewhat uncertain [49]. A strong suppression of J/ψ mesons in HIC has been shown [50, 51] but the suppression pattern is still puzzling and the interpretation of data is not totally clear yet since quarkonium is also suppressed in proton-nucleus collisions [52]. Recent

data on bottomonium suppression through the study of Υ mesons have been published by LHC [51] and RHIC [53] allowing a better theoretical understanding of this channel.

The high energy jets produced in a collision are severely affected by a strongly interacting medium. When a high-momentum parton is produced in the initial stage of a nucleus-nucleus collision, it will multiply interact with the medium constituents before its hadronization. The energy of such partons is reduced due to collisional energy loss [54] and medium-induced gluon radiation [55]. The energy of these partons is stored in the QGP and propagates as a collective excitation or conical flow [56]. This effect leads to peaks in particle correlations that have been experimentally observed [57]. The effect of jet quenching in the QGP is the main motivation for studying jets as well as high-momentum particle spectra and particle correlations in HIC. The study of high energy jets is one of the best hard probes to investigate the nuclear medium as their production occurs at very high energy scales where perturbative QCD guarantees a good theoretical description. Similarly, many of the properties of jets in vacuum are also controlled by physics at high energy scales and are thus well understood theoretically. The observed deviations of different properties in HIC and in vacuum must be due to the interaction of the different jet components with the nuclear medium. Accurate jet reconstruction allows measurements of the jet fragmentation functions and provide insight on the properties of the hot and dense QGP. Evidences of parton energy loss were first observed at RHIC from the suppression of high p_T particles studying the nuclear modification factor [58] and the suppression of back-to-back correlations [59]. LHC also observed jet quenching [60] and SPS partially did [61].

Besides hard probes, many other signatures of the medium created in HIC have been discussed. Large topological fluctuations in the QCD vacuum may induce the breaking of parity in nucleus-nucleus collisions leading to the Chiral Magnetic Effect [63], which predicts a charge separation across the reaction plane. In addition, photons and dileptons (same-flavour lepton and antilepton pairs) are considered powerful probes due to their negligible interactions with the final state hadrons. We will explain these two aspects in detail in the following sections.

1.4 The Chiral Magnetic Effect

A different effect that has received a lot of attention is the charge separation detected in nucleus-nucleus collisions at STAR [62]. The measurement of a non-trivial three-particle observable reflects that event-by-event same- and opposite- charge azimuth correlations lead to a small separation of charges across the reaction plane in a HIC. This observable has the advantage of suppressing the background correlations unrelated to the reaction plane. The measurement of this effect has been assumed to be an experimental confirmation of the Chiral Magnetic Effect (CME) [63], which assumes that local parity-odd domains may appear in HIC. We will discuss this effect in more detail in Chapter 2. The pair correlations of same and opposite charge due to the CME are expected to be similar in magnitude and opposite in sign. This could be modified by

the medium resulting in the dilution of the correlations between opposite sign particles [63]. A clear difference in the correlation strength between the same and opposite charge particle combinations seems to be observed (see Fig. 1.4). The simulation of opposite-charge correlations of three particle correlations is similar to the measured signal but the same-charge signal is much larger and of opposite sign compared to the predicted one. Such phenomenon has also been observed at ALICE in LHC [64].
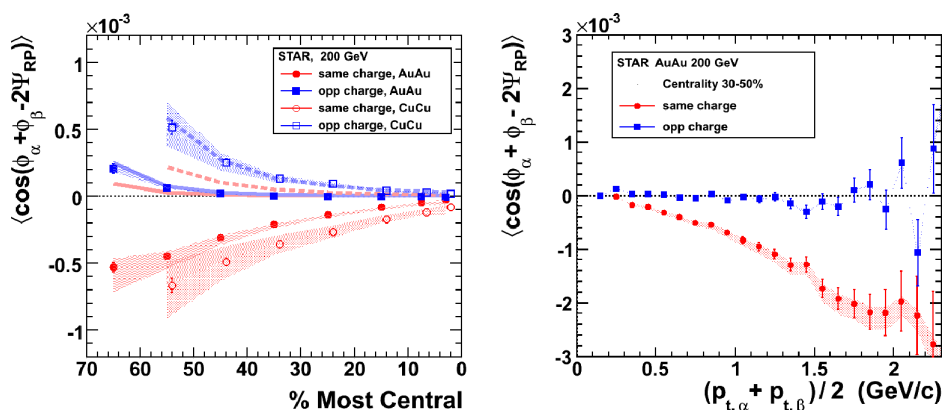
Figure 1.4: The observable that reflects same- and opposite- charge azimuth correlations is displayed depending on the centrality of the collision for Au+Au collisions and Cu+Cu collisions (left) and the semi-sum of transverse momenta only for Au+Au collisions (right) extracted from [62]. In the left panel, the thick solid (Au+Au) and dashed (Cu+Cu) lines represent theoretical calculations of 3-particle correlations.

The centrality dependence shown in the left panel of Fig. 1.4 agrees with the charge separation relative to the reaction plane. On the other hand, the magnitude of the effect for same charge particles increases with average pair p_T both at RHIC and LHC. This observation is in contradiction with the initial expectation [63], which predicts the dominance of low p_T particles. In any case, no definite conclusions can be stated due to the lack of realistic model calculations for the dependences on the centrality and pair momentum.

Different magnetic field dynamics are expected to be induced in LHC and RHIC, a fact that should be quantified. The parity-breaking signal indicates the presence of a charge separation whose magnitude shrinks with diminishing beam energy, suggesting that the QGP volume shrinks with lower energy collisions, leading to less charge separation. It has been argued that at higher energies the strength of the CME should decrease since the magnetic field decays much faster [65].

The analysis of different charge azimuthal correlations in order to search for charge separations in a deconfined state of matter may hint to the possibility of probing new effects in hot and dense QCD. In particular, the appearance of local large topological fluctuations inducing metastable P- and CP-odd domains could be detected together with the electromagnetic current induced by large angular momentum or magnetic field in non-central HIC. In addition to the presented study, analyses of higher order

harmonic correlations are planned and may help to provide a deeper insight into the charge dependent correlations observed at RHIC and LHC.

1.5 The problem of low-mass dileptons

Dileptons are considered the most useful electromagnetic probe to unravel the main features of the hot medium created in HIC. They are produced continuously carrying information of the entire evolution of the system and due to the existence of an additional variable, their invariant mass $M_{\ell\ell}$, dileptons possess a better signal to background ratio compared to photons. Depending on the stage of the collision, dileptons are emitted from different sources. Before the collision dileptons are produced through coherent bremsstrahlung due to the electromagnetic repulsion among the two nuclei [66] but this contribution is negligible compared to other processes that follow [67]. During the heating of the nuclear system and before equilibrium is reached, Drell-Yan annihilation provides the main source of dileptons that may be dominant above $M_{\ell\ell} \simeq 3$ GeV [68]. When the system enters the QGP and thermalizes, dileptons are mainly created from perturbative quark-antiquark scattering. Next, the plasma evolves to a hadron gas where dileptons are emitted from pion and kaon annihilation (among other channels) [69]. The presence of light vector meson resonances like ρ, ω and ϕ are responsible for an enhancement of such processes due to their connection between the initial two-meson states and the final dileptons [70]. The dilepton invariant mass corresponds to the vector meson mass distribution at the precise moment of the decay allowing to obtain a deep insight into the hot medium. At the final stages of the collision when freezout is reached, only long-lived hadronic states (mainly mesons) like π^0, η and ω are able to produce lepton pairs through their Dalitz decay as they do not interact among themselves [71]. These processes correspond to an initial state decaying into a pair of particles, one of them being a virtual photon that subsequently leads to a lepton pair. Due to the kinematics of these decays, all the mentioned meson sources are relevant for the production of dileptons with an invariant mass below 1 GeV.

Due to the relevance of dileptons, many studies have been undertaken in order to unravel the main properties of the nuclear medium. Perhaps one of the most important and oldest analysis consists in measuring the dilepton invariant mass distribution, which has been analysed by different experimental collaborations during the last decades. In proton-proton collisions the shape of the detected distribution can be well reproduced by the so-called hadronic 'cocktail', the sum of several final-state hadron decays with known abundances. In fact, pp data is normally used to fit the weight of the different hadrons in order to be used for other predictions. And while proton-nucleus data can be well understood from pp results, central nucleus-nucleus collisions have presented severe discrepancies with respect to the expected theoretical contribution [45, 46, 47], in particular, a strong enhancement of dileptons with invariant mass below 1 GeV. This disagreement reflects that in-medium effects have to be considered to explain the abnormal AA results.

The anomalous dilepton yield from nucleus-nucleus collisions has been a long-standing problem that has been under investigation by many different groups, both theoretical and experimental (for a review see [72]). No dilepton measurements were performed at the AGS accelerator, where high baryon densities were expected. The DLS collaboration at BEVALAC released the first dielectron results for fixed target Ca+Ca, C+C, He+Ca and Nb+Nb reactions at a beam energy of 1 GeV per nucleon. The first generation of DLS data [73] were consistent with the results from transport model calculations [74] including the conventional dileptons sources as pn bremsstrahlung, light meson Dalitz decays, direct decays of vector mesons and pion-pion annihilation, without incorporating any medium effects. However, an updated version of the DLS measurement on the full data sample and an improved analysis showed an enhancement of almost one order of magnitude in the cross section compared to the previous results [75]. This discrepancy has persisted for years and many attempts have been addressed to disentangle the newest DLS data. In fact, all in-medium scenarios that successfully have explained the dilepton enhancement at higher energies in more powerful accelerators failed to describe the new DLS dilepton data, a problem that was soon known as the 'DLS puzzle'.

The DLS puzzle motivated the HADES experiment at SIS, a new generation experiment that was designed to study C+C, Ni+Ni and Au+Au collisions at beam energies up to 8A GeV with a fixed target. The dielectron excess observed at DLS was confirmed by HADES data [76] running C+C collisions at 1A and 2A GeV. Recently, new approaches have been trying to tackle this problem. On the one hand, the effect was partially interpreted as being due to enhanced η meson production in proton-neutron scattering [77]. On the other hand, an enhanced bremsstrahlung contribution in line with one boson exchange calculations, led to a rather successful agreement with the published DLS and HADES data on C+C collisions [78]. However, the same calculations still underestimate the dilepton production in Ca+Ca reactions and thus, the issue still remains controversial.

At SPS the low-mass dilepton excess in central nucleus-nucleus collisions was observed again. Two different beams were used: a sulphur beam at 200 GeV/nucleon and a lead one at 158 GeV/nucleon. CERES collaboration reported a dielectron excess [45] where fixed target S+Au and Pb+Au reactions were analysed. In addition, they showed that the enhancement, particularly important in the mass region around 400-600 MeV, covered a wide range in transverse momentum, but was largest at low transverse momentum. Similar abnormal results for low-mass dimuons were observed at HELIOS/3 [79] with S+W reactions. The results from S+Cu and S+U reactions studied by the NA38 collaboration together with the Pb+Pb collisions at NA50 revealed no significant excess of dimuons [80], a fact that could most probably related to a large M_T-cut applied in their analysis. These independent measurements of the low-mass dilepton excess at the SPS triggered a huge theoretical research also motivated by a possible connection to the breaking of chiral symmetry. The importance of baryon density suggested by in-medium effects on the ρ meson encouraged the CERES collaboration to measure low-mass dielectron in Pb+Au collisions at the lower energy of 40A

1. INTRODUCTION

GeV where a higher baryon density and a lower temperature were expected [81]. Many different approaches were addressed to describe the dilepton excess at SPS, where it is not clear that thermal equilibrium was reached. Finally, the data could apparently be explained by means of in-medium modifications of the ρ meson due to its strong hadronic coupling and other less conventional assumptions [38, 41, 44, 78, 82].

The dilepton physics program of the NA38/NA50, HELIOS/3 and CERES collaboration was continued by the NA60 experiment also at SPS. Nucleus-nucleus collisions were investigated via dimuon production in In+In reactions at 158 GeV/nucleon with a fixed target. The experiment exhibited a clear excess of dimuons at low energies that increases with centrality and low pair p_T [83]. The most successful models at that time were compared with the high quality data of NA60, which could isolate the ρ channel from the rest of hadronic sources. In particular, the dropping mass and broadening scenarios show similar results for masses below the ω resonance peak due to the limited precision of the data, but between the ω and the ϕ resonance peaks the dropping mass case seems to be ruled out [46]. The broadening mass scenario [38] is reinforced by the NA60 data, together with other recent calculations that are claimed to reproduce the dilepton excess [39, 40]. Yet, the still considerable experimental uncertainties may allow other effects to be accommodated.

RHIC is the first accelerator with two highly energetic beams running at $\sqrt{s_{NN}} = 200$ GeV/nucleon, where Au+Au collisions are currently carried out and analysed by PHENIX and STAR experiments. PHENIX has measured a serious dielectron excess at low energies that is present at all p_T but it is more pronounced at low pair p_T [47]. A very strong centrality dependence is observed for the low-mass continuum. The enhancement appears in central collisions where it reaches a factor of almost 8 (see Fig. 1.5). PHENIX results appear different from those observed at the SPS: while at SPS the excess was closer to the ρ meson resonance peak, at PHENIX it spreads towards lower invariant masses. In addition, the integrated yield increases faster with the centrality of the collisions than the number of participating nucleons. The contribution of correlated pairs from the semi-leptonic decays of open charm mesons, negligible at SPS energies, is an important source that has to be included in the hadronic cocktail at RHIC energies. In contrast to previous experiments, PHENIX low-mass dilepton results have not been correctly reproduced by any of the successful models that apparently explained the excess before.

The STAR collaboration also reported a dielectron enhancement below the ω peak [84] but it was observed to be significantly lower than what was measured by PHENIX. Due to this moderate excess, theoretical calculations including an in-medium broadened ρ meson can possibly explain the STAR data. The centrality and p_T dependence is also comparable with expectations from model calculations.

Finally, low invariant mass dilepton measurements have not yet been published by LHC collaborations.

A similar dilepton excess with invariant mass between 1 and 3 GeV has been also measured at SPS and RHIC. All experiments at SPS reported an excess with respect
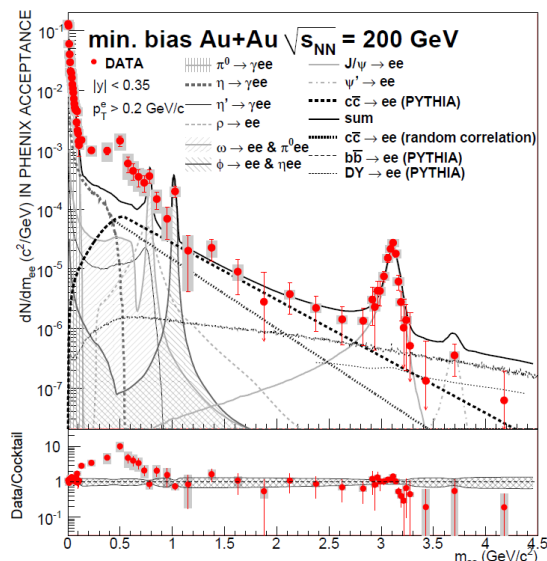
Figure 1.5: Dielectron mass spectrum in minimum-bias Au+Au collisions at PHENIX compared to the cocktail of known hadronic sources extracted from [47]. The ratio of data to the cocktail is shown in the bottom panel. A clear enhancement of almost one order of magnitude is observed at low invariant masses.

to the expected yield from the two main contributions in this mass region, Drell-Yan and semi-leptonic charm decay [79, 85]. Several explanations were investigated based in the phenomenological hypothesis of an enhanced charm production, such as secondary Drell-Yan emission, final-state rescatterings that broaden the m_T distribution of charmed mesons enhancing the yield, and all sources of lepton pairs from secondary meson interactions. NA60 concluded that the excess of dimuons in the intermediate mass region corresponds to the thermal radiation emitted in the early stages of the collision [86]. However, PHENIX showed that the inclusive production seems to agree with the simulated open charm contribution [47].

We are living an era with plenty of ongoing experiments that may obtain relevant information about QCD matter. Many models have tried to solve or explain different problems with the addition of new parameters or observables that need to be measured. Thanks to the current experimental work, the measurement of such parameters may help to confirm or rule out all these models. In addition, one cannot exclude the fact that new phenomena could be detected. This scenario constitutes an encouraging source of motivation for both theoretical and experimental research.

1.6 Scope and overview

In the context of HIC, new effects can be studied in QCD due to high temperatures and densities. In particular, in this thesis we will explore the possibility that the QCD vacuum breaks parity in a finite volume. The Vafa-Witten theorem [87] forbids the

spontaneous breaking of discrete symmetries in gauge theories. However, this theorem does not apply when one deals with a dense system. The high temperatures and densities reached in the strongly interacting medium induced in HIC lead to a realistic scenario where the violation of parity in QCD could be perceptible.

The violation of parity in QCD has been already studied by different collaborations and approaches [63, 88] that we will discuss. Here we are interested in describing the thermodynamic conditions that could lead to this phenomenon in HIC as well as the phenomenology associated to it. If this effect takes place, the properties of in-medium hadrons would be severely distorted leading to unexpected modifications of the distributions of final state particles. We will show in detail how scalar and vector mesons are influenced by a parity-odd medium and in addition, we will search for possible signatures that could help to detect this effect at RHIC or LHC.

In Chapter 2 we will focus on the possible existence of a new phase characterised by the violation of parity in QCD. We will analyse two different approaches to explore this effect. The first of them corresponds to the study of QCD at finite density by means of effective lagrangian techniques coupled to a non-trivial baryon chemical potential. A generalised linear sigma model retaining the two lightest multiplets of scalar and pseudoscalar fields of $SU(2)$ and satisfying the QCD symmetries in vacuum shows that for a given range of $\mu \neq 0$ a non-vanishing pseudoscalar condensate may arise leading to a new phase of QCD [88]. The second possibility is related to the presence of metastable $P-$ and $CP-$ odd bubbles in hot matter due to large topological fluctuations in a finite volume. In this context a large magnetic field or angular momentum could induce an electric field perpendicular to the reaction plane and hence an electric dipole moment [63]. This is the Chiral Magnetic Effect that we already presented in Section 1.4 and has been claimed to be detected in peripheral HIC at STAR [62]. Following the lines of the latter approach we will investigate the violation of parity in QCD as a consequence of large topological fluctuations corresponding to a non-equilibrium effect that may be driven by an external axial chemical potential μ_5.

In Chapter 3 we will implement the Nambu–Jona-Lasinio model with a vector and an axial chemical potentials at zero temperature in order to investigate the phase diagram of the model searching for possible phases with pseudoscalar condensation leading to parity violation. We will see that a non-zero μ_5 severely modifies the known properties of the NJL model while the presence of μ does not affect much our considerations. Provided that some numerical relations between the parameters of the model hold, spontaneous breaking of parity is found to be stable. In particular, we will find a phase with a non-trivial isospin singlet pseudoscalar condensate as well as a scalar condensate down to a critical value of the axial chemical potential. However, NJL with such characteristic parameters has nothing to do with QCD since the masses of the known states in vacuum are not compatible with the phenomenology. Despite being unable to draw definite conclusions for QCD, the values of μ_5 leading to a thermodynamically stable phase with parity violation suggest the range of the axial chemical potential where a parity-breaking phase has to be searched in HIC experiments.

After investigating the possible values of μ_5 that could lead parity violation, we address a detailed study of the in-medium modifications of mesons. First of all, Chapter 4 is devoted to the study of scalar and pseudoscalar mesons in a medium characterised by a non-trivial axial chemical potential. We will implement a generalised sigma model including the lightest scalar and pseudoscalar mesons in the $SU(3)$ representation in order to investigate the mixing among states of different parity and same flavour induced by a parity-odd medium, where in fact, the distinction of scalar and pseudoscalar states is meaningless. The axial chemical potential will be introduced as an external spurious axial-vector field through a covariant derivative. In-medium mesons will exhibit energy-dependent properties as spectrum and widths. We will see that the lightest degrees of freedom in each isospin channel become tachyonic states at high energies. In addition, the pion gas that constitutes the heavy ion fireball in the hadronic phase could instead be a gas of distorted pions due to the breaking of parity. We will thus compute the widths of all these states into distorted pions so as to search for possible broad resonances that could suffer from a regeneration process as the ρ meson does. In particular, the distorted η meson seems to be in thermal equilibrium inside the 'pion' gas due to its remarkably large width, unlike in vacuum.

Vector mesons are treated in Chapter 5. We will introduce the parity-breaking effect through the Chern-Simons term since the mixing of vector mesons with different parity is rather uncertain. By means of the Vector Meson Dominance model (VMD), we will introduce the lightest states in the $SU(3)$ representation. However, as we will argue in the next chapter, the ϕ meson decouples from the rest of the system and it can be simplified to $SU(2)$. A mixing will be found among photons and ρ and ω mesons due to the VMD mechanism itself and the parity-violating effect. After resolving the mixed system we will find a distorted dispersion relation for vector mesons while photons are not affected by parity-odd effects. As in the case of spin-zero mesons, vector mesons will show a frame-dependent effective mass and a tachyonic behaviour for one of their polarizations. The in-medium modifications of vector mesons can be tested through their decays into dileptons. The distorted shape of the ρ and ω spectral functions predicts an enhancement of the dilepton production around their resonance peak. We will show that this enhancement could help to partially explain the low-mass dilepton excess that has been presented in Section 1.5 for the NA60/PHENIX/STAR experiments. But this signal can be rather tricky to detect. The distorted shape of the ρ and ω spectral functions reveal a polarization asymmetry around the vacuum peak. Hence, we will also describe how the parity-breaking effect may be detected in HIC by means of a restriction of the angular coverage of the final lepton states. Two suitable angular variables will be presented in order to search for polarization dependencies and we will explain how a combined analysis of one of these variables together with the dilepton invariant mass could be an important signature to detect the possible violation of parity in HIC.

Finally, in Chapter 6 we present the main conclusions and future perspectives of this work.

1. INTRODUCTION

Chapter 2

A new phase of QCD with parity violation

During the last years the behaviour of baryonic matter under extreme conditions has received a lot of attention [89, 90, 91]. Many different models and approximations have appeared trying to obtain a deeper insight into the dynamics of heavy ion collisions. A particular investigation line has been recently studied triggering a significant spark among the scientific community: the possibility that QCD breaks parity at finite temperature and/or density. Indeed, one of the very few non-perturbative analytic results of QCD is the Vafa-Witten theorem [87]. According to it, vector-like global symmetries such as parity, charge conjugation, isospin and baryon number in vector-like gauge theories like QCD cannot be spontaneously broken while the θ angle is zero (see Eq. (2.1) and subsequent discussion). However this theorem does not apply to dense QCD matter where the partition function is not any more positive definite due to the presence of a highly non-trivial fermion determinant. In addition, out-of-equilibrium symmetry-breaking effects driven by finite temperatures are not forbidden by the Vafa-Witten theorem. Lorentz–non-invariant P-odd operators are allowed to have non-zero expectation values at finite density $\mu \neq 0$ [92] and finite temperature if the system is out of equilibrium [93]. The possibility that in extreme conditions of temperature and baryon density such discrete symmetries might be broken in QCD has been discussed recently by different collaborations [63, 88, 94, 95], whose different approaches we will describe with some detail in this section.

Invariance under parity or charge conjugation are some of the characteristic footprints of strong interactions. However, the QCD Lagrangian may exhibit some terms explicitly break the CP symmetry. The corresponding operators with dimension 4 (or less) read

$$\mathcal{O}_g = \frac{1}{2}\varepsilon^{\mu\nu\rho\sigma}\mathrm{Tr}\left(G_{\mu\nu}G_{\rho\sigma}\right) \equiv \mathrm{Tr}\left(G^{\mu\nu}\widetilde{G}_{\mu\nu}\right), \qquad \mathcal{O}_q = i\bar{q}\hat{m}_q\gamma_5 q. \qquad (2.1)$$

The dimension-4 operator $\mathcal{O}_g$ normally appears coupled to a constant *angle* θ, the so-called θ-term. If one introduces the QCD Lagrangian with complex quark masses

2. A NEW PHASE OF QCD WITH PARITY VIOLATION

including the quark operator $\mathcal{O}_q$, a $U(1)_A$ transformation of the quark fields $q_f \rightarrow \exp(i\gamma_5 \theta_f/2)q_f$ can remove the imaginary part of quark masses [4] with an appropriate choice of the coefficients $\theta_f = \arctan(\hat{m}_q/m)$, following the notation introduced in Eq. (1.1). However, eliminating the term $\mathcal{O}_q$ from the Lagrangian involves the replacement $\theta \rightarrow \theta + \sum_f \theta_f$ due to the partial conservation of the axial current, which is explained below (see Eq. (2.13)). Therefore, as the quark operator can be rotated away and reabsorbed by the gluon operator $\mathcal{O}_g$, one usually forgets about the former and focuses in the gluon one. Experimental measurements [96] lead to a a strong bound $\theta \lesssim 10^{-9}$. The particularly small value of this parameter represents a case of fine-tuning that is known as the *strong CP problem*. In the next section more details will be given concerning the θ-term.

Several solutions have been addressed to solve the strong CP problem. The most accepted one consists in introducing a new global chiral $U(1)_{PQ}$ symmetry whose spontaneous breaking produces a Nambu-Goldstone (pseudoscalar) boson called axion [97]. The axion interacts with the gluon fields through a θ-like term that explicitly breaks the axial $U(1)_{PQ}$ symmetry. The minimum of the axion potential provides a relation where the axion condensate cancels the θ-term. The resulting Lagrangian is invariant under CP thus explaining the small bound on the effective θ parameter. Nowadays the axion is still considered as a viable solution of the strong CP problem, and one of the plausible dark matter candidates. Several experimental groups are currently searching for axions (see [98] and references therein). While strong interactions preserve P and CP invariances at present time, this scenario suggests that in the early universe these symmetries could have been substantially violated leading to an asymmetry between matter and antimatter. This imbalance resulted in a substantial amount of residual matter that forms the present universe.

We will now explore the possibility that strong interactions do not respect parity after all. Two different approaches have been carried out in order to investigate the possible violation of parity in QCD. On the one hand, analytical studies with effective theories suggest that parity may be broken in dense systems. A generalised sigma model containing the two lightest $SU(2)$ multiplets of scalar and pseudoscalar fields reveals that a meson lagrangian realizing all the QCD properties at low energies may lead to a phase where parity is spontaneously broken due to a neutral isotriplet pseudoscalar condensation [88, 99]. It seems that the necessary conditions for this parity-breaking phase may be satisfied for a definite window of baryonic chemical potentials. On the other hand, it has been proposed that $P-$ and $CP-$ odd bubbles may appear in a finite volume due to large topological fluctuations [63, 94] in a hot (rather than dense) medium. The presence of a large magnetic field or angular momentum may induce an electric field perpendicular to the reaction plane through the θ-term and correspondingly, a net electric dipole moment. This is the Chiral Magnetic Effect that we already introduced in the previous chapter. This scenario can be regarded as a pseudo-equilibrium effect showing that a charge separation should be present in peripheral HIC.

2.1 Spontaneous parity breaking in dense systems

The simplest hadronic effective theory is the linear sigma model. Spontaneous chiral symmetry breaking (CSB) emerges due to a non-zero value for $\langle\sigma\rangle \sim \langle\bar{q}q\rangle/\Lambda^2$, $\Lambda \simeq 4\pi f_\pi$ with f_π being the weak pion decay coupling constant. A generalised model may be built containing two $SU(2)$ multiplets of scalar/pseudoscalar fields that include the two lowest lying resonances in each channel. The presence of two multiplets constitutes the minimal model having the possibility of describing spontaneous parity breaking (SPB) [88]. One should think of these two chiral multiplets as representing the two lowest-lying radial states for a given J^{PC}

$$H_j = \sigma_j \mathbf{I} + i\hat{\pi}_j, \quad j = 1, 2, \ \text{with} \ \hat{\pi}_j \equiv \pi_j^a \tau^a, \qquad (2.2)$$

where τ^a are Pauli matrices. This kind of parameterization preserves the parities of σ_2 and π_2 to be even and odd respectively (in the absence of SPB) and realizes manifestly the masslessness of Goldstone bosons. Current algebra techniques indicate that in order to relate this model to QCD one has to choose a real condensate for the scalar density, with its sign opposite to current quark masses, and avoid any parity breaking due to a v.e.v. of the pseudoscalar density. The introduction of a chemical potential does not change the phase of the condensate and therefore does not generate any parity breaking. This is just fine because in normal conditions parity breaking does not take place in QCD. The general effective potential of this model is given by

$$
\begin{aligned}
V_{\text{eff}} = \ &\frac{1}{2}\text{Tr}\Bigg\{ -\sum_{j,k=1}^{2} H_j^\dagger \Delta_{jk} H_k + \lambda_1 (H_1^\dagger H_1)^2 + \lambda_2 (H_2^\dagger H_2)^2 + \lambda_3 H_1^\dagger H_1 H_2^\dagger H_2 \\
&+ \frac{1}{2}\lambda_4 (H_1^\dagger H_2 H_1^\dagger H_2 + H_2^\dagger H_1 H_2^\dagger H_1) + \frac{1}{2}\lambda_5 (H_1^\dagger H_2 + H_2^\dagger H_1) H_1^\dagger H_1 \\
&+ \frac{1}{2}\lambda_6 (H_1^\dagger H_2 + H_2^\dagger H_1) H_2^\dagger H_2 \Bigg\} + \mathcal{O}\left(\frac{|H|^6}{\Lambda^2}\right) \quad (2.3)
\end{aligned}
$$

and contains 9 real constants. The neglected terms are suppressed by powers of $\langle H\rangle^2/\Lambda^2$. Indeed, this is a good approximation if one assumes the v.e.v. of H_j to be of the order of the constituent quark mass $\simeq 300$ MeV and the CSB scale $\Lambda \simeq 1.2$ GeV.

In order to guess the order of magnitude of the couplings, it may be useful to consider a particular model. In particular, a quasi-local quark model [100] the general Lagrangian is given by

$$\mathcal{L}_{\text{QQM}} = \bar{q}i\slashed{\partial}q + \sum_{k,l=1}^{2} a_{kl}\left[\bar{q}f_k(s)q\bar{q}f_l(s)q - \bar{q}f_k(s)\tau^a\gamma_5 q\bar{q}f_l(s)\tau^a\gamma_5 q\right], \qquad (2.4)$$

where a_{kl} is a symmetric matrix of real coupling constants and $f_k(s)$ are a set of polinomial form factors depending on $s \equiv -\partial^2/\Lambda^2$, which specify the quasilocal interaction

in momentum space. The polynomial form factors are usually taken to be orthogonal as the results do not depend on a concrete choice in the large-log approximation. For a convenient selection $f_1(s) = 2 - 3s$ and $f_2(s) = -\sqrt{3}s$, the values of the couplings λ_i in (2.3) are fixed for $i = 2, ..., 6$: $\lambda_2 = \frac{9N_c}{32\pi^2}$, $\lambda_3 = \frac{3N_c}{8\pi^2}$, $\lambda_4 = \frac{3N_c}{16\pi^2}$, $\lambda_5 = -\frac{5\sqrt{3}N_c}{8\pi^2}$ and $\lambda_6 = \frac{\sqrt{3}N_c}{8\pi^2}$.

A further simplification may be performed by a (real) rotation the H_j fields when the chemical potential and temperature are zero so that it is sufficient to select $\Delta_{ij} = \Delta\delta_{ij}$ and $\lambda_5 = 0$. The chiral multiplet H_1 is taken to be coupled to the quark fields and the global invariance of the model allows the parametrization

$$H_1(x) = \sigma_1(x)\xi^2(x) = \sigma_1(x)\exp\left(i\frac{\pi_1^a(x)\tau_a}{F_0}\right); \quad H_2(x) = \xi(x)\Big(\sigma_2(x) + i\hat{\pi}_2(x)\Big)\xi(x). \tag{2.5}$$

One could add some more terms to the potential (2.3) that manifestly break parity but in this representation of the doublets, these operators identically vanish. There are also two more operators but they are redundant as they can be expressed as a linear combination of operators with constants λ_3 and λ_4.

The potential (2.3) may exhibit several solutions for σ_1 and σ_2. A necessary and sufficient condition for the absence of SPB is given by

$$(\lambda_3 - \lambda_4)\sigma_1^2 + \lambda_6\sigma_1\sigma_2 + 2\lambda_2\sigma_2^2 > \Delta. \tag{2.6}$$

In absence of SPB, the landscape of parameters shows a maximum of 9 extrema where only two of them at most are minima (see Fig. 2.1). The specific values of the constants determines which one is the true minimum of the theory.
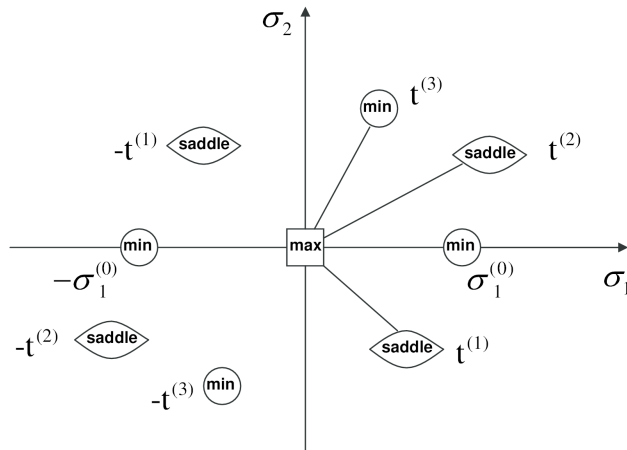
Figure 2.1: Extrema of effective potential in the reduction basis [99]: the maximum is placed in the square, four minima are located in the circles and the corresponding four saddle points are depicted by the lentils. Which one corresponds to the true minimum depends on the actual value of the phenomenological constants.

It is assumed that the scalars under consideration are generated in the quark sector of QCD. The baryon chemical potential μ is transmitted to the meson sector via a local quark-meson coupling

$$\Delta\mathcal{L} = -(\bar{q}_R H_1 q_L + \bar{q}_L H_1^\dagger q_R) \longrightarrow -\bar{q}\sigma_1 q. \tag{2.7}$$

After integrating out the constituent quarks, the temperature and chemical potential dependence are included in the gap equation of σ_1 through the one-loop contribution to the effective potential (2.3), ΔV_{eff}. The saturation point to nuclear matter can be found at finite densities due to the presence of two multiplets, avoiding the chiral restoration that takes place in simpler models with only one multiplet like NJL. This effective potential is normalized to reproduce the baryon density for quark matter

$$\varrho_B = -\frac{1}{3}\partial_\mu \Delta V_{\text{eff}}(\mu) = \frac{N_c N_f}{9\pi^2}p_F^3 = \frac{N_c N_f}{9\pi^2}(\mu^2 - \sigma_1^2)^{3/2}, \tag{2.8}$$

where the quark Fermi momentum is $p_F = \mu^2\sigma_1^2$. Normal nuclear density is $\varrho_B \simeq 0.17$ fm$^3 \simeq (1.8\text{fm})^3$ that corresponds to the average distance 1.8 fm between nucleons in nuclear matter. An accurate description of the condensation point, i.e. the critical density where nuclei become stable requires the introduction [88, 99] of an isosinglet repulsive interaction driven by the ω meson, but this will not be considered here.

A phase with SPB may take place due to condensation of π_2^0 together with non-trivial scalar condensates. A direct relation seems to connect the eventual presence of a SPB phase with the absence of chiral collapse in the model provided that $\Delta > 0$. The transition from the CSB to the SPB phase is found to be possible at zero temperature, and at finite temperature with lower chemical potential. However, this relation strongly depends on the generic parameters of the model. In addition to the breaking of chiral symmetry that converts the triplet of light pions in massless Goldstone bosons, spontaneous condensation in the isotriplet channel breaks the isospin symmetry $SU(2)_V$ down to $U(1)$ and two charged excited π' mesons are expected to be massless throughout this phase while the neutral state becomes massless only at the very transition phase. Notice that convexity around the minimum of the potential (2.3) implies that all diagonal elements are non-negative. This gives positive masses for two scalar and one pseudoscalar mesons, whereas the triplet of pions and charged doublet of π' mesons remain massless. In Fig. 2.2 this behaviour is displayed.

Once fixed the interaction to quark matter is fixed, there is no freedom in the choice of the kinetic term for scalar fields. Namely one cannot rotate two fields and rescale the doublet H_1 without changes in the chemical potential driver through ΔV_{eff}. However the rescaling of H_2 is possible at the expense of an appropriate redefinition of other coupling constants and this freedom can be used to fix one of the constants which appear in the kinetic term. Thus the general kinetic term symmetric under $SU(2)_L \times SU(2)_R$ global reads

$$\mathcal{L}_{\text{kin}} = \frac{1}{4}\sum_{j,k=1}^{2} A_{jk}\text{Tr}\left\{\partial_\mu H_j^\dagger \partial^\mu H_k\right\}. \tag{2.9}$$
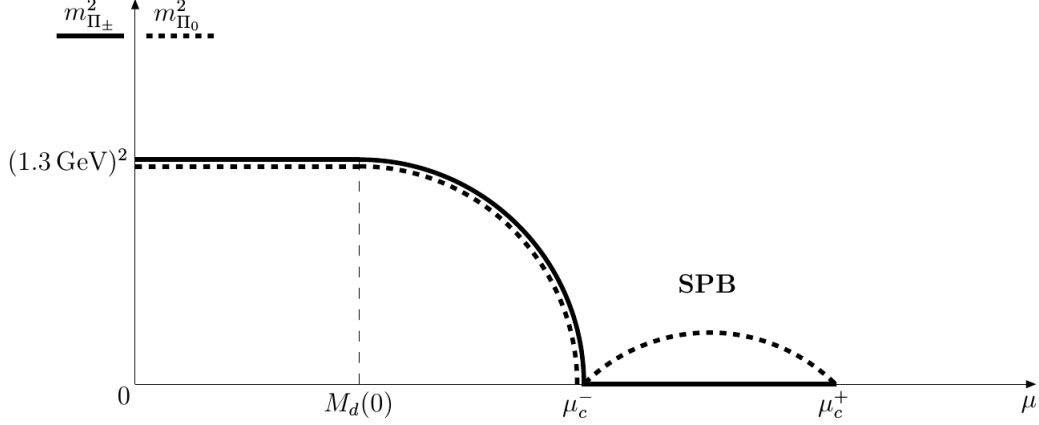
Figure 2.2: Qualitative behaviour of excited pions depending on the quark chemical potential μ when the SPB phase is entered [101]. $M_d(0)$ is the constituent quark mass at zero μ. Charged pions become massless in the SPB phase while the neutral component only aquires zero mass at the very transition point.

In general, π_1 and π_2 are mixed and their diagonalization leads to the physical mass states π and Π. By means of the parametrization (2.5), the mass of the heavy pion triplet in the parity-even phase can be written as

$$m_\Pi^2 = \frac{-\Delta + (\lambda_3 - \lambda_4)\sigma_1^2 + \lambda_6\sigma_1\sigma_2 + 2\lambda_2\sigma_2^2}{A_{22} - \zeta^2}, \tag{2.10}$$

with

$$F_0^2 = \sum_{j,k=1}^{2} A_{jk}\sigma_j\sigma_k, \quad \zeta \equiv \frac{1}{F_0}\sum_{j=1}^{2} A_{j2}\sigma_j. \tag{2.11}$$

In the SPB phase, the expected mixing among scalar and pseudoscalar states is explicit in the kinetic term, where the notation $\langle\pi_2^0\rangle = \rho$ is used. This kinetic term has the following form

$$\mathcal{L}_{\text{kin}} = \partial_\mu\pi^\pm\partial^\mu\pi^\mp + \frac{1}{2}\left(1 + \frac{A_{22}\rho^2}{F_0^2}\right)\partial_\mu\pi^0\partial^\mu\pi^0 + (A_{22} - \zeta^2)\partial_\mu\Pi^\pm\partial^\mu\Pi^\mp$$

$$+ \frac{1}{2}\left(A_{22} - \frac{F_0^2}{F_0^2 + A_{22}\rho^2}\zeta^2\right)\partial_\mu\Pi^0\partial^\mu\Pi^0 \tag{2.12}$$

$$+ \frac{1}{2}\sum_{j,k=1}^{2}\frac{A_{jk}F_0^2 + \rho^2\det(A)\delta_{1j}\delta_{1k}}{F_0^2 + A_{22}\rho^2}\partial_\mu\Sigma_j\partial^\mu\Sigma_k - \frac{F_0\rho}{F_0^2 + A_{22}\rho^2}\zeta\partial_\mu\Pi^0\sum_{j=1}^{2}A_{j2}\partial^\mu\Sigma_j.$$

It is interesting to note that even in the massless pion sector the isospin breaking occurs: neutral pions become less stable with a larger decay constant. Furthermore, in the charged meson sector the relationship between massless π and Π remain the same as in the symmetric phase. If a small quark mass is considered without an explicit isospin

breaking, one finds two massless charged pions $\pi^{\pm}$ and three light pseudoscalars $\pi^0, \Pi^{\pm}$ with masses linear in the current quark mass.

A relevant example to be examined corresponds to models with residual discrete chiral symmetry $Z_2 \times Z_2$ after the breaking of $SU(2)_L \times SU(2)_R \rightarrow SU(2)_V$. This extra symmetry is related to the independent reflections $H_j \rightarrow -H_j$. This subset of particular models requires $\lambda_5 = \lambda_6 = A_{12} = 0$ but $\lambda_4 \neq 0$. One can always fix $A_1 = A_2$ redefining the other parameters. The gap equations and stability conditions are significantly simplified allowing to get a feeling of the possible scales involved in the system. A few plausible assumptions such as $F_0 = 100$ MeV and a constituent quark mass $M_d = \sigma_1 = 300$ MeV allow to get an insight into this model obtaining a reasonable mass spectrum in the parity-even phase provided that $\Delta \simeq 2.7 F_0^2$, $\lambda_1 \simeq 0.15$ and $\lambda_4 \simeq 0.35$. With these values and taking $M_{d,\text{crit}} \simeq 1.8 F_0$, one finds that SPB occurs at dense nuclear matter with a typical density $\varrho_{B,\text{crit}} \simeq 0.5$ fm$^{-3} \simeq 3 \varrho_{B,\text{nuclear}}$. Thus the possibility of SPB emerges naturally for reasonable values of the meson physics parameters and low-energy constants.

The parity-breaking effect triggered by an isotriplet pseudoscalar condensation has some characteristic footprints that could eventually lead to the detection of this phase. The isospin breaking could affect the heavy pion decay constant as shown in Eq. (2.12) enhancing their electroweak decays. Higher-mass meson resonances (radial excitations) do not have a definite parity and therefore the same resonance can decay both in two and three pions (in general into even and odd number of pions). As already mentioned, at the very point of the phase transition leading to parity breaking one has six massless pion-like states. After crossing the phase transition, in the parity broken phase, the massless charged Π remain as Goldstone bosons enhancing charged pion production, whereas the additional neutral pseudoscalar state becomes massive. Finally, a reinforcement of long-range correlations in the pseudoscalar channel could be hunted in lattice simulations.

Despite dealing with a simple model, the feature of parity breaking could be a rather generic feature of QCD at finite density. A rigorous proof does not exist in QCD yet due to the difficulties of dealing with non-vanishing chemical potentials in the lattice [102]. A vector chemical potential in gauge theories like QCD cannot be easily treated and therefore simpler models hopefully reproducing the main features of the theory may be useful. Needless to say, non-equilibrium effects are also notoriously difficult to study non-perturbatively. In spite of this, the conclusions of the analysis in [88] seem rather robust: there is a range of densities where a parity violating vacuum is energetically favourable.

Such a parity-violating state could be produced in HIC in conditions which are expected at the FAIR facility or at the planned NICA accelerator. An illustrative simulation for the time evolution of the medium density in central and semicentral collisions is presented in Fig. 2.3 based on a particular transport code [103]. In the center-of-mass frame of the colliding ions the density fastly increases in the pre-equilibrium stages and then slowly decreases eventually entering in the hadron phase. Once entered this phase,
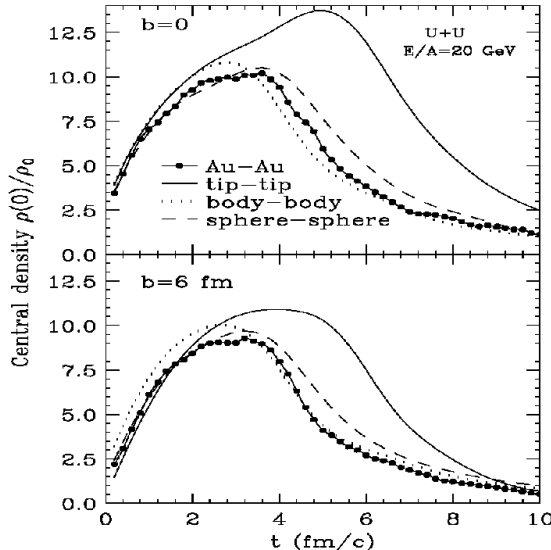
Figure 2.3: Central density as a function of time for central Au+Au collisions (dotted line) and tip-on-tip U+U collisions (solid line) at 20A GeV as calculated with the ART transport code [103] (upper plot). Same for semi-central collisions (b=6 fm) (lower plot).

the decreasing density suggests a time-dependent neutral pion condensate (if any) with a relatively smooth time dependence. The latter just produces a modification of quantum electrodynamics (QED) via parity-breaking term $\sim \langle \Pi(t) \rangle F_{\mu\nu} \widetilde{F}^{\mu\nu}$ that describes the neutral pion decay into two photons. If we assume that $\langle \Pi(t) \rangle \propto t$ the presence of pion condensation distorts the photon spectrum and its two transversal (circular) polarizations obtain different masses [104]. One of them becomes massive and growing with the photon 3-momentum and the other one appears as a tachyon. It is remarkable that the generation of photon mass is also predicted in the presence of a neutral pion condensate [105]. As a result, photons with momenta $|\vec{k}| > 4m_\ell^2/\eta$ start to decay into lepton pairs $\gamma \to \ell^+ \ell^-$, with $\eta \sim \alpha \langle \dot{\Pi} \rangle / f_\pi$. A hierarchy of thresholds appears for different leptons, mostly electrons and muons. The decay width $\sim \alpha\eta$ is suppressed by the fine structure constant α but may be considerably enhanced if the pion condensate derivative η rapidly changes.

However, this scenario is not completely accurate as it is known that vector mesons mix with photons and the calculation of dilepton rates only from photons is a crude approximation at low energies. We will investigate this effect in detail in Chapter 5.

2.2 Topological fluctuations as a source for parity breaking

A remarkable feature of gauge theories like QCD is the existence of topologically non-trivial configurations of gauge fields [106], the so-called instantons. They correspond

to a connection of different degenerate vacua which are related by topologically non-trivial gauge transformations. The amplitudes of such transitions vanish order by order in perturbation theory and therefore they are associated to non-perturbative phenomena. Typical calculations of quantum tunnelling between states with diferent topology suggested that these transitions were suppressed by factors of the order of $\exp(-2\pi/\alpha)$, where α is the interaction strength of the gauge theory.

At high temperature the suppression factor disappears [107] since there is enough energy to pass over the potential barrier that separates the topological inequivalent vacua. This phenomenon is called a sphaleron transition [108] and it could be responsible for the appearance of metastable domains where the QCD vacuum breaks P and CP [63] in the vicinity of the deconfinement phase transition. P-even, but CP-odd metastable states have also been argued to exist in hot gauge theories [109]. Several dynamical scenarios for the decay of P-odd bubbles have been considered [94], and numerical lattice calculations of the fluctuations of topological charge in classical Yang-Mills fields have been performed [32, 110, 111, 112]. Progress in understanding the vacuum structure of gauge theories, especially supersymmetric ones [113], also points to the possible existence of P- and CP-odd vacuum states. A parity broken phase also exists in lattice QCD with Wilson fermions [114], but this phenomenon has been recognized as a lattice artifact.

The experimental study of metastable P and CP-odd domains at LHC or RHIC provides a unique link to the QCD phase transition in the early universe when probably $\theta \neq 0$. Such a large CP violation during the QCD phase transition might have lead to a separation of matter and anti-matter. Current experiments show that the very tiny amount of CP violation from the electroweak part of SM is probably not sufficient to explain the baryon number density observed today.

As it is well known, QCD with massless quarks shows an exact chiral $SU(2)_L \times SU(2)_R$ symmetry. However, the $U(1)_A$ symmetry is not satisfied at the quantum level leading to the axial anomaly. As a result, the colour- and iso-singlet axial current $J_{5,\mu} = \bar{q}\gamma_\mu\gamma_5 q$ is no longer conserved despite considering massless quarks. The local partial conservation of the axial current (PCAC) relation is afflicted with the gluon anomaly (for N_f flavours)

$$\partial^\mu J_{5,\mu} - 2i\bar{q}\hat{m}_q\gamma_5 q = \frac{N_f g^2}{8\pi^2}\mathrm{Tr}\left(G^{\mu\nu}\widetilde{G}_{\mu\nu}\right), \qquad (2.13)$$

where $\hat{m}_q$ is the quark mass matrix and $\widetilde{G}_{\mu\nu} \equiv \frac{1}{2}\varepsilon_{\mu\nu\rho\sigma}G^{\rho\sigma}$ with $\varepsilon_{0123} = -\varepsilon^{0123} = +1$. Here g denotes the QCD coupling constant with generators normalized as $\mathrm{Tr}(t_a t_b) = \delta_{ab}/2$. The term at the r.h.s. of Eq. (2.13) can be expressed as a total derivative of the Bardeen current K^μ

$$K_\mu = \frac{g^2}{2}\epsilon_{\mu\nu\rho\sigma}\mathrm{Tr}\left(G^\nu\partial^\rho G^\sigma - i\frac{2}{3}g G^\nu G^\rho G^\sigma\right), \qquad \partial_\mu K^\mu = \frac{g^2}{4}\mathrm{Tr}\left(G^{\mu\nu}\widetilde{G}_{\mu\nu}\right). \quad (2.14)$$

2. A NEW PHASE OF QCD WITH PARITY VIOLATION

As already mentioned in the previous section, including the vacuum structure is equivalent to adding a new θ-term in the QCD Lagrangian

$$\Delta\mathcal{L}_\theta = \theta \frac{g^2}{16\pi^2} \mathrm{Tr}\left(G^{\mu\nu}\widetilde{G}_{\mu\nu}\right), \qquad (2.15)$$

where unless θ vanishes, parity is violated. Discarding a total derivative from the QCD Lagrangian seems legitimate in case of an homogeneous in space and time $\theta \neq 0$. However, local dependences may trigger local parity breaking (LPB) in the small domains quoted by [63]. Gauge field configurations can be characterised by an integer topological (invariant) charge T_5 (equivalent to the winding number with this normalization) given by

$$T_5 = \frac{g^2}{16\pi^2} \int_{t_i}^{t_f} dt \int_{\mathrm{vol.}} d^3x \, \mathrm{Tr}\left(G^{\mu\nu}\widetilde{G}_{\mu\nu}\right) \in \mathbb{Z}, \qquad (2.16)$$

where the integration limits explicitly reflect that a finite volume is considered[1]. The integration over a finite space volume of the PCAC in Eq. (2.13) allows to associate a non-zero topological charge with a non-trivial quark axial charge Q_5^q

$$\frac{d}{dt}(Q_5^q - 2N_f T_5) \simeq 2i \int_{\mathrm{vol.}} d^3x \, \bar{q}\hat{m}_q \gamma_5 q \,, \quad Q_5^q = \int_{\mathrm{vol.}} d^3x \, \bar{q}\gamma_0\gamma_5 q. \qquad (2.17)$$

Perturbative interactions between quarks and gluons cannot induce a difference between the number of right- and left-handed quarks. A mass term always will tend to wash out such difference [115]. For massless quarks a topological charge induces a net chirality in a finite volume.

It was pointed out that the presence of non-zero angular momentum in peripheral HIC may trigger a charge separation in P- and CP- odd domains [63]. In such collisions, an induced electric field perpendicular to the reaction plane was found to appear of order $E \sim -(e\,\theta/2\pi)\,l$, where $l \sim b$ is the angular momentum in a collision at impact parameter b. Another way to understand this effect comes from considering the angular momentum of a peripheral collision as an equivalent magnetic field orthogonal to the reaction plane. The θ-term can be written as $L_\theta \sim \theta \vec{E}\vec{B}$ so a coupling between the electric and magnetic fields arises. At non-trivial θ angle, a magnetic field induces a parallel electric field $\vec{E} \sim \theta\vec{B}$ through the axial anomaly and a corresponding electric dipole moment.

A further explanation for this charge separation in peripheral HIC can be provided. In a domain with a non-trivial topological charge and massless quarks, it was proved from Eq. (2.17) that an imbalance of the left- and right-handed quarks arises, which is

---

[1]The topological current flux through the boundary is normally neglected. Then, the following definition of T_5 is also used

$$T_5 = \frac{1}{4\pi^2} \int_{t_i}^{t_f} dt \int_{\mathrm{vol.}} d^3x \, \partial_0 K^0 = \frac{1}{4\pi^2} \int_{\mathrm{vol.}} d^3x \, \left[K^0(\vec{x}, t_f) - K^0(\vec{x}, t_i)\right].$$

translated into a net helicity. If an electrodynamic magnetic field is applied, positively charged quarks will orient their spin along the direction of the magnetic field due to the magnetic moment interaction. Likewise, negatively charged quarks will orient in the opposite direction. Since a net helicity is conserved in the domain, the quark spins will preferentially orientate in the direction of their momenta. Therefore, positively charged quarks will move in the direction of the magnetic field, and negatively charged ones will move opposite to it. A resulting electromagnetic current will set up in the direction of the magnetic field. Due to this conception, the charge separation induced by an angular momentum or magnetic field in a small domain characterised with a non-trivial topological charge was called the Chiral Magnetic Effect (CME). For a review of this and other related 'environmental symmetry violations' in heavy ion collisions, see [116].

The CME could be used to determine whether a deconfined chirally symmetric phase of matter is created in HIC. Deconfinement is a necessary requirement for this effect to work since it requires that quarks can separate over distances much greater than the radius of the nucleon. Moreover, chiral symmetry restoration is essential, because a chiral condensate will tend to erase any asymmetry between the number of right- and left-handed fermions.

An experimental observable measuring the CME charge separation with respect to the reaction plane was proposed shortly afterwards [117]. More recently, it has been claimed that this signal is observed in the STAR experiment at RHIC [62] (see Fig. 1.4), although the issue still remains controversial. The effect should be most visible for ultra-peripheral HIC where large angular momenta induce large magnetic fields contributing to the axial charge separation.

2.3 Quasi-equilibrium treatment of a conserved quark axial charge

We already mentioned that the two parity-violating operators presented in Eq.(2.1) can be related by a $U(1)_A$ transformation. Indeed, due to the axial anomaly (2.13) the θ-term in Eq. (2.15) can be transformed into

$$\frac{1}{2N_f}\partial_\mu\theta\bar{\psi}\gamma^\mu\gamma^5\psi. \tag{2.18}$$

For massless quarks, QCD with a topological charge $\langle T_5 \rangle \neq 0$ can be equally described at the Lagrangian level by a conserved topological chemical potential μ_θ or by an axial chemical potential μ_5 [63, 112, 118]. Their relation arises from (2.17)

$$\langle T_5 \rangle = \frac{1}{2N_f}\langle Q_5^q \rangle \quad \Longleftrightarrow \quad \mu_5 = \frac{1}{2N_f}\mu_\theta. \tag{2.19}$$

This quasi-equilibrium situation can be treated simply adding to the QCD Lagrangian $\Delta\mathcal{L}_{\text{top}} = \mu_\theta T_5$ or, alternatively, $\Delta\mathcal{L}_q = \mu_5 Q_5^q$. The latter realization together with Eq.

(2.18) allows to identify

$$\mu_5 = \frac{1}{2N_f} \partial_0 \theta \quad \Longrightarrow \quad \mu_\theta = \partial_0 \theta. \tag{2.20}$$

Thus we assume that a time dependent but approximately spatially homogeneous pseudoscalar axion-like background is induced at the energy densities reached in HIC with $\partial_\mu \theta(x) \sim (\mu_5, 0, 0, 0)$. We could refer the reader to [104] where it has been shown that a pseudoscalar field slowly evolving in time drastically changes the electromagnetic properties of the vacuum. In particular a photon propagating in this background with sufficiently high energy may decay on shell in medium into dileptons.

For massive light quarks the axial charge is conserved provided that the quark mass term breaking chiral symmetry remains subdominant. The characteristic oscillation time is governed by inverse quark masses. Evidently for u, d quarks the characteristic time $1/\hat{m}_q \sim 1/5 \text{ MeV}^{-1} \sim 40$ fm is much bigger than the fireball lifetime ($\tau_{\text{fireball}} \simeq 5 - 10$ fm) and the left-right quark mixing can be neglected. But it is not the case for strange quarks as $1/m_s \sim 1/150 \text{ MeV}^{-1} \sim 1$ fm $\ll \tau_{\text{fireball}}$ and even if a topological charge persists during the fireball lifetime, the mean value of the strange quark axial charge is around zero due to left-right oscillations.

When nuclear matter is superdense, pseudoscalar condensation in the $I = 1$ channel may occur too, as it has been outlined in the previous section 2.1. This situation corresponds to introducing a vector chemical potential μ. Thus for light quarks in hot and dense nuclear matter, the matrix structure of the axial chemical potential μ_5 in flavour space generically includes not only $SU(3)_f$ singlet but also neutral components of $SU(3)_f$ octet, that corresponds to including both a μ_5 and a μ term, respectively. Note that the appearance of a condensate in the τ_3 direction implies in addition a breaking of the isospin symmetry of the vacuum.

This thesis is mostly concerned with the possibility of LPB associated to the appearance of an isosinglet axial chemical potential. This case is expected to be the dominant one in experiments where the temperature in the nuclear fireball is much larger than the chemical potential $T \gg \mu$, as it is the case for the LHC or RHIC. The issue of isotriplet condensation induced by finite density[2] will not be discussed in this approach. This scenario corresponds to the region where $\mu \gg T$ that will be explored in future experiments at FAIR and NICA. Although we will work with an isosinglet μ_5 throughout, some indications will be provided along the text for the case that one could be interested in selecting an isotriplet pseudoscalar condensate.

Unlike the case of having a dense system with a non-trivial μ, an axial chemical potential is tractable on the lattice [119] and with other methods [120]. For central collisions and light quarks, local topological fluctuations may correspond to the existence of an ephemeral phase characterised by LPB with non-trivial axial chemical potential. In Fig. 2.4, the phase diagram of QCD is showed depending on the temperature and

---

[2]Finite density may contribute to isosinglet pseudoscalar condensation too.

the baryon density. The hypothetical location of the LPB phase is displayed suggesting that this phenomenon may be important in heavy ion experiments where the produced system is very hot but not specially dense. We conjecture that the CME and topological fluctuations may be complementary effects revealing two facets associated to the formation of a thermodynamic phase where parity is locally broken. The red lines in the graphic show the compression and later expansion of the system.

The treatment of μ_5 is a non-trivial task due to the complex dynamics of HIC. During the first stages of the collision, nuclear matter is quickly compressed and heated with a very short thermalization time $\tau_{\text{heating}} < 0.5$ fm (attempts to explain this process in holographic QCD can be found in [121]) and it may enter the LPB phase. After reaching the QGP, the system slowly expands and cools down reentering the LPB phase where large topological fluctuations may take place. Of course, the cooling time greatly exceeds the time taken for the LPB phase to form so most of the expected effects should come from this latter period. At this stage the nuclear matter cools down (for the fireball lifetime) until freeze-out. During this period the topological charge is supposedly conserved and the system may reach thermal equilibrium. The effect of having a non-trivial axial charge could trigger the main phenomenological effects that are discussed all along this thesis. It is not clear that the value of the axial chemical potential is uniform but we shall assume so here and consider an average μ_5 which has to be understood as an effective value extracted from such dynamics.
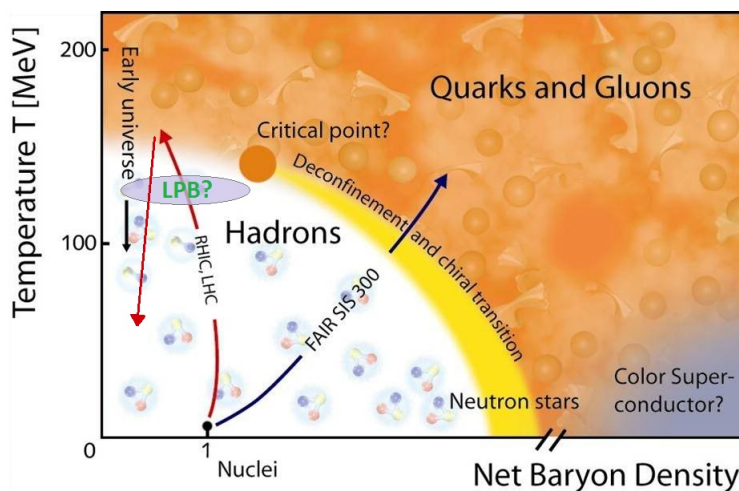
Figure 2.4: QCD phase diagram depending on the temperature and the baryon density where the approximate situation of the hypothetical LPB phase is showed. For rather hot (but not dense) HIC, the system may enter this phase and remain there for a time similar to the nuclear fireball lifetime $\tau_{\text{fireball}} \simeq 5 - 10$ fm.

If this new thermodynamic phase really exists, experiments should be able to encounter it. By means of both a vector and an axial chemical potential, we describe how the symmetry breaking mechanism works from the theoretical point of view and

its implications. Finding observables that could be measured at the mentioned experiments constitutes one of the main goals of our research. This is a field in between high energy physics, nuclear physics and lattice numerical studies, and one where theory and experiment still work close together.

Chapter 3

Parity breaking in the Nambu–Jona-Lasinio model

As already discussed, QCD with a vector chemical potential presents serious difficulties to be treated. Therefore, the study a simpler model reproducing the main symmetries of the QCD may provide some qualitative and quantitative ideas that could help in a further understanding of strong interactions.

In the present chapter we shall consider the Nambu–Jona-Lasinio model (NJL) [122, 123, 124, 125, 126], which shares interesting features with QCD. Although it may be implemented with an exact chiral symmetry with massless quarks, this symmetry is spontaneously broken due to the formation of a dynamical chiral (quark) condensate. Such phenomenon inspired many theories of the breaking of electroweak symmetry such as technicolor.

In the NJL modelization, QCD gluon interactions among quarks are assumed to be replaced by some effective four-fermion couplings. The appearance of these dimension 6 operators makes the model a non-renormalizable effective theory valid up to some physical scale Λ. The absence of gluons permits the model to be bosonised, replacing the 4-fermion couplings by composed degrees of freedom that are normally associated with light mesons such as σ and pions.

Confinement is absent in the NJL model, but global symmetries can be arranged to be identical in both QCD and NJL. When the chiral condensate forms, the chiral symmetry is spontaneously broken into a diagonal subgroup $SU(2)_V$ since the condensate leads to a pairing of the left-handed and the right-handed flavours. The broken symmetries lead to massless pseudoscalar bosons which are the associated Goldstone bosons, in this case, pions.

The NJL model has been used recently by some authors [127] to investigate the nature of the Aoki phase in QCD [114]. This is a phase in lattice QCD with Wilson fermions where parity and possibly isospin symmetry is broken. It does not survive the continuum (note that the NJL does not have a 'continuum limit' either). It is however conceivable that the introduction of the chemical potential may enlarge the scope of

the Aoki phase and allow for a sensible continuum interpretation. This is what should happen if the effective theory analysis described in [88] is correct.

Previously some authors have studied the effect of a vector chemical potential μ with three flavours [128] in the NJL model for a study the nonet meson characteristics. An analysis of the QCD phase diagram at finite temperature including an axial chemical potential μ_5 has also been considered by several groups [120]. Nevertheless, the consequences of including both a vector and an axial chemical potentials have not been considered so far to our knowledge.

In this work NJL constitutes a toy model for the implementation of parity-breaking effects. With the help of both a vector and an axial chemical potentials, we shall investigate the phase diagram of the model with special interest in the appearance of possible pseudoscalar condensates leading to spontaneous breaking of parity. It turns out that the inclusion of μ_5 changes radically the phase structure of the model and shows that μ is not a key player in ushering a thermodynamically stable phase where parity is violated in the NJL model, but μ_5 is. The introduction of μ_5 constitutes an explicit source for parity violation. However, a spontaneous breaking of this symmetry points towards a region where pseudoscalar condensation may be thermodynamically stable. The characteristic values of the external drivers allowing for this possible new stable phase may provide some hints on the realistic values of such magnitudes reached in HIC.

However, NJL is definitely not QCD and the present work does not attempt to draw definite conclusions on the latter theory; just to point out possible phases requiring further analysis.

This chapter is organized as follows. In Sec. 3.1 the NJL Lagrangian with the incorporation of μ and μ_5 will be introduced. We describe how an effective potential is extracted when one introduces some effective light meson states and integrates out the fermion degrees of freedom. In Sec. 3.2 we show the gap equations of the model and the conditions for their stability. After that, the different stable phases of this model are presented and discussed. We show in Sec. 3.3 that a phase with an isospin singlet pseudoscalar condensate in addition to a scalar condensate is possible. It turns out that the conditions for this phase to be stable and exhibit chiral symmetry breaking too are such that one gets an inverted mass spectrum with $m_\pi > m_{\eta_q}$ and $m_\sigma > m_{a_0}$, which is quite different from QCD. In Sec. 3.3 we also present the main results of this work with plots of the evolution of the scalar and pseudoscalar condensates together with the main features of the phase transition.

3.1   Nambu–Jona-Lasinio Lagrangian with μ and μ_5

The starting point of this chapter is the NJL Lagrangian where we incorporate a vector and an axial chemical potentials μ and μ_5, respectively. For two flavours and N colours,

we have [123]

$$\mathcal{L} = \bar{\psi}(\slashed{\partial}+m-\mu\gamma_0-\mu_5\gamma_0\gamma_5)\psi-\frac{G_1}{N}[(\bar{\psi}\psi)^2+(\bar{\psi}i\gamma_5\vec{\tau}\psi)^2]-\frac{G_2}{N}[(\bar{\psi}\vec{\tau}\psi)^2+(\bar{\psi}i\gamma_5\psi)^2], \quad (3.1)$$

with a full $U(2)_L \times U(2)_R$ chiral invariance in the case that $G_1 = G_2$, while if these constants differ, the $U(1)_A$ symmetry breaks and only $SU(2)_L \times SU(2)_R \times U(1)_V$ remains. In the case of an isotriplet axial chemical potential would appear attached to the quark bilinear $\bar{\psi}\gamma_0\gamma_5\tau^3$. One may introduce two doublets of bosonic degrees of freedom $\{\sigma, \vec{\pi}\}$ and $\{\eta, \vec{a}\}$ by adding the following chiral invariant term

$$\Delta\mathcal{L} = \frac{Ng_1^2}{4G_1}(\sigma^2 + \vec{\pi}^2) + \frac{Ng_2^2}{4G_2}(\eta^2 + \vec{a}^2). \quad (3.2)$$

These would be identified with their namesake QCD states (actually η_q and $\vec{a}_0$ for the last two). Euclidean conventions will be used throughout this chapter. We bosonize the model following the same procedure as in [124].

After shifting each bosonic field with the quark bilinear operator that carries the corresponding quantum numbers

$$\sigma \to \sigma + \frac{2G_1}{Ng_1}\bar{\psi}\psi, \qquad \vec{\pi} \to \vec{\pi} + \frac{2G_1}{Ng_1}\bar{\psi}i\gamma_5\vec{\tau}\psi,$$

$$\eta \to \eta + \frac{2G_2}{Ng_2}\bar{\psi}i\gamma_5\psi, \qquad \vec{a}_0 \to \vec{a}_0 + \frac{2G_2}{Ng_2}\bar{\psi}\vec{\tau}\psi, \quad (3.3)$$

the Lagrangian (3.1) may be rewritten as

$$\mathcal{L} = \bar{\psi}[\slashed{\partial}+m - \mu\gamma_0 - \mu_5\gamma_0\gamma_5 + g_1(\sigma + i\gamma_5\vec{\tau}\vec{\pi}) + g_2(i\gamma_5\eta + \vec{\tau}\vec{a})]\psi$$

$$+ \frac{Ng_1^2}{4G_1}(\sigma^2 + \vec{\pi}^2) + \frac{Ng_2^2}{4G_2}(\eta^2 + \vec{a}^2), \quad (3.4)$$

which shows a redundancy related to the coupling constants $g_{1,2}$ that appear attached to each doublet and it is eventually related to their wave function normalization. In other words, these coefficients will be absorbed in the fields once they are renormalised $g_1\sigma \to \sigma^r$. Without further ado we will take $g_1 = g_2 = 1$.

Integration of the fermions will produce a bosonic effective potential (or free energy) and will allow to study the different phases of the model. We will work in the mean field approximation and accordingly neglect fluctuations. The results will be exact in the large N limit.

$$V_{\text{eff}} = \frac{N}{4G_1}(\sigma^2 + \vec{\pi}^2) + \frac{N}{4G_2}(\eta^2 + \vec{a}^2) - \text{Tr}\log\mathcal{M}(\mu, \mu_5), \quad (3.5)$$

where the trace is understood to be performed in the isospin and Dirac spaces in addition to a 4-momentum integration of the operator in the momentum space. We will assume that $\mu > 0$, namely we consider a baryon (as opposed to antibaryon) finite

density. The invariance under CP of the action ensures that the free energy (3.5) only depends on the modulus of μ.

We also define the fermion operator

$$\mathcal{M}(\mu, \mu_5) = \slashed{\partial} + (M + \vec{\tau}\vec{a}) - \mu\gamma_0 - \mu_5\gamma_0\gamma_5 + i\gamma_5(\vec{\tau}\vec{\pi} + \eta), \tag{3.6}$$

with the introduction of a constituent quark mass $M \equiv m + \sigma$.

In appendix A we show that the dependence on both vector and axial chemical potentials does not change the reality of the fermion determinant. However, its sign remains undetermined, and in order to ensure a positive determinant, we shall consider an even number of 'colours'[1] N so that one can safely assume

$$\det[\mathcal{M}(\mu, \mu_5)] = \sqrt{\det[\mathcal{M}(\mu, \mu_5)]^2} \tag{3.7}$$

and hence, use the calculations in Appendix A. If we just retain the neutral components of the triplets, this determinant can be written in the following way

$$\begin{aligned}
\log \det \mathcal{M}(\mu, \mu_5) =& \operatorname{Tr} \log \mathcal{M}(\mu, \mu_5) \\
=& \frac{1}{8} \operatorname{Tr} \sum_{\pm} \left\{ \log\left[-(ik_0 + \mu)^2 + (|\vec{k}| \pm \mu_5)^2 + M_+^2 \right] \right. \\
& \left. + \log\left[-(ik_0 + \mu)^2 + (|\vec{k}| \pm \mu_5)^2 + M_-^2 \right] \right\},
\end{aligned} \tag{3.8}$$

where

$$M_\pm^2 \equiv (M \pm a)^2 + (\eta \pm \Pi)^2 \tag{3.9}$$

and

$$\operatorname{Tr}(1) = 8NT \sum_n \int \frac{d^3\vec{k}}{(2\pi)^3} \left[k_0 \to \omega_n^F = \frac{(2n+1)\pi}{\beta} \right]. \tag{3.10}$$

From now on, when we refer to the neutral pion condensate, we will write Π. Note that, as explained in appendix A, one is able to write the determinant as the trace of an operator that is the identity in flavour space in spite of the initial non-trivial flavour structure. This facilitates enormously the calculations.

In the search for stable configurations in the potential (3.5) we will need the derivatives of the fermion determinant, which are basically given by the function K_1 that we define as

$$4NK_1 = \operatorname{Tr} \sum_{\pm} \frac{1}{(ik_0 + \mu)^2 - [(|\vec{k}| \pm \mu_5)^2 + M^2]}, \tag{3.11}$$

---

[1]The choice of an even number of colours, unlike QCD, is simply a technical restriction to ensure the fermion determinant to be positive definite.

which is clearly divergent in the UV. We will deal with the NJL model using dimensional regularization (DR) and a 3-momentum cut-off (Λ) both at zero temperature [129, 130]. The function K_1 depending on the regulator can be written as follows

$$
\begin{aligned}
K_1^{\mathrm{DR}}(M, \mu, \mu_5) = & \frac{1}{2\pi^2} \left[\Theta(\mu - M) \left\{ \mu\sqrt{\mu^2 - M^2} + (2\mu_5^2 - M^2) \log\left(\frac{\mu + \sqrt{\mu^2 - M^2}}{M} \right) \right\} \right. \\
& \left. - \frac{1}{2}M^2 + \frac{1}{2}(M^2 - 2\mu_5^2) \left(\frac{1}{\epsilon} - \gamma_E + 2 - \log\frac{M^2}{4\pi\mu_R^2} \right) \right],
\end{aligned}
\tag{3.12}
$$

$$
\begin{aligned}
K_1^{\Lambda}(M, \mu, \mu_5) = & \frac{1}{2\pi^2} \left[\Theta(\mu - M) \left\{ \mu\sqrt{\mu^2 - M^2} + (2\mu_5^2 - M^2) \log\left(\frac{\mu + \sqrt{\mu^2 - M^2}}{M} \right) \right\} \right. \\
& \left. - \frac{1}{2}M^2 + \frac{1}{2}(M^2 - 2\mu_5^2) \log\frac{4\Lambda^2}{M^2} - \Lambda^2 \right].
\end{aligned}
\tag{3.13}
$$

The quadratically divergent term in the cut-off regularization can be reabsorbed in the couplings $G_{1,2}$. After the redefinition, the two results are then identical if we identify

$$
\frac{1}{\epsilon} - \gamma_E + 2 \;\longleftrightarrow\; \log\frac{\Lambda^2}{\pi\mu_R^2}.
\tag{3.14}
$$

However in both cases the logarithmic divergence cannot be absorbed [131] unless we include extra terms in the Lagrangian like $(\partial\sigma)^2$ and σ^4. This is of course a manifestation of the non-renormalizability of the model. For this reason, we shall assume the scale Λ (or equivalently μ_R) to represent a physical cut-off and write

$$
\begin{aligned}
K_1(M, \mu, \mu_5) = & \frac{1}{2\pi^2} \left[\Theta(\mu - M) \left\{ \mu\sqrt{\mu^2 - M^2} + (2\mu_5^2 - M^2) \log\left(\frac{\mu + \sqrt{\mu^2 - M^2}}{M} \right) \right\} \right. \\
& \left. - \frac{M^2}{2} + (M^2 - 2\mu_5^2) \log\frac{2\Lambda}{M} \right].
\end{aligned}
\tag{3.15}
$$

Note that K_1 increases with μ and decreases with μ_5. The derivative of this function will also be used

$$
\begin{aligned}
L_1(M, \mu, \mu_5) \equiv & \frac{1}{M}\frac{\partial K_1}{\partial M} = -\frac{1}{\pi^2} \left[\Theta(\mu - M) \left\{ \frac{\mu\mu_5^2}{M^2\sqrt{\mu^2 - M^2}} + \log\left(\frac{\mu + \sqrt{\mu^2 - M^2}}{M} \right) \right\} \right. \\
& \left. + 1 - \frac{\mu_5^2}{M^2} - \log\frac{2\Lambda}{M} \right].
\end{aligned}
\tag{3.16}
$$

It verifies the property $L_1(\mu_5 = 0) > 0$.

3.2 Search for stable vacuum configurations

We will now explore the different phases that are allowed by the effective potential (3.5) by solving the gap equations and analysing the second derivatives to investigate the stable configurations of the different scalar and pseudoscalar condensates. The gap equations for the system read

$$\frac{\sigma}{2G_1} + \sum_{\pm}(M \pm a)K_1^{\pm} = 0, \qquad \frac{\eta}{2G_2} + \sum_{\pm}(\eta \pm \Pi)K_1^{\pm} = 0$$

$$\frac{\Pi}{2G_1} + \sum_{\pm}\pm(\eta \pm \Pi)K_1^{\pm} = 0, \qquad \frac{a}{2G_2} + \sum_{\pm}\pm(M \pm a)K_1^{\pm} = 0 \qquad (3.17)$$

where $K_1^{\pm} \equiv K_1(M_{\pm}, \mu, \mu_5)$ (the same convention applies to L_1). The second derivatives of the potential are

$$V_{\sigma\sigma} = \frac{1}{2G_1} + \sum_{\pm}\left[(M \pm a)^2 L_1^{\pm} + K_1^{\pm}\right], \qquad V_{\eta\eta} = \frac{1}{2G_2} + \sum_{\pm}\left[(\eta \pm \Pi)^2 L_1^{\pm} + K_1^{\pm}\right]$$

$$V_{\pi\pi} = \frac{1}{2G_1} + \sum_{\pm}\left[(\eta \pm \Pi)^2 L_1^{\pm} + K_1^{\pm}\right], \qquad V_{aa} = \frac{1}{2G_2} + \sum_{\pm}\left[(M \pm a)^2 L_1^{\pm} + K_1^{\pm}\right]$$

$$V_{\sigma\eta} = V_{\pi a} = \sum_{\pm}(M \pm a)(\eta \pm \Pi)L_1^{\pm}, \qquad V_{\sigma\pi} = V_{\eta a} = \sum_{\pm}\pm(M \pm a)(\eta \pm \Pi)L_1^{\pm}$$

$$V_{\sigma a} = \sum_{\pm}\pm\left[(M \pm a)^2 L_1^{\pm} + K_1^{\pm}\right], \qquad V_{\eta\pi} = \sum_{\pm}\pm\left[(\eta \pm \Pi)^2 L_1^{\pm} + K_1^{\pm}\right] \qquad (3.18)$$

To keep the discussion simple we will assume in the subsequent that $a = 0$. However, in Sec. 4 we will see that in a very tiny region of the parameter space there is evidence of the existence of a phase with $a \neq 0$.

3.2.1 Chirally symmetric phase

We will first consider the phase where none of the fields condenses (in the chiral limit with $m = 0$ and $\mu = \mu_5 = 0$ for simplicity). The gap equations are automatically satisfied, while the second derivatives read in this case

$$V_{\sigma\sigma} = V_{\pi\pi} = \frac{1}{2G_1} + 2K_1, \qquad V_{\eta\eta} = V_{aa} = \frac{1}{2G_2} + 2K_1,$$

$$V_{\sigma\eta} = V_{\sigma\pi} = V_{\sigma a} = V_{\eta\pi} = V_{\eta a} = V_{\pi a} = 0. \qquad (3.19)$$

After absorbing the quadratic divergence from the cut-off regularization into the coupling constants as mentioned previously

$$\frac{1}{2G_i} - \frac{\Lambda^2}{\pi^2} = \frac{1}{2G_i^r} \qquad (3.20)$$

the stability conditions for this phase are $G_{1,2}^r > 0$. For simplicity, we will drop the superindex r throughout this study.
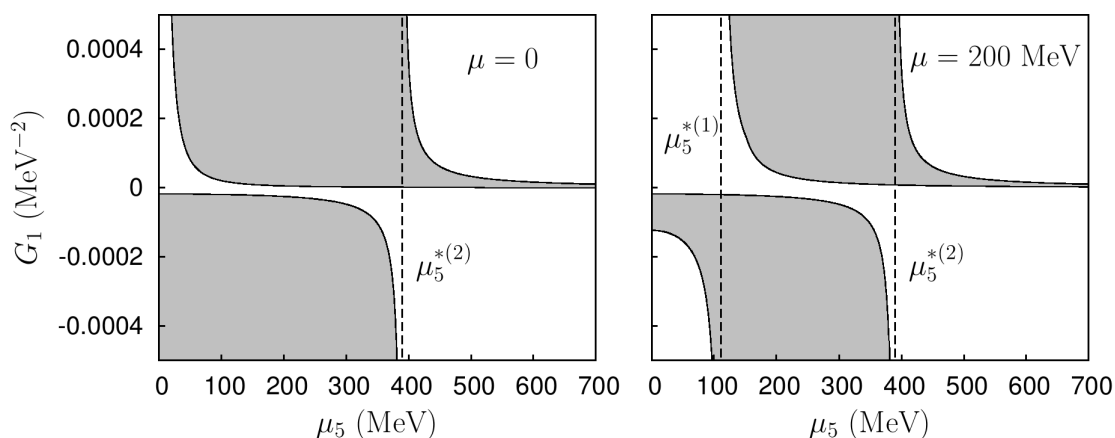
3.2.2 Chirally broken phase

In this section we will explore the phase where the field σ, and only this field, condenses. The gap equations reduce just to one

$$K_1 = -\frac{1}{4G_1}\left(1 - \frac{m}{M}\right).$$ (3.21)

Let us first assume $\mu = \mu_5 = 0$. Then the condition for CSB after absorbing the quadratic divergence into the coupling constants (or right away in DR for that matter) reads

$$M^2\left(\frac{1}{2} - \log\frac{2\Lambda}{M}\right) = \frac{\pi^2}{2G_1}\left(1 - \frac{m}{M}\right).$$ (3.22)

Figure 3.1: Allowed region of G_1 as a function of μ_5 with fixed μ for a stable CSB phase (dark region). The left panel shows $\mu = 0$ while the right one corresponds to $\mu = 200$ MeV. The figure corresponds to $m = 0$ and $\Lambda = 1$ GeV.

In Fig. 3.1 we show the region of G_1 that provides a stable CSB phase with $m = 0$ for non-trivial values of the external drivers. All dimensional quantities scale with Λ, which we take to be $\Lambda = 1$ GeV throughout. Two discontinuities appear in the plot. The first one is found at

$$\left(\mu_5^{*(1)}\right)^2 = \frac{\mu^2}{2}\left[\Theta(\mu - \mu^*)\left(1 - \frac{1}{2\ln\frac{2\Lambda}{\mu}}\right) + \Theta(\mu^* - \mu)\frac{1}{\ln\frac{\Lambda}{\mu}}\right]$$

with

$$\mu^* \equiv \exp\left[-\frac{1}{4}\left(3 - 2\ln 2 + \sqrt{9 + 4\ln 2 + 4\ln^2 2}\right)\right]\Lambda \approx 0.265\Lambda,$$

while the second one can be written analytically only if $\mu < 2\exp[-\frac{1}{4}(1 + \sqrt{5})]\Lambda \approx 0.891\Lambda$. In this case, the second discontinuity is given by

$$\left(\mu_5^{*(2)}\right)^2 = (3 - \sqrt{5})\Lambda^2\exp\left[-\frac{1}{2}\left(1 + \sqrt{5}\right)\right] \approx (0.389\Lambda)^2.$$

41

3. PARITY BREAKING IN THE NAMBU–JONA-LASINIO MODEL

For $\mu = 0$ and $\mu = 200$ MeV, the condition $\mu < 0.891\Lambda$ is satisfied and the previous equation can be used to find the discontinuity, which is clearly independent of μ. The limit $\mu \to 0$ reduces to $G_1 < 0$, a known result from a previous work on the NJL model in DR [130]. Finally, note that the restriction for G_2 is simply $\frac{1}{G_2} > \frac{1}{G_1}$.

A similar analysis could be done setting $m \neq 0$ but except for the complications appearing due to the inclusion of this extra parameter, no big differences would appear with respect to the curves presented in Fig. 3.1. Therefore, we omit the details of such calculation.

Let us set $m \neq 0$ again. The meson spectrum for any value of the external chemical potentials is given by the second derivatives at the local minimum

$$V_{\sigma\sigma} = \frac{m}{2G_1 M} + 2M^2 L_1, \qquad V_{\eta\eta} = \frac{m}{2G_1 M} + \frac{1}{2}\left(\frac{1}{G_2} - \frac{1}{G_1}\right)$$

$$V_{\pi\pi} = \frac{m}{2G_1 M}, \qquad V_{aa} = \frac{m}{2G_1 M} + \frac{1}{2}\left(\frac{1}{G_2} - \frac{1}{G_1}\right) + 2M^2 L_1$$

$$V_{\sigma\eta} = V_{\sigma\pi} = V_{\sigma a} = V_{\eta\pi} = V_{\eta a} = V_{\pi a} = 0, \tag{3.23}$$

where one has to use a bare quark mass m of the same sign as the coupling G_1 so as to provide a positive pion mass.

The stability conditions read

$$\frac{1}{G_2} > \frac{1}{G_1}\left(1 - \frac{m}{M}\right), \qquad 2M^2 L_1 > \max\left[-V_{\pi\pi}, -V_{\eta\eta}\right]. \tag{3.24}$$

Let us set once again $\mu = \mu_5 = 0$. Then $L_1 > 0$ and the second covexity condition is always met if the first one is fulfilled. In this case the mass spectrum obeys the relation

$$m_\sigma^2 - m_\pi^2 = m_a^2 - m_\eta^2 > 0$$

in analogy to the situation in QCD. In addition the following relation also holds

$$m_a^2 - m_\sigma^2 = m_\eta^2 - m_\pi^2,$$

and the difference $m_\eta^2 - m_\pi^2$ is positive (like the analogous one in QCD [87]) provided that $\frac{1}{G_2} - \frac{1}{G_1} > 0$.

Let us now examine in detail the dependence of the chiral condensate on the external chemical potentials. In Figure 3.2 we present the evolution of the constituent quark mass as a function of the vector chemical potential for different values of the current quark mass and coupling G_1 (left and right panels respectively) with $\mu_5 = 0$. Both the bare quark mass and the coupling G_1 are taken to be negative, as just explained above. There is chiral restoration around a certain value of the chemical potential that depends mostly on G_1; this phenomenon of chiral restoration is well known in the NJL model [132] and it is possibly the main reason that this simple model fails to reproduce
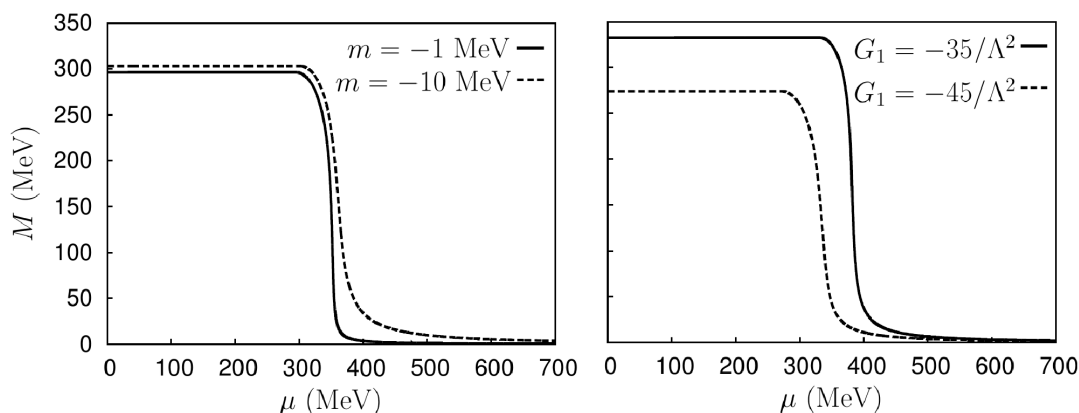
Figure 3.2: Evolution of the constituent quark mass M depending on μ. For both plots we set $G_2 = -45/\Lambda^2$ with $\Lambda = 1$ GeV and $\mu_5 = 0$. In the left panel, we fixed $G_1 = -40/\Lambda^2$ and plot for different values of m. In the right panel instead, we fixed $m = -5$ MeV in order to examine the variation of G_1. The transition becomes sharper as m decreases.
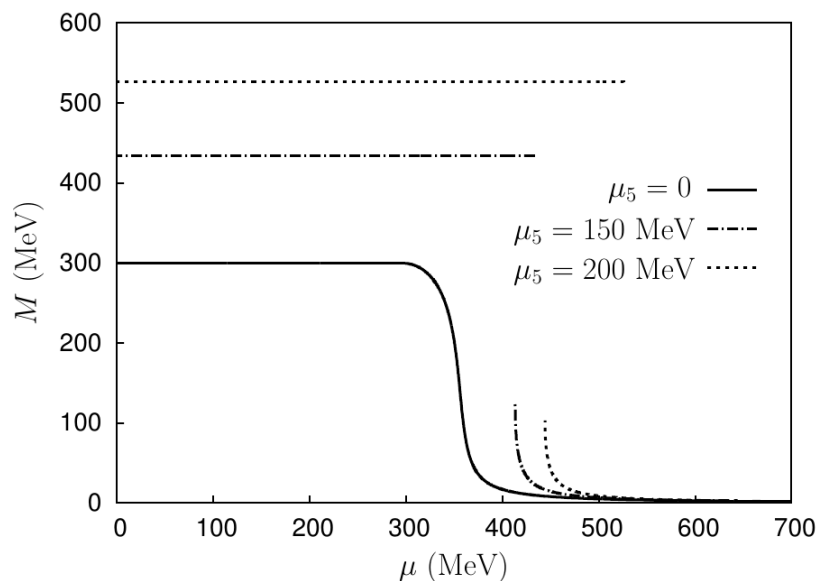
Figure 3.3: Evolution of the constituent quark mass M depending on μ for different values of the axial chemical potential μ_5 setting $m = -5$ MeV, $G_1 = -40/\Lambda^2$ and $G_2 = -45/\Lambda^2$. The drawn lines correspond to locally stable phases and accordingly the absence of a continuous line in the cases where $\mu_5 \neq 0$ is due to the fact that the Hessian matrix is not positive definite. The transition to a chirally restored phase changes to a first order one as μ_5 increases.

correctly the transition to nuclear matter. The transition becomes sharper as the value $m = 0$ is approached.

In Fig. 3.3 we observe the influence of the axial chemical potential μ_5 on the

restoration of chiral symmetry that always takes place in the NJL as μ increases. For high values of the axial chemical potential, the plateau appearing for $M > \mu$ acquires bigger values and spreads over a wider range of μ. At some point, the solution of the gap equation shows a stable and a metastable solution that must necessarily flip thus implying a jump of the constituent quark mass at some value of the chemical potential where both solutions coexist. Between these solutions, another unstable solution exists, but is not shown in the plot since the Hessian matrix is not positive definite. The jump represents a first order phase transition from $\mu < M$ (=constant) to a non-constant M smaller than the chemical potential.

It may be helpful to show a plot of the same constituent quark mass depending on μ_5 for different values of μ. In the left panel of Fig. 3.4 we display such evolution for $\mu = 0$ and 390 MeV[2]. The first curve is valid for any $\mu < M \approx 300$ MeV while the second one shows a small discontinuity that represents a first order phase transition within the CSB phase. A detail of the jump is presented in the inset. Note that both curves coincide after the jump and stop at $\mu_5 \sim 280$ MeV since beyond this value, the phase becomes unstable, as presented previously in Fig. 3.1.
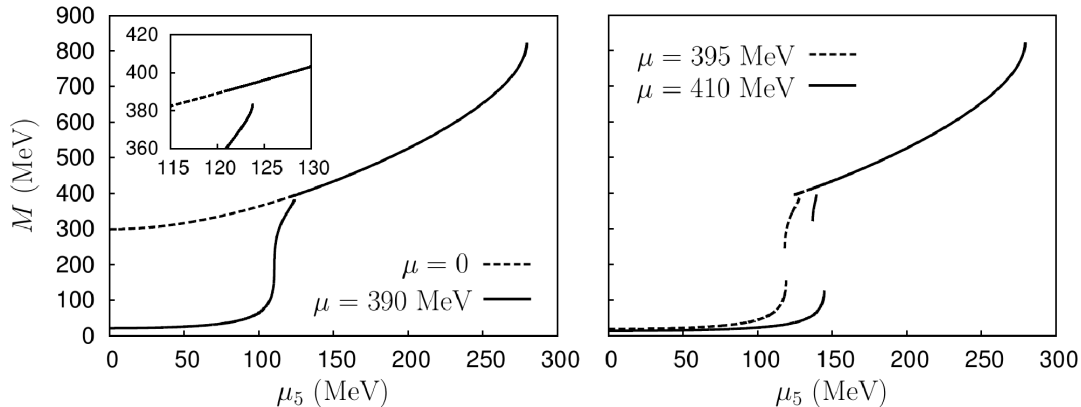
Figure 3.4: Evolution of the constituent quark mass M depending on μ_5 for different values of the chemical potential μ setting $m = -5$ MeV, $G_1 = -40/\Lambda^2$ and $G_2 = -45/\Lambda^2$. Both graphics show the regions where all the second derivatives are positive. Certain values of μ_5 exhibit coexisting solutions implying first order phase transitions. In the left panel, we show a plot for $\mu = 0$ (or indeed for any $\mu < M$) and $\mu = 390$ MeV. The second curve exhibits a small jump that is shown more detailed in the inset. The right panel corresponds to $\mu = 395$ (two jumps) and 410 MeV (probably only one jump). This plot shows that the NJL with external drivers has a rather complex phase diagram.

In the right panel, we present the values of $\mu = 395$ and 410 MeV, which correspond to qualitatively different cases. The curve for $\mu = 395$ MeV shows two separate regions where the function is bivaluated. First, the lower and intermediate branches share some common values of μ_5 even that it cannot be appreciated in the plot. Thus, a first order phase transition must take place within this region. The same behaviour happens for

---

[2]The solid and dashed lines were interchanged in [123]. This new version is corrected.

the intermediate and the upper branches, implying another first order phase transition. For bigger values of μ_5 one recovers the tendency of $\mu = 0$ as in the previous case. The curve $\mu = 410$ MeV is somewhat similar to the previous one but now with a trivaluated region: for a certain small range of μ_5 the three branches may be reached and therefore one or two jumps may take place. For bigger values of μ, the intermediate branch disappears and only one jump may take place.

All the jumps in Fig. 3.4 are due to the presence of unstable regions that would connect the different branches of the same curve. Here, it can be shown that $V_{\sigma\sigma} < 0$ is the responsible for these unstable zones. On the other hand, V_{aa} is simply $V_{\sigma\sigma}$ with a positive shift and the restriction $V_{aa} > 0$ does not add anything new.

We want to stress that all the first order phase transitions just explained are a direct consequence of the addition of μ_5 to the problem. No other assumptions are made beyond using the mean field approximation.

3.3 Isosinglet pseudoscalar condensation and parity breaking

Next we focus in the analysis of parity violating phases. It turns out that the only stable one corresponds to condensation in the isoscalar channel [123]. Neutral pseudoscalar isotriplet condensation, either with or without CSB, does not lead to a stable termodynamical phase[3]. Now, in addition to the scalar condensate σ that was explored in the previous section we will allow for a non-vanishing isosinglet pseudoscalar condensate η. The gap equations now turn to be

$$M = \frac{m}{G_1} \frac{1}{\frac{1}{G_1} - \frac{1}{G_2}}, \qquad K_1 = -\frac{1}{4G_2}. \tag{3.25}$$

The first gap equation shows that the scalar condensate exhibits a remarkable independence on the external chemical potentials as it turns out to be constant once the parameters of the model are fixed. Unlikely the η condensate does depend on the external drivers through the second equation. Moreover, from the first equation one finds that in the parity-breaking phase $m = 0$ iff $G_1 = G_2$; namely, the parity-breaking η condensate is a stationary point of the effective potential (3.5) only when the chiral and $U(1)_A$ symmetries are explicitly preserved or broken at the same time in the NJL Lagrangian (3.1). However this stationary point would not be a true minimum but a stationary point with two flat directions. The more general case where $m \neq 0$ and $G_1 \neq G_2$ is thus the only possibility to have a genuine parity-breaking phase. We will see in a moment how as one takes the limit $m \to 0$, the narrow window to have access to this phase disappears.

---

[3]This is at variance with the QCD- inspired effective theory analysis of [88] where the possibility of a condensation in the isotriplet channel was proven.

The second derivatives read

$$V_{\sigma\sigma} = \frac{1}{2}\left(\frac{1}{G_1} - \frac{1}{G_2}\right) + 2M^2 L_1, \qquad V_{\eta\eta} = 2\eta^2 L_1, \qquad V_{\sigma\eta} = 2M\eta L_1$$

$$V_{\pi\pi} = \frac{1}{2}\left(\frac{1}{G_1} - \frac{1}{G_2}\right) + 2\eta^2 L_1, \qquad V_{aa} = 2M^2 L_1, \qquad V_{\pi a} = 2M\eta L_1$$

$$V_{\sigma\pi} = V_{\sigma a} = V_{\eta\pi} = V_{\eta a} = 0.$$

We find that the Hessian matrix is not diagonal but has a block structure with two isolated sectors $\sigma - \eta$ and $\pi - a$ that reflect the mixing of states with different parity [88, 118]. This mixing will be carefully studied in Chapter 4, where more degrees of freedom will be included. As already stressed, the focal point of this chapter is the analysis of the stable thermodynamic phases and therefore, the mixing effect will be omitted here. The determinants of these blocks are

$$\det(V^{\sigma,\eta}) = \eta^2 L_1 \left(\frac{1}{G_1} - \frac{1}{G_2}\right), \qquad \det(V^{\pi,a}) = M^2 L_1 \left(\frac{1}{G_1} - \frac{1}{G_2}\right),$$

and thus, the resulting conditions for this phase to be stable reduce to

$$L_1 > 0, \qquad \left(\frac{1}{G_1} - \frac{1}{G_2}\right) > 0. \tag{3.26}$$

The second of the previous conditions leads to a peculiar ordering of the physical meson spectrum. Recall that in the chiral symmetry breaking phase we had

$$m_a^2 - m_\sigma^2 = m_\eta^2 - m_\pi^2 = -\frac{N}{2}\left(\frac{1}{G_1} - \frac{1}{G_2}\right),$$

and therefore, a stable parity-breaking phase is not compatible with a fit to the phenomenology. Thus parity breaking in the NJL model corresponds to a choice of parameters that makes this model quite different from QCD predictions [87]. In other words, the NJL model with a stable parity-breaking phase will have nothing to do with QCD. Note that the above differences are independent of the external drivers μ and μ_5.

The rest of the possible phases with a vanishing a require $m = 0$ to satisfy the gap equations; they are not true minima. In particular, there is no phase with parity breaking and $\sigma = 0$.

3.3.1 Transition to the parity-breaking phase

In this section we will analyse the characteristics of the transition to the phase where parity is broken. First of all, let us define M_0 as the solution to $M_0 = M(G_1, \mu = \mu_5 = 0)$ in the CSB phase given by Eq. (3.21). Recall the inequality $V_{\eta\eta} > 0$ of the same phase given in Eq. (3.23) and the stability condition of the parity-breaking phase in Eq. (3.26). Putting all of them together yields the following inequalities

$$0 < \frac{1}{G_1} - \frac{1}{G_2} < \frac{m}{G_1 M_0}.$$

The second inequality can be inserted in the first gap equation of the parity-breaking phase (see Eq. (3.25)) to show that in this phase, $M > M_0$. The same set of inequalities can be rewritten as

$$\frac{1}{G_1}\left(1 - \frac{m}{M_0}\right) < \frac{1}{G_2} < \frac{1}{G_1}, \tag{3.27}$$

which means that G_1 and G_2 necessarily have the same sign, while in the CSB phase G_2 had no restriction and could have opposite sign. This set of inequalities represents the necessary condition to have a transition from the CSB to a parity-breaking phase, as they provide the stability conditions of both phases. Notice that the model allows a narrow window of G_2 (once G_1 is fixed) so that both phases may take place depending on the value of the external drivers. In the limit $m \to 0$, this window closes and no parity breaking can be found.

Let us recall the gap equation in the CSB phase Eq. (3.21) and assume $\mu = \mu_5 = 0$. Provided that Eq. (3.27) is satisfied, it follows that

$$K_1 = -\frac{1}{4G_1}\left(1 - \frac{m}{M_0}\right) > -\frac{1}{4G_2}.$$

In the parity-odd phase, the gap equation is $K_1 = -\frac{1}{4G_2}$. In order to reach this phase from the parity-even one, K_1 has to decrease as a function of the external chemical potentials. From (3.21) this statement is equivalent to an increasing chiral condensate $M(\mu, \mu_5) > M_0$ in the parity-even phase. All this discussion is in agreement with the fact that $M > M_0$ in the parity-odd phase, as we explained above.

Let us point out the fact that the condition $L_1 > 0$ from the parity broken phase in Eq. (3.26) is stronger than the one from the CSB one in Eq. (3.24) so the former will remain to provide stability to both phases. Let us describe how the phase transition takes place first for $\mu = 0$ and finally for $\mu \neq 0$.

3.3.2 Phase transitions with $\mu = 0$

Let us simplify the analysis by setting $\mu = 0$ and let us study the dependence on μ_5, which makes M increase from its initial value M_0. At some critical value such that

$$M^c \equiv M(\mu_5^c) = \frac{m}{G_1}\frac{1}{\frac{1}{G_1} - \frac{1}{G_2}}, \tag{3.28}$$

where the critical value of the axial chemical potential is

$$(\mu_5^c)^2 = \frac{M_c^2}{2} - \frac{1}{4\log\frac{2\Lambda}{M_c}}\left(M_c^2 - \frac{\pi^2}{G_2}\right),$$

m_η vanishes, and from here on, we get into the parity-breaking phase via a second order phase transition, where M remains frozen as discussed while the dependence on μ_5 is absorbed into a non-vanishing η condensate. The dependence of K_1 on $M_\pm^2$ will be now on $M_c^2 + \eta^2$. Note that $(\mu_5^c)^2 > 0$ and therefore, a threshold in M^c follows.
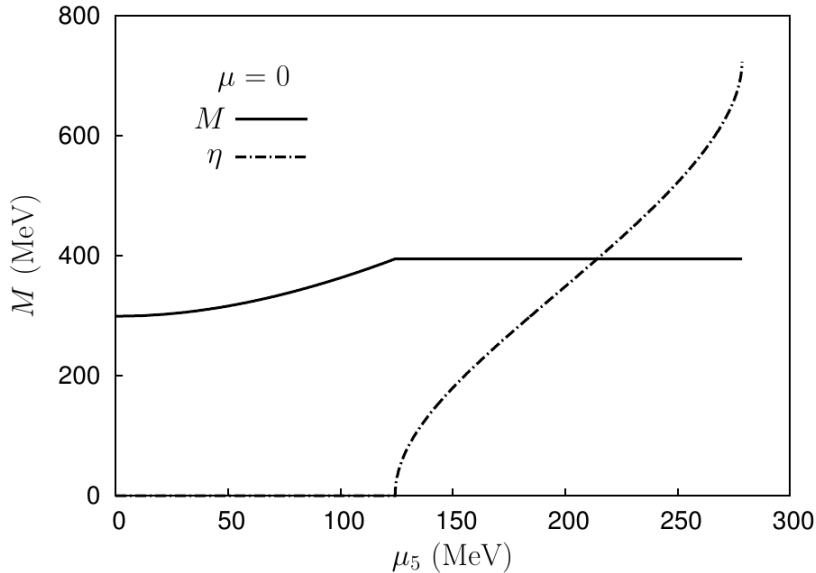
Figure 3.5: M and η dependence on μ_5 for $\mu < M_0$, $G_1 = -40/\Lambda^2$, $G_2 = -39.5/\Lambda^2$, $m = -5$ MeV and $\Lambda = 1$ GeV.

In Fig. 3.5 we present a plot showing the evolution of M and η with respect to μ_5 for $\mu = 0$ (or any $\mu < M_0 \approx 300$ MeV). In the CSB phase M grows with μ_5 up to the critical value M^c, the point where this magnitude freezes out and η condensates acquiring non-trivial values, also growing with the axial chemical potential. At $\mu_5 \simeq 0.28\Lambda$, this phase shows an endpoint and beyond, no stable solution exists. This point is the same one that we found in the CSB phase, meaning that the model becomes unstable at such value of μ_5, no matter which phase one is exploring.

3.3.3 Phase transitions with $\mu > 0$

The presence of both chemical potentials makes the function K_1 exhibit more complicated features. As K_1 decreases with μ_5 and μ does the opposite job, μ_5 needs larger values than μ to reach the parity-breaking phase. In Fig. 3.6, we present a set of plots with the evolution of both M and η for non-vanishing values of the chemical potential. As before we take the value $\Lambda = 1$ GeV to make the model in order to have some QCD-inspired intuition. Of course everything scales with Λ.

In the upper panels, we set $\mu = 375$ MeV (left) and $\mu = 390$ MeV (right), both of them $M_0 < \mu < M^c$, where jumps in M are observed in the parity even phase together with tiny metastable regions. This behaviour is very similar to the one described in Fig. 3.4 with the subtlety that we inverted the sign of $\frac{1}{G_1} - \frac{1}{G_2}$ and therefore, the parity-odd phase may be reached.

In addition, this change of sign shifts the second derivative V_{aa}, which is the only responsible for the apparent big jump in the $\mu = 390$ MeV window (the one with
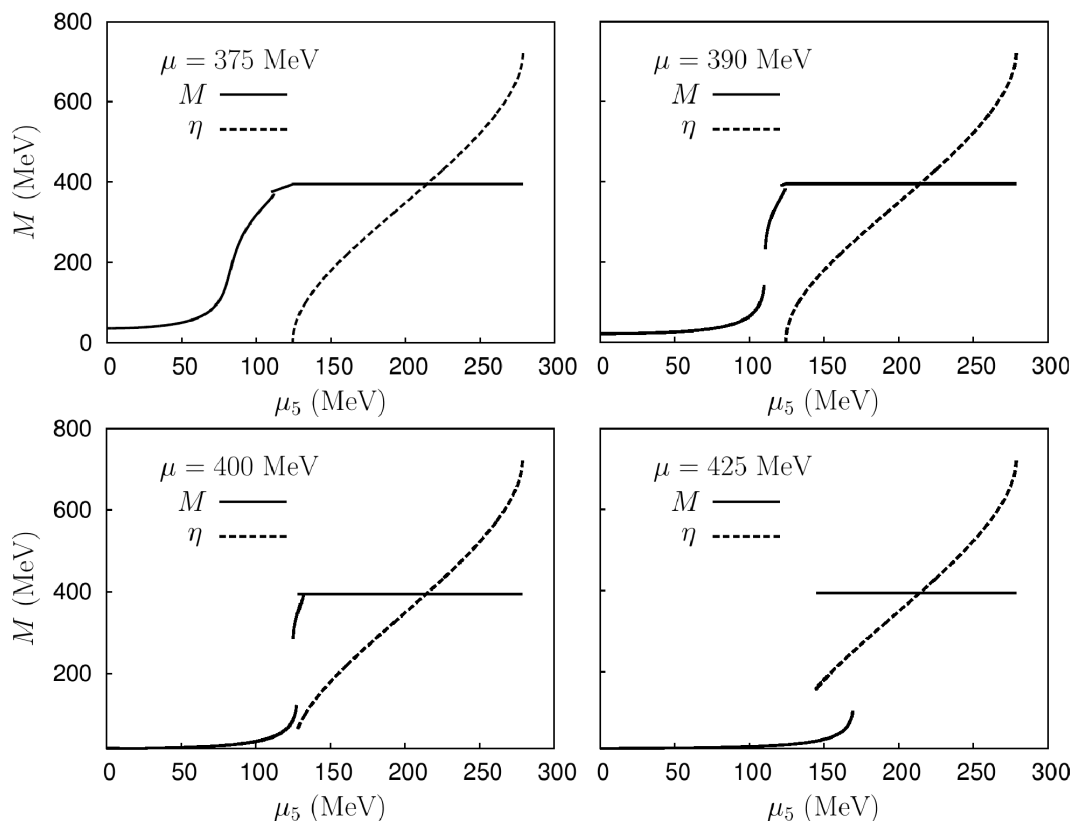
Figure 3.6: M and η dependence on μ_5 for $\mu = 375$, 390, 400 and 425 MeV, $G_1 = -40/\Lambda^2$, $G_2 = -39.5/\Lambda^2$, $m = -5$ MeV and $\Lambda = 1$ GeV. The graphics show the regions where all the second derivatives are positive. Certain values of μ_5 exhibit coexisting solutions implying first order phase transitions. The first jump in the plot for $\mu = 390$ MeV shows a very small region of μ_5 where the function is not defined. This region is characterised by $V_{aa} < 0$, thus suggesting a phase with a non-trivial scalar isotriplet condensate. This is the only region where we have found indications for a phase with $a \neq 0$. The landscape of first order phase transitions in the constituent quark mass is essentially the same as the one explained in Fig. 3.4.

lower μ_5). V_{aa} becomes negative while all the other derivatives remain positive. If for a moment we forgot V_{aa}, the curve would be smoothly increasing and we would only have the other tiny jump close to the flat region of constant M, as in the CSB case. However, the fact that this second derivative becomes negative leads to a small range of μ_5 where no stable solution exists. Hence, it seems natural to think that the system goes away from the phase with $a = 0$ and acquires a non-trivial scalar isotriplet condensate. We emphasize this region is really tiny and depends crucially on the specific values for the parameters, even disappearing for $G_1 > -30/\Lambda^2$. Both graphics show a smooth transition to the parity-odd phase, say, via a second order phase transition with the same characteristics of the previous section with $\mu = 0$.

In the lower panels of Fig. 3.6 we set $\mu = 400$ MeV (left) and $\mu = 425$ MeV (right) with $\mu > M^c$ and observe what we could more or less expect from Fig. 3.4 with the same landscape of first order phase transitions in the parity-even phase. The main difference of these two latter values appears in the finite jump of η, implying now a first order phase transition towards the parity-breaking phase.

Finally, we present the phase transition line in a $\mu^c(\mu_5^c)$ plot in Fig. 3.7. For $\mu < M^c \approx 395$ MeV (or equivalently, for $\mu_5^c = \mu_5^c(\mu = 0)$), the transition is smooth (second order) while beyond that there is a jump in the condensates (first order), as it was also observed in the previous figure.
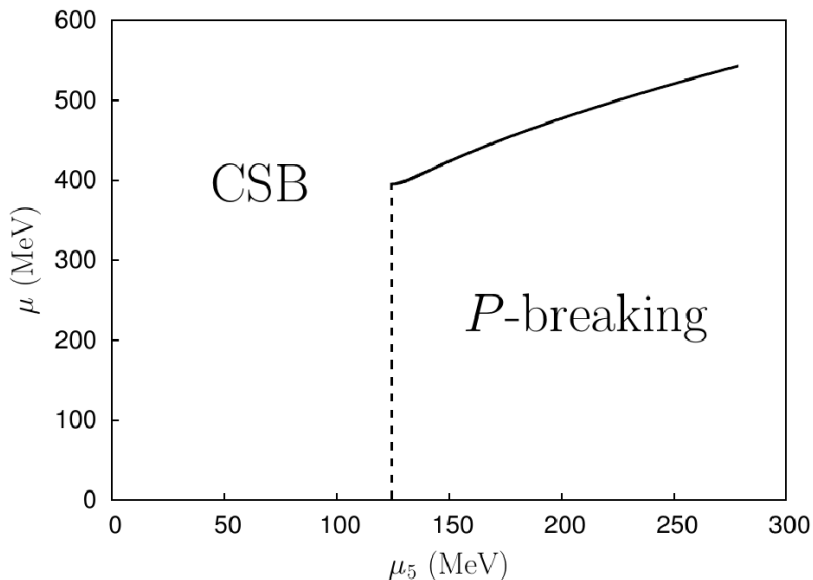
Figure 3.7: Transition line from the CSB to the P-breaking phase with $G_1 = -40/\Lambda^2$, $G_2 = -39.5/\Lambda^2$, $m = -5$ MeV and $\Lambda = 1$ GeV. The vertical dashed line is related to a second order phase transition while the solid one corresponds to a first order one.

3.4 Summary

In this chapter we worked in the continuum and explored in detail the different phases that arise in the Nambu–Jona-Lasinio model in the presence of both vector and axial chemical potentials at zero temperature. The axial chemical potential changes considerably the thermodynamical properties of the model. Interestingly, when the full $U(2)_L \times U(2)_R$ global symmetry is broken to $SU(2)_L \times SU(2)_R \times U(1)_V$ (i.e. $G_1 \neq G_2$) a phase where parity is spontaneously broken by the presence of an isosinglet condensate η appears. However, we have not found any phase where parity and flavour symmetry are simultaneously broken thus indicating the presence of a non-zero value for $\langle \bar{\psi} \gamma_5 \tau^3 \psi \rangle$. On the contrary we have found an extremely small region in the space of

parameters where flavour symmetry is broken by a non-zero value of $\langle \bar{\psi} \tau^3 \psi \rangle$ but parity is not broken yet.

Demanding stability of such a phase however leads to a region of the parameter space where the spectrum has little resemblance to QCD. We have investigated all the properties of the transition from the parity-even to the parity-odd phase providing results on the evolution of both condensates, which exhibit finite jumps under certain conditions, and finally examining the phase transition line, where it was shown that for $\mu < M^c$ we have a 2nd order transition while for $\mu > M^c$, it corresponds to a 1st order one.

The discussion presented here on the phase structure of the NJL model in the presence of external chemical potentials is rather general and, as discussed above, the model -in spite of its simplicity- exhibits an enormously rich phase structure.

Chapter 4

An effective theory for spin 0 mesons in a parity-breaking medium

After a careful study of a phase where parity breaks spontaneously in the NJL model due to the presence of $\mu_5 \neq 0$ (see also [88]), it seems rather realistic to assume that such phase may really exist in QCD. If this is the case, the order of magnitude of the axial chemical potential reached in HIC should be similar to the one explored in the previous chapter in order the new phase to be thermodynamically stable. Another naive estimate would be assuming simply that $\mu_5 \sim \tau_{\text{heating}}^{-1}$ so a formation time of the fireball $\tau_{\text{heating}} \sim 0.5 - 1$ fm leads to $\mu_5 \sim 200 - 400$ MeV. On the other hand, we can also estimate μ_5 by assuming that the change in the free energy has to be of order f_π and the average change in the quark axial charge $\langle \Delta Q_5^q \rangle \sim 1$. Then, assuming a linear response, $\mu_5 \sim f_\pi \simeq 100$ MeV. Therefore, in the rest of this thesis we shall assume μ_5 to take values in the range of hundreds of MeV. Note that this parameter may take different values from collision to collision so the magnitude we are dealing with has to be understood as an effective one. In any case, the dependence of the results on μ_5 will be discussed everywhere it is needed.

It seems interesting to investigate how hadronic physics is modified by the presence of μ_5. In this chapter we will address the treatment of the spin zero resonances while we postpone to Chapter 5 the case of vector mesons.

The appearance of an axial chemical potential as a consequence of local large topological fluctuations in a hot medium constitutes an explicit source of parity violation. It generates new in-medium effects on resonances that can be unambiguously predicted in terms of the axial chemical potential alone. As introduced in the previous chapter if parity breaks, the regular classification of particles into scalars and pseudoscalars is meaningless. The consequences are far reaching; parity ceases to be a guidance for allowing/forbidding strong interaction processes, and states that have opposite parities, but otherwise equal quantum numbers, mix. In this scenario two new processes are then

4. AN EFFECTIVE THEORY FOR SPIN 0 MESONS IN A PARITY-BREAKING MEDIUM

likely to be most relevant inside the fireball thermodynamics: the decays $\eta, \eta' \to \pi\pi$ that are strictly forbidden in QCD on parity grounds.

The fireball created from a HIC is usually treated as a pion gas. The $\rho(770)$ meson plays a significant role in this context as its large width $\Gamma_{\rho \to \pi\pi} \simeq 150$ MeV allows it to decay and regenerate in-medium several times. As a consequence, this channel has been deeply analysed [38] and suggested to reach thermal equilibrium within the pion gas in experiments like RHIC or LHC. In a similar way, the new decays $\eta, \eta' \to \pi\pi$ in a parity-odd medium could eventually lead to large widths and a thermalization of the corresponding channels. In this chapter we shall address a detailed study of this effect.

In order to introduce the axial chemical potential to an effective theory we have to recall that, just as the ordinary baryonic potential is introduced as the zero-th component of a spurious vector field, the axial chemical potential μ_5 can be implemented as the time component of a fictitious axial-vector field. We follow the arguments for strange quark suppression already mentioned in Chapter 2 of parity-breaking effects in a finite volume. Let us recall that according to Eq. (2.13), due to the unavoidable left-right oscillations the mean value of strange quark axial charge is washed out as the strange quark mass is comparable with the decay width of fireballs. Therefore, we will use axial chemical potential in the non-strange sector only.

At the level of an effective meson Lagrangian, μ_5 will appear using the spurion technique through the action of the covariant derivative

$$\partial_\mu \to D_\mu = \partial_\mu - i\{\mathbf{I}_q \mu_5 \delta_{\mu 0}, \cdot\} = \partial_\mu - 2i\mathbf{I}_q \mu_5 \delta_{\mu 0} \qquad (4.1)$$

in the same way an external axial-vector field would be introduced through $D_\mu = \partial_\mu - i\{A_\mu, \cdot\}$. In the case one considered an isotriplet μ_5, the non-strange $\mathbf{I}_q$ should be replaced by the neutral Pauli matrix τ^3 and the anticommutator structure should be preserved due to the non-trivial flavour structure of a general lagrangian.

To get a rough estimate of the relevance of the previously forbidden processes $\eta, \eta' \to \pi\pi$ we introduced μ_5 to the Chiral Lagrangian. However, it can be checked that there is no contribution from dimension two operators, but dimension four terms (see e.g. [133]) which lead to

$$\sim \frac{16\mu_5}{F_\Pi f_\pi^2} L\, \partial\eta\, \mathrm{Tr}\, (\partial\hat{\pi}\partial\hat{\pi})\,; \quad \Pi = \eta,\, \eta', \qquad (4.2)$$

where L is a combination of the Gasser-Leutwyler constants $L_{1,2,3} \sim 10^{-3}$. In order to obtain a numerical estimate we take the average pion momenta to be $\sim m_\eta/2$. The effective coupling constant affecting this operator can be estimated to be ~ 0.4, which is large enough to induce substantial η meson regeneration in the hot pion gas. A very rough estimate of the partial width for the exotic process under discussion gives $\Gamma_{\eta \to \pi\pi} \simeq 100\,\mathrm{MeV}$, when we assume $\mu_5 \simeq 150$ MeV, to be compared for instance to $\Gamma_{\rho \to \pi\pi} \simeq 150$ MeV. Clearly if ρ mesons are in thermal equilibrium in the pion bath, so will the η. A similar analysis leads to an even larger width for the η' due to the above parity-breaking operator.

However at this point, one should be aware that the previous estimate using the Chiral Lagrangian may not be reliable at all because the decay width grows quadratically with the axial chemical potential and a slight increase of μ_5 would lead to abnormally large widths and a violation of unitarity. Thus, μ_5 has to be understood as a perturbatively small parameter. In addition, one expects substantial mixing with the scalar partners of η, η' (i.e. σ, f_0, glueballs, etc.) with comparable masses. For this reason, we will build a more sophisticated effective theory in order to investigate this effect. In the next section, we introduce a generalised sigma model with the lightest meson states with different parities to account for the mixing due to the parity violation.

This chapter is organized as follows. In Sec. 4.1 a generalised sigma model is presented. Mass-gap equations for three v.e.v. of neutral scalar fields are derived and solved analytically. Then we determine the best fit of parameters of the model comparing with the experimental inputs for scalar and pseudoscalar meson spectral data [134]. In Sec. 4.2 the axial chemical potential is introduced. We obtain the modification of the mass-gap equations and find the distortion of a_0- and π- meson spectra caused by the parity breaking. In Sec. 4.3 a more complicated mixing of three meson states, σ, η, η', is investigated when the medium has an axial charge. At certain energies some particle states become tachyons (recall we are in-medium so this actually does not represent a fundamental problem). In Sec. 4.4 all decay widths are calculated for both the rest frame and for moving particles (we note that when an axial charge fills the medium, the Lorentz invariance is broken). In Sec. 4.5 the problem of isosinglet axial-vector meson condensation and its interference with the axial chemical potential is examined.

4.1   Generalised sigma model

Our starting point will be the following Lagrangian, invariant under $SU(3)_F$ [118]

$$
\begin{aligned}
\mathcal{L} =& \frac{1}{4}\mathrm{Tr}\left(D_\mu H D^\mu H^\dagger\right) + \frac{b}{2}\mathrm{Tr}\left[M(H + H^\dagger)\right] + \frac{M^2}{2}\mathrm{Tr}\left(HH^\dagger\right) \\
& - \frac{\lambda_1}{2}\mathrm{Tr}\left[(HH^\dagger)^2\right] - \frac{\lambda_2}{4}\left[\mathrm{Tr}\left(HH^\dagger\right)\right]^2 + \frac{c}{2}(\det H + \det H^\dagger) \\
& + \frac{d_1}{2}\mathrm{Tr}\left[M(HH^\dagger H + H^\dagger HH^\dagger)\right] + \frac{d_2}{2}\mathrm{Tr}\left[M(H + H^\dagger)\right]\mathrm{Tr}\left(HH^\dagger\right)
\end{aligned}
\tag{4.3}
$$

where $H = \xi\Sigma\xi$, $\xi = \exp\left(i\frac{\Phi}{2f}\right)$, $\Phi = \lambda^a\phi^a$ and $\Sigma = \lambda^b\sigma^b$. This model can be confronted to similar models in [135, 136, 137] with the important difference (see below) in the trilinear vertices with couplings d_1, d_2. These interaction terms are needed if a fit to phenomenology wants to be performed accurately. The piece with the determinant is responsible for providing the breaking of $U(1)_A$ and a non-degenerate mass to η and η' in the chiral limit. The neutral v.e.v. of the scalars are defined as $v_i = \langle\Sigma_{ii}\rangle$ where $i = u, d, s$, and satisfy the following gap equations:

$$
M^2 v_i - 2\lambda_1 v_i^3 - \lambda_2 \bar{v}^2 v_i + c\frac{v_u v_d v_s}{v_i} = 0.
\tag{4.4}
$$

4. AN EFFECTIVE THEORY FOR SPIN 0 MESONS IN A PARITY-BREAKING MEDIUM

Let us stress that the parameter f, which is commonly identified with the pion decay constant, appears attached to the fields throughout and therefore, it will be absorbed in the field renormalization. Here the role of the pion decay constant is assigned to the chiral quark condensates v_i.

For further purposes we need the non-strange meson sector and η_s. In terms of v.e.v. and physical scalar and pseudoscalar states, the parametrization used here is

$$\Phi = \begin{pmatrix} \eta_q + \pi^0 & \sqrt{2}\pi^+ & 0 \\ \sqrt{2}\pi^- & \eta_q - \pi^0 & 0 \\ 0 & 0 & \sqrt{2}\eta_s \end{pmatrix}, \qquad \Sigma = \begin{pmatrix} v_u + \sigma + a_0^0 & \sqrt{2}a_0^+ & 0 \\ \sqrt{2}a_0^- & v_d + \sigma - a_0^0 & 0 \\ 0 & 0 & v_s \end{pmatrix}. \quad (4.5)$$

In the scalar sector, besides considering different flavour vacuum expectation values, we included in our model the isosinglet σ meson and the isotriplet $a_0(980)$. In the pseudoscalar sector, we introduced pions and the strange and non-strange components of the η and $\eta'(958)$ mesons. η_q corresponds to the same degree of freedom that we introduced in the NJL model in Chapter 3. That description was rather poor for an accurate fit to phenomenology since the strange sector was not accounted for. Therefore a more precise phenomenological treatment was postponed to this section. Indeed η_q and η_s are not mass eigenstates of the strong interaction as they appear to be mixed mainly due to the determinant term in (4.3). However, dealing with these states will simplify considerable our analysis. The mixing among them leading to the genuine mass eigenstates η and η' is defined by a rotation of angle ψ

$$\begin{pmatrix} \eta_q \\ \eta_s \end{pmatrix} = \begin{pmatrix} \cos\psi & \sin\psi \\ -\sin\psi & \cos\psi \end{pmatrix} \begin{pmatrix} \eta \\ \eta' \end{pmatrix}. \quad (4.6)$$

As stated in Chapter 2, an axial charge can only be effectively generated for nearly massless quarks. Due to the non-negligible strange quark mass, even that an axial charge is generated in the strange sector from a HIC, it will not be transmitted to hadron physics. Therefore we exclude kaons and their scalar partners κ from the analysis as they will not be affected by a non-strange μ_5. Let us take for the time being $\mu_5 = 0$ and assume $v_u = v_d = v_s = v_0 \equiv f_\pi \approx 92$ MeV because we only consider the effect of masses perturbatively. As a function of the Lagrangian parameters, the main physical magnitudes derived from this model are

$$v_0 = \frac{c \pm \sqrt{c^2 + 4M^2(2\lambda_1 + 3\lambda_2)}}{2(2\lambda_1 + 3\lambda_2)}, \qquad m_\pi^2 = \frac{2}{v_0}(b + (d_1 + 3d_2)v_0^2)m,$$

$$m_a^2 = 2(-M^2 + 3(2\lambda_1 + \lambda_2)v_0^2 + cv_0 - 2(3d_1 + 2d_2)mv_0 - 2d_2 m_s v_0),$$

$$m_\sigma^2 = 2(-M^2 + (6\lambda_1 + 7\lambda_2)v_0^2 - cv_0 - 6(d_1 + 2d_2)mv_0 - 2d_2 m_s v_0),$$

$$m_{\eta,\eta'}^2 = \frac{m_\pi^2}{2m}(m + m_s) + 3cv_0 \mp \sqrt{8c^2 v_0^2 + \left[\frac{m_\pi^2}{2m}(m - m_s) + cv_0\right]^2},$$

$$\Gamma_a^2 = \frac{(-4m_\eta^2 m_\pi^2 + (-m_a^2 + m_\eta^2 + m_\pi^2)^2)(m_a^2 - m_\eta^2 + 4d_1 mv_0)^4}{(48m_a^3 \pi v_0^2)^2},$$

$$\Gamma_\sigma^2 = \frac{9(m_\sigma^2 - 4m_\pi^2)(m_\sigma^2 - m_\pi^2 + 4(d_1 + 2d_2)mv_0)^4}{(32m_\sigma^2\pi v_0^2)^2},$$

$$\sin(2\psi) = \frac{4\sqrt{2}cv_0}{m_{\eta'}^2 - m_\eta^2}, \tag{4.7}$$

with $m/m_s = (m_u + m_d)/(2m_s) \simeq 1/25$. The angle ψ is not really necessary for our subsequent discussion but we can use it as a test of the model. v_0 is found via gap equations. These equations are inserted in MINUIT in order to find the minimum of the χ^2 estimator using the following experimental numbers (in MeV):

$$v_0^{\text{exp}} = 92 \pm 5, \quad m_\pi^{\text{exp}} = 137 \pm 5, \quad m_a^{\text{exp}} = 980 \pm 50,$$
$$m_\sigma^{\text{exp}} = 600 \pm 120, \quad m_\eta^{\text{exp}} = 548 \pm 50, \quad m_{\eta'}^{\text{exp}} = 958 \pm 100,$$
$$\Gamma_a^{\text{exp}} = 60 \pm 30, \quad \Gamma_\sigma^{\text{exp}} = 600 \pm 120. \tag{4.8}$$

The σ mass is assumed to be relatively large as we are not considering any glueballs, so this σ is a sort of average of the real σ and other 0^+ light states. We have assigned generous error bars to include the uncertainties in the model itself. In the minimization process there are several control variables:

- The value of the potential at the minimum has to be $V(v_0) < 0$ since $v = 0$ is an extremal point with $V(v = 0) = 0$ but in the case the latter is a minimum, the true vacuum has to have a lower energy. Also, there is a control of the third extremal, which has to be higher than the true minimum, given by

$$V(v_0) = \frac{1}{4}v_0^2(-6M^2 + 3(2\lambda_1 + 3\lambda_2)v_0^2 - 4cv_0).$$

- The Hessian matrix has degenerate eigenvalues and there are only two different eigenvalues whose positivity should be provided

$$(V'')_1(v_0) = -M^2 + 3(2\lambda_1 + \lambda_2)v_0^2 + cv_0,$$
$$(V'')_2(v_0) = -M^2 + 3(2\lambda_1 + 3\lambda_2)v_0^2 - 2cv_0.$$

The final result of the minimization process is given in Table 4.1.

All the requirements concerning the control parameters are satisfied at this global solution. The fit makes the cubic (in H) terms in (4.3) actually more relevant than the linear one. As a last point, the ψ angle is treated as a prediction. Experimentally [134], $\psi \simeq -18° + \arctan\sqrt{2} \simeq -18° + 54.7° \approx 36.7°$, while our result is $\psi_{\text{MINUIT}} \approx 35.46°$, in excellent agreement.

4.2 Introducing the axial chemical potential

The introduction of the axial chemical potential μ_5 is carried out following the prescription described by the spurion technique in Eq. (4.1). An extra piece which is

4. AN EFFECTIVE THEORY FOR SPIN 0 MESONS IN A PARITY-BREAKING MEDIUM

Magnitude	MINUIT value (MeV)	Experimental value (MeV)	Error
v_0	92.00	92	-3.52×10^{-7}
m_π	137.84	137	$+6.10 \times 10^{-3}$
m_a	980.00	980	-1.26×10^{-6}
m_σ	599.99	600	-1.66×10^{-5}
m_η	497.78	548	-9.16×10^{-2}
$m_{\eta'}$	968.20	958	$+1.06 \times 10^{-2}$
Γ_a	60.00	60	$+2.04 \times 10^{-5}$
Γ_σ	600.00	600	$+6.81 \times 10^{-6}$

Table 4.1: Comparison of the experimental data with the values obtained in the model using the MINUIT routine to find the minimum of the χ^2 estimator.

proportional to μ_5 appears in the P-even Lagrangian

$$\Delta\mathcal{L} = \frac{i}{2}\mu_5 \mathrm{Tr}\left[\mathbf{I}_q\left(\partial_0 H H^\dagger - H \partial_0 H^\dagger\right)\right] + \mu_5^2 \mathrm{Tr}\left(\mathbf{I}_q H H^\dagger\right). \tag{4.9}$$

For non-vanishing μ_5, we will assume isospin symmetry and thus, we impose to our solutions to have $v_u = v_d = v_q \neq v_s$. The corresponding gap equations are

$$M^2 - 2(\lambda_1 + \lambda_2)v_q^2 - \lambda_2 v_s^2 + c v_s + 2\mu_5^2 = 0, \tag{4.10}$$

$$v_s(M^2 - 2\lambda_2 v_q^2 - (2\lambda_1 + \lambda_2)v_s^2) + c v_q^2 = 0. \tag{4.11}$$

The correct solution of this system of coupled equations is taken imposing the correct limit to the chiral condensates $v_q, v_s \to v_0$ when $\mu_5 \to 0$ (see Figure 4.1 for the μ_5 evolution of the solution). This solution can be checked to be the global minimum independently on the value of the axial chemical potential.
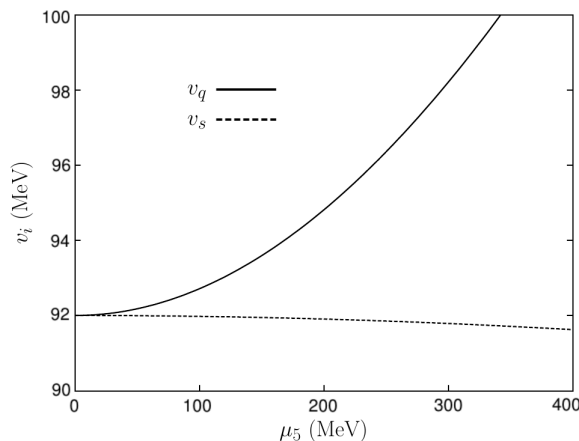
Figure 4.1: v_q and v_s dependence on μ_5.

As an example of such a mixing let us consider the two isotriplets of opposite parity π and a_0. After normalization of the states, let us consider the piece of the effective

Lagrangian that is bilinear in the π and a_0 fields

$$\mathcal{L} = \frac{1}{2}(\partial a_0)^2 + \frac{1}{2}(\partial \pi)^2 - \frac{1}{2}m_1^2 a_0^2 - \frac{1}{2}m_2^2 \pi^2 - 4\mu_5 a_0 \dot{\pi}, \qquad (4.12)$$

where

$$
\begin{aligned}
m_1^2 &= -2(M^2 - 2(3\lambda_1 + \lambda_2)v_q^2 - \lambda_2 v_s^2 - cv_s + 2(3d_1 + 2d_2)mv_q + 2d_2 m_s v_s + 2\mu_5^2), \\
m_2^2 &= \frac{2m}{v_q}\left[b + (d_1 + 2d_2)v_q^2 + d_2 v_s^2\right].
\end{aligned}
\qquad (4.13)
$$

Notice that the resulting Lagrangian is not Lorentz invariant, which is obvious from (4.1). We will perform a diagonalization in momentum space, so the Lagrangian operator is written as

$$\mathcal{L} = -\frac{1}{2}\begin{pmatrix} a_0^*(k) & \pi^*(k) \end{pmatrix} \begin{pmatrix} -k^2 + m_1^2 & 4i\mu_5 k_0 \\ -4i\mu_5 k_0 & -k^2 + m_2^2 \end{pmatrix} \begin{pmatrix} a_0(k) \\ \pi(k) \end{pmatrix}. \qquad (4.14)$$

Recall that fields in the momentum representation satisfy $A^*(k) = A(-k)$. Note also the fact that the mixing term has been rewritten as $-4\mu_5 a_0 \dot{\pi} = -2\mu_5(a_0 \dot{\pi} - \dot{a}_0 \pi)$ in order the matrix to be hermitian. The eigenvalues are $\frac{1}{2}(k^2 - m_{\text{eff}}^2)$, where the (energy dependent) effective masses are

$$m_{\text{eff}\,\pm}^2(k_0) = \frac{1}{2}\left[m_1^2 + m_2^2 \pm \sqrt{(m_1^2 - m_2^2)^2 + (8\mu_5 k_0)^2}\right]. \qquad (4.15)$$

The new eigenstates $X_{1,2}$ are defined through

$$a_0 = \sum_{j=1}^{2} C_{aj} X_j, \quad \pi = \sum_{j=1}^{2} C_{\pi j} X_j, \qquad (4.16)$$

$$C_{a1} = iC_{\pi 2} = C_+, \quad C_{a2} = -iC_{\pi 1} = -C_-,$$

with

$$C_\pm = \frac{1}{\sqrt{2}}\sqrt{1 \pm \frac{m_1^2 - m_2^2}{\sqrt{(m_1^2 - m_2^2)^2 + (8\mu_5 k_0)^2}}}. \qquad (4.17)$$

We can also use the notation $X_1, X_2 \equiv \tilde{a}, \tilde{\pi}$, indicating that X_1 (resp. X_2) is the state that when $\mu_5 = 0$ goes over to a_0 (resp. π).

In Fig. 4.2, we present the results for the evolution of $\tilde{\pi}$ and $\tilde{a}_0$ effective masses with respect to the axial chemical potential μ_5 for different values of the 3-momentum. As stressed, both states tend to the known physical ones in the limit $\mu_5 \to 0$. In general terms, we find a growing mass depending on μ_5 for $\tilde{a}_0$ while the opposite holds for $\tilde{\pi}$. A remarkable feature of this model is the appearance of in-medium tachyonic states at high energies (or momenta). It is evident from Eq. (4.15) that for energies higher than a critical value $k_0, |\vec{k}| > m_1 m_2/(4\mu_5) \equiv k_{\tilde{\pi}}^c$, the square root term dominates, thus leading to a negative squared mass for pions, as shown in the right panel of Fig. 4.2.
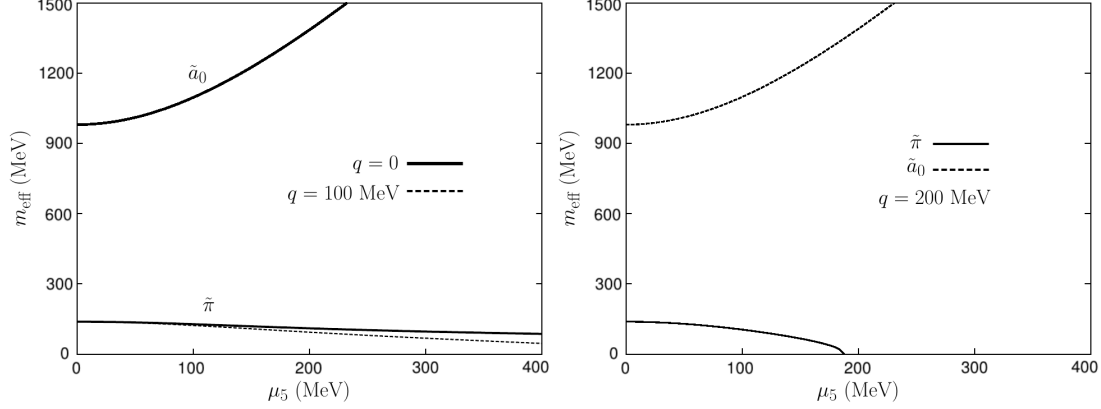
Figure 4.2: Effective mass dependence on μ_5 for $\tilde{\pi}$ and $\tilde{a}_0$. Left panel: comparison of masses at rest and at low momentum $q = 100$ MeV. Right panel: masses at $q = 200$ MeV, where the $\tilde{\pi}$ mass goes tachyonic, as discussed in the text. For such momenta, the variations in $\tilde{a}_0$ are almost invisible and only slightly visible for large values of μ_5 for $\tilde{\pi}$.

Such a behaviour does not represent a serious physical obstacle since it can be checked that the energies are always positive and no vacuum instabilities appear. The group velocity can also be checked to be smaller than the speed of light independently of μ_5. On the other hand, the $\tilde{a}_0$ mass shows an important enhancement, but in this model μ_5 has to be understood as a perturbatively small parameter, and very high values are beyond the domain of applicability of the effective Lagrangian. A better treatment of $\tilde{a}_0$ would require the inclusion of heavier degrees of freedom such as $\pi(1300)$ for instance.

4.3 Mixing $\eta - \sigma - \eta'$

A similar analysis applies to the isosinglet case. We shall consider three states here: η, η' and σ. As before, the starting point will be the piece of the effective Lagrangian (4.3) that after the inclusion of μ_5 is bilinear in the fields, i.e. the properly normalized kinetic part

$$\mathcal{L} = \frac{1}{2}[(\partial\sigma)^2 + (\partial\eta_q)^2 + (\partial\eta_s)^2] - \frac{1}{2}m_3^2\sigma^2 - \frac{1}{2}m_4^2\eta_q^2 - \frac{1}{2}m_5^2\eta_s^2 - 4\mu_5\sigma\dot{\eta}_q - 2\sqrt{2}cv_q\eta_q\eta_s. \quad (4.18)$$

The constants appearing in the previous equation are given by[1]

$$m_3^2 = -2(M^2 - 6(\lambda_1 + \lambda_2)v_q^2 - \lambda_2 v_s^2 + cv_s + 6(d_1 + 2d_2)mv_q + 2d_2 m_s v_s + 2\mu_5^2),$$

$$m_4^2 = \frac{2m}{v_q}\left[b + (d_1 + 2d_2)v_q^2 + d_2 v_s^2\right] + 4cv_s,$$

$$m_5^2 = \frac{2m_s}{v_s}[b + 2d_2 v_q^2 + (d_1 + d_2)v_s^2] + \frac{2cv_q^2}{v_s}. \quad (4.19)$$

---

[1]There were two miswritten numerical factors in [118]. This version is corrected.

In this case two different mixing pieces appear: the first one is indeed proportional to the axial chemical potential μ_5 and the other is proportional to the coupling c that breaks the axial anomaly due to the determinant term in Eq. (4.3) as already mentioned before. In matrix form, the previous lagrangian can be written as

$$\mathcal{L} = -\frac{1}{2} \begin{pmatrix} \sigma^*(k) & \eta_q^*(k) & \eta_s^*(k) \end{pmatrix} \begin{pmatrix} -k^2 + m_3^2 & 4i\mu_5 k_0 & 0 \\ -4i\mu_5 k_0 & -k^2 + m_4^2 & 2\sqrt{2}cv_q \\ 0 & 2\sqrt{2}cv_q & -k^2 + m_5^2 \end{pmatrix} \begin{pmatrix} \sigma(k) \\ \eta_q(k) \\ \eta_s(k) \end{pmatrix}. \tag{4.20}$$

The equation for the eigenvalues (effective masses) is now a cubic one and the solution is determined numerically

$$-8c^2 v_q^2 (m_{\text{eff}}^2 - m_3^2) + (m_{\text{eff}}^2 - m_5^2) \tag{4.21}$$

$$\times \left[\left(m_{\text{eff}}^2 - \frac{1}{2}(m_3^2 + m_4^2) \right)^2 - \frac{1}{4}(m_3^2 - m_4^2)^2 - (4\mu_5 k_0)^2 \right] = 0.$$

As before the eigenstates are defined via

$$\sigma = \sum_j C_{\sigma j} X_j, \qquad \eta_q = \sum_j C_{\eta_q j} X_j, \qquad \eta_s = \sum_j C_{\eta_s j} X_j, \tag{4.22}$$

where

$$C_{\sigma j} = \frac{4i\mu_5 k_0 (m_5^2 - m_j^2)}{N_j \prod_{k \neq j}(m_j^2 - m_k^2)}, \quad C_{\eta_q j} = \frac{(m_5^2 - m_j^2)(m_3^2 - m_j^2)}{N_j \prod_{k \neq j}(m_j^2 - m_k^2)},$$

$$C_{\eta_s j} = \frac{-2\sqrt{2}cv_q(m_3^2 - m_j^2)}{N_j \prod_{k \neq j}(m_j^2 - m_k^2)}, \quad \frac{1}{N_j} = \sqrt{1 + \frac{(4\mu_5 k_0)^2}{(m_j^2 - m_3^2)^2} + \frac{8c^2 v_q^2}{(m_j^2 - m_5^2)^2}}. \tag{4.23}$$

N_j is the proper (eigen)field normalization factor.

The μ_5-dependence of the effective masses is plotted in Fig. 4.3 for different values of the 3-momentum. As in the previous example, the heavy degrees of freedom $\tilde{\sigma}$ and $\tilde{\eta}'$ become heavier as one increases μ_5 while the opposite applies for the light $\tilde{\eta}$. The latter state eventually becomes tachyonic for high energies or momenta $k_0, |\vec{k}| > k_{\tilde{\eta}}^c$ with $k_{\tilde{\eta}}^c \equiv m_3/(4\mu_5 m_5)\sqrt{m_4^2 m_5^2 - 8c^2 v_q^2}$, as shown in the right panel of Fig. 4.3. As in the previous example, vacuum is stable and group velocities are checked to be smaller than the speed of light. The tachyon critical energy presents a similar behaviour as the one in the triplet case. In Fig. 4.4, both isotriplet $k_{\tilde{\pi}}^c$ and isosinglet critical energies $k_{\tilde{\eta}}^c$ are plotted together.
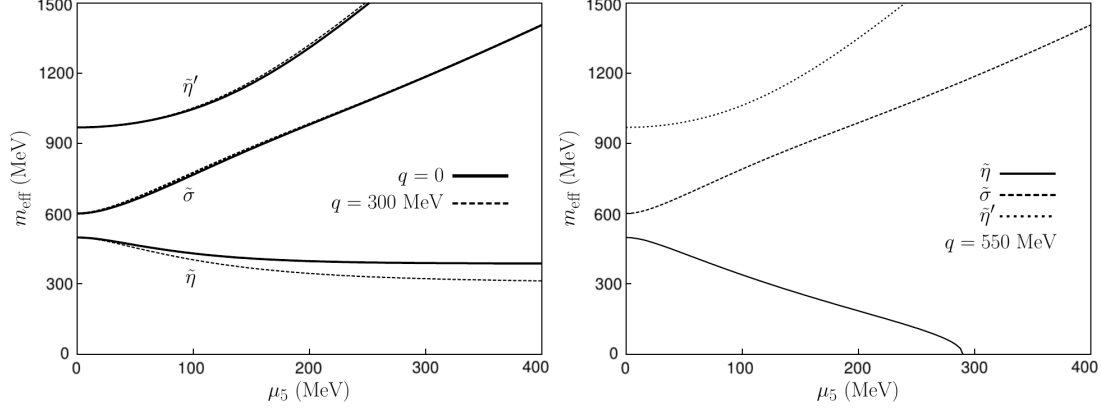
Figure 4.3: Effective mass dependence on μ_5 for $\tilde{\eta}$, $\tilde{\sigma}$ and $\tilde{\eta}'$. Left panel: comparison of masses at rest and at low momentum $q = 300$ MeV. Right panel: masses at $q = 550$ MeV, where the $\tilde{\eta}$ mass goes tachyonic, as discussed in the text. As in the previous example, for this range of momenta, the variations in the heavier degrees of freedom $\tilde{\sigma}$ and $\tilde{\eta}'$ are almost invisible and only slightly visible for large values of μ_5 for $\tilde{\eta}$.
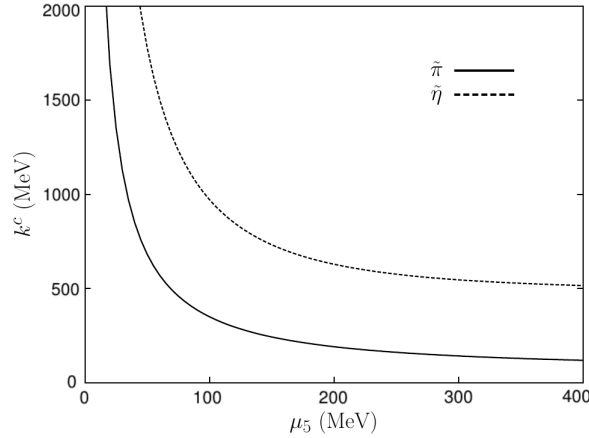
Figure 4.4: μ_5-dependence of the tachyon critical energy for isotriplet $k_{\tilde{\pi}}^c$ and isosinglet case $k_{\tilde{\eta}}^c$.

4.4 New interactions and decay widths

After the inclusion of μ_5 the cubic couplings present in the effective Lagrangian (4.3) containing one isosinglet and two isotriplets are

$$\mathcal{L}_{\sigma aa} = 2[(3d_1 + 2d_2)m - 2(3\lambda_1 + \lambda_2)v_q]\sigma\vec{a}^2,$$

$$\mathcal{L}_{\sigma\pi\pi} = \frac{1}{v_q^2}\left[(\partial\vec{\pi})^2 v_q - (b + 3(d_1 + 2d_2)v_q^2 + d_2 v_s^2)m\vec{\pi}^2\right]\sigma,$$

$$\mathcal{L}_{\eta a\pi} = \frac{2}{v_q^2}[\partial\eta_q\vec{a}\partial\vec{\pi}v_q - (b + (3d_1 + 2d_2)v_q^2 + d_2 v_s^2)m\eta_q\vec{a}\vec{\pi}],$$

$$\mathcal{L}_{\sigma a\pi} = -\frac{4\mu_5}{v_q}\sigma\vec{a}\dot{\vec{\pi}}, \quad \mathcal{L}_{\eta aa} = -\frac{2\mu_5}{v_q}\dot{\eta}_q\vec{a}^2, \quad \mathcal{L}_{\eta\pi\pi} = 0. \tag{4.24}$$

62

As seen in the previous expressions, interactions (and therefore decays) that are normally forbidden on parity conservation grounds are now possible with a strength proportional to the parity-breaking parameter μ_5. However, the previous interaction terms are not physical because the genuine eigenstates are now X_i rather than the original fields π, a_0, etc. Going to the physical basis requires using the diagonalization process defined in the previous section.

Our ultimate purpose is to check the relevance of dynamically generated parity breaking through topological charge fluctuations in heavy ion collisions. It is natural then to ask how the previously derived masses and vertices may influence the physics in the hadronic fireball.

It should be clear that the influence may be very important if μ_5 is such that the induced parity-breaking effects are significant. After the initial collision of two heavy ions in a central or quasi-central process a fireball is formed. This fireball could be described in rather simplistic terms as a hot and dense pion gas. Pion-pion interaction is dominated by σ and ρ -particle exchanges and processes such as $\eta \to \pi\pi$ or $\eta' \to \pi\pi$ are forbidden. If parity is no longer a restriction, these two processes, or rather processes such as $X_i \to \tilde{\pi}\tilde{\pi}$ ($i = 3, 4, 5$) are for sure relevant and the new eigenstates produced due to parity breaking could thermalize inside the fireball.

Let us now try to be more quantitative. It should be clear from the mass evolution as a function of μ_5 (Figure 4.2) that $\tilde{\pi}$ is the lightest state and it dominates the partition function in the fireball. To get an estimate of the relevance of the new states X_i we will compute their width to distorted pions $\tilde{\pi}$. A non-negligible decay width comparable (or higher) to the inverse fireball lifetime would correspond to a state with a mean free path smaller than the size of the fireball. As a consequence, such state would decay in-medium into (distorted) pions meaning that it could be regenerated as in the case of the ρ meson, even opening the possibility of reaching thermal equilibrium. To do so we need the following S-matrix element corresponding to $X_i(q) \to \tilde{\pi}^+(p)\tilde{\pi}^-(p')$

$$
\begin{aligned}
i\mathcal{M} =& 4i[(3d_1 + 2d_2)m - 2(3\lambda_1 + \lambda_2)v_q]C_{\sigma i}C_{a2}^+ C_{a2}^- + \frac{4\mu_5}{v_q}C_{\sigma i}(E_{p'}C_{a2}^+ C_{\pi 2}^- + E_p C_{a2}^- C_{\pi 2}^+) \\
& - \frac{i}{v_q^2}\left[(m_{X_i}^2 - m_{\tilde{\pi}^+}^2 - m_{\tilde{\pi}^-}^2)v_q + 2(b + 3(d_1 + 2d_2)v_q^2 + d_2 v_s^2)m\right]C_{\sigma i}C_{\pi 2}^+ C_{\pi 2}^- \\
& - \frac{4\mu_5 E_q}{v_q}C_{\eta_q i}C_{a2}^+ C_{a2}^- + \frac{i}{v_q}(m_{\tilde{\pi}^+}^2 - m_{\tilde{\pi}^-}^2)C_{\eta_q i}(C_{a2}^- C_{\pi 2}^+ - C_{a2}^+ C_{\pi 2}^-) \\
& - \frac{i}{v_q^2}[2(b + (3d_1 + 2d_2)v_q^2 + d_2 v_s^2)m - m_{X_i}^2 v_q]C_{\eta_q i}(C_{a2}^+ C_{\pi 2}^- + C_{a2}^- C_{\pi 2}^+). \qquad (4.25)
\end{aligned}
$$

We are dealing with a relativistic non-invariant theory and therefore the widths do not a priori transform as one would naively think. We shall compute them first at rest, then for different values of the 3-momentum of the decaying particle.

4. AN EFFECTIVE THEORY FOR SPIN 0 MESONS IN A PARITY-BREAKING MEDIUM

4.4.1 Widths at rest

The width of X_i is calculated from the amplitude shown in Eq. (4.25) since we do not include further decaying processes. Recall that all masses are energy dependent. At the X_i rest frame, $\vec{q} = \vec{0}$ and $E_p = E_{p'} = m_{X_i}(\vec{q} = \vec{0})/2 \equiv m_0^{X_i}/2$. Here, a momentum-dependent effective mass is taken instead of an energy-dependent one since we assume the decaying particle to be on-shell so both $m(\vec{k})$ and $m(k_0)$ coincide. Thus, the rest width is given by

$$\Gamma_{X_i \to \tilde{\pi}\tilde{\pi}} = \frac{3}{2} \frac{1}{2m_0^{X_i}} |\mathcal{M}|^2 \frac{1}{4\pi} \frac{p_{\tilde{\pi}}}{m_0^{X_i} \frac{dp_{\tilde{\pi}}^2}{dE_p^2}}, \quad \frac{dp_{\tilde{\pi}}^2}{dE_p^2} = 1 + \frac{(4\mu_5)^2}{\sqrt{(m_1^2 - m_2^2)^2 + (8\mu_5 E_p)^2}} \quad (4.26)$$

where $p_{\tilde{\pi}}(E_p) = \sqrt{E_p^2 - m_{\tilde{\pi}}^2(E_p)}$ and the factor $3/2$ accounts for the decay both to neutral and charged $\tilde{\pi}$. The results of the widths are shown in Figure 4.5.

The new state $\tilde{\eta}$ exhibits a smooth behaviour with an average value ~ 60 MeV, corresponding to a mean free path ~ 3 fm, which is smaller than the typical fireball size $L_{\text{fireball}} \sim 5 - 10$ fm. Hence, the thermalization of this channel via regeneration of $\tilde{\pi}$ within the gas seems to be possible.

Another striking point concerning $\tilde{\sigma}$ takes place down to $\mu_5 \sim 100$ MeV, when the decay width decreases dramatically leading to scenarios where this state becomes stable. The visible bumps in these two latter channels seem to reflect the tachyonic nature of the decaying $\tilde{\pi}$.
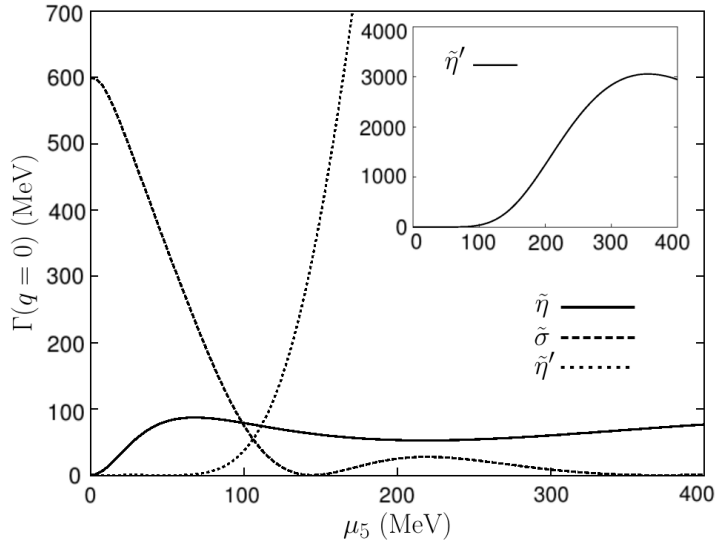
Figure 4.5: $\tilde{\eta}$, $\tilde{\sigma}$ and $\tilde{\eta}'$ widths at rest depending on μ_5. Down to $\mu_5 = 50$ MeV, $\tilde{\eta}$ acquires a width of order 60 MeV, with a characteristic mean free path smaller than the typical fireball size of $5 - 10$ fm and hence implying that thermalization may occur in this channel. Nevertheless, $\tilde{\sigma}$ shows a pronounced fall and beyond $\mu_5 = 100$ MeV, it becomes a stable channel. Inset: Detail of $\tilde{\eta}'$ width reaching the GeV scale, a clear violation of unitarity since we do not include heavier degrees of freedom in our model.

Finally, we present in the inset of Fig. 4.5 the detail of the $\tilde{\eta}'$ width, that grows up to the GeV scale, showing clear violations of unitarity. As in the case of $\tilde{a}_0$, more hadronic degrees of freedom are needed to obtain a reliable result, such as $f_0(980)$, etc.

4.4.2 Decay widths of moving particles

Next, let us compute the width when the decaying particle is not at rest. As explained before in a non-invariant relativistic theory this cannot be obtained from the one at rest by simply taking into account the time dilatation effect. The explicit calculation of such width is given by

$$\Gamma_{X \to \tilde{\pi}\tilde{\pi}} = \frac{3}{2} \frac{1}{2E_q} \frac{1}{8\pi q} \int \frac{|\mathcal{M}|^2 p \, dp}{E_p \frac{dp_{\tilde{\pi}}^2}{dE_p^2}}. \tag{4.27}$$

In our numerical calculation we controlled that all the magnitudes are implemented coherently, like for example $|\cos\theta| < 1$ and $E_{p'} > 0$. Of course, the limit $q \to 0$ coincides with the calculation at rest performed before.

In the $\tilde{\eta}$ channel (see the left section of Fig. 4.6), one may observe the time dilatation effect by which the width should decrease as the 3-momentum grows. However, this cannot explain the small variations at low 3-momenta with respect to the width at rest, namely, two initial bumps at $\mu_5 \sim 80$ MeV and 550 MeV (the latter being beyond the plot range) that slowly separate as one increases q. The two-dimensional representation $\Gamma_{\tilde{\eta}}(\mu_5, q)$ exhibits a saddle point around $\mu_5^* \sim 240$ MeV and $q^* \sim 500$ MeV, and in consequence, for large 3-momenta, a third intermediate bump appears opening the possibility of creating two different $\tilde{\pi}$ tachyons at the same time. The latter maximum grows fast as one increases q and becomes the global one when the 3-momentum goes beyond $q \gtrsim 700$ MeV.
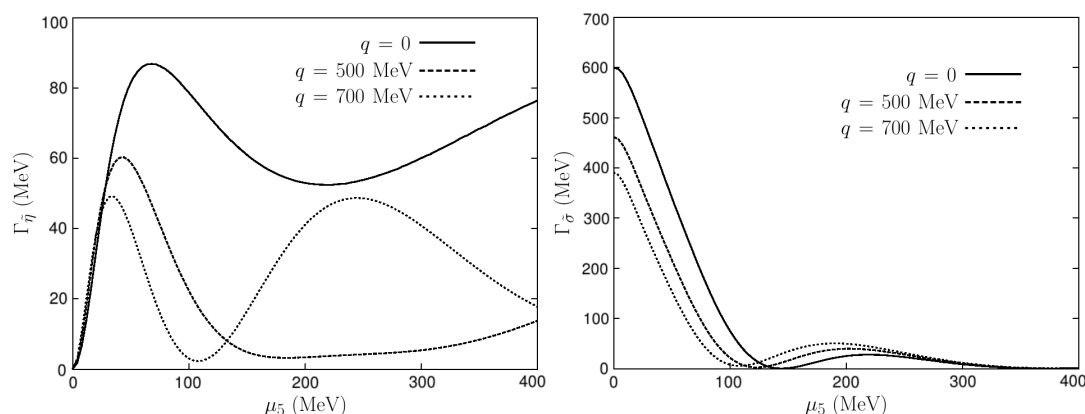
Figure 4.6: $\tilde{\eta}$ (left) and $\tilde{\sigma}$ (right) widths depending on μ_5 for different values of the incoming 3-momentum: $q = 0, 500, 700$ MeV. The first plot shows a non-trivial dependence on q (see text) while the second one shows a fall that is mainly due to the Lorentz factor.

On the other hand, in the $\tilde{\sigma}$ and $\tilde{\eta}'$ channels no huge differences arise when boosting
the decaying particle. In the right panel of Fig. 4.6, we show the $\tilde{\sigma}$ width for different
values of q and the most salient behaviour is, as in the previous case, the separation of
the two minima as one increases q.

4.5 Axial-vector meson condensation

The introduction of an axial chemical potential into the quark-meson model interferes
with the flavour-singlet axial-vector channel as this potential is just the time component
of some axial-vector field, as discussed at the beginning of this chapter. Therefore if one
includes the coupling of the singlet axial-vector quark current with the corresponding
meson field h_μ one expects mixing and renormalization of the bare axial chemical
potential due to condensation of the time component of the axial-vector field $h^\mu \simeq$
$\langle h^0 \rangle \delta^{0\mu}$. This phenomenon is in full analogy to the condensation of the time component
of the ω meson field when a baryon chemical potential enters the Lagrangian [138] which
is quite important to understand the repulsive nuclear forces in this channel.

Let us elucidate this phenomenon in more details. The relevant Lagrangian for
axial-vector mesons reads

$$\Delta\mathcal{L} = -\frac{1}{4}h_{\mu\nu}h^{\mu\nu} + \frac{1}{2}m_h^2 h_\mu h^\mu + \bar{q}\gamma_\mu\gamma_5(g_h h^\mu + \delta^{\mu 0}\mu_5)\mathbf{I}_q q, \tag{4.28}$$

where h stands for the $SU(2)$ singlet axial-vector meson $h_1(1170)$ [134] and g_h denotes
its coupling to the quark current. We assume the condensation of $h^\mu \simeq \langle h^0 \rangle \delta^{0\mu}$ and
thus, the effective chemical potential $\bar{\mu}_5 \equiv \mu_5 + g_h\langle h_0 \rangle$ can be defined. The equation of
motion for h

$$\frac{\delta\Delta\mathcal{L}}{\delta h_0} = m_h^2\langle h_0 \rangle + g_h\langle \bar{q}\gamma_0\gamma_5\mathbf{I}_q q \rangle = 0 \tag{4.29}$$

determines the relation among the effective non-strange axial charge density $\rho_5 = \langle \bar{q}\gamma_0\gamma_5\mathbf{I}_q q \rangle$ and the isosinglet axial-vector condensate.

$$\rho_5(\bar{\mu}_5) = \frac{\mu_5 - \bar{\mu}_5}{G_h} = \frac{\delta\Delta\mathcal{L}}{\delta\bar{\mu}_5}, \quad \Delta V = -\frac{1}{2}m_h^2\langle h_0 \rangle^2 = -\frac{1}{2}\frac{(\bar{\mu}_5 - \mu_5)^2}{G_h}, \tag{4.30}$$

where $G_h = g_h^2/m_h^2$. After including ΔV (Eq. (4.30)) in Eq. (4.9) the stationary point
equation (or equivalently, the equation of motion for the axial-vector condensate) can
be derived

$$\frac{\delta\mathcal{L}}{\delta\bar{\mu}_5} = \frac{\delta}{\delta\bar{\mu}_5}\left[2\bar{\mu}_5^2 v_q^2 + \frac{1}{2}\frac{(\bar{\mu}_5 - \mu_5)^2}{G_h}\right] = 0 \tag{4.31}$$

that allows to relate the bare and effective axial chemical potentials

$$\bar{\mu}_5\left[1 + 4G_h v_q^2(\bar{\mu}_5)\right] = \mu_5. \tag{4.32}$$

We stress that in the mass-gap equations for v_q, v_s the effective axial chemical potential
$\bar{\mu}_5$ must be used. The relation (4.32) is smooth against the decoupling of axial-vector

mesons $g_h \rightarrow 0$. It determines unambiguously the axial charge density, $\rho_5(\bar{\mu}_5) = 4\bar{\mu}_5 v_q^2(\bar{\mu}_5)$, which exhibits, in general, lower values when affected by axial meson forces, $|\bar{\mu}_5| < |\mu_5|$.

4.6 Summary

In this chapter we have analysed the physics of the lightest scalar and pseudoscalar mesons in the presence of a parity-odd medium driven by an axial chemical potential. By means of a generalised sigma model, we introduced some of the main resonances with spin zero in the $SU(3)$ representation. The presence of an axial chemical potential as an explicit source for parity violation induces a mixing among the states of different parity and same flavour content. The properties of in-medium mesons are energy dependent due to the breaking of Lorentz invariance when μ_5 is implemented as a time-dependent axial-vector field. Then, meson physics is frame-dependent with the natural consequence that masses and decay widths do depend non-trivially on the momentum of the corresponding particle.

We have given convincing arguments that, if $\mu_5 \neq 0$ the pion gas in the fireball forming after a central heavy ion collision may actually not be made of the usual pions, but instead of some states of non-defined parity and energy-dependent effective mass. In addition the lightest spin zero states in each isospin channel become tachyons for high enough energies. As a consequence of this feature, the decay widths of the singlet states into distorted pions show non-trivial dependences on the axial chemical potential. Perhaps more importantly, the distorted η meson seems to be in thermal equilibrium with the 'pion' gas, as indicated by the characteristic large width, completely different from the ones in vacuum.

4. AN EFFECTIVE THEORY FOR SPIN 0 MESONS IN A PARITY-BREAKING MEDIUM

Chapter 5

Vector Meson Dominance approach to local parity breaking

It is natural to ask whether the mixing of states of different parities as studied in the previous chapter occurs in the vector/axial-vector sector. There are many models dealing with vector particles phenomenologically. If we assume that the vector mesons appear as part of a covariant derivative (as postulated e.g. in hidden symmetry models [139]), no mixing term can be generated by operators of dimension 4 if μ_5 is an isos-inglet. However, such a mixing is not forbidden on (global) symmetry grounds if μ_5 is present, appearing as the time component of an axial-vector field (see e.g. [137]). This means that this coupling is very much model dependent and, unfortunately, not much phenomenological information is present. Therefore, in the present chapter we will omit the mixing of vector and axial-vector mesons due to parity violation.

The parity-breaking effect will be introduced through the Chern-Simons term assuming a time-dependent pseudoscalar (axion-like) condensate as pointed out in Chapter 2. As we will see, this form of LPB can be incorporated by adding a parity-odd term in the Lagrangian; however, this breaking, while being technically 'soft', can be numerically large, leading to important consequences. We shall review in detail how in-medium vector mesons are influenced by this effect and discuss possible ways to verify its existence.

We are interested in providing experimental signatures that allow to detect the LPB effect in the vector meson sector. Their hadronic decays are not useful channels as the decay products will be severely affected by the strongly interacting medium created within the HIC fireball. The cleanest way to extract reliable properties of in-medium vector mesons is through their electromagnetic decays. If we want to investigate LPB in HIC with the help of electromagnetic probes, we have to account for the photon contribution to the singlet axial anomaly. Following the lines of Eq. (2.17) an electromagnetic topological piece may to be added to the quark axial charge via

$$Q_5^q \rightarrow \tilde{Q}_5 = Q_5^q - T_5^{\text{em}}, \quad T_5^{\text{em}} = \frac{N_c e^2}{8\pi^2} \int_{\text{vol.}} d^3x \, \varepsilon_{jkl} \, \text{Tr}\left(\hat{A}^j \partial^k \hat{A}^l\right). \qquad (5.1)$$

5. VECTOR MESON DOMINANCE APPROACH TO LOCAL PARITY BREAKING

Now μ_5 is conjugated to the conserved $\tilde{Q}_5$ in the limit of vanishing quark masses but not to Q_5 itself [140]. We will bosonize QCD in the light vector meson sector using the Vector Meson Dominance model prescription [141, 142] with vector meson and photon fields appearing in the quark covariant derivative.

The VMD mechanism induces a mixing among photons and vector mesons independently on the preservation or violation of parity. This effect allows to reproduce the electromagnetic decays of vector mesons. In this chapter we will focus on the phenomenology related to the decay of vector mesons into lepton pairs (dileptons). Experimental results from different collaborations [46, 47, 62] are available so that a comparison with our theoretical predictions can be performed.

As described in Chapter 1, in central HIC an abnormal dilepton excess has been observed [46, 47]. In the PHENIX experiment, for instance, an excess is seen for dileptons in the range $M < 1.2$ GeV, for centrality $0 - 20\%$ and $p_T < 1$ GeV [47]. Theorists have so far been unable to account for the total dilepton excess convincingly. Thermal effects inducing vector resonance broadening and/or mass dropping fall short of providing a full explanation [38, 39, 40, 41, 78]. On the other hand, these effects seem to be able to explain most of the abnormal yield for NA60[46, 86]. The study of vector meson decays into dileptons within a parity-odd medium may be a helpful tool in order to investigate such dilepton excess around the $\rho - \omega$ resonance peak. The dilepton excess is conspicuously absent for peripheral HIC (where the CME should be more visible). We conjecture that the CME and the 'anomalous' dilepton excess may be complementary effects revealing two facets associated to the formation of a thermodynamic phase where parity is locally broken. We investigate whether LPB modifications of vector mesons may induce a large dilepton excess in certain HIC. We will briefly discuss how other hadronic decays may be relevant for the dilepton enhancement due to their substantial modification induced by LPB.

The modifications of ρ and ω induced by LPB will reveal distorted spectral functions. Distortion of the $\rho - \omega$ spectrum is well known to happen in HIC. Conventional explanations exist [38, 39, 40, 78] and if LPB occurs, all effects need to be treated jointly as long as they do not represent double counting. Due to the precision of current experiments, the distorted spectral function itself may be difficult to be accurately measured. In our analysis, we will see that this distortion is characterised by a polarization asymmetry around the $\rho - \omega$ resonance position. This feature could, in principle, be detected. Therefore, we will address a careful treatment of the polarization distribution associated to the lepton pairs produced in the decay of these mesons and to give possible signatures for experimental detection of LPB that could potentially be seen by the PHENIX and STAR collaborations are discussed.

Current HIC experiments have investigated possible polarization dependencies in dilepton angular distributions with no significant results [143]. We claim that the conventional angular variables used in such studies are not efficient enough to convey all the information related to the parity-breaking effect. The dilepton invariant mass plays a key role in this game, which is normally missed. If not considered, dilepton polar-

ization dependencies wipe out and no net effect can be extracted from experimental data. We will see that a combined analysis of some characteristic angles together with the dilepton invariant mass constitutes the appropriate framework to investigate the possible polarization asymmetry predicted by LPB.

This chapter is organised as follows: in Section 5.2, we introduce the Vector Meson Dominance model approach to LPB and derive in detail the distorted dispersion relation that affects the lightest meson states ρ and ω. In Section 5.3 their spectral functions are presented together with some considerations of a possible partial explanation of the abnormal dilepton production in the vicinity of their resonance peak position. An experimentally oriented study of the polarization asymmetry found in the spectral functions is discussed in Section 5.4. Two different analysis of the dilepton angular distribution are presented in order to reflect how the LPB effect may be experimentally detected.

5.1   Summary of the Vector Meson Dominance model

Before the formulation of QCD, hadron physics was deeply investigated through a variety of models incorporating approximate symmetries. The interaction between photons and hadronic matter is a subject of a particular interest in this work that the Vector Meson Dominance model (VMD) can address satisfactorily (for reviews, see [144]). The main idea behind this model is assuming that the quark loops appearing in the vacuum polarization of the photon can be described exclusively by vector mesons. This approximation results to be very accurate in the regions around the vector meson masses. In QED the photon self-energy can be reasonably well approximated using bare propagators and vertices for electron-positron loops due to higher order suppressions. However, the strong coupling of hadronic constituents requires considering the dressing of quark loops in this context.

The success of the principles of quantum field theories in QED led to a formulation of strong interactions based in the same principles. In particular, the notion of conserved currents, the gauge principle and the universality of couplings should be applied to strong-interaction physics. The VMD model was introduced as the theory of the strong interaction mediated by vector mesons and based on a non-abelian Yang-Mills theory [141]. Its simplest realization conceives the hadronic contribution to the photon polarization as a propagating vector meson that replaces the quark loop. This assumption is equivalent to considering the hadronic electromagnetic current operator (in the neutral isotriplet channel) given by the current-field identity

$$j_\mu^{\text{em}}(x)\Big|_{I=1} = \frac{m_\rho^2}{g_\rho}\rho_\mu^0(x) \tag{5.2}$$

is proportional to the vector meson field operator. As the electromagnetic current has null divergence, so will the field ρ_μ, both its neutral and its charged components so $\partial_\mu \vec{\rho}^\mu = 0$. The breaking of gauge invariance due to vector meson masses was ignored

5. VECTOR MESON DOMINANCE APPROACH TO LOCAL PARITY BREAKING

since local gauge transformations were considered as the way to create interactions with universal couplings among nucleons and vector mesons, say $g_\rho \equiv g_{\rho NN} = g_{\rho\pi\pi} = g_{\rho\rho\rho}$.

VMD was particularly successful in the description of the electromagnetic form factors of the nucleons. The nucleon was regarded as a core surrounded by a pion cloud and the form factor measurements were interpreted as an evidence for an isoscalar vector meson ω and for an isovector meson ρ^0 decaying into 3 and 2 pions, respectively. This picture of the nucleon form factors was subsequently generalised to all photon-hadron interactions. Based on the previous considerations, the electromagnetic current was associated to a linear combination of vector meson fields. A complete realization of the VMD model involves other light resonances such as ω and ϕ to be incorporated in the game equivalently to the ρ meson in Eq. (5.2) through the extension of the current-field identity

$$j_\mu^{\mathrm{em}} = \frac{m_\rho^2}{g_\rho}\rho_\mu^0 + \frac{m_\omega^2}{g_\omega}\omega_\mu + \frac{m_\phi^2}{g_\phi}\phi_\mu, \tag{5.3}$$

which generalises Eq. (5.2). With this notation the $SU(3)$ ratios $g_\rho : g_\omega : g_\phi = 1 : 3 : -3/\sqrt{2}$ hold. This treatment implies that the amplitudes of photon interactions are proportional to the corresponding vector meson processes. In this sense, a virtual photon is understood to fluctuate to a vector meson which is the responsible for interactions with hadronic matter. A parallel derivation of the ρ meson coupling can be obtained without any recurrence to gauge invariance.

Another way to derive Eq. (5.3) is from the hadronic electromagnetic current of the SM in terms of the quark fields in the $SU(3)$ representation [145] given by

$$j_\mu^{\mathrm{em}} = \frac{2}{3}\bar{u}\gamma_\mu u - \frac{1}{3}\bar{d}\gamma_\mu d - \frac{1}{3}\bar{s}\gamma_\mu s, \tag{5.4}$$

which can be rewritten identically as

$$j_\mu^{\mathrm{em}} = \frac{1}{\sqrt{2}}j_\mu^\rho + \frac{1}{3\sqrt{2}}j_\mu^\omega - \frac{1}{3}j_\mu^\phi, \tag{5.5}$$

where the vector meson currents can be expressed in terms of their quark content via

$$j_\mu^\rho = \frac{1}{\sqrt{2}}\left(\bar{u}\gamma_\mu u - \bar{d}\gamma_\mu d\right),$$
$$j_\mu^\omega = \frac{1}{\sqrt{2}}\left(\bar{u}\gamma_\mu u + \bar{d}\gamma_\mu d\right),$$
$$j_\mu^\phi = \bar{s}\gamma_\mu s. \tag{5.6}$$

With this definition the matrix element can be expressed as

$$\langle 0|j_\mu^{\mathrm{em}}|V\rangle = \frac{M_V^2}{g_V}\epsilon_\mu^{(V)}, \tag{5.7}$$

where $\epsilon_\mu^{(V)}$ is a polarization vector and $g_\omega \simeq g_\rho \equiv g \simeq 6 < g_\phi \simeq 7.8$ and $M_V^2 = 2g_V^2 f_\pi^2$. We will use this notation for the couplings throughout this analysis.

The fact that the electromagnetic current is made of vector meson fields suggests an underlying lagrangian with a mixing term proportional to $\rho_\mu A^\mu$ but this piece breaks gauge invariance. One of the consistent ways to introduce both gauge invariance and the photon-vector meson mixing is given by the current-mixing form [146] with an explicit mixing of vector mesons and photons both in the mass and kinetic terms. In the limit of universality $g_\rho = g_{\rho\pi\pi} = g_{\rho NN} = \ldots$, an alternative description of VMD can be equivalently used with a mixing of vector mesons with photons in the mass term and a non-trivial photon mass (mass-mixing form) [141]. In any of these formulations the photon remains massless when one computes its propagator to all orders. Despite the second formulation is not as elegant as the first due to a photon mass term, it has been established as the most popular representation of VMD [141, 142]. From now on we will use this representation. Quark-meson interactions are described by [95]

$$\mathcal{L}_{\text{int}} = \bar{q}\gamma_\mu V^\mu q; \quad V_\mu \equiv -eA_\mu Q + \frac{1}{2}g_\omega \omega_\mu \mathbf{I}_q + \frac{1}{2}g_\rho \rho_\mu \lambda_3 + \frac{1}{\sqrt{2}}g_\phi \phi_\mu \mathbf{I}_s, \qquad (5.8)$$

where $Q = \frac{\lambda_3}{2} + \frac{1}{6}\mathbf{I}_q - \frac{1}{3}\mathbf{I}_s$, $\mathbf{I}_q$ and $\mathbf{I}_s$ are the identities in the non-strange and strange sector, respectively; and λ_3 is the corresponding Gell-Mann matrix. Then the Maxwell and mass terms of the VMD lagrangian are

$$\mathcal{L}_{\text{kin}} = -\frac{1}{4}\left(F_{\mu\nu}F^{\mu\nu} + \omega_{\mu\nu}\omega^{\mu\nu} + \rho_{\mu\nu}\rho^{\mu\nu} + \phi_{\mu\nu}\phi^{\mu\nu}\right) + \frac{1}{2}V_{\mu,a}\hat{m}^2_{ab}V_b^\mu,$$

$$\hat{m}^2 = m_V^2 \begin{pmatrix} \frac{4e^2}{3g^2} & -\frac{e}{3g} & -\frac{e}{g} & \frac{\sqrt{2}eg_\phi}{3g^2} \\ -\frac{e}{3g} & 1 & 0 & 0 \\ -\frac{e}{g} & 0 & 1 & 0 \\ \frac{\sqrt{2}eg_\phi}{3g^2} & 0 & 0 & \frac{g_\phi^2}{g^2} \end{pmatrix}, \ \det\left(\hat{m}^2\right) = 0, \qquad (5.9)$$

where $(V_{\mu,a}) \equiv \left(A_\mu, \omega_\mu, \rho_\mu^0 \equiv \rho_\mu, \phi_\mu\right)$ and $m_V^2 \equiv m_\rho^2 = 2g_\rho^2 f_\pi^2 \simeq m_\omega^2$. This matrix reflects the VMD relations at the quark level [141, 142].

The pion form factor $F_\pi(q^2)$ represents the contribution from the intermediate vector mesons connecting the photon to pions in a process like $\gamma \to \pi^+\pi^-$. The form factor is the multiplicative deviation from a point-like behaviour of photon-pion coupling. In the limit of zero momentum transfer $(q^2 \to 0)$, the photon is only affected by the charge of the pions and therefore one expects $F_\pi(0) = 1$. This relation is automatically satisfied by the pion form factor derived from the current-mixing Lagrangian [146] while for the mass-mixing scenario [141], it is necessary to impose universality via $g_\rho = g_{\rho\pi\pi}$. This is the basis of the argument for universality given in [141], where the photon couples to the ρ due to the imposition of local gauge symmetry. Therefore $g_{\rho\pi\pi}$ must equal g_ρ. This is a direct consequence of assuming complete ρ dominance of the form factor.

5.2 Vector Meson Dominance Lagrangian in the presence of P-breaking background

Once we introduced the VMD model in the $SU(3)$ representation, let us recall the arguments given in Chapter 2 about the approximate decoupling of the strange quark flavour from the rest due to intensive left-right oscillations as $m_s \gg \tau_{\text{fireball}}^{-1}$. Hence, even if an axial charge appears in the strange sector, its average will be essentially zero. In addition the role of the ϕ meson is negligible as its typical mean free path ~ 40 fm makes it less sensitive to medium effects. In this sense, we will deal with a non-strange axial chemical potential like in the previous chapters and decouple the strange sector reducing the symmetry of our initial VMD Lagrangian (5.9) from $SU(3)$ to $SU(2)$. This simplification does not introduce significant changes to the Lagrangian except for the reduction of the group matrix λ_3 to τ^3 and the mass matrix

$$\hat{m}^2 = m_V^2 \begin{pmatrix} \frac{10e^2}{9g^2} & -\frac{e}{3g} & -\frac{e}{g} \\ -\frac{e}{3g} & 1 & 0 \\ -\frac{e}{g} & 0 & 1 \end{pmatrix}, \qquad \det(\hat{m}^2) = 0, \tag{5.10}$$

As previously discussed, parity-breaking effects cannot be transmitted to the vector sector by means of an axial chemical potential playing the role of the time component of a spurious axial-vector field. Therefore, we will neglect the mixing among states of different parity and only use the parity-odd Chern-Simons term to include the effect an axial quark charge

$$\mathcal{L}_{\text{CS}} = -\frac{1}{4}\varepsilon^{\mu\nu\rho\sigma} \text{Tr}\left[\hat{\zeta}_\mu V_\nu V_{\rho\sigma}\right] = \frac{1}{2}\text{Tr}\left[\hat{\zeta}\,\epsilon_{jkl}\,V_j\,\partial_k V_l\right] = \frac{1}{2}\,\zeta\,\epsilon_{jkl}\,V_{j,a}\,\hat{N}_{ab}\,\partial_k V_{l,b}, \tag{5.11}$$

where a time-dependent pseudoscalar axion-like background is considered in order to accommodate an axial chemical potential associated to large topological fluctuations (recall Eq. (2.20)). By means of the PCAC (2.13) and the introduction of electromagnetism in the investigation of LPB (5.1) it is possible to relate the gluon and the photon contributions and therefore relate the VMD bosonization with the θ angle appearing in the QCD Lagrangian (2.15). With this definition, the relation $\zeta = N_c\,g^2\mu_5/8\pi^2 \simeq 1.37\mu_5$ holds. The presence of this term in the VMD Lagrangian induces an additional mixing among photons and vector mesons due to LPB. Note that in this chapter, ζ will appear naturally in the vector meson dispersion relation and thus, we will refer to either this magnitude or the axial chemical potential indifferently as they are proportional.

For an isosinglet pseudoscalar background $\hat{\zeta} = 2\zeta/g^2 \mathbf{I}_q$, the mixing matrix reads

$$(\hat{N}^\theta) \simeq \begin{pmatrix} \frac{10e^2}{9g^2} & -\frac{e}{3g} & -\frac{e}{g} \\ -\frac{e}{3g} & 1 & 0 \\ -\frac{e}{g} & 0 & 1 \end{pmatrix} = \frac{(\hat{m}^2)}{m_V^2}\bigg|_{SU(2)_f}, \quad \det(\hat{N}^\theta) = 0. \tag{5.12}$$

5.2 Vector Meson Dominance Lagrangian in the presence of P-breaking background

In the case of an isotriplet pion-like condensate with $\hat{\zeta} = 10\zeta/(3g^2)\tau^3$, the corresponding mixing matrix is

$$
(\hat{N}^\pi) \simeq \begin{pmatrix} \frac{2e^2}{3g^2} & -\frac{e}{g} & -\frac{e}{3g} \\ -\frac{e}{g} & 0 & 1 \\ -\frac{e}{3g} & 1 & 0 \end{pmatrix}, \quad \det\left(\hat{N}^\pi\right) = 0. \tag{5.13}
$$

The VMD coefficients in (5.9), (5.10), (5.12) and (5.13) are obtained from the anomalous Wess-Zumino action [147] and related to the phenomenology of radiative decays of vector mesons [148]. The ratios of matrix elements for an isotriplet condensate in (5.13) are in direct agreement with the experimental decay constants for the processes $\pi^0 \to \gamma\gamma$, $\omega \to \pi^0\gamma$, $\rho^0 \to \pi^0\gamma$ [147] and for the decay $\omega \to \pi\pi\pi$ [145] taken from [134]. Likewise the VMD coefficients in (5.12) can be estimated from the experimental decay constants for the processes $\eta \to \gamma\gamma$, $\eta' \to \gamma\gamma$, $\omega \to \eta\gamma$ and $\rho^0 \to \eta\gamma$ after taking into account a strong $\eta_8 - \eta_0$ mixing [149]. Only the ratio of the decay widths $\omega \to \eta\gamma$, $\rho^0 \to \eta\gamma$ is a little sensitive to the mixing and confirms the off-diagonal elements of (5.12). Armed with the above information one can easily determine the modifications on the vector meson spectrum and their eventual relevance.

With an isosinglet μ_5 the mass-shell equations for vector mesons read

$$
K^{\mu\nu}_{ab} V_{\nu,b} = 0; \quad k^\nu V_{\nu,b} = 0, \quad K^{\mu\nu} \equiv g^{\mu\nu}(k^2\mathbf{I} - \hat{m}^2) - k^\mu k^\nu \mathbf{I} + i\varepsilon^{\mu\nu\rho\sigma}\zeta_\rho k_\sigma \hat{N}^\theta \tag{5.14}
$$

and select three physical polarizations vectors $(\varepsilon_+, \varepsilon_-, \varepsilon_L)$ for massive vector fields that couple to conserved fermion currents. Following the lines of [104] let us now define

$$
S^\nu_\lambda \equiv \varepsilon^{\mu\nu\alpha\beta}\zeta_\alpha k_\beta \, \varepsilon_{\mu\lambda\rho\sigma}\zeta^\rho k^\sigma, \tag{5.15}
$$

which satisfies the following properties

$$
S^\nu_\lambda \zeta^\lambda = S^\nu_\lambda k^\lambda = 0, \quad S^{\mu\nu}S_{\nu\lambda} = \frac{S}{2}S^\mu_\lambda, \quad S = S^\nu_\nu = 2[(\zeta \cdot k)^2 - \zeta^2 k^2]. \tag{5.16}
$$

For a time-like and spatially isotropic pseudoscalar condensate we find $S = 2\zeta^2 \vec{k}^2 > 0$. It is convenient to introduce the two orthonormal hermitian projectors

$$
P^{\mu\nu}_\pm \equiv \frac{S^{\mu\nu}}{S} \pm \frac{\mathrm{i}}{\sqrt{2S}}\varepsilon^{\mu\nu\alpha\beta}\zeta_\alpha k_\beta, \tag{5.17}
$$

which satisfy the following properties:

$$
P^{\mu\nu}_\pm \zeta_\nu = P^{\mu\nu}_\pm k_\nu = 0, \quad g_{\mu\nu}P^{\mu\nu}_\pm = 1,
$$
$$
P^{\mu\lambda}_\pm P_{\pm\lambda\nu} = P^\mu_{\pm\nu}, \quad P^{\mu\lambda}_\pm P_{\mp\lambda\nu} = 0, \quad P^{\mu\nu}_+ + P^{\mu\nu}_- = \frac{2}{S}S^{\mu\nu}. \tag{5.18}
$$

A pair of complex and space-like chiral polarization vectors can be constructed by means of a constant and space-like 4-vector ϵ^μ in such a manner that we can set

$$
\varepsilon^\mu_\pm(k) \equiv \left[\frac{\vec{k}^2 - (\epsilon \cdot k)^2}{2\vec{k}^2}\right]^{-1/2} P^{\mu\nu}_\pm \epsilon_\nu, \tag{5.19}
$$

5. VECTOR MESON DOMINANCE APPROACH TO LOCAL PARITY BREAKING

which satisfy the orthogonality relations

$$- g_{\mu\nu} \, \varepsilon_\pm^{\mu\,*}(k) \, \varepsilon_\pm^\nu(k) = 1, \qquad g_{\mu\nu} \, \varepsilon_\pm^{\mu\,*}(k) \, \varepsilon_\mp^\nu(k) = 0, \tag{5.20}$$

as well as the closure relation

$$\varepsilon_+^{\mu\,*}(k) \, \varepsilon_+^\nu(k) + \varepsilon_-^{\mu\,*}(k) \, \varepsilon_-^\nu(k) \; + \; \text{c.c.} = -\frac{4}{S} \, S^{\mu\nu}. \tag{5.21}$$

The longitudinal polarization ε_L^μ is orthogonal to k_μ and to ζ_μ

$$\varepsilon_L^\mu = \frac{\zeta^\mu k^2 - k^\mu(\zeta \cdot k)}{\sqrt{k^2\big((\zeta \cdot k)^2 - \zeta^2 k^2\big)}}, \quad \varepsilon_L \cdot \varepsilon_L = -1, \tag{5.22}$$

for $k^2 > 0$. Its projector can be easily found through the relation

$$\sum_\epsilon P_\epsilon^{\mu\nu} = g^{\mu\nu} - \frac{k^\mu k^\nu}{k^2} \quad \implies \quad P_L^{\mu\nu} = g^{\mu\nu} - \frac{k^\mu k^\nu}{k^2} - 2\frac{S^{\mu\nu}}{S} \tag{5.23}$$

where the sum in ϵ is understood to be performed over all the physical polarizations. The expression of a projector as a function of the polarization vectors is given by

$$\varepsilon_\epsilon^\mu \varepsilon_{\epsilon'}^{*\nu} = -P_\epsilon^{\mu\nu} \delta_{\epsilon\epsilon'}. \tag{5.24}$$

Taking into account the relations (5.18) we may rewrite (5.14) as

$$K^{\mu\nu}\varepsilon_\nu(k) = \left(g^{\mu\nu}(k^2 \mathbf{I} - \hat{m}^2) - k^\mu k^\nu \mathbf{I} + \sqrt{(\zeta \cdot k)^2 - \zeta^2 k^2} \, \left(P_+^{\mu\nu} - P_-^{\mu\nu} \right) \hat{N}^\theta \right) \varepsilon_\nu(k) = 0. \tag{5.25}$$

The mass spectrum can be found after simultaneous diagonalization of $\hat{m}^2|_{SU(2)} \propto \hat{N}^\theta$ with $\zeta_\mu \simeq (\zeta, 0, 0, 0) = \text{constant}$

$$\hat{N} = \text{diag}\left[0,\, 1,\, 1 + \frac{10e^2}{9g^2}\right] \simeq \text{diag}\left[0,\, 1,\, 1\right],$$

$$\hat{m}^2 = m_V^2 \, \text{diag}\left[0,\, 1,\, 1 + \frac{10e^2}{9g^2}\right] \simeq m_V^2 \, \text{diag}\left[0,\, 1,\, 1\right].$$

We notice that in the case of pure isosinglet pseudoscalar background, a null eigenvalue is found corresponding to massless photons that are not distorted by the mixing with massive vector mesons or the parity-breaking effect.

In turn massive vector mesons do exhibit a distortion due to the violation of parity. Due to the orthogonality of the longitudinal polarization vector ε_L to the $\pm$ projectors (5.18), its mass is the same as in vacuum. However, the transversal polarizations satisfy

$$K^\mu_\nu \varepsilon_\pm^\nu = \left(k^2 \mathbf{I} - \hat{m}^2 \pm \sqrt{(\zeta \cdot k)^2 - \zeta^2 k^2} \, \hat{N} \right)\varepsilon_\pm^\mu; \quad m_{V,\pm}^2 \equiv k_0^2 - \vec{k}^2 = m_V^2 \mp \zeta|\vec{k}|. \tag{5.26}$$

We may combine the longitudinal and transverse polarizations into a unique expression [95]

$$m_{V,\epsilon}^2 = m_V^2 - \epsilon\zeta|\vec{k}|, \tag{5.27}$$

where ϵ accounts for the polarization of the vector meson ($\epsilon = \pm 1$ for the transverse polarizations and $\epsilon = 0$ for the longitudinal one). The breaking of Lorentz invariance through the 3-momentum dependence in the dispersion relation is due to the time-dependent background. The parity-breaking effect is unambiguously reflected in the polarization dependence of masses $m_{V,+}^2 < m_{V,L}^2 < m_{V,-}^2$. For large enough $|\vec{k}| \geq m_V^2/\zeta$ ($\simeq 1.5$ GeV for $\zeta = 400$ MeV corresponding to $\mu_5 \approx 290$ MeV) vector meson states with positive polarization become tachyons in the same way we observed in the scalar sector in Chapter 4. However their group velocity remains less than the speed of light provided that $\zeta < 2m_V \approx 1.6$ GeV. For higher values of ζ the vacuum state becomes unstable, namely, polarization effects give an imaginary part for the vacuum energy. However, this threshold is much above the scales we are considering to obtain a stable parity-breaking phase as we showed in Chapter 3. Note that the position of the resonance poles for $\pm$ polarized mesons is moving with wave vector $|\vec{k}|$. Therefore they appear as broadened resonances, leading to an enhancement of their spectral function away from their nominal vacuum resonance position and a reduction at the very peak. In this work we will only consider $|\zeta|$ since a change of sign simply interchanges the $\pm$ polarizations but does not affect the separation of the polarization-dependent vector meson masses.

5.3   Dilepton production rate in a P-breaking medium

In this section we want to link the in-medium modifications of vector mesons with the phenomenology associated to them. Our aim consists in finding possible experimental signatures of parity violation effects through the decays of such distorted vector mesons. Hadronic decays may be severely distorted due to the new dispersion relations of scalar and pseudoscalar mesons as we discussed in Chapter 4. The cleanest way to extract reliable properties of in-medium vector mesons is through their electromagnetic (rather than strong) interactions. In what follows we will consider the modifications in the dilepton spectrum due to the ρ and ω decays.

The dilepton production from the $V(k) \to \ell^-(p)\ell^+(p')$ decays is governed by

$$\frac{dN_V}{dM} = \int \frac{d\tilde{M}}{\sqrt{2\pi}\Delta} \exp\left[-\frac{(M-\tilde{M})^2}{2\Delta^2}\right] c_V \frac{\alpha^2}{24\pi^2\tilde{M}} \Theta(\tilde{M} - n_V m_\pi) \left(1 - \frac{n_V^2 m_\pi^2}{\tilde{M}^2}\right)^{3/2}$$

$$\times \int \frac{d^3\vec{k}}{E_k} \frac{d^3\vec{p}}{E_p} \frac{d^3\vec{p}'}{E_{p'}} \delta^4(p + p' - k) \sum_\epsilon \frac{m_{V,\epsilon}^4 \left(1 + \frac{\Gamma_V^2}{m_V^2}\right)}{\left(\tilde{M}^2 - m_{V,\epsilon}^2\right)^2 + m_{V,\epsilon}^4 \frac{\Gamma_V^2}{m_V^2}}$$

$$\times P_\epsilon^{\mu\nu}(\tilde{M}^2 g_{\mu\nu} + 4p_\mu p_\nu) \frac{1}{e^{\tilde{M}_T/T} - 1}, \tag{5.28}$$

5. VECTOR MESON DOMINANCE APPROACH TO LOCAL PARITY BREAKING

where $V = \rho, \omega$ and $n_V = 2, 0$ respectively[1], and $\tilde{M} > n_V m_\pi$. Note that the coupling to pions is only relevant for the position of the threshold and therefore we do not complicate the calculations by considering distorted pions as in the previous chapter. A dilepton invariant mass smearing of width Δ is taken into account to relate the measured M with the physical $\tilde{M}$. From now on this smearing will be omitted (together with dropping the tilde of $\tilde{M}$) for the sake of simplicity but considered in our numerical calculations. M_T is the transverse mass $M_T^2 = M^2 + \vec{k}_T^2$ where $\vec{k}_T$ is the vector meson transverse momentum and M is the dilepton invariant mass. The projectors $P_\epsilon^{\mu\nu}$ have been detailed in (5.18). p and p' correspond to the lepton and anti-lepton momenta. A Boltzmann distribution is included with an effective temperature T [47, 150] that may in fact depend on the range of M, p_T and centrality. A simple thermal average is appropriate only for central collisions and moderate values of p_T. No serious attempt will be made here to extrapolate to peripheral processes, but an appropriate mixture of distorted and non-distorded vector mesons should be adequate. The constants c_V normalize the contribution of the respective resonances parametrizing in an effective way their total cross sections. Since they are not known with precision, particularly their off-shell values, the relative weights are used as free parameters in the 'cocktail' of hadronic sources used to fit the experimental data [45, 46, 47, 79, 83]. The usual 'cocktail' contains weights normalized to the peripheral collisions result (roughly agreeing with existing pp and p-nucleus data). Finally, modified form factors due to LPB are included according to our previous discussion.

In order to make our plots meaningful we should implement some values relevant for the main HIC experiments. A prediction of the parity-breaking effect for the NA60 experiment is certainly appealing. However, their earlier results [83] are not corrected for the detector acceptance and therefore a valid comparison with our theoretical predictions cannot be done. Their newest data [86, 151] are already acceptance corrected but they do not exactly correspond to the same variables we are describing. For these reasons, we will compare our results with NA60 data but we understand that this is a crude connection.

The temperature appearing in the previous formula is not the 'true' temperature of the hadron gas; it rather corresponds to the effective temperature T_{eff} of the hadrons that best describes the slope of the multipliplicity distribution $d^3N/dp^3(M_T)$ for a given range of invariant masses. In fact, one should not confuse the theoretical and the phenomenological approaches for the calculation of multiplicities in ultra-relativistic collisions. The first one is the direct contribution to the invariant one-particle multiplicity distribution given by

$$\frac{1}{M_T}\frac{dN}{dy\,dM_T} = AE\int_V d^3x \exp\left[-\frac{p\cdot u(x)}{T}\right] = AE\int_V d^3x \exp\left[-\frac{\gamma(x)[E - \vec{p}\,\vec{u}(x)]}{T}\right],$$
(5.29)

where T is the real temperature, A is an arbitrary normalization constant and $u(x)$ corresponds to the collective 4-velocity. The (phenomenological) transverse one-particle

---

[1]$n_\omega = 0$ is taken since we do not include the threshold to 3 pions.

multiplicity distribution depends on the specific type of particle and reaction and is governed by a simpler expression

$$\frac{1}{M_T}\frac{dN}{dy\ dM_T} = A' \exp\left(-\frac{M_T}{T_{\text{eff}}}\right), \tag{5.30}$$

T_{eff} being an effective temperature or slope parameter and A' a different arbitrary normalization constant. In the limit where the particle velocity is large compared an average collective velocity v and specializing to the transverse direction, one may neglect the pre-exponential energy dependence and obtain the relation among the two temperatures [152]

$$T_{\text{eff}} = \frac{M_T}{M_T - p_T v}\sqrt{1-v^2}\,T. \tag{5.31}$$

For massless particles, this expression is reduced to

$$T_{\text{eff}} = \sqrt{\frac{1+v}{1-v}}\,T. \tag{5.32}$$

For a typical value of an average transverse collective velocity $v = 0.4c$, a temperature $T = 150$ MeV leads to an effective temperature (or slope) of the order of $T_{\text{eff}} \simeq 230$ MeV. Obviously $T_{\text{eff}} > T$ and therefore it is quite possible that T_{eff} exceeds the deconfinement temperature while one is still dealing with hadrons.

NA60 has obtained accurate results for the ρ spectral function [46, 83] by measuring the $\mu^+\mu$ spectrum with unprecedented precision and by carefully subtracting the contributions from the 'cocktail' except the ρ itself. If one implements the NA60 acceptance with an experimental cut in rapidity ($3.3 < y < 4.3$ in the laboratory frame which is translated to $0.42 < y < 1.42$ in the center of mass frame where we work) together with a temperature $220 \lesssim T \lesssim 300$ MeV [46, 83] (for all p_T), we obtain a ρ spectral function similar to the experimental one using $m_\rho = 750$ MeV. In Fig. 5.1 (left) we show two plots with $\mu_5 = 300$ MeV and $T = 220, 300$ MeV in order to compare them with experimental data (right). Of course, other explanations for such distortion [38, 39, 40, 78] would need to be also considered if one attempted to reproduce the data.

The noticeable discrepancy below $M \lesssim 600$ MeV may be due to a broad variety of facts. First, we recall that NA60 data are not corrected for the detector acceptance, subject that we did not pursue and therefore, strict comparison is misleading. Next, thermal effects inducing ρ broadening and other effects have not been accounted for. And finally, it may be revealing that the upper kinematical limit for the Dalitz process $\omega \to \mu^+\mu^-\pi^0$ is 643 MeV, suggesting that this process could play a significant role as its contribution is subtracted from the total dilepton yield assuming a vacuum contribution. In fact, Dalitz decays are thought to take place after hadron freezout and therefore they should not be affected by in-medium effects, but the possibility that the parity-breaking phase still survives at lower temperatures is an interesting subject to be explored. We address this possibility in Appendix B.

## 5. VECTOR MESON DOMINANCE APPROACH TO LOCAL PARITY BREAKING
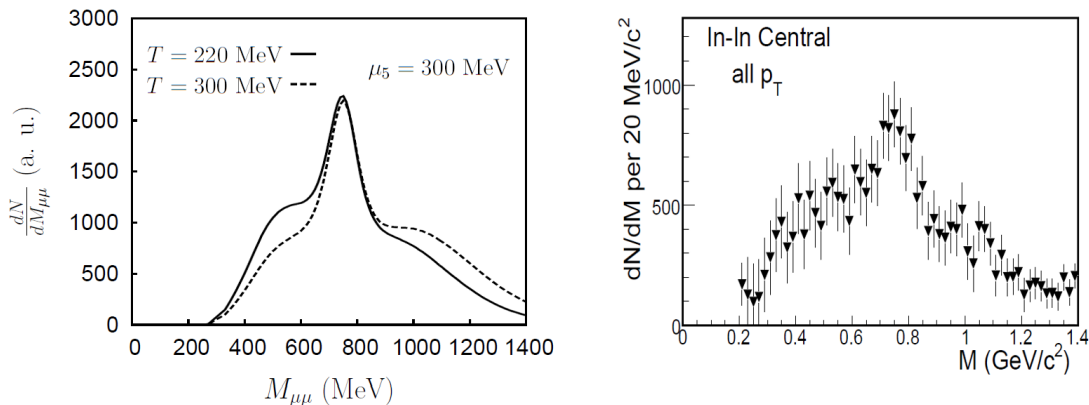
Figure 5.1: The ρ spectral function is presented depending on the invariant mass M with $\mu_5 = 300$ MeV and $T = 220, 300$ MeV (left). For comparison NA60 experimental data [46, 83] is shown in the right panel. Experimental results are not corrected for NA60 experimental acceptance. We use arbitrary units in our fit.

Another remarkable consideration that can also be extracted from Fig. 5.1 is the dilepton production near the threshold. While in our computation we implemented the two-pion threshold that corresponds to $2m_\pi \approx 280$ MeV, the experimental data seem to reflect a different behaviour showing a threshold due to the muon mass corresponding to $2m_\mu \approx 210$ MeV. The presence of dimuon events within these two values could entail the disappearance of the in-medium two-pion threshold. In any case, the main results of our work are not affected by this subtlety.

We will implement now the experimental cuts of the PHENIX experiment ($p_T > 200$ MeV and $|y_{ee}| < 0.35$ in the center of mass frame) and $T \simeq 220$ MeV together with a Gaussian invariant mass smearing of width 10 MeV [47, 153]. We have not implemented the single electron cut $|y_e| < 0.35$ because in practice it makes no visible difference with simply imposing a cut on the dilepton pair momentum as a whole but we will check this issue explicitly more below. The value of the temperature is extracted from the measurement of direct photons, but it has to be understood as a representative value. In fact, NA60 reports even higher temperatures when the ρ spectral function is decomposed into the peak and the continuum contributions [46, 83]. Note that with such value for the effective temperature, vector mesons with high energy will be produced with very low probability like the tachyonic states with $+$ transverse polarization which require at least $|\vec{k}| > 1.5$ GeV.

Then one is lead to the dilepton production result that is shown in Figure 5.2, where the ρ spectral function is presented together with the separate contributions of each polarization for $\zeta = 400$ MeV (corresponding to $\mu_5 = 290$ MeV) and a comparison with $\zeta = 0$ (no LPB). The $\pm$ transversely polarized mesons exhibit two different peaks aside the vacuum resonance. Their combination with the longitudinal polarization results in a distorted spectral function that could be experimentally measured.
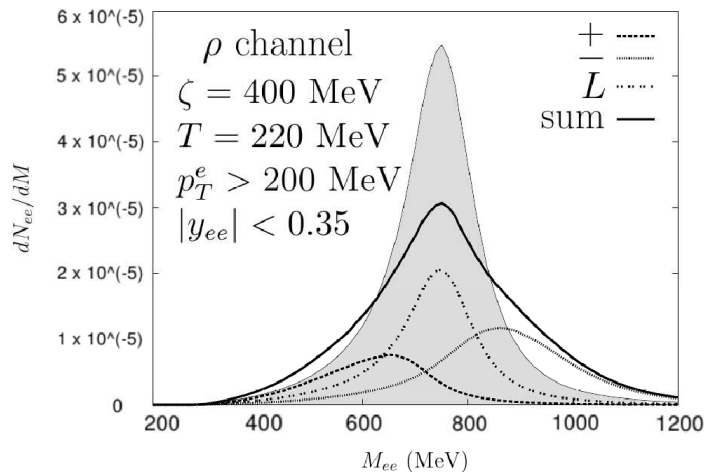
Figure 5.2: The polarization splitting of the ρ contribution to dilepton production is shown for LPB with $\zeta = 400$ MeV ($\mu_5 \simeq 290$ MeV). The comparison with a parity-even medium with $\zeta = 0$ (shaded region) is presented. The vertical units are taken to coincide with PHENIX experimental data [47], as well as experimental detector cuts and temperature.

A remarkable feature of the ρ spectral function in Fig. 5.2 is the polarization asymmetry observed aside the vacuum peak. Longitudinally polarized mesons seem to dominate the vacuum peak while the transverse ones are more important in the vicinity of the resonance. Therefore a measure of dilepton polarization event-by-event could reveal in an unambiguous way the existence of LPB, confirming the hypothesis of pseudoscalar condensate formation in HIC. We will come back to this important characteristic in Section 5.4 where we will deeply investigate how this effect may be experimentally detected. Let us stress that similar results may be obtained modifying ζ so when it increases, the circularly polarized peaks appear more separated from the vacuum one. If the effective temperature T increased, we would see an enhancement of the upper mass tail. However, the main qualitative results from this plot are not affected by (reasonable) temperature modifications.

The simulation of ω meson production [154] shows that a significant fraction of them decay inside of the nuclear fireball and therefore LPB distorted ω mesons may also play a significant role in this game. In Fig. 5.3 the separate contributions of ρ and ω are presented for $\zeta = 400$ MeV to be compared with their vacuum results. An enhancement factor 1.8 is included for the ratio ρ/ω in central HIC, particularly at low p_T. This enhancement is due to the ρ meson regeneration into pions within the fireball (a plausible consequence of the 'ρ clock' effect [151, 155]) and the in-medium ω suppression [156]. There are no published reports of a direct determination of the ρ/ω ratio at PHENIX and we have decided to use the above value that is very close to the average value for the ratio of the respective cross sections reported by NA60 [83]. We note that the η/ω ratios measured both by NA60 and PHENIX collaborations

roughly agree. Note too that due to the assumed effective thermal distribution and the
fact that the ρ and ω are nearly degenerate in mass the ratio c_ρ/c_ω is identical to the
ratio of the respective cross-sections. However it should be stated right away that our
conclusions do not depend substantially on the precise value of the ratio c_ρ/c_ω.
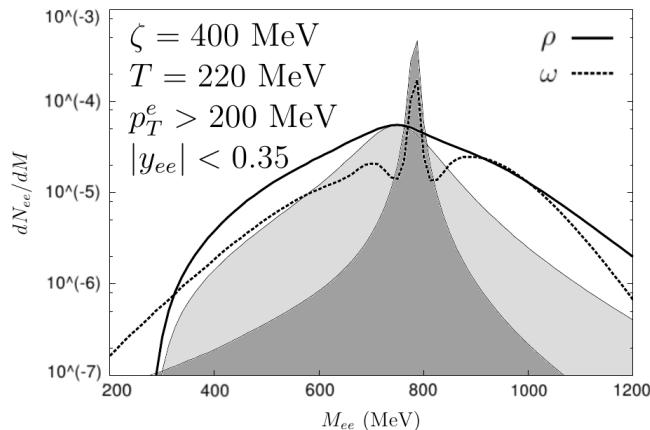

Figure 5.3: The in-medium contribution in the ρ and ω channels (solid and dashed line,
respectively) is presented for $\zeta = 400$ MeV together with their vacuum contributions (light
and dark shaded regions, respectively). The in-medium ρ yield is enhanced by a factor 1.8
(see text). The vertical units are taken to coincide with PHENIX experimental data [47],
as well as experimental detector cuts and temperature.

The parity-breaking effect shows an important increase in the dilepton production
away from the $\rho-\omega$ peak due to the mass shifting of the circularly polarized resonances.
Such enhancement suggests the appealing possibility of perhaps partially explaining the
abnormal dilepton yield found in central HIC at low p_T in the low invariant mass region
quoted by PHENIX and STAR [46, 47]. However, direct comparison with PHENIX or
STAR experimental data is not possible due to the lack of results for the ρ and ω spectral
functions. The measurement of the PHENIX dielectron continuum has a much poorer
precision compared to NA60 and a numerical subtraction of the 'cocktail' sources in
order to determine different individual contributions is meaningless. In this sense, the
only possible comparison of our results with PHENIX data consists in removing the
vector meson contributions included in the 'cocktail' and replace them by the distorted
spectral functions previously presented. We will only focus in the region near the $\rho-\omega$
resonance peak. Fig. 5.4 shows the predicted e^+e yield by the 'cocktail' of hadronic
sources without any parity-breaking effect and for local parity breaking with $\mu_5 = 150$
and 300 MeV as well as PHENIX experimental data. As already stressed, we apply an
enhancement factor 1.8 to the ratio ρ/ω and the ω is normalized to fit the resonance
peak. The precision of the data does not allow for clear conclusions but it is clear
that LPB noticeably improves the agreement to the data as compared to the 'cocktail'.
In addition, if the ω peak was accurately measured, we could provide a more definite
prediction of our results, i.e., we normalized the peak to coincide with 'cocktail', which

might not coincide with the experiment. Finally, in the inset of Fig. 5.4 we present the ρ spectral function for the same values of μ_5, which has notably increased as compared to the vacuum case.
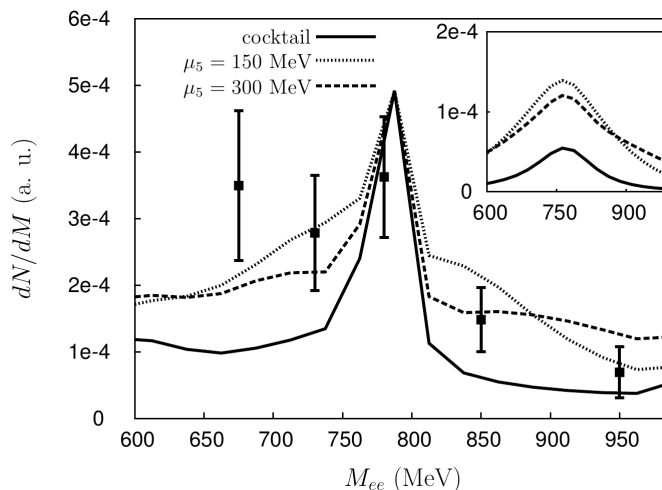
Figure 5.4: The meson contribution to dilepton production is shown for parity symmetric nuclear matter $\mu_5 = 0$ (solid line) and for local parity breaking with $\mu_5 = 150$ and 300 MeV (dotted line and discontinuous line, respectively) compared to the PHENIX measurements for $p_T^e > 200$ MeV, $|y_{ee}| < 0.35$ and $T = 220$ MeV. The $\mu_5 = 0$ line is just the 'cocktail' contribution as quoted by PHENIX [157]. The $\mu_5 \neq 0$ results show an enhancement of the / ratio by a factor 1.8 (see text) normalizing the ω contribution to fit the 'cocktail' peak. Data for $M < 650$ MeV is not shown as the contribution from Dalitz processes has not been included and they are expected to be relevant. Inset: the ρ spectral function for the same values of the axial chemical potential is compared to the cocktail one with the same assumptions.

Dileptons are produced in a variety of decays. The dominant processes in the range of invariant masses 200 MeV $< M <$ 1200 MeV are assumed to be the ρ and ω decays into lepton pairs, the $\omega \to \pi^0 \ell^+ \ell^-$ Dalitz decay and the $\eta, \eta' \to \gamma \ell^+ \ell^-$ Dalitz decays. These are the basic ingredients of the hadronic 'cocktail' [38, 46, 47], conventionally used to predict the dilepton yield[2]. Naturally, the dispersion relations of ρ, ω, etc. are modified due to conventional in-medium thermal effects such as a dropping mass and/or broadening resonance. These investigations claim to explain the abnormal dilepton yield but the issue is still unclear and it may not be excluded that the distortion due to parity breaking may play a role.

We have to retain the very important point that a number of light hadronic states will be in thermal equilibrium (so their respective abundances will be governed by the Boltzmann distribution) and regeneration of these resonances will take place in the fireball similarly to the one taking place for ρ mesons. They will be much more

---

[2]In addition there is a substantial $c\bar{c}$ background that is not affected by the present considerations.

abundant in the fireball if there is LPB and the decays of these resonances could be an important source of dileptons so far unaccounted for.

The Dalitz processes are described by the Kroll-Wada formula [158] that includes the contribution of vector mesons and it remains valid in the case of LPB provided that we replace the vector meson masses by the values in (5.26) according to the intermediate meson polarization $(L, \pm)$. The fact that the decaying meson is distorted by the medium complicates analytically and numerically the calculation due to the lack of Lorentz invariance generated by a polarization and momentum dependent meson mass. We address the calculations of Dalitz decays in Appendix B.

5.4 Dilepton polarization analysis in $V \to \ell^+\ell^-$ decays

In this section we want to address a careful analysis of the polarization distribution associated to the lepton pairs produced in the decay of vector mesons. Motivated by the results from Fig. 5.2 where a clear polarization asymmetry was found aside the ρ vacuum resonance peak, we will study the angular distribution of the outgoing leptons searching for polarization dependences.

Current angular distribution analysis [159, 160] are not the most suitable way to extract all the information related to the parity-breaking effects we present [161]. First, they omit the non-trivial dependence on M where one could be able to see the resonances associated to the transverse polarized mesons. And second, the usual angular variables considered are not able to isolate the different polarizations. We will perform a two-dimensional study of the decay product with the dilepton invariant mass M and a certain angle that we will introduce below. Our aim is to elucidate which other angular variables of the decay process should be taken into account when experimental data is analysed.

From now on the overall constants c_V in Eq. (5.28) are chosen in such a way that after integrating the entire phase space the total production at the vacuum resonance peak is normalized to 1 unless otherwise is stated. This choice will help us to quantify the number of events found when the phase space is restricted in the following discussion. We define the normalized number of events as

$$N_\theta(M) = \frac{\int_{\Delta\theta} \frac{dN}{dM\,d\cos\theta}(M, \cos\theta)\, d\cos\theta}{\int_{-1}^{+1} \frac{dN}{dM\,d\cos\theta}(M = m_V, \cos\theta)\, d\cos\theta}, \tag{5.33}$$

being θ one of the two different angular variables that we will consider in the next sections.

5.4.1 Case A

The first variable we will investigate is the angle θ_A between the two outgoing leptons in the laboratory frame. Some basic algebraic manipulations lead us from Eq. (5.28)

to

$$\frac{dN_V}{dM d\cos\theta_A} = c_V \frac{\alpha^2}{6\pi M} \left(1 - \frac{n_V^2 m_\pi^2}{M^2}\right)^{3/2} \int \frac{p^2 p'^2 dp d\cos\theta d\phi}{E_p \sqrt{(M^2 - 2m_\ell^2)^2 - 4m_\ell^2(E_p^2 - p^2 \cos^2\theta_A)}}$$

$$\sum_\epsilon \frac{m_{V,\epsilon}^4 \left(1 + \frac{\Gamma_V^2}{m_V^2}\right)}{\left(M^2 - m_{V,\epsilon}^2\right)^2 + m_{V,\epsilon}^4 \frac{\Gamma_V^2}{m_V^2}} P_\epsilon^{\mu\nu}(M^2 g_{\mu\nu} + 4p_\mu p_\nu) \frac{1}{e^{M_T/T} - 1}, \quad (5.34)$$

where θ is the angle between p and the beam axis (not to be confused with θ_A previously defined) and ϕ is the azimuthal angle of p' with respect to p. The lepton energies are given by $E_p^2 - p^2 = E_{p'}^2 - p'^2 = m_\ell^2$ and $p' = |\vec{p}'|(\theta_A, p, M, m_\ell)$ can be found from the decay kinematics that lead to the following equation:

$$E_p E_{p'} - pp' \cos\theta_A = \frac{M^2}{2} - m_\ell^2. \quad (5.35)$$

In the left panels of Fig. 5.5 we present the results of the dilepton production in the ρ channel as a function of its invariant mass M integrating small bins of $\Delta \cos\theta_A = 0.2$. The different curves displayed in the plot correspond to $\cos\theta_A \in [-0.2, 0], [0, 0.2], [0.2, 0.4], [0.4, 0.6]$ and $[0.6, 0.8]$. The upper panel corresponds to the vacuum case with $\mu_5 = 0$ while the lower one represents a parity-breaking medium with $\mu_5 = 300$ MeV. The LPB effect produces a secondary peak corresponding to a transverse polarization in the low invariant mass region in addition to the vacuum resonance. This graphic does not imply a larger abundance of transversely polarized mesons with respect to the longitudinal ones but the fact that transverse mesons can be selected (and almost isolated) with a suitable angular coverage. If the effective temperature T increased, we would see an enhancement of the upper mass tail making the secondary peak smaller in comparison to the vacuum one. As $\cos\theta_A$ increases, the outgoing leptons are more collimated, meaning a higher meson 3-momentum and from the dispersion relation in Eq. (5.27), a larger separation between the two peaks together with a Boltzmann suppression. Note that the highest peaks in the figures with $\mu_5 \neq 0$ have a value $\simeq 0.1$, this is a 10% of the total production at the vacuum peak when the total phase space is considered (except for the detector cuts). We took a representative value $\mu_5 = 300$ MeV so as to show two different visible peaks. If the axial chemical potential acquires smaller values, the secondary peak approaches the vacuum one. The smaller μ_5 is taken, the more collinear the leptons have to be in order to obtain a large meson momentum and thus, a visible and significant secondary peak (recall Eq. (5.27)).

Dealing with quantities smaller than 10% may be tricky. As the main information related to LPB is focused in $\cos\theta_A \approx 1$, in the right panels of Fig. 5.5 we show a somewhat more experimentally oriented set of plots where we integrated $\cos\theta_A$ down to -0.2, 0, 0.2 and 0.4. The upper panel corresponds to vacuum and the lower one represents a parity-breaking medium with $\mu_5 = 300$ MeV. The number of events grows when more
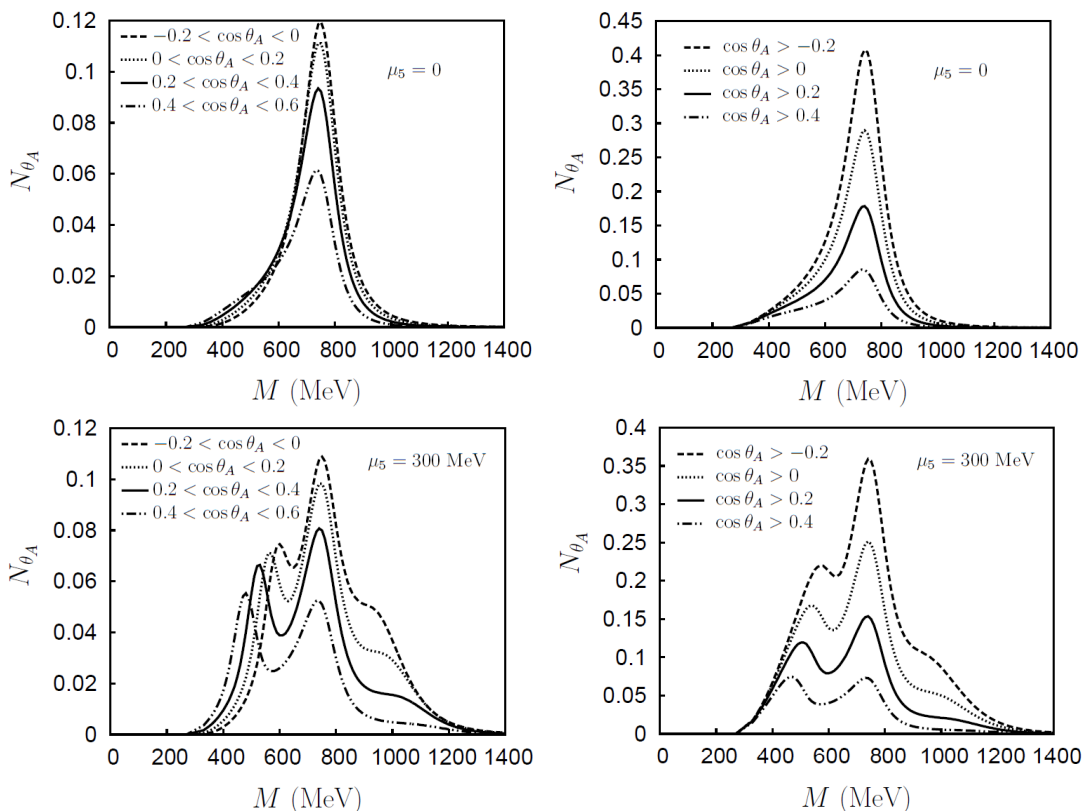
Figure 5.5: The ρ spectral function is presented depending on the invariant mass M in vacuum ($\mu_5 = 0$) and in a parity-breaking medium with $\mu_5 = 300$ MeV (upper and lower panels, respectively) for different ranges of the angle between the two outgoing leptons in the laboratory frame θ_A. We display the curves corresponding to $\cos\theta_A \in [-0.2, 0], [0, 0.2], [0.2, 0.4], [0.4, 0.6]$ and $[0.6, 0.8]$ in the left panels, and $\cos\theta_A \geq -0.2, 0, 0.2, 0.4$ in the right ones. The total production at the vacuum peak is normalized to 1 when the entire phase space is considered. Results are presented for the experimental cuts quoted by PHENIX [47].

and more separated leptons are considered but the secondary peak smears and becomes much less significant. Therefore, an optimization process should be performed in every different experiment so as to find the most suitable angular coverage.

At this point, we recover the discussion about introducing a realistic cut in single-electron rapidity. In principle, all accelerator experiments have to account for this cut (independently on the particle type) in order not to accumulate a large number of tracks and energy amounts in the forward direction that would be rather tricky to isolate. However, for the PHENIX experiment there is no clear information about this cut [47] and therefore we decided to omit it. In Fig. 5.6 we show one of the curves already presented in Fig. 5.5 including a single-electron cut $|y_e| < 0.35$ and without it. One may observe that the qualitative behaviour already discussed holds if this cut

is added. In fact, the vacuum peak slightly decreases whereas the secondary peak due to LPB does not substantially change. Indeed, this small distortion does not affect the results already explained regarding the ρ spectral function measured by NA60 or the improvement of the PHENIX cocktail.
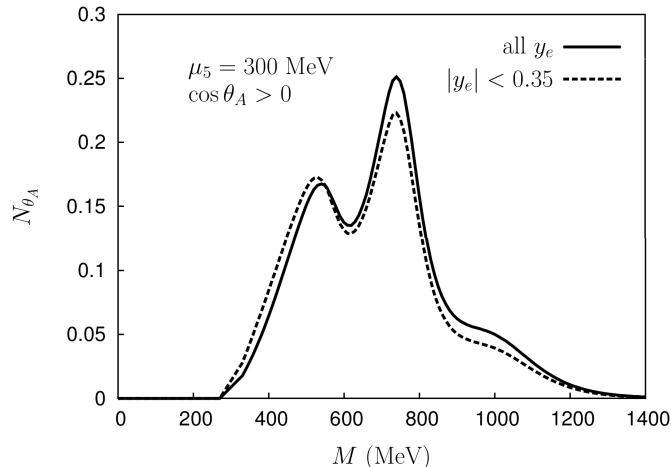
Figure 5.6: One of the curves presented in Fig. 5.5 is displayed (solid line) together with its modification when an additional single-electron cut $|y_e| < 0.35$ is included (dashed line). No significant changes are observed concerning the significance of the secondary peak that appears due to a non-trivial μ_5.

Another issue that could be experimentally addressed is the analysis of μ_5 for a particular (and fixed) coverage of θ_A. If the secondary peaks due to the transversally polarized mesons were found, their positions would be an unambiguous measurement of μ_5 (more precisely, $|\mu_5|$). In Fig. 5.7 we integrate the forward direction of the two outgoing leptons, i.e. $\cos\theta_A \geq 0$, and examine how the transverse polarized peaks move with respect to the vacuum one when we change the values of the axial chemical potential. The ρ and ω spectral functions are displayed in the upper panels for $\mu_5 = 100$, 200 and 300 MeV. The same tendency is found in both graphics except for the fact that both transverse peaks are observed in the ω channel (one below and one above the vacuum resonance). For small values like $\mu_5 \simeq 100$ MeV the vacuum peak hides the transverse one due to the ρ width, being impossible to discern if one or two resonances are present. In the ω channel all the peaks are visible even for such small μ_5. The latter channel could be the most appropriate one in order to search for polarization asymmetry. For completeness, we also present their combination in the lower panel normalized to PHENIX data. The normalized number of events are defined in this case as

$$N_\theta^{\text{PH}}(M) = \frac{dN^{\text{PH}}}{dM}\left(M = m_V\right) \frac{\int_{\Delta\theta_A} \frac{dN}{dM d\cos\theta}\left(M, \cos\theta\right) d\cos\theta}{\int_{-1}^{+1} \frac{dN}{dM d\cos\theta}\left(M = m_V, \cos\theta\right) d\cos\theta}, \qquad (5.36)$$

where $\frac{dN^{\text{PH}}}{dM}(M)$ is the theoretical spectral function used in the PHENIX hadronic

cocktail. As it was discussed in Section 5.3 an enhancement factor 1.8 is included for the ratio ρ/ω due to the ρ meson regeneration into pions within the HIC fireball [151, 155] and the in-medium ω suppression [156]. As already mentioned, our conclusions do not depend substantially on the precise value of this ratio as the experimental signal that we propose is amply dominated by the ω when the two resonances are considered together (see. Fig. 5.7).
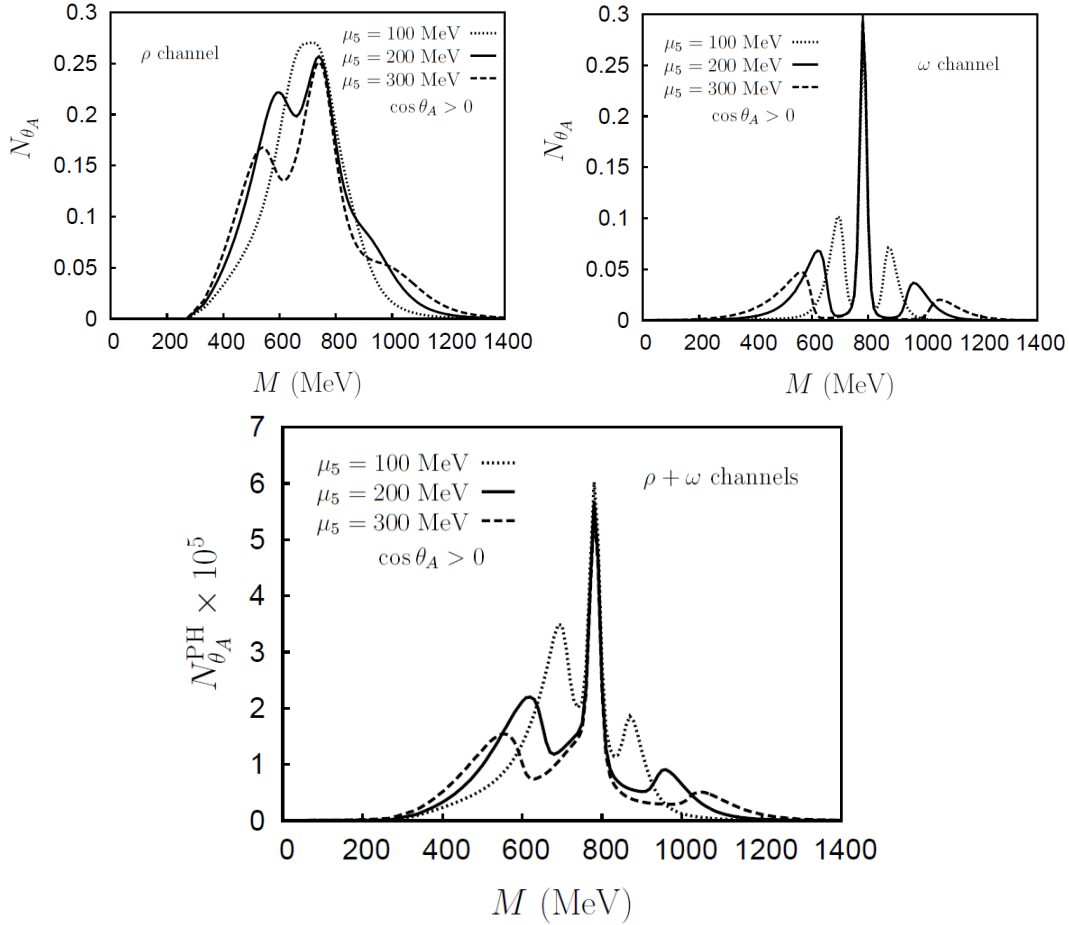
Figure 5.7: The ρ (upper-left panel) and ω (upper-right panel) spectral functions and their combination (lower panel) are showed depending on the invariant mass M and integrating the forward direction $\cos\theta_A \geq 0$ for $\mu_5 = 100, 200$ and 300 MeV. In the upper panels the total production at the vacuum peak is normalized to 1 when the entire phase space is considered whereas the lower panel is normalized to PHENIX data. Results are presented for the experimental cuts quoted by PHENIX [47].

5.4.2   Case B

The second variable we present is the angle θ_B between one of the two outgoing leptons in the laboratory frame and the same lepton in the dilepton rest frame. The angle

is exactly the same if one chooses the lepton with positive or negative charge. The dilepton production is given by

$$
\frac{dN_V}{dM} = c_V \frac{\alpha^2}{6\pi M} \left(1 - \frac{4m_\pi^2}{M^2}\right)^{3/2} \int \frac{k^2 dk\, d\cos\theta}{E_k} \frac{p^2 d\cos\psi\, d\phi}{\sqrt{M^4 - 4m_\ell^2(E_k^2 - k^2\cos\psi^2)}}
$$

$$
\sum_\epsilon \frac{m_{V,\epsilon}^4 \left(1 + \frac{\Gamma_V^2}{m_V^2}\right)}{\left(M^2 - m_{V,\epsilon}^2\right)^2 + m_{V,\epsilon}^4 \frac{\Gamma_V^2}{m_V^2}} P_\epsilon^{\mu\nu}(M^2 g_{\mu\nu} + 4p_\mu p_\nu) \frac{1}{e^{M_T/T} - 1}, \qquad (5.37)
$$

where $k(p)$ and $E_k(E_p)$ are the meson (selected lepton) momentum and energy. ψ and ϕ are the polar and azimuthal angles respectively of the lepton with respect to the meson momentum. The beam direction forms an angle θ with the vector meson. One may extract p from the decay kinematics. All these variables are defined in the laboratory frame. The new angle θ_B is defined via

$$
\frac{M}{2} \cos\theta_B \sqrt{M^2 - 4m_\ell^2} = p(M\sin^2\psi + E_k\cos^2\psi) - kE_p\cos\psi. \qquad (5.38)
$$

Regarding the fact that we would like to perform experimental cuts in θ_B, our numerical computations integrate the whole phase space of the decay and reject the regions with unwanted values of θ_B instead of treating this angle as an integration variable, which makes the calculations more complicated.

Events with $\cos\theta_B \simeq 1$ correspond to one lepton being produced in approximately the same direction in the laboratory frame and in the meson rest frame, implying that in the laboratory frame the vector meson is almost at rest. Vector mesons with low momentum are not suppressed by the Boltzmann weight but do not carry relevant information about μ_5. Therefore the opposite limit (high momenta) will be the important one for our purposes.

In the left panel of Fig. 5.8 the ρ spectral function is presented in small bins of $\Delta\cos\theta_B = 0.1$. The curves correspond to $\cos\theta_B \in [0.3, 0.4], [0.4, 0.5], [0.5, 0.6]$ and $[0.6, 0.7]$ with a fixed $\mu_5 = 300$ MeV. At first glance, the plot looks as the one showed in the previous section for θ_A with a similar secondary peak below the vacuum resonance. The main difference with the previous section is the number of events. The analysis of θ_B is more sensitive to the Boltzmann suppression than the previous case with θ_A. In the right panel of Fig. 5.8 it may be readily checked that the number of events at the highest secondary peak is 0.14, whereas in Fig. 5.5 it corresponds to 0.22, a considerable enhancement of around a 60%.

A phenomenological analysis of μ_5 depending on the position of the secondary peak as well as a comparison with the vacuum contributions may be equally described in this section but no new features are found so we omit the corresponding details.
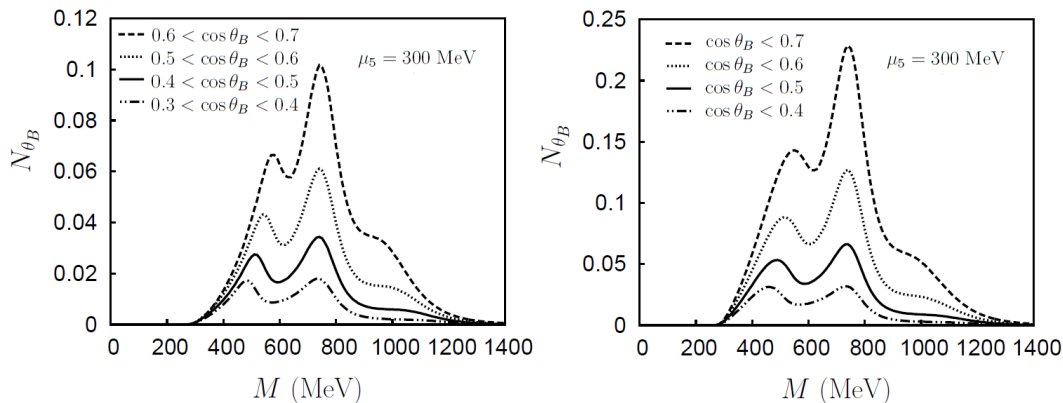
Figure 5.8: The ρ spectral function is presented depending on the invariant mass M for different ranges of the angle θ_B between one of the outgoing leptons in the laboratory frame and the same lepton in the dilepton rest frame for fixed $\mu_5 = 300$ MeV. We display the curves corresponding to $\cos\theta_B \in [0.3, 0.4], [0.4, 0.5], [0.5, 0.6]$ and $[0.6, 0.7]$ in the left panel, and $\cos\theta_B \leq 0.4, 0.5, 0.6, 0.7$ in the right one. The total production at the vacuum peak is normalized to 1 when the entire phase space is considered. Results are presented for the experimental cuts quoted by PHENIX [47].

5.5 Summary

In this chapter we have seen that in the presence of an isosinglet time-dependent pseudoscalar background vector mesons are severely distorted. They acquire an effective mass depending on their polarization, 3-momentum and the axial chemical potential. Such dispersion relation predicts that massive vector mesons split into three polarizations with different masses. The resonance poles associated to the transverse mesons appear separated of vacuum peak implying a polarization asymmetry. We have computed this effect and found that it naturally tends to produce an overabundance of lepton pairs in the vicinity of the $\rho - \omega$ resonance peak. Thus LPB seems relevant to explaining the PHENIX/STAR 'anomaly'.

As possible signatures for experimental detection of LPB we presented a description in two angular variables that are not considered in the literature when angular distribution analysis are investigated. The first one is the angle between the two outgoing leptons produced from the meson decay in the laboratory frame. The second one is defined as the angle between one of the leptons at the laboratory frame and the same lepton in the dilepton rest frame. These angles are the most suitable ones so as to extract information about LPB. Without a careful choice of angular observables the effects of LPB on the different polarizations can be easily missed. We claimed that a two-dimensional study of the decay product with the variables angle-dilepton mass allows to distinguish at least two of the resonance poles and confirm the parity-breaking hypothesis. We displayed the ρ and ω spectral functions in order to illustrate this effect and discuss the most efficient ways to search for polarization asymmetry.

The study presented here is still not fully realistic and several improvements could be made such as e.g. including a complete hydrodynamical treatment, a non-trivial baryon chemical potential, finite volume effects, thermal broadening of the resonances and a more detailed study of the time and (effective) temperature dependence. Yet none of these are expected to erase the traces of LPB if the latter is present and we would like to encourage the experimental collaborations to actively search for this interesting possibility.

5. VECTOR MESON DOMINANCE APPROACH TO LOCAL PARITY BREAKING

Chapter 6

Conclusions and outlook

The high temperatures and densities reached at current HIC experiments allow to access new regions of the QCD phase diagram that had not been investigated before. In this work we have studied the possibility that QCD breaks parity in the nuclear fireball by means of an isosinglet axial chemical potential μ_5. We saw that a phase where this symmetry is spontaneously broken may appear in the Nambu–Jona-Lasinio model, a feature that NJL may possibly share with QCD. The order of magnitude of μ_5 that allows to enter this phase is the one expected to occur in HIC experiments. Armed with this tool as the only input for parity violation, we studied how in-medium mesons are distorted. When parity is broken, the distinction between scalars and pseudoscalars is meaningless. We found the new eigenstates of QCD in the scalar sector and investigated their energy-dependent masses and decay widths. Interestingly, the distorted $\tilde{\eta}$ meson may reach thermal equilibrium in the *pion* gas forming the fireball. In the vector sector, the parity-breaking effect induces a mixing between the different vector mesons and photons. The light vector meson states ρ and ω are distorted in a similar way as spin zero resonances. Their masses are energy- and polarization-dependent, which implies an overproduction of lepton pairs from their decay. A crude comparison of our in-medium ρ spectral function with NA60 data reflects a similar behaviour. In the case of the PHENIX experiment, we improved the 'cocktail' of hadronic sources with the distorted ρ and ω contributions and observed a better agreement with the data around the resonance peak. We also described how this abnormal yield may be detected experimentally by restricting the angular coverage of the final lepton states. In this way, the possibility that QCD breaks parity in HIC has been carefully discussed together with the main implications derived of this effect. More work is needed before definite conclusions can be drawn but we believe that sufficient evidence is accumulated at present to bring these tentative conclusions to the attention of the interested readers. The possible detection of this phenomenon constitutes an encouraging source of motivation to continue working in these lines with the conviction that QCD still hold many surprises for us.

In Chapter 2 we presented the possibility that the discrete symmetries of gauge theories like parity or charge conjugation may be broken in a hot and/or dense medium.

6. CONCLUSIONS AND OUTLOOK

Two different approaches were described in detail. The first one corresponds to an analysis of dense systems with effective Lagrangian techniques. It was shown that a general sigma model containing two $SU(2)$ multiplets of scalar/pseudoscalar fields that include the two lowest lying resonances in each channel may induce a stable pseudoscalar condensate at non-trivial baryon chemical potential. Of course, the necessary conditions of this phase along with its stability depend on the exact values of the generic parameters.

The second hypothesis of parity violation in QCD may only take place in a finite volume. In HIC, the nuclear fireball reaches extremely high temperatures and densities that allow the system to enter the QGP. QCD exhibits a non-trivial and degenerate vacuum structure with different topologically inequivalent sectors. Many authors support the idea that large topological fluctuations connecting different vacua may be possible in a hot medium leading to visible effects via the Chiral Magnetic Effect. In this case, not only peripheral collisions (where CME is present) will show traces of parity breaking. While the system cools down to the hadronic phase, we claim that a new phase characterised by LPB may be crossed. The topological charge resulting from these fluctuations is transmitted to the quark sector inducing a non-trivial axial charge Q_5^q, namely an imbalance between the left- and right-handed quarks. In the case of light quarks (u, d) and a fireball living for $\tau_{\text{fireball}} \simeq 5 - 10$ fm, this axial charge is approximately conserved. In the strange sector, although an axial charge is formed, it will be wiped out due to non-trivial left-right oscillations as a consequence of the large strange quark mass. We introduced an axial chemical potential μ_5 conjugated to Q_5^q in order to investigate the parity-breaking effect. This is the approach we used throughout this thesis.

The axial chemical potential is proportional to the time derivative of a spatially homogeneous pseudoscalar axion-like condensate and it may have an isospin structure. In this work we only considered the isosinglet case, which should be more relevant for experiments like RHIC and LHC. However, the isotriplet case can also be implemented as we gave the main indications to work with it. The future experiments FAIR and NICA could be scenarios where the triplet condensate is actually more important.

In Chapter 3 we presented the NJL model as a toy model for QCD when parity is violated. This model has received a lot of attention in order to study QCD in extreme conditions. It is not clear that NJL is a good modellisation of QCD. Yet one expects the results of NJL to be qualitatively similar to those in QCD like the mechanism of chiral symmetry breaking through a scalar isosinglet condensation. The study of μ_5 in QCD has been performed in lattice simulations. Unlikely, finite density calculations present serious difficulties both analytically and in the lattice. The simplicity of the NJL model allows to work in a regime where $\mu, \mu_5 \neq 0$ and its results may help to obtain some realistic insights of QCD.

We implemented the NJL model in the presence of both a vector and an axial chemical potentials at zero temperature so as to investigate the different phases of the model. The presence of a non-trivial μ_5 constitutes a source for explicit parity breaking. The interplay of both external drivers in this model was never considered before. We

found that the axial chemical potential plays an essential role in the game (unlike μ). First, in the chirally broken phase it leads to a non-trivial dependence of the scalar condensate introducing finite jumps under certain conditions. And second, it may trigger a spontaneous breaking of parity via an isosinglet pseudoscalar condensation $\eta \neq 0$ as long as massive quarks are considered and the full $U(2)_L \times U(2)_R$ global symmetry is broken to $SU(2)_L \times SU(2)_R \times U(1)_V$ (i.e. $G_1 \neq G_2$). We considered for simplicity $a_0^0 = \langle \bar{\psi} \tau^3 \psi \rangle = 0$ thus forbidding flavour violation together with parity conservation. With these considerations, it is remarkable the absence of a phase with a pion-like condensation with a simultaneous violation of flavour and parity symmetries. However, we found an extremely small region in the $\mu - \mu_5$ space of parameters where flavour symmetry may be broken by a non-trivial a_0^0 condensate and parity is preserved.

We investigated the main features of the chirally broken phase in NJL considering a slightly modified DR scheme to treat UV divergences. We showed the allowed parameter space (including μ and μ_5) for this phase to be stable. A deep discussion of the jumps in the chiral condensate was presented depending on the values of the external drivers. As it is well known, chiral restoration was found at high values of μ with a sharper transition as one approaches the limit $m \to 0$.

The stability of the parity-breaking phase requires a set of conditions for the parameters that make the model very different of QCD. Due to a non-conventional order relation between G_1 and G_2, the NJL mass spectrum in the chirally broken phase shows that the σ and π mesons are heavier than $a_0(980)$ and η_q respectively. We set the appropriate conditions for both the chirally- and parity-broken phases to be stable in order to analyse the possible phase transition. In this context, μ_5 is determinant (unlike μ) in order to enter the parity-breaking phase. We showed the evolution of the scalar and pseudoscalar condensates with respect the axial chemical potential and also the phase transition line, which was displayed in the $\mu - \mu_5$ plane. For $\mu < M^c$ we have a second order transition while for $\mu > M^c$, it corresponds to a first order one.

The addition of an axial chemical potential induces new features in the NJL that had not been observed before. The model itself remains rather simple but all the subtleties arising from a non-trivial μ_5 seem to reflect that QCD may still exhibit many features that we do not understand yet. On the other hand, the fact that an axial chemical potential of the order or a few hundreds of MeV may induce the stability of a parity-violating phase has to be understood as a generic feature of QCD and not only about this specific model. Therefore, we explored how hadronic physics is affected by LPB.

In Chapter 4 we studied the main effects that parity-violation induces to spin zero mesons. We introduced a generalised sigma model with some of the lightest degrees of freedom in $SU(3)$. Masses and widths of the different states were calculated and a fit to QCD was performed in order to set the parameters of the model. We introduced an axial chemical potential as the time component of a spurious axial-vector field and consequently, new terms mixing states of different parity arose in the Lagrangian. In addition to parity breaking, this mechanism also introduces a Lorentz-symmetry violation that is manifest in the dispersion relation of the different states. Therefore, the

6. CONCLUSIONS AND OUTLOOK

properties of in-medium mesons are frame-dependent.

First we described the mixing between the scalar and pseudoscalar triplets a_0 and π and next we solved the system in the isosinglet sector where σ, η and η' are all mixed. As expected due to the Lorentz violation, the masses of the new eigenstates are energy-dependent. In both cases, we found that the lightest states corresponding to the distorted $\tilde{\pi}$ and $\tilde{\eta}$ become tachyonic for high enough energies. However, that was not a problem since energies are well defined and vacuum remains stable.

Due to the breaking of parity, new in-medium *exotic* processes and decays may take place. In the presence of μ_5 the pion gas that commonly forms the HIC fireball may actually be composed of distorted pions. We computed the decay widths of the singlet states into $\tilde{\pi}$ and observed a non-trivial dependence on the axial chemical potential. The energy-dependent widths show different bumps that have nothing to do with the Lorentz factor but most probably reflect the tachyonic nature of the final state *pions*. The distorted η meson acquired a width of order 60 MeV, comparable to the inverse fireball lifetime. Accordingly, we stressed that this state may reach thermal equilibrium within the HIC fireball, fact that could help in understanding the anomalous dilepton production that was studied in Chapter 5.

We explained that the isosinglet axial-vector meson channel interferes with the axial chemical potential. The condensation of its time component induces a renormalization of the bare μ_5 leading to an effective $\bar{\mu}_5$. We provided the relation between them and stressed that the effective one should be introduced in the mass-gap equations of the model.

In Chapter 5 we investigated how the violation of parity affects vector mesons. We discussed that the mixing of states of different parities may also take place in the vector/axial-vector sector. However, this coupling is very model dependent since it is not forbidden but it does not appear from a spurious μ_5. Thus the LPB effect was implemented through the Chern-Simmons term. It was shown that LPB affects the dispersion relation of the lightest vector mesons ρ and ω. In the presence of an axial chemical potential their effective masses depend on their polarization and 3-momentum reflecting the breaking of Lorentz and parity symmetries. Accordingly, vector mesons split into three polarizations with different masses. The transversely polarized mesons have their corresponding resonance peak aside the vacuum peak leading to a distorted spectral function that strongly indicates a polarization asymmetry around the vacuum peak.

In order to search for possible manifestations of the LPB effect in the vector meson channel, we computed the dilepton production from vector meson decays in central collisions and observed that a non-trivial axial chemical potential leads to an overproduction of dileptons around the $\rho - \omega$ resonance peak. We computed the shape of the ρ spectral function applying the experimental conditions of NA60 and saw that there is a suggesting similarity between our results and the experimental data for $\mu_5 \simeq 300$ MeV. However, this comparison was not completely significant as data is not acceptance corrected. We also investigated the case of the PHENIX dilepton excess in the

low invariant mass region. The combination of the ρ and ω contributions compared to the vacuum case showed a clear enhancement of the dielectron production around the resonance peak that strongly depends on the axial chemical potential. We took the theoretical prediction of the PHENIX dilepton yield based 'cocktail' of known hadronic sources and replaced the vacuum ρ and ω contributions by our in-medium calculations and observed a better agreement with the experimental data around the peak. In addition, the fact that distorted η mesons are in thermal equilibrium within the *pion* gas leads to an enhancement of their production of lepton pairs. These considerations together with other many body or in-medium corrections [38, 39, 40, 78] may help to explain the anomalous results from PHENIX and STAR. And moreover, LPB may also play a non-trivial role in NA60, where current explanations for the in-medium ρ spectral function could not be the only answer due to the large experimental uncertainty in the data.

A clear signal of LPB would be the verification that dileptons produced for values of the invariant mass above and below the $\rho - \omega$ pole are predominantly of opposite circular polarizations. This requires searching for asymmetries among longitudinal and transverse polarization for different values of the dilepton invariant mass in event-by-event measurements. An angular analysis of the final lepton states could reveal polarization dependences. We presented two angular variables that are not considered in the literature and carry the main information related to the LPB effect. The first one is the angle between the two outgoing leptons produced from the meson decay in the laboratory frame. The second one is defined as the angle between one of the leptons at the laboratory frame and the same lepton in the dilepton rest frame. We stressed that the effects of LPB may be missed if one does not carefully choose the appropriate angular variables. A two-dimensional study of one of the previous angles and the dilepton invariant mass may allow to distinguish (at least) one extra peak aside the resonance pole. We showed the ρ and ω spectral functions to illustrate this effect and discussed the most efficient ways to search for polarization asymmetry.

6.1 Future perspectives

We would like to emphasize the simplicity of the approach presented here. The features of both scalar and vector mesons only depend on a free parameter μ_5, which is expected to depend on the characteristics of the HIC. In particular, the fits presented in Chapter 5 use the values (effective temperatures, normalizations, etc.) quoted by the experiments themselves. A method to measure the axial chemical potential was also presented. The work developed about parity breaking in HIC seems interesting by itself. Even more if one considers the consequent phenomenological implications that we found so far and the expected ones. Several appealing investigation lines could be followed in order investigate more details of this phenomenon.

A deep study about the origin of a parity-odd medium through the generation of large local topological fluctuations could be helpful to understand the nature of the axial

chemical potential and the essence of parity violation in QCD. Some analysis based on the evolution of classical Yang-Mills fields [32] reveal the possibility that some *tubular* structure may be generated after a HIC with a characteristic $\vec{E}\vec{B} \neq 0$. The connections between these domains and topological fluctuations have been briefly analysed in this context. Going into detail about this topic and relate it with the work already done represents one of the more significant analysis that could be immediately performed.

Another open line of research is performing some numerical and analytical studies on the lattice, possibly doing strong coupling expansions to tackle the $\mu \neq 0$ problem. This work could complement other works in this field. Other possible extensions of the present work could be an analysis of the ρ and ω line shapes comparing with the NA60 results. Also the inclusion of heavier degrees of freedom, both vector and scalar mesons may also lead to more accurate conclusions. Other objects such as glueballs may also help in a better description of the effective theories we considered. The mixing of states of different parity in the vector sector was not treated due to its model dependency. However, this is an interesting point to analyse in the future as it may result in phenomenological observables that could be eventually detected. On the other hand, a generalisation of the concept of axial chemical potential could be addressed. We assumed this magnitude to be similar to the derivative of a time-dependent axion-like field. However, it is well known that in accelerator collisions, spatial isotropy is a crude approximation. As a matter of fact, the study of a space-dependent axion-like field is already under study [162]. Finally, a parallel study of an isotriplet axial chemical potential could be performed to examine dense systems and draw possible predictions for future experiments like FAIR and NICA.

On the other hand, parity is globally conserved so if a topological fluctuation occurs in a certain domain, another one with different sign must also take place. Hence it is plausible to think that if lepton production from vector mesons is dominated by a sign of the chemical potential (on average); there will be a different reaction that carries the opposite sign, like jets or other phenomena. This is a topic that could spark some interest.

Although this thesis does not provide definite answers to the open question of the possibility of local parity breaking in heavy ion collisions, the main conclusions of this thesis should lead us to a deeper understanding of the nature of QCD. And hopefully, our results will be soon contrasted with experiments like ALICE at LHC. In any case, we are living in a fascinating era where theory and experiment may be contrasted very quickly. Remarkable synergies among different sectors of the scientific community are emerging and so in the near future we may witness rapid advances in this area.

6.2   List of publications

6.2.1   Publications in journals

- A. A. Andrianov, V. A. Andrianov, D. Espriu and X. Planells, *Analysis of dilepton angular distributions in a parity breaking medium*, Phys. Rev. D 90 (2014)

034024, arXiv:1402.2147 [hep-ph].

- A. A. Andrianov, D. Espriu and X. Planells, *Chemical potentials and parity breaking: the Nambu–Jona-Lasinio model*, Eur. Phys. J. C 74 (2014) 2776, arXiv:1310.4416 [hep-ph].

- A. A. Andrianov, D. Espriu and X. Planells, *An effective QCD Lagrangian in the presence of an axial chemical potential*, Eur. Phys. J. C 73 (2013) 2294, arXiv:1210.7712 [hep-ph].

- A. A. Andrianov, V. A. Andrianov, D. Espriu and X. Planells, *Dilepton excess from local parity breaking in baryon matter*, Phys. Lett. B 710 (2012) 230, arXiv:1201.3485 [hep-ph].

- A. A. Andrianov, V. A. Andrianov, D. Espriu and X. Planells, *Abnormal enhancement of dilepton yield in central heavy-ion collisions from local parity breaking*, Theor. Math. Phys. 170 (2012) 17.

6.2.2 Other publications

- A. A. Andrianov, D. Espriu and X. Planells, *An effective theory for QCD with an axial chemical potential*, PoS QFTHEP 2013 (2014) 049, arXiv:1310.4434 [hep-ph].

- A. A. Andrianov, V. A. Andrianov, D. Espriu and X. Planells, *Implications of local parity breaking in heavy ion collisions*, PoS QFTHEP 2011 (2013) 025, arXiv:1310.4428 [hep-ph].

- A. A. Andrianov, V. A. Andrianov, D. Espriu and X. Planells, *Abnormal dilepton yield from parity breaking in dense nuclear matter*, AIP Conf. Proc. 1343 (2011) 450, arXiv:1012.0744 [hep-ph].

- A. A. Andrianov, V. A. Andrianov, D. Espriu and X. Planells, *The problem of anomalous dilepton yield in relativistic heavy-ion collisions*, PoS QFTHEP 2010 (2010) 053.

6.2.3 Unpublished

- A. A. Andrianov, V. A. Andrianov, D. Espriu and X. Planells, *Abnormal dilepton yield from local parity breaking in heavy-ion collisions* (2010), arXiv:1010.4688 [hep-ph].

Chapter 7

Resumen en castellano

La fuerza nuclear fuerte es conocida como la responsable de ligar los núcleos atómicos a pesar de la repulsión electromagnética entre los protones. Esta interacción es una de las cuatro fuerzas fundamentales de la naturaleza, al igual que la gravedad y las fuerzas electromagnética y débil. Las últimas dos interacciones pueden ser tratadas conjuntamente por medio de la teoría unificada de la interacción electro-débil. Las interacciones electro-débiles y fuertes, aunque no la gravedad, pueden ser formuladas en términos de una teoría cuántica de campos que es conocida como el Modelo Estándar (SM) de las partículas elementales. El comportamiento de las partículas elementales se rige por esta exitosa teoría que ha sido contrastada en numerosas ocasiones con experimentos.

Los primeros intentos de tratar con las interacciones fuertes se encuentran en la mitad del siglo pasado. En 1961 Gell-Mann propuso un modelo fenomenológico [1] para estructurar el gran número de nuevos hadrones que se estaban encontrando en experimentos con aceleradores en aquella época. Durante la década siguiente la fuerza nuclear fuerte fue formulada a nivel cuántico por la Cromodinámica Cuántica (QCD) [2], una teoría de Yang-Mills no abeliana formulada en $SU(3)$ que describe las interacciones fundamentales entre quarks y gluones [3], llamados partones. Los quarks y gluones fueron introducidos como los componentes básicos de los hadrones y tienen asociado un número cuántico de color debido a la simetría del grupo de QCD. El lagrangiano de QCD viene dado por

$$\mathcal{L}_{\text{QCD}} = -\frac{1}{4} G^{\mu\nu,a} G^a_{\mu\nu} + \bar{q}(i\gamma^\mu D_\mu - m)q,$$
$$D_\mu = \partial_\mu - ig G^a_\mu \lambda^a, \quad G^a_{\mu\nu} = \partial_\mu G^a_\nu - \partial_\nu G^a_\mu + g f^{abc} G^b_\mu G^c_\nu, \tag{7.1}$$

donde q es el campo del quark con dos índices implícitos en los espacios de color y sabor y el campo dependiente de color del gluón es G^a_μ. También se usan la constante de acoplo fuerte g y las matrices de Gell-Mann λ^a en la representación adjunta de $SU(3)$. Existen 3 colores y 6 sabores de quarks. Los quarks son estados fermiónicos masivos en la representación fundamental de la simetría de grupo de QCD mientras que

los gluones son los portadores de la fuerza (sin masa), equivalentemente a los fotones en el electromagnetismo, y pertenecen a la representación adjunta de $SU(3)$.

La atracción fuerte entre pares de quark-antiquark requiere una gran cantidad de energía para separarlos. Esta energía excita el estado de vacío hasta un punto en que la creación de otro nuevo par de quarks se vuelve energéticamente favorable y las nuevas partículas rápidamente apantallan la carga original. Este es la descripción cualitativa del confinamiento de los quarks, que es responsable del hecho que los estados de color no pueden ser observados de forma aislada en la naturaleza. Este fenómeno sólo es conocido en QCD y se cree que está ligado a su estructura no abeliana. La falta de una prueba rigurosa del confinamiento aún constituye un reto notable para los físicos teóricos en la actualidad.

Se observó experimentalmente que sólo existen dos estructuras principales formadas por quarks. Los hadrones se separan en bariones y mesones. Los bariones son estados de 4 quarks mientras que los mesones están compuestos de una pareja de quark y antiquark. Con tal de preservar el principio de exclusión de Pauli en la formación de bariones, un nuevo número cuántico se introdujo: la carga de color. Suponiendo que cada quark lleva un color asociado, ambas estructuras pueden ser organizadas de manera que no tengan color. Esta es la razón por la que se dice comúnmente que sólo estados sin color (o blancos) son observables en la naturaleza.

Además de la simetría gauge, el lagrangiano de QCD (7.1) muestra una invariancia bajo tres simetrías globales discretas [4, 5]. La paridad P invierte la orientación del espacio que corresponde a revertir el momento de una partícula sin girar su espín. La transformación de paridad viene dada por

$$q(\vec{x},t) \rightarrow \eta_P \gamma^0 q(-\vec{x},t), \qquad G_\mu(\vec{x},t) \rightarrow G_\mu(-\vec{x},t), \tag{7.2}$$

donde η_P es una posible fase genérica que es tomada normalmente como 1 para quarks y leptones sin pérdida de generalidad. Para antipartículas, se elige $\eta_P = -1$. La conjugación de carga C intercambia partículas por antipartículas sin ninguna modificación de momento o espín a través de la transformación

$$q(\vec{x},t) \rightarrow -i\eta_C C \bar{q}^T(\vec{x},t), \qquad G_\mu(\vec{x},t) \rightarrow -G_\mu^T(\vec{x},t), \tag{7.3}$$

donde η_C es otra fase y C es la matriz de conjugación de carga que obedece las siguientes relaciones

$$C\gamma_\mu C^{-1} = -\gamma_\mu^T, \qquad C\gamma_5 C^{-1} = \gamma_5^T, C^\dagger = C^{-1} = -C \tag{7.4}$$

y en la representación de Dirac viene dada por $C = i\gamma^0\gamma^2$. Finalmente, la reversión temporal T corresponde al intercambio de los conos de luz delantero y trasero, correspondiendo a invertir el momento y el espín de una partícula vía

$$q(\vec{x},t) \rightarrow -i\eta_T \gamma_5 C q(\vec{x},-t), \qquad G_\mu(\vec{x},t) \rightarrow G_\mu(\vec{x},-t), \tag{7.5}$$

donde η_T es de nuevo una fase arbitraria. QCD, como cualquier otra teoría cuántica de campos local e invariante Lorentz con un hamiltoniano hermítico es también invariante bajo la simetría simultánea CPT.

El espectro de quarks se extiende sobre un amplio rango de masas desde $m_{u,d} \sim 5$ MeV hasta $m_t \sim 175$ GeV, que lleva a una clara jerarquía de masa/energía. A una cierta escala de energía Λ, los quarks pueden separarse en quarks ligeros con masa m_q y quarks pesados con m_Q de tal manera que se satisface la relación $m_q \lesssim \Lambda \ll m_Q$. En este contexto a bajas energías, el efecto de los quarks pesados equivale a redefiniciones de las masas de los quarks ligeros m_q y las constantes de acoplo que involucran los quarks ligeros con correcciones del orden de Λ/m_Q. Esto es conocido como el teorema del desacoplo [6]. Las teorías de bajas energías [7] normalmente se formulan para describir la física de las interacciones fuertes bajo la escalar de ruptura de simetría quiral $\Lambda \sim 1$ GeV y de ahí el número de sabores de quarks se toma generalmente como $N_f = 2, 3$ incluyendo siempre los quarks u y d, y en ocasiones el quark s. Para análisis a escalas de energías más elevadas, se usan otras técnicas como la teoría efectiva de quarks pesados [9].

En el límite de quarks sin masa, QCD exhibe una simetría global $U(N_f)_L \times U(N_f)_R$ exacta a nivel clásico, donde N_f es el número de sabores de quarks considerados. Bajo esta transformación los campos de quarks se ven modificados de la siguiente manera:

$$q_{L,R}(x) \rightarrow \exp\left(\frac{i}{2}\theta_{L,R}^a T^a\right) q_{L,R}(x), \qquad q_{L,R}(x) \rightarrow \exp\left(\frac{i}{2}\tilde{\theta}_{L,R}\right) q_{L,R}(x), \qquad (7.6)$$

donde T^a pertenecen a la representación adjunta de $SU(N_f)$ y $\theta_{L,R}^a, \tilde{\theta}_{L,R}$ son unas constantes arbitrarias que parametrizan la transformación. Los campos gluónicos no se ven afectados por esta simetría global. Cualquier transformación $U(N)$ puede descomponerse en $SU(N) \times U(1)$ y por ello, la simetría global previa puede ser reescrita como $SU(N_f)_L \times SU(N_f)_R \times U(1)_V \times U(1)_A$, donde la parte vectorial V es la suma de los números cuánticos de quarks derechos e izquierdos y la componente axial A corresponde a la resta de estas cantidades.

Las correcciones cuánticas revelan que la corriente vector axial singlete asociada a la simetría bajo $U(1)_A$, que se conserva a nivel clásico, desarrolla una anomalía y por tanto, la verdadera simetría de la teoría cuántica se reduce a $SU(N_f)_L \times SU(N_f)_R \times U(1)_V$. En el Capítulo 2 abordaremos una explicación más detallada de la anomalía axial. La simetría $U(1)_V$ se relaciona con la conservación del número bariónico mientras que el resto se trata de simetría quiral. Si la simetría quiral fuese una verdadera simetría de QCD, uno esperaría un espectro de estados degenerados con paridad opuesta. Sin embargo, esto no se observa en la naturaleza implicando que la simetría está rota. De hecho, la simetría se rompe espontáneamente ya que los generadores del subgrupo $SU(N_f)_A$ no aniquilan el estado fundamental y por tanto, cada uno de ellos se asocia a un bosón de Goldstone sin masa. Los estados físicos correspondientes a estos bosones de Goldstone son los mesones más ligeros π, η y K, siendo el último importante sólo si $N_f = 3$. Las masas finitas de estas partículas se entienden como consecuencia de la ruptura explícita de simetría debido a las masas finitas de los quarks en el lagrangiano de QCD. A pesar de que la simetría quiral exacta no se satisface realmente en QCD, este tratamiento puede usarse como una aproximación para trabajar en QCD a bajas

energías desarrollando la llamada Teoría de Perturbaciones Quirales (χPT), que se discute más abajo.

La constante de acoplo de QCD g determina la fuerza de las interacciones entre quarks y gluones y las auto-interacciones de gluones. éstas últimas son permitidas debido a la naturaleza no abeliana de QCD, al contrario el caso del electromagnetismo donde los fotones sólo pueden interaccionar con otras partículas. La renormalización de una teoría cuántica conduce a la movilidad de su constante de acoplo, que no es realmente constante sino que depende de la escala de energía μ a la que un proceso tiene lugar. Una teoría gauge $SU(N_c)$ con N_f sabores de quarks muestra [10] que la función β a un loop

$$\beta(g)_{\text{1-loop}} = \frac{\partial g}{\partial \log \mu} = -\frac{g^3}{16\pi^2}\left(\frac{11}{3}N_c - \frac{2}{3}N_f\right) \tag{7.7}$$

es negativa para $N_f < \frac{11}{2}N_c$. En particular, el hecho de que QCD con $N_c = 3$ y $N_f = 6$ quarks se caracteriza por una función β negativa implica una constante de acoplo decreciente con una energía creciente. A altas energías, QCD ya no es una teoría que interaccione fuertemente y se acerca al límite libre. Este efecto es conocido como libertad asintótica y de alguna manera corresponde al comportamiento opuesto al confinamiento descrito a bajas energías.

Esta visión de QCD permite usar técnicas perturbativas para cálculos de procesos a altas energías. Las secciones eficaces perturbativas de partones a cortas distancias y las cantidades no perturbativas de largas distancias pueden combinarse gracias a los teoremas de factorización de QCD [11]. La contribución de largas distancias incluye las funciones de distribución de los partones, funciones de fragmentación, diferentes tipos de factores de forma, etc. Efectivamente, este método se vuelve más preciso así como las energías aumentan debido a la libertad asintótica de QCD.

A bajas energías, los cálculos perturbativos no tienen sentido debido al gran acoplo entre quarks y gluones. Los efectos no perturbativos no se pueden evitar en este régimen y por tanto, aparecen muchas dificultades haciendo que QCD sea muy difícil de solucionar analítica o numéricamente. Diversas aproximaciones han sido abordadas para superar estos problemas como las simulaciones numéricas en el retículo [12], teorías de campos efectivas [7] o expansiones en $1/N_c$ [13].

Una posibilidad de definir rigurosamente una teoría cuántica de campos consiste en discretizarla. Los cálculos en el retículo son un mecanismo no perturbativo donde QCD se formula en una cuadrícula de puntos en un espacio-tiempo euclídeo. Una separación fija y finita entre los puntos de la cuadrícula representa un regulador UV. Si el tamaño del retículo se toma infinitamente grande y la separación de sus puntos infinitesimalmente pequeña, se recupera el continuo de QCD [12]. La aproximación de integral de caminos de Feynman se usa para calcular las funciones de correlación de operadores hadrónicos y elementos de matriz de cualquier operador entre estados hadrónicos en función de los grados de libertad fundamentales de quarks y gluones. La masa del pión

m_π se usa normalmente para examinar la fiabilidad de los cálculos en el retículo ya que éste es el estado hadrónico más ligero y por tanto su longitud de onda correspondiente es la más larga. Si el retículo no es lo suficientemente grande, la función de onda del pión no cabe en el retículo. Por este motivo normalmente se usan grandes masas para los quarks en esta descripción que conducen a un valor no físico para el valor de la masa del pión. Sin embargo, grandes retículos con espaciado pequeño corresponden a un gran número de puntos en la cuadrícula y por tanto, simulaciones computacionales que necesitan mucho más tiempo para ser ejecutadas. Además, las correcciones de efectos de volumen finito tienen que ser calculadas para una comparación realista con los experimentos.

Una aproximación diferente QCD a bajas energías consiste en usar teorías de campos efectivas (EFT). Como no son visibles a grandes distancias, los quarks y gluones pueden ser eliminados del modelo mientras que los hadrones se convierten en los grados de libertad relevantes a bajas energías. Imponiendo las simetrías de QCD a la teoría, cualquier observable puede ser calculado mediante una especie de expansión perturbativa en la que el esquema de contado de potencias determina la importancia de las amplitudes cuánticas. De la misma manera que el aumento de la potencia de una constante de acoplo pequeña se usa en teoría de perturbaciones, EFT normalmente aprovecha el ratio de un parámetro pequeño como masa, momento/energía. Estas teorías corresponden a la realización a bajas energías de QCD y por consiguiente éstas son sólo válidas hasta una cierta escala máxima, haciéndolas no-renormalizables. χPT ha demostrado ser una teoría efectiva de mucho éxito donde se describen las interacciones entre los estados mesónicos ligeros (para un análisis detallado ver [7]). Debido a la gran masa del quark s, la convergencia de la expansión en el sector $SU(3)$ es en cierto modo más lenta comparada con la versión de $SU(2)$. Es posible generalizar esta teoría mediante la introducción de estados bariónicos en la teoría que involucra interacciones barión-barión y barión-mesón adicionales. Nótese que χPT sólo usa como ingredientes las simetrías de QCD y por ello no se trata de un modelo sino de una realización a bajas energías.

En esta tesis usaremos dos modelos de bajas energías: el modelo de Nambu–Jona-Lasinio (NJL) y el modelo sigma. NJL es un modelo microscópico que incluye vértices de 4 fermiones que reemplazan las interacciones de los gluones en QCD. Debido a la presencia de estos términos, el modelo no es renormalizable pero la ausencia de gluones permite que la teoría sea bosonizada. Después de este proceso, se obtiene una teoría de mesones con campos escalares y pseudoescalares que puede ser asociada a un modelo sigma con valores concretos de sus parámetros. Por otro lado, el modelo sigma corresponde a una teoría particular que deriva de una EFT basada en χPT asumiendo dominancia escalar en la interacción a bajas energías. Tanto en NJL como en el modelo sigma, la simetría quiral se rompe espontáneamente debido a la formación de un condensado dinámico de quarks quirales. Este condensado transmite una masa constituyente a los quarks. En el sector u, d se espera que ésta sea del orden de unos 300 MeV (en base a la masa de los nucleones) en contraste con la ligera masa de los quarks desnudos, del orden de 5 MeV.

Cuando ninguno de los otros métodos funciona, la única forma de investigar el comportamiento de QCD a bajas energías consiste en hacer una expansión en términos del pequeño parámetro $1/N_c$. El límite de gran N_c de una teoría gauge $SU(N_c)$ puede llevar a pensar que este mayor grupo gauge complica la teoría ya que conlleva un aumento del número de los grados de libertad dinámicos. Sin embargo, es posible demostrar que este límite es una aproximación razonable aún en el caso de QCD donde $N_c = 3$ [13]. En el límite de gran N_c el número de especies de gluones aumenta como N_c^2 mientras el número de quarks lo hace como N_c. QCD se convierte en una teoría de un número infinito de resonancias sin interacción ni anchura de desintegración [14], que son mesones y bolas de gluones ya que las masas de los bariones crece con N_c y pueden desacoplarse de la teoría y ser ignorados sin peligro. La expansión $1/N_c$ normalmente se formula asignando a cada diagrama de Feynman una potencia de N_c [15], que es determinada por la topología del diagrama. Las contribuciones dominantes son 'planares' y no contienen *loops* de quarks mientras que los términos subdominantes van suprimidos por un factor $1/N_c$ debido a *loops* de quarks y cada intercambio de gluones no planar es suprimido por $1/N_c^2$. El punto cualitativamente importante de esta aproximación es el comportamiento de escala en N_c de los diferentes diagramas que permite clasificarlos dependiendo de su relevancia. Dado que $1/N_c$ no es un parámetro muy pequeño, una expansión perturbativa en $1/N_c$ puede requerir la inclusión de un gran número de términos de orden superior si se busca un resultado preciso.

7.1 Diagrama de fases de QCD

El hecho de que partones altamente energéticos puedan interaccionar casi libremente sugiere la posibilidad de que la materia confinada pueda sufrir con el tiempo una transición de fase. El sistema es dirigido a un régimen de deconfinamiento donde los grados de libertad relevantes de QCD son los quarks y gluones en lugar de los hadrones y por tanto los estados sin color no existirían más.

El estudio del deconfinamiento ha sido abordado por muy diferentes colaboraciones y técnicas. Los cálculos de QCD en el retículo pueden dar resultados fiables de las propiedades termodinámicas de la materia que interacciona fuertemente sólo para valores muy pequeños del potencial químico bariónico. En este caso se predice una transición de deconfinamiento de tipo híbrido [16]. QCD en el retículo sugiere una transición de fase desde la fase hadrónica al QGP a $T_c \sim 140 - 190$ MeV [17] (para un análisis detallado ver [18]).

Esta nueva fase, el llamado plasma de quarks y gluones (QGP), podría ser alcanzado a altas temperaturas y densidades, condiciones que son factibles en colisiones de iones pesados (HIC). De hecho, los recientes resultados del Acelerador Relativista de Iones Pesados (RHIC) muestran una fuerte evidencia de que el QGP ha sido creado en colisiones Au+Au a $\sqrt{s_{NN}} = 200$ GeV[19].

Modificando las condiciones experimentales como la energía de la colisión o el parámetro de impacto es posible explorar un amplio rango de temperaturas y den-

sidades desentrañando las diferentes fases de QCD. Mientras el sistema se comprime y calienta, se espera que los hadrones ocupen cada vez más y más espacio, lo que lleva a un solapamiento final que desencadena una 'percolación' de partones entre hadrones y éstos acaban siendo liberados. Además, los quarks ligeros pierden su masa constituyente dentro de los hadrones y adquieren su masa real (desnuda) restaurando la simetría quiral. Uno de los objetivos científicos del programa actual de iones pesados de alta energía es la cuantificación de las propiedades de la materia del QGP, como por ejemplo su ecuación de estado.

En un experimento de HIC, los núcleos pesados son acelerados a velocidades ultra-relativistas antes de su impacto. Inmediatamente después de su colisión, los núcleos crean un medio que interacciona fuertemente y alcanza temperaturas extremadamente altas del orden de varios centenares de MeV, y la densidad de la materia nuclear puede ser ampliamente rebasada. Entender el comportamiento de la caliente y densa bola de fuego constituye uno de los retos más notables en QCD. Se cree que estas extremas condiciones termodinámicas existen en dos contextos astrofísicos: algunos microsegundos después del 'Big Bang' una etapa transitoria de materia fuertemente interactuante sobrevivió con una temperatura ~ 200 MeV (alrededor de 10^{12} K) y un pequeño exceso neto de bariones; en el núcleo de las estrellas de neutrones se cree que las densidades se son varias veces la densidad nuclear. Nuevas regiones del diagrama de fases de QCD pueden ser exploradas mediante los actuales experimentos en aceleradores [20, 21]. Las primeras colisiones se llevaron a cabo en el Sincrotrón de Nivelado Alternado (AGS) en Brookhaven (BNL) con una energía en el centro de masas de alrededor de $\sqrt{s} \sim 5$ GeV por nucleón y más tarde, el Súper Sincrotrón de Protones (SPS) del CERN alcanzó $\sqrt{s} \sim 20$ GeV por nucleón entre muchos otros experimentos de aceleradores. Actualmente RHIC en BNL y LHC en el CERN llegan a energías de hasta $\sqrt{s} \sim 200$ GeV y 5 TeV por nucleón, respectivamente.

El fenómeno del deconfinamiento ha sido investigado también en experimentos con aceleradores. La transición híbrida hacia la fase deconfinada que predice QCD en el retículo parece ser confirmada por recientes experimentos en RHIC [23]. En este régimen de densidades moderadas, diferentes aproximaciones predicen una posible transición de fase de primer orden hacia la fase de deconfinamiento sugiriendo la existencia de un punto crítico que ha sido buscado intensamente en RHIC. Uno de los mayores objetivos del programa de bajas energías de RHIC es encontrar este punto crítico escaneando diferentes regiones del espacio de fases de los núcleos de oro que se hacen colisionar a diversas energías. Para encontrar un posible punto crítico se miden momentos superiores de las distribuciones netas de protones en colisiones Au+Au en un amplio rango de potenciales químicos. Se han observado desviaciones de algunos momentos con respecto a las expectativas teóricas a energías del haz por debajo de $\sqrt{s_{NN}} = 27$ GeV por nucleón [24]. Sin embargo, se necesita más estadística para obtener conclusiones definitivas. Desde el punto de vista teórico, muchas aproximaciones diferentes han planteado e investigado este punto crítico.

Tratar con materia acoplada fuertemente complica el entendimiento teórico de las
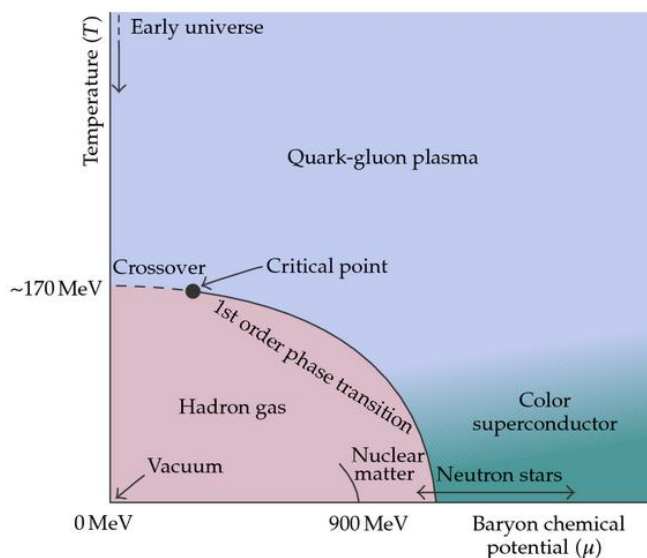
Figure 7.1: Diagrama de fases de QCD dependiendo de la temperatura y densidad extraído de [22]. Se indican las fases reales y las especulativas.

propiedades y la dinámica del medio. En los últimos años un creciente interés en técnicas de acoplo fuerte conllevó el estudio de los plasmas líquidos que aparecen como fases calientes de deconfinamiento en teorías gauge no abelianas que tienen descripciones holográficas duales como las teorías gravitacionales en 4+1 dimensiones conteniendo un horizonte de agujero negro. Un ejemplo simple de esta dualidad gauge/gravedad ha sido aplicado en una teoría supersimétrica de Yang-Mills $\mathcal{N} = 4$ fuertemente acoplada en el límite de un gran número de colores. Este tipo de análisis han proporcionado numerosos conocimientos cualitativos de las propiedades del QGP [25]. En particular, en el límite donde el acoplo de QCD es grande a todas las energías relevantes, la dualidad gauge/gravedad permitió usar cálculos holográficos para obtener información dinámica detallada de procesos con pérdida de energía.

Los estudios teóricos de la termodinámica del QGP revelaron que éste se comporta como un líquido de Fermi casi ideal, a pesar de que la investigación de las características de flujo aún está en marcha. Un importante desarrollo en los últimos años ha sido la conjetura de que para cualquier fluido térmico puede existir un límite fundamental en el valor de la viscosidad [26]. El principio de indeterminación requiere una viscosidad diferente de cero. De forma más precisa la conjetura indica que el ratio de la viscosidad sobre entropía debe satisfacer la relación $\eta/s \geq 1/4\pi$ y se han desarrollado diferentes investigaciones para medir experimentalmente este ratio [27]. La combinación de diferentes resultados parece concluir que la materia producida está dentro de un factor 2-3 del límite conjeturado y por tanto, éste debería corresponder al fluido más ideal que ha sido medido jamás. Sin embargo, existen evidencias de que la materia no se comporta como un estado casi ideal de quarks y gluones libres sino más bien como un fluido denso

casi perfecto con una absorción casi completa de pruebas de gran momento [28].

Además del QGP y la fase hadrónica, otras fases termodinámicas han sido discutidas junto con sus correspondientes transiciones de fase. En la Fig. 7.1 se muestra un diagrama de fases de QCD tentativo dependiendo de la temperatura y densidad. Por ejemplo, se cree que la transición líquido-gas de la materia nuclear al gas hadrónico ocurre a temperaturas del orden de $T \lesssim 10$ MeV y potenciales químicos $\mu \simeq 900$ MeV. Otra fase es la llamada fase de color-sabor cerrado (CFL) [29]. A densidades muy altas los 3 quarks más ligeros u, s, d pueden formar parejas de Cooper que correlacionan sus propiedades de color y sabor conllevando un comportamiento de superconductividad de color. La fase CFL rompería las simetrías de QCD y exhibiría un espectro y unas propiedades de transporte muy diferentes. Hasta la fecha no se han encontrado evidencias experimentales de esta fase pero se conjetura que esta forma de materia puede existir en los núcleos de las estrellas de neutrones. Con todo, la estructura del diagrama de fases a altas densidades bariónicas permanece bastante incierta.

7.2 Explorando el diagrama de fases con colisiones de iones pesados

La dinámica de la bola de fuego nuclear creada en HIC no es trivial. En la Fig. 7.2 presentamos un boceto de una HIC evolucionando en el tiempo y la correspondiente fase donde el sistema se encuentra en cada momento. En las primeras etapas la bola de fuego se comprime por un corto periodo de tiempo entre 0.5 y 1 fm. Durante este tiempo se cree que el sistema alcanza temperaturas de hasta $\sim$600-700 MeV dependiendo del modelo y el experimento (ver [30] y las referencias en su interior) y entra el QGP. En la próxima etapa toda la fenomenología asociada a la fase de deconfinamiento tiene lugar mientras el sistema empieza a termalizar debido a las fuertes interacciones entre los componentes del medio. La temperatura cae lentamente hasta los ~ 200 MeV, una situación donde aún no está claro si existe una fase mixta. Después de la expansión que dura entre 5 y 10 fm, los modelos hidrodinámicos convencionales y los cálculos en el retículo sugieren que alrededor de $T_c \sim 140 - 190$ MeV, una transición de fase lleva al sistema a la fase hadrónica, donde los quarks y los gluones se reagrupan de nuevo para formar hadrones. Las pruebas experimentales de interacciones hadrónicas pueden proporcionar valiosos conocimientos del QGP y de la transición de fase de deconfinamiento. Finalmente, cuando el sistema está lo suficientemente frío, es decir $T \sim 100$ MeV, las colisiones entre hadrones cesan y los componentes del medio quedan congelados, sobreviviendo como partículas en el estado final.

A altas energías, o equivalentemente, a pequeños valores de la x de Bjorken, las densidades de gluones son muy elevadas. Bajo estas circunstancias QCD puede ser descrita por una teoría de muchos cuerpos de partones acoplados débilmente, el llamado Condensado de Vidrio de Color (CGC) [31]. En las primeras etapas de una HIC dos núcleos a velocidades relativistas pueden ser considerados como dos tortitas de CGC. Los gluones en las funciones de onda nucleares se encuentran desordenadas

7. RESUMEN EN CASTELLANO
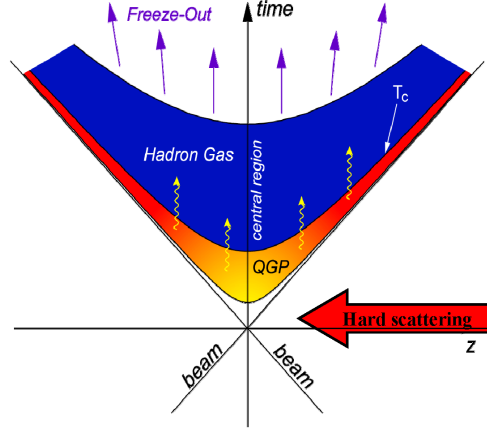
Figure 7.2: Evolución del medio nuclear creado en HIC dependiendo del tiempo. Después de la colisión el sistema se calienta y entra en el QGP donde los quarks y gluones quedan deconfinados. A continuación, un proceso de enfriamiento lento tiene lugar llevando al sistema a la fase hadrónica donde los partones se agrupan en bariones y mesones. Finalmente, cuando la temperatura de congelamiento es alcanzada, los hadrones dejan de interactuar.

y evolucionan muy lentamente en comparación con la escala de tiempo de una HIC, similar al comportamiento de los vidrios. Su alta densidad es la responsable del término condensado. Esta visión de la materia nuclear consiste en un campo clásico coherente que se desintegra en partones cercanos a su capa másica y eventualmente se termaliza para formar el QGP. Esta aproximación permite el estudio de las condiciones iniciales y el proceso de equilibrio de las HIC. De hecho, el CGC ha de ser considerado como la etapa de no-equilibrio precedente del QGP. Por esta razón, a esta materia se la denomina normalmente Glasma [32, 33].

Una manera de analizar las propiedades de la materia de QCD en HIC es vía el estudio de la anisotropía azimutal inducida en colisiones no centrales (para análisis detallados ver [34, 35]). El fluido colectivo anisotrópico, es decir, anisotropías en las distribuciones de momentos de las partículas con respecto al plano de reacción, es altamente sensible a las propiedades del sistema en las primeras etapas de su evolución (ver Fig. 7.3). Esto es debido a que las asimetrías iniciales en la geometría del sistema que rápidamente se desvanecen mientras el sistema se enfría. La distribución azimutal de partículas medida con respecto al plano de reacción es convenientemente expandida en una serie de Fourier [36]. Los diferentes harmónicos, generalmente llamados n-ésimo orden del fluido, de esta expansión dependen de la rapidez, del momento transverso y del parámetro de impacto de la colisión y han sido medidos en diferentes experimentos [37]. Se han abordado muchos cálculos hidrodinámicos diferentes para proporcionar descripciones cualitativas de los fluidos colectivos (ver [25] y las referencias en el interior).

Cuando la bola de fuego de una HIC se enfría y entra en la fase hadrónica, los quarks y gluones se reagrupan para formar hadrones. La materia se deja de tener color
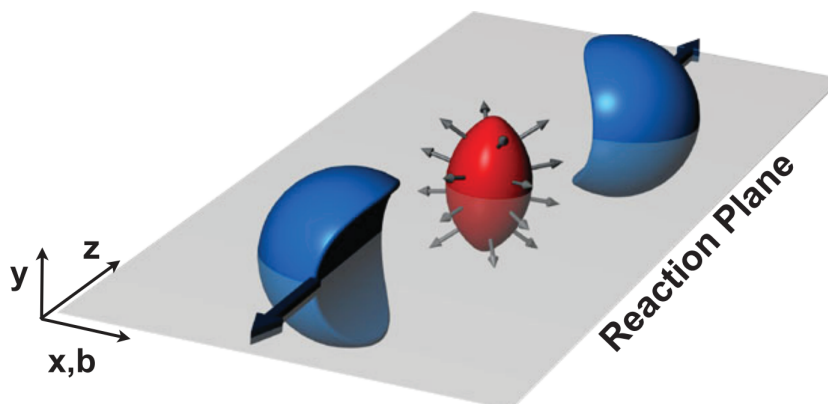
Figure 7.3: En colisiones no centrales, la región central donde los dos núcleos se solapan presenta una forma parecida a una almendra (gráfico extraído de [35]) que acarrea una anisotropía inicial con respecto al plano de reacción. Esto se traduce en anisotropías en las distribuciones de momentos de las partículas.

de nuevo creando un gas de hadrones. Se ha argumentado que tanto en RHIC como en LHC se ha alcanzado el equilibrio térmico a diferencia de otras máquinas previas como SPS. Este medio puede estar formado por muchas partículas diferentes pero la función de partición viene dominada por los grados de libertad más ligeros. Por tanto, la bola de fuego puede aproximarse por un gas de piones. Otros estados mesónicos ligeros pueden estar presentes en pequeñas cantidades pero los bariones son ciertamente demasiado pesados para jugar un papel significativo en este contexto.

La evolución dinámica del gas de hadrones necesita entenderse correctamente ya que corresponde al paso intermedio entre el QGPP y los estados finales que se miden en los detectores. El mesón ρ juega un papel clave en la termalización del gas de hadrones. Primero de todo, los mesones ρ interactúan fuertemente con los piones y su corto recorrido libre medio permite múltiples procesos de dispersión que lleva a la regeneración de éstas partículas a partir de los piones, es decir, el número efectivo de mesones ρ se ve incrementado con respecto a su producción directa en el proceso de hadronización. Y en segundo lugar, parece ser que diversos estudios basados en teorías hadrónicas efectivas coinciden en que la función espectral del mesón ρ se ve modificada severamente por efectos del medio nuclear conllevando un fuerte ensanchamiento de la resonancia [38, 39, 40] con sólo un pequeño desplazamiento de la masa [41].

Por otra parte, un ensanchamiento de la función espectral del mesón ρ puede resultar de su creación a partir de los bariones en el denso medio hadrónico [38]. Un modelo hadrónico de muchos cuerpos extendido de la ρ en materia masónica caliente que incluye excitaciones de resonancias y un incremento Bose de piones en la autoenergía de la ρ implica un ensanchamiento de alrededor de $\Delta\Gamma_\rho \sim 80$ MeV a una temperatura de $T = 150$ MeV y una densidad piónica $\varrho_\pi \simeq 0.75\varrho_0$ [42], donde ϱ_0 es la densidad nuclear. En materia nuclear fría otras investigaciones han sido desarrolladas en modelos de resonancia ρN incluyendo la nube de piones en el medio [43] mostrando un

ensanchamiento aún más fuerte de ~ 300 MeV a $\varrho_N \simeq \varrho_0$ y un desplazamiento de masa comparable de unos ~ 40 MeV. Por otro lado, el escenario de caída de masa de los mesones vectoriales en la densa bola de fuego [44] establece un vínculo entre las masas hadrónicas y el condensado de quarks, el parámetro de orden de la restauración de la simetría quiral. La masa de la ρ escala [41] con el condensado de quarks y éste último cae debido a la alta densidad bariónica más que por una alta temperatura. Nótese que ambas aproximaciones se basan en una alta densidad bariónica. Los relativos méritos de estas dos diferentes aproximaciones han atraído mucho debate intentando explicar el exceso de dileptones de baja masa invariante que han sido medidos en diferentes experimentos [45, 46, 47].

7.3 Pruebas duras en colisiones de iones pesados

Se ha propuesto una gran variedad de señales del medio nuclear y su dinámica. Las llamadas pruebas duras, es decir procesos que involucran intercambios de grandes momentos, pueden explorar la física de pequeñas distancias siempre que los quarks constituyentes sean lo suficientemente pesados, un régimen que puede ser bien descrito por QCD perturbativa que conduce a un buen control teórico del asunto.

Una prueba dura importante es el conjunto de diferentes estados de quarkonio pesado y sus modificaciones en el medio [48]. La presencia del QGP apantalla la fuerza atractiva de un par quark-antiquark. La máxima distancia que permite la formación del quarkonio disminuye con la temperatura del medio. La interacción de estos estados con un medio caliente conlleva la modificación de sus propiedades y su completa disociación a temperaturas suficientemente altas. La dualidad gauge/gravedad ha mostrado que los mesones de quarkonio pesado permanecen ligados en el plasma y el hecho de que su temperatura de disociación cae con una creciente velocidad del mesón [25]. Esta ruptura implica la supresión de la producción de quarkonio en colisiones nucleares en comparación con su equivalente protón-protón. La mayoría de estudios sobre el quarkonio se han centrado en estados de charmonio como por ejemplo el mesón J/ψ debido a la pequeña sección eficaz de producción del quark b a bajas energías. Sin embargo, los quarks c no son lo suficientemente pesados para una descripción teórica fiable y por tanto, sus interacciones con el QGP y su mecanismo de producción en HIC son relativamente inciertos [49]. Se ha mostrado una supresión fuerte de los mesones J/ψ en HIC [50, 51] pero el patrón de supresión es aún confuso y la interpretación de datos no está totalmente clara ya que el quarkonio también queda suprimido en colisiones protón-núcleo [52]. Recientemente se han publicado datos sobre la supresión del bottomonio a través del estudio de los mesones Υ en LHC [51] y RHIC [53] permitiendo un mejor entendimiento teórico de este canal.

Los jets de alta energía producidos en una colisión se ven severamente afectados por un medio que interacciona fuertemente. Cuando un partón de gran momento se produce en la primera fase de una colisión núcleo-núcleo, éste interactuará múltiplemente con los constituyentes del medio antes de su hadronización. La energía de estos partones

se ve reducida debido a la pérdida de energía por colisión [54] y a la radiación de gluones inducida por el medio [55]. La energía de estos partones se almacena en el QGP y se propaga como una excitación colectiva o fluido cónico [56]. Este efecto conlleva la aparición de picos en correlaciones de partículas que han sido observados experimentalmente [57]. El efecto de la extinción de jets en el QGP es la motivación principal para el estudio de jets al igual que del espectro de partículas de gran momento y correlaciones de partículas en HIC. El estudio de jets altamente energéticos es una de los mejores pruebas duras para investigar el medio nuclear ya que su producción ocurre a escalas de energía muy altas donde QCD perturbativa garantiza una buena descripción teórica. De forma similar, muchas de las propiedades de los jets en el vacío también están controladas por la física a altas escalas de energía y por tanto están bien entendidas desde un punto de vista teórico. Las desviaciones observadas en las diferentes propiedades en HIC y en vacío han de ser debidas a la interacción de diferentes componentes del jet con el medio nuclear. La precisa reconstrucción de jets permite la medida de las funciones de fragmentación de los jets y permiten entender mejor las propiedades del caliente y denso QGP. Las primeras evidencias de pérdida de energía en partones fueron observadas en RHIC a partir de la supresión de partículas con alto p_T estudiando el factor de modificación nuclear [58] y la supresión de correlaciones de partículas que salen en direcciones opuestas [59]. El LHC también ha observado la extinción de jets [60] y SPS parcialmente también [61].

Además de las pruebas duras, otras señales del medio creado en HIC han sido discutidas. Grandes fluctuaciones topológicas en el vacío de QCD pueden inducir la ruptura de paridad en colisiones núcleo-núcleo que llevan al Efecto Magnético Quiral [63], que predice una separación de carga a lo largo del plano de reacción. Además, los fotones y dileptones (parejas de leptón y antileptón del mismo sabor) son considerados como potentes pruebas debido a su despreciable interacción con los estados hadrónicos finales. Explicaremos estos dos aspectos en detalle en las próximas secciones.

7.4   El Efecto Magnético Quiral

Un efecto diferente que ha recibido mucha atención es la separación de cargas detectada en colisiones núcleo-núcleo en STAR [62]. La medida de un observable no trivial de 3 partículas refleja que las correlaciones azimutales de igual y opuesta carga en cada evento conducen a una pequeña separación de cargas sobre el plano de reacción en una HIC. Este observable tiene la ventaja de suprimir las correlaciones de fondo que no están relacionadas con el plano de reacción. Se ha supuesto que la medida de este efecto es la confirmación del Efecto Magnético Quiral (CME) [63], que asume que dominios locales con paridad impar pueden aparecer en HIC. Se espera que las correlaciones de pares con la misma y opuesta carga debido al CME sean similares en magnitud y de signo opuesto. Esto podría verse modificado por el medio que resultaría en la dilución de las correlaciones entre partículas de signo opuesto [63]. Parece observarse una diferencia clara en la fuerza de correlación entre las combinaciones de partículas de carga igual y opuesta (ver Fig. 7.4). La simulación de correlaciones de carga opuesta

de la correlación de 3 partículas es similar a la señal medida pero la señal de igual carga es mucho mayor y de signo opuesto a la predicha. Este fenómeno también ha sido observado en ALICE en LHC [64].
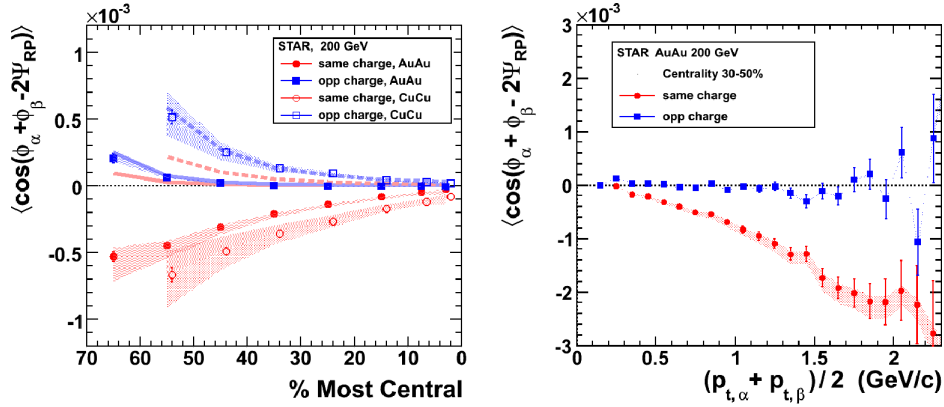
Figure 7.4: El observable que refleja las correlaciones azimutales de igual y opuesta carga se muestra dependiendo de la centralidad de la colisión para choques Au+Au y Cu+Cu (izquierda) y de la semi-suma de los momentos transversos sólo para colisiones Au+Au (derecha) extraído de [62]. En el panel izquierdo las líneas continua (Au+Au) y discontinua (Cu+Cu) representan los cálculos teóricos de correlaciones de 3 partículas.

La dependencia en la centralidad que se muestra en el panel izquierdo de la Fig. 7.4 coincide con la separación de carga relativa al plano de reacción. Por otro lado, la magnitud del efecto para partículas de igual carga aumenta con la media de p_T del par tanto en RHIC como en LHC. Esta observación se encuentra en contradicción con la expectativa inicial [63], que predice el dominio de partículas con bajo p_T. En cualquier caso, no se pueden exponer conclusiones definitivas debido a la falta de cálculos de modelos realistas para las dependencias en la centralidad y el momento del par.

Se esperan diferentes dinámicas de campo magnético en LHC y RHIC, un hecho que debería ser cuantificado. La señal de ruptura de paridad indica la presencia de una separación de carga cuya magnitud se encoge con una energía decreciente del haz, sugiriendo que el volumen del QGP se reduce con colisiones de menor energía, lo que conlleva una menor separación de carga. Se ha argumentado que a altas energías la fuerza del CME debería decrecer ya que el campo magnético decae mucho más rápido [65].

El análisis de diferentes correlaciones azimutales de carga para buscar separaciones de carga en un estado deconfinado de la materia puede ayudar en la posibilidad de probar nuevos efectos en QCD a altas temperaturas y densidades. En particular, la aparición de grandes fluctuaciones topológicas locales que inducen dominios metaestables con P y CP impar podrían ser detectados junto con la corriente electromagnética inducida por grandes momentos angulares o campos magnéticos en HIC no centrales. Además del estudio presentado, se planea el análisis de correlaciones de harmónicos de orden superior, que puede ayudar a proporcionar un mayor entendimiento de las

correlaciones dependientes de la carga observadas en RHIC y LHC.

7.5 El problema de los dileptones de baja masa

Se considera que los dileptones son la prueba electromagnética más útil para desentrañar los rasgos principales del medio caliente creado en HIC. éstos son producidos de forma continua transportando información de toda la evolución del sistema y dada la existencia de una variable adicional, su masa invariante $M_{\ell\ell}$, los dileptones poseen un mejor ratio señal/fondo comparado con los fotones. Dependiendo de la fase de la colisión, los dileptones son emitidos desde diferentes fuentes. Antes de la colisión, los dileptones se producen a través de una radiación de frenado coherente debido a la repulsión electromagnética entre los dos núcleos [66] pero esta contribución es despreciable comparada con otros procesos que le siguen [67]. Durante el calentamiento del sistema nuclear y antes de que se alcance el equilibrio, la aniquilación Drell-Yan proporciona la fuente principal de dileptones que puede ser dominante por encima de $M_{\ell\ell} \simeq 3$ GeV [68]. Cuando el sistema entra en el QGP y termaliza, los dileptones se crean principalmente de la dispersión perturbativa de quarks y antiquarks. A continuación, el plasma evoluciona a un gas de hadrones donde los dileptones se emiten de la aniquilación de piones y kaones (entre otros canales) [69]. La presencia de resonancias mesónicas vectoriales ligeras como ρ, ω y ϕ son responsables de un incremento de estos procesos debido a su conexión entre los estados de dos mesones iniciales y los dileptones finales [70]. La masa invariante de los dileptones corresponde a la distribución de masas del mesón vectorial en el preciso momento de la desintegración permitiendo entender mejor el medio a altas temperaturas. En las fases finales de la colisión cuando se congelan las interacciones entre hadrones, sólo los estados hadrónicos de larga vida (principalmente mesones) como π^0, η y ω son capaces de producir pares de leptones a través de su desintegración Dalitz ya que éstos ya no interactúan entre ellos [71]. Estos procesos corresponden a un estado inicial que se desintegra en un par de partículas, una de ellas es un fotón virtual que posteriormente decae en una pareja de leptones. Debido a la cinemática de estas desintegraciones, todas las fuentes de mesones mencionadas son relevantes para la producción de dileptones con una masa invariante por debajo de 1 GeV.

Debido a la relevancia de los dileptones, se han llevado a cabo numerosos estudios para desentrañar las principales características del medio nuclear. Posiblemente uno de los análisis más importantes y antiguos consiste en medir la distribución de masa invariante de los dileptones, que ha sido analizado por diferentes colaboraciones experimentales durante las últimas décadas. En colisiones protón-protón la forma de la distribución detectada puede ser correctamente reproducida por el llamado 'coctel' hadrónico, la suma de diversas desintegraciones de hadrones en el estado final con abundancias conocidas. De hecho, los datos pp normalmente se usan para ajustar el peso de los diferentes hadrones para ser usados para otras predicciones. Y mientras los datos protón-núcleo se pueden entender a partir de los resultados pp, las colisiones centrales núcleo-núcleo han presentado severas discrepancias con respecto a la contribución

teórica esperada [45, 46, 47], en particular, un fuerte incremento de dileptones con masa invariante por debajo de 1 GeV. Este desacuerdo refleja que los efectos en el medio han de ser considerados para explicar los resultados anormales en colisiones AA.

La producción anómala de dileptones en colisiones núcleo-núcleo ha sido un problema de larga duración que ha sido investigado por muchos grupos diferentes, tanto teóricos como experimentales (para un análisis detallado ver [72]). No se efectuaron medidas de dileptones en el acelerador AGS, donde se esperaban altas densidades bariónicas. La colaboración DLS en BEVALAC lanzó los primeros resultados de dielectrones para reacciones Ca+Ca, C+C, He+Ca y Nb+Nb con objetivo fijo a una energía del haz de 1 GeV por nucleón. La primera generación de datos de DLS [73] era consistente con los resultados de cálculos de modelos de transporte [74] incluyendo las fuentes convencionales de dileptones como la radiación de frenado pn, desintegraciones Dalitz de mesones ligeros, desintegraciones directas de mesones vectoriales y aniquilación pión-pión, sin incorporar efectos en el medio. Sin embargo, una versión actualizada de las medidas de DLS que incluía toda la muestra de datos y con un análisis mejorado mostró un incremento de casi un orden de magnitud en la sección eficaz comparado con los resultados previos [75]. Esta discrepancia ha persistido durante años y se han abordado numerosos intentos para desenredar los nuevos datos de DLS. De hecho, todos los escenarios en el medio que han explicado con éxito el incremento de dileptones a más altas energías en aceleradores más potentes fallan al describir los nuevos datos de dileptones de DLS, un problema que pronto fue conocido como el 'puzle DLS'.

El puzle DLS motivó el experimento HADES en SIS, un experimento de nueva generación que fue diseñado para estudiar colisiones C+C, Ni+Ni y Au+Au a unas energías del haz de hasta 8A GeV con un objetivo fijo. El exceso de dielectrones observado en DLS fue confirmado por los datos de HADES [76] haciendo colisionar C+C a 1A y 2A GeV. Recientemente, nuevas aproximaciones han intentado atacar este problema. Por un lado, el efecto fue parcialmente interpretado como si fuese debido a un incremento de la producción del mesón η en la dispersión protón-neutrón [77]. Por otro lado, un incremento en la contribución de radiación de frenado de acuerdo con cálculos de intercambio de un bosón condujo a un acuerdo bastante exitoso con los datos publicados por DLS y HADES en colisiones C+C [78]. Sin embargo, los mismos cálculos aún subestiman la producción de dileptones en reacciones Ca+Ca y por tanto, el tema aún es discutible.

En SPS el exceso de dileptones de baja masa en colisiones centrales núcleo-núcleo fue observado de nuevo. Se usaron dos haces diferentes: un haz de azufre a 200 GeV/nucleón y uno de plomo a 158 GeV/nucleón. La colaboración CERES presentó un exceso de dielectrones [45] donde se analizaban reacciones S+Au y Pb+Au con objetivo fijo. Además, mostraron que el incremento, particularmente importante en la región de masa alrededor de 400-600 MeV, cubría un amplio rango de momento transverso, pero era mayor a bajo momento transverso. Se observaron resultados anormales similares para dimuones de baja masa en HELIOS/3 [79] con reacciones S+W. Los resultados de reacciones S+Cu y S+U estudiadas por la colaboración NA38 junto con las colisiones

Pb+Pb en NA50 revelaron un exceso poco significante de dimuones [80], un hecho que muy probablemente pudo estar relacionado con un gran corte en M_T aplicado en su análisis. Estas medidas independientes del exceso de dileptones de baja masa en SPS desencadenaron una gran investigación teórica también motivada por una posible conexión con la ruptura de simetría quiral. La importancia de la densidad bariónica sugerida por efectos en el mesón ρ en el medio animaron a la colaboración CERES a medir dielectrones de baja masa en colisiones Pb+Au a una energía baja de 40A GeV donde se esperaba una alta densidad bariónica y una menor temperatura [81]. Se llevaron a cabo numerosas aproximaciones para describir el exceso de dileptones en SPS, donde no está claro que se alcanzase un equilibrio térmico. Finalmente, los datos pudieron ser aparentemente explicados mediante modificaciones en el medio del mesón ρ debido a su fuerte acoplo hadrónico y otras hipótesis menos convencionales [38, 41, 44, 78, 82].

El programa de física de dileptones de las colaboraciones NA38/NA50, HELIOS/3 y CERES fue continuado por el experimento NA60 también en SPS. Se investigaron colisiones núcleo-núcleo vía producción de dimuones en reacciones In+In a 158 GeV/nucleón con un objetivo fijo. El experimento exhibió un claro exceso de dimuones a bajas energías que aumentaba con la centralidad y bajo p_T del par [83]. Los modelos con más éxito de la época fueron comparados con los datos de alta calidad de NA60, que pudieron aislar el canal ρ del resto de fuentes hadrónicas. En particular, los escenarios de caída de masa y de ensanchamiento muestran resultados similares para masas por debajo del pico de resonancia del mesón ω debido a la limitada precisión de los datos, pero entre las resonancias ω y ϕ el caso de caída de masa parece ser descartado [46]. El escenario de ensanchamiento de masa [38] se refuerza con los datos de NA60, junto con otros cálculos recientes que aseguran reproducir el exceso de dileptones [39, 40]. Con todo, las aún considerables incertidumbres experimentales pueden permitir que otros efectos también tengan lugar.

RHIC es el primer acelerador con dos haces altamente energéticos impactando a $\sqrt{s_{NN}} = 200$ GeV/nucleón, donde actualmente se llevan a cabo colisiones Au+Au y son analizadas en los experimentos PHENIX y STAR. PHENIX ha medido un serio exceso de dielectrones a bajas energías que está presente a todo p_T pero éste es más pronunciado a bajo p_T del par [47]. Se observa una fuerte dependencia en la centralidad para el continuo de baja masa. El incremento aparece en colisiones centrales donde éste alcanza un factor casi 8 (ver Fig. 7.5). Los resultados de PHENIX son diferentes de los observados en SPS: mientras que en SPS el exceso era próximo al pico resonante del mesón ρ, en PHENIX éste se extiende hacia masas invariantes más bajas. Además, la producción integrada aumenta más rápido con la centralidad de las colisiones que el número de nucleones participantes. La contribución de pares correlacionados a partir de desintegraciones semileptónicas de mesones con el quark c, despreciable a las energías de SPS, es una fuente importante que ha de ser incluida en el coctel hadrónico en las energías de RHIC. Al contrario que en previos experimentos, los resultados de dileptones de baja masa de PHENIX no han sido reproducidos correctamente por ningún modelo con éxito que haya aparentemente explicado el exceso anteriormente.
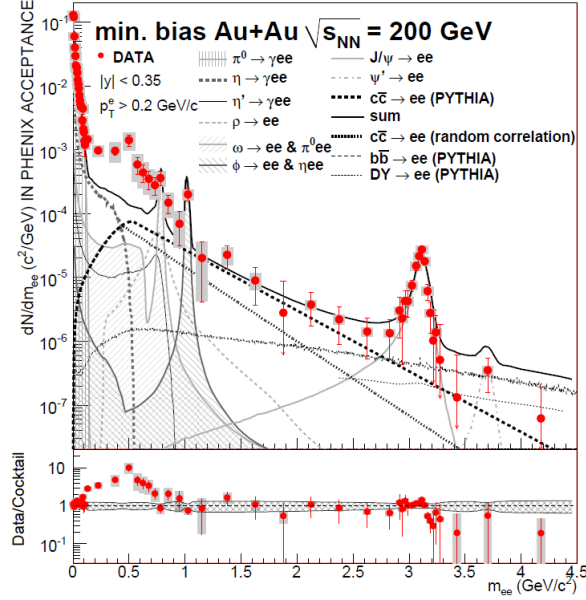
Figure 7.5: Espectro de masa de dielectrones en colisiones Au+Au con mínimo sesgo en PHENIX comparado con el coctel de las conocidas fuentes hadrónicas extraído de [47]. El ratio de los datos sobre el coctel se muestra en el panel inferior. Se observa un claro incremento de casi un orden de magnitud a bajas masas invariantes.

La colaboración STAR también presentó un incremento de dielectrones bajo el pico del mesón ω [84] pero se observó que era significantemente inferior que el medido en PHENIX. Debido a este exceso moderado, los datos de STAR posiblemente se pueden explicar mediante cálculos teóricos incluyendo un mesón ρ ensanchado en el medio. La centralidad y la dependencia en p_T también es comparable con las expectativas de cálculos a partir de modelos.

Finalmente, las colaboraciones de LHC aún no se han publicado medidas de dileptones de baja masa invariante.

También se ha medido un exceso de dileptones similar con una masa invariante de entre 1 y 3 GeV en SPS y RHIC. Todos los experimentos en SPS presentaron un exceso con respecto a la producción esperada a partir de las dos contribuciones principales en esta región de masas, las desintegraciones Drell-Yan y semileptónicas del quark c [79, 85]. Se investigaron diversas explicaciones basadas en hipótesis fenomenológicas de una producción incrementada c, como emisiones secundarias Drell-Yan, re-dispersiones en los estados finales que ensanchen la distribución de m_T de los mesones encantados aumentando la producción, y todas las fuentes de parejas de leptones a partir de interacciones mesónicas secundarias. NA60 concluyó que el exceso de dimuones en la región de masas intermedias corresponde a la radiación térmica emitida en las primeras etapas de la colisión [86]. Por el contrario, PHENIX mostró que la producción inclusiva parece estar de acuerdo con la contribución simulada de mesones encantados [47].

Vivimos en una era con numerosos experimentos en curso que pueden obtener infor-

mación relevante sobre la materia de QCD. Muchos modelos han intentado solucionar o explicar diferentes problemas con la adición de nuevos parámetros u observables que necesitan ser medidos. Gracias al duro trabajo experimental actual, la medida de estos parámetros puede ayudar a confirmar o descartar todos estos modelos. Además, uno no puede excluir el hecho de que podrían detectarse nuevos fenómenos. Este escenario constituye una fuente estimulante de motivación para la investigación tanto teórica como experimental.

7.6 Alcance y visión de conjunto

En el contexto de HIC, se pueden estudiar nuevos efectos en QCD debido a altas temperaturas y densidades. En particular, en esta tesis exploraremos la posibilidad de que el vacío de QCD rompa paridad en un volumen finito. El teorema de Vafa-Witten [87] prohíbe la ruptura espontánea de simetrías discretas en teorías gauge. Sin embargo, este teorema no se aplica cuando uno trata con un sistema denso. Las altas temperaturas y densidades alcanzadas en el medio fuertemente interactuante inducido en HIC nos llevan a un escenario realista donde la violación de paridad en QCD podría ser perceptible.

La violación de paridad en QCD ya ha sido estudiada por diferentes colaboraciones y aproximaciones [63, 88] que discutiremos. Aquí estamos interesados en describir las condiciones termodinámicas que podrían conducir a este fenómeno en HIC al igual que la fenomenología asociada a él. Si este efecto tiene lugar, las propiedades de los hadrones en el medio se verían severamente distorsionadas, lo que provocaría modificaciones inesperadas de las distribuciones de las partículas en el estado final. Mostraremos en detalle cómo los mesones escalares y vectoriales se ven influenciados por un medio de paridad impar y además, buscaremos posibles trazas que puedan ayudar a detectar este efecto en RHIC o LHC.

Primeramente, nos centramos en la posible existencia de una nueva fase caracterizada por la violación de paridad en QCD. Hemos analizado dos aproximaciones diferentes para explorar este efecto. La primera de ellas corresponde al estudio de QCD a densidad finita mediante técnicas de lagrangianos efectivos acoplados a un potencial químico bariónico no trivial. Un modelo sigma lineal generalizado que retiene los dos multipletes más ligeros de campos escalares y pseudoescalares de $SU(2)$ y que satisface las simetrías de QCD en el vacío muestra que para un rango dado de $\mu \neq 0$, un condensado pseudoescalar puede aparecer llevándonos a una nueva fase de QCD [88]. La segunda posibilidad está relacionada con la presencia de burbujas metaestables con P y CP impar en materia caliente debido a grandes fluctuaciones topológicas en un volumen finito. En este contexto un gran campo magnético o momento angular podría inducir un campo eléctrico perpendicular al plano de reacción y de ahí un momento dipolar eléctrico [63]. Este es el Efecto Magnético Quiral que ya ha sido presentado previamente y se dice que ha sido detectado en HIC periféricas en STAR [62]. Siguiendo los argumentos de esta última aproximación, investigamos la violación de paridad

en QCD como consecuencia de grandes fluctuaciones topológicas correspondiendo a un efecto de no-equilibrio que puede ser tratado por un potencial químico axial externo μ_5.

A continuación implementamos el modelo NJL con un potencial químico vectorial y axial a temperatura cero para investigar el diagrama de fases del modelo en busca de posibles fases con un condensado pseudoescalar que violen paridad. Vemos que un μ_5 diferente de cero modifica severamente las propiedades conocidas del modelo NJL mientras que la presencia de μ no afecta demasiado a nuestras consideraciones. Siempre que ciertas relaciones numéricas entre los parámetros del modelo se satisfagan, se encuentra que la ruptura de paridad espontánea es estable. En particular, encontramos una fase con un condensado pseudoescalar singlete de isospín no trivial al igual que un condensado escalar a partir de un valor crítico del potencial químico axial. Sin embargo, NJL con tales parámetros característicos no tiene nada que ver con QCD ya que las masas de los conocidos estados mesónicos en el vacío no son compatibles con la fenomenología. A pesar de no poder dar conclusiones definitivas para QCD, los valores de μ_5 que llevan a una fase termodinámicamente estable con violación de paridad sugieren el rango de potenciales químicos axiales donde se ha de buscar la fase de ruptura de paridad en experimentos de HIC.

Después de investigar los posibles valores de μ_5 que podrían conllevar una violación de paridad, estudiamos detalladamente las modificaciones de los mesones en el medio. Primero de todo, analizamos los mesones escalares y pseudoescalares en un medio caracterizado por un potencial químico axial no trivial. Implementamos un modelo sigma generalizado incluyendo los mesones escalares y pseudoescalares más ligeros en la representación de $SU(3)$ para investigar la mezcla entre los estados de diferente paridad y mismo sabor inducidos por un medio de paridad impar donde de hecho, la distinción entre estados escalares y pseudoescalares no tiene ya sentido. Se introduce el potencial químico axial como un espurio campo vector axial externo a través de una derivada covariante. Los mesones en el medio exhiben propiedades dependientes de la energía como el espectro y las anchuras de desintegración. Vemos que los grados de libertad más ligeros en cada canal de isospín se convierten en estados taquiónicos a altas energías. Además, el gas de piones que constituye la bola de fuego en una colisión de HIC una vez alcanza la fase hadrónica podría ser un gas de piones distorsionados debido al efecto de ruptura de paridad. Calculamos las anchuras de desintegración de todos estos estados a piones distorsionados para buscar posibles resonancias anchas que pudiesen sufrir un proceso de regeneración como en el caso del mesón ρ. En particular, el mesón η distorsionado parece estar en equilibrio térmico dentro del gas de 'piones' debido a su gran anchura, a diferencia de lo que sucede en el vacío.

En el sector de los mesones vectoriales introducimos el efecto de ruptura de paridad a través del término de Chern-Simons ya que la mezcla de estados de diferente paridad es bastante incierta. Mediante el modelo de Dominancia de Mesones Vectoriales (VMD) introducimos los estados más ligeros en la representación de $SU(3)$. Sin embargo, el mesón ϕ se desacopla del resto del sistema y éste puede ser simplificado a $SU(2)$. Se en-

cuenta una mezcla entre fotones y los mesones ρ y ω debido al propio mecanismo VMD y al efecto de violación de paridad. Después de resolver el sistema mezclado encontramos una relación de dispersión distorsionada para los mesones vectoriales mientras que los fotones no se ven afectados por los efectos de ruptura de paridad. Como en el caso de los mesones de espín nulo, los mesones vectoriales muestran una masa efectiva dependiente del sistema de referencia y un comportamiento taquiónico para una de sus polarizaciones. Las modificaciones en el medio de los mesones vectoriales pueden ser examinadas a través de sus desintegraciones en dileptones. La forma distorsionada de las funciones espectrales de ρ y ω predice un incremento de la producción de dileptones alrededor de su pico de resonancia. Vemos que este incremento podría ayudar a explicar parcialmente el exceso de dileptones de baja masa presentado en la Section 7.5 para los experimentos NA60/PHENIX/STAR. Pero esta señal puede ser bastante complicada de detectar. La forma distorsionada de las funciones espectrales de ρ y ω revelan una asimetría en sus polarizaciones alrededor del pico en el vacío. De ahí, describimos cómo el efecto de ruptura de paridad puede ser detectado en HIC a partir de la restricción de la cobertura angular en los estados leptónicos finales. Se presentan dos variables angulares adecuadas para buscar posibles dependencias en la polarización y explicamos cómo un análisis combinado de una de estas variables junto con la masa invariante de los dileptones puede ser una traza importante para detectar la ruptura de paridad en HIC.

7.7 Lista de publicaciones

7.7.1 Publicaciones en revistas

- A. A. Andrianov, V. A. Andrianov, D. Espriu and X. Planells, *Analysis of dilepton angular distributions in a parity breaking medium*, Phys. Rev. D 90 (2014) 034024, arXiv:1402.2147 [hep-ph].

- A. A. Andrianov, D. Espriu and X. Planells, *Chemical potentials and parity breaking: the Nambu–Jona-Lasinio model*, Eur. Phys. J. C 74 (2014) 2776 [arXiv:1310.4416 [hep-ph]].

- A. A. Andrianov, D. Espriu and X. Planells, *An effective QCD Lagrangian in the presence of an axial chemical potential*, Eur. Phys. J. C 73 (2013) 2294 [arXiv:1210.7712 [hep-ph]].

- A. A. Andrianov, V. A. Andrianov, D. Espriu and X. Planells, *Dilepton excess from local parity breaking in baryon matter*, Phys. Lett. B 710 (2012) 230 [arXiv:1201.3485 [hep-ph]].

- A. A. Andrianov, V. A. Andrianov, D. Espriu and X. Planells, *Abnormal enhancement of dilepton yield in central heavy-ion collisions from local parity breaking*, Theor. Math. Phys. 170 (2012) 17.

7.7.2 Otras publicaciones

- A. A. Andrianov, D. Espriu and X. Planells, *An effective theory for QCD with an axial chemical potential*, PoS QFTHEP 2013 (2014) 049 [arXiv:1310.4434 [hep-ph]].

- A. A. Andrianov, V. A. Andrianov, D. Espriu and X. Planells, *Implications of local parity breaking in heavy ion collisions*, PoS QFTHEP 2011 (2013) 025 [arXiv:1310.4428 [hep-ph]].

- A. A. Andrianov, V. A. Andrianov, D. Espriu and X. Planells, *Abnormal dilepton yield from parity breaking in dense nuclear matter*, AIP Conf. Proc. 1343 (2011) 450 [arXiv:1012.0744 [hep-ph]].

- A. A. Andrianov, V. A. Andrianov, D. Espriu and X. Planells, *The problem of anomalous dilepton yield in relativistic heavy-ion collisions*, PoS QFTHEP 2010 (2010) 053.

7.7.3 Trabajos sin publicar

- A. A. Andrianov, V. A. Andrianov, D. Espriu and X. Planells, *Abnormal dilepton yield from local parity breaking in heavy-ion collisions* (2010) [arXiv:1010.4688 [hep-ph]].

Appendix A

Calculation of the fermion determinant in Chapter 3

In this appendix we address the analysis of the determinant of the fermion operator presented in Eq. (3.6)

$$\mathcal{M}(\mu, \mu_5) = \slashed{\partial} + (M + \vec{\tau}\vec{a}) - \mu\gamma_0 - \mu_5\gamma_0\gamma_5 + i\gamma_5(\vec{\tau}\vec{\pi} + \eta).$$

As it has been already stressed in [127], the fermion determinant can be proven to be real. The presence of both a vector and an axial chemical potentials does not modify this feature. Invariance under parity and time reversal symmetries also provide some equalities that will be useful for our purposes. Let us introduce some useful formulæ in the Dirac representation where the superscripts P and T stand for parity and time reversal transformations:

$$\det(\mathcal{M}) = \det(\mathcal{M}^P) = \det(\mathcal{M}^T), \quad \Gamma \equiv -i\gamma_0\gamma_5 = \Gamma^\dagger, \quad \gamma_2\gamma_\mu\gamma_2^\dagger = \gamma_\mu^*, \quad \Gamma^2 = \gamma_2\gamma_2^\dagger = 1$$

$$\mathcal{M}^\dagger(\mu, \mu_5) = \slashed{\partial} + (M + \vec{\tau}\vec{a}) - \mu\gamma_0 + \mu_5\gamma_0\gamma_5 - i\gamma_5(\vec{\tau}\vec{\pi} + \eta)$$

$$\gamma_0\slashed{\partial}\gamma_0 = \slashed{\partial}^P, \qquad \Gamma\slashed{\partial}\Gamma^\dagger = \slashed{\partial}^T, \qquad \gamma_2\slashed{\partial}\gamma_2^\dagger = \slashed{\partial}^*, \qquad \gamma_0^* = \gamma_0, \qquad \gamma_5^* = \gamma_5$$

Let us recall that external fields are constant and the parity and time reversal transformations do not modify them. Invariance under parity leads to

$$\det(\mathcal{M}(\mu, \mu_5)) = \det(\mathcal{M}^P(\mu, \mu_5))$$
$$= \det(\slashed{\partial} + (M + \vec{\tau}\vec{a}) - \mu\gamma_0 + \mu_5\gamma_0\gamma_5 - i\gamma_5(\vec{\tau}\vec{\pi} + \eta)) = \det(\mathcal{M}^\dagger(\mu, \mu_5)),$$

where we multiplied the expression by $\gamma_0[\ldots]\gamma_0$. This equality shows that the determinant is real independently on the external values. The same process may be done using invariance under time reversal and multiplying by $\Gamma^\dagger[\ldots]\Gamma$:

$$\det(\mathcal{M}(\mu, \mu_5)) = \det(\mathcal{M}^T(\mu, \mu_5))$$
$$= \det(\slashed{\partial} + (M + \vec{\tau}\vec{a}) + \mu\gamma_0 - \mu_5\gamma_0\gamma_5 - i\gamma_5(\vec{\tau}\vec{\pi} + \eta)) = \det(\mathcal{M}^\dagger(-\mu, -\mu_5)).$$

A. CALCULATION OF THE FERMION DETERMINANT IN CHAPTER 3

Finally, let us stress that we are only interested in the neutral components of the isotriplet external fields and then we can compute the conjugate of the determinant and multiply at both sides of the expression by $\gamma_2^\dagger[\dots]\gamma_2$

$$[\det(\mathcal{M}(\mu, \mu_5))]^* = \det(\mathcal{M}^*(\mu, \mu_5))$$
$$= \det(\slashed{\partial} + (M + \vec{\tau}\vec{a}) + \mu\gamma_0 - \mu_5\gamma_0\gamma_5 + i\gamma_5(\vec{\tau}\vec{\pi} + \eta)) = \det(\mathcal{M}(-\mu, \mu_5)).$$

The last two expressions are useful to show

$$\det(\mathcal{M}(\mu, \mu_5)) = \det(\mathcal{M}(-\mu, -\mu_5)) = \det(\mathcal{M}(-\mu, \mu_5)) = \det(\mathcal{M}(\mu, -\mu_5)).$$

In particular, we will use

$$\det(\mathcal{M}(\mu, \mu_5)) = \det(\mathcal{M}^\dagger(\mu, \mu_5)) = \det(\mathcal{M}(\mu, -\mu_5)) = \det(\mathcal{M}^\dagger(\mu, -\mu_5)).$$

We shall use N to be even in order the determinant to be positive defined and use the fact that $\det(\mathcal{M})^2 = \det(\mathcal{M}^2)$. The development of the product

$$\mathcal{M}(\mu, \mu_5)\mathcal{M}^\dagger(\mu, -\mu_5) = -\partial^2 + M^2 + \vec{\pi}^2 + (\eta^2 + \vec{a}^2) + 2M\vec{\tau}\vec{a} + 2\eta\vec{\tau}\vec{\pi}$$
$$+ 2\gamma_5(\vec{a} \times \vec{\pi})\vec{\tau} - \mu^2 + \mu_5^2 + 2\mu\partial_0 - 2\mu_5\gamma_0\vec{\gamma}\vec{\partial}\gamma_5$$

provides a result which is scalar in flavour except for the term proportional to μ_5. An additional product produces

$$\mathcal{M}(\mu, \mu_5)\mathcal{M}^\dagger(\mu, -\mu_5)\mathcal{M}(\mu, -\mu_5)\mathcal{M}^\dagger(\mu, \mu_5) = A' + \vec{\tau}(\vec{\alpha}' + \vec{\epsilon}'\gamma_5)$$

with

$$A' = A^2 + \vec{\alpha}^2 + \vec{\epsilon}^2 + 4\mu_5^2\vec{\partial}^2, \qquad \vec{\alpha}' = 2A\vec{\alpha}, \qquad \vec{\epsilon}' = 2A\vec{\epsilon}$$
$$A = -\partial^2 + M^2 + \vec{\pi}^2 + (\eta^2 + \vec{a}^2) - \mu^2 + \mu_5^2 + 2\mu\partial_0,$$
$$\vec{\alpha} = 2(M\vec{a} + \eta\vec{\pi}),$$
$$\vec{\epsilon} = 2(\vec{a} \times \vec{\pi}), \qquad \vec{\alpha}\vec{\epsilon} = 0$$

with the property $\vec{\alpha}'\vec{\epsilon}' = 0$. The logarithm of a quantity with such characteristics can be calculated and all the non-diagonal operators in Dirac or flavour space disappear leading to

$$\log[A + \vec{\tau}(\vec{\alpha} + \vec{\epsilon}\gamma_5)] = \frac{1}{2}\log[A^2 - \vec{\alpha}^2 - \vec{\epsilon}^2].$$

The evaluation of the argument leads us to

$$A'^2 - \vec{\alpha}'^2 - \vec{\epsilon}'^2 = \prod_{\pm} \left[-(ik_0 + \mu)^2 + (|\vec{k}| \pm \mu_5)^2 + M_+^2\right]\left[-(ik_0 + \mu)^2 + (|\vec{k}| \pm \mu_5)^2 + M_-^2\right]$$

where $M_{\pm}^2 = (M \pm a)^2 + (\eta \pm \pi)^2$. Finally the fermion determinant can be written as

$$
\begin{aligned}
\log \det(\mathcal{M}(\mu, \mu_5)) =& \mathrm{Tr} \log \mathcal{M}(\mu, \mu_5) = \frac{1}{8} \mathrm{Tr} \log(A'^2 - \vec{\alpha}'^2 - \vec{\epsilon}'^2) \\
=& \frac{1}{8} \mathrm{Tr} \sum_{\pm} \left\{ \log \left[-(ik_0 + \mu)^2 + (|\vec{k}| \pm \mu_5)^2 + M_+^2 \right] \right. \\
& \left. + \log \left[-(ik_0 + \mu)^2 + (|\vec{k}| \pm \mu_5)^2 + M_-^2 \right] \right\},
\end{aligned}
\tag{A.1}
$$

where the trace operator is given by

$$
\mathrm{Tr}(1) = 8NT \sum_n \int \frac{d^3\vec{k}}{(2\pi)^3} [k_0 \to \omega_n^F],
$$

with $\omega_n^F = (2n+1)\pi/\beta$.

A.1 Inclusion of temperature

A finite temperature can be included with the formalism of the Matsubara frequencies [163]

$$
\int \frac{dk_0}{2\pi} f(k_0) = iT \sum_{n=-\infty}^{\infty} f(i\omega_n)
$$

where $\beta T = 1$ and

$$
\omega_n^B = \frac{2n\pi}{\beta}, \qquad \omega_n^F = \frac{(2n+1)\pi}{\beta}
$$

are the Matsubara frequencies for fermions or bosons. In our case, we are intersted in integrating Eq. (3.11) which can be written as

$$
\sum_n \frac{1}{E^2 - (i\omega_n^F + \mu)^2} = \frac{1}{2E} \sum_n \left[\frac{1}{(E + \mu) + i\omega_n^F} - \frac{1}{(-E + \mu) + i\omega_n^F} \right].
$$

In order to sum the previous expression, we take the function

$$
f(\tau) = n^F(E + \mu)e^{(E+\mu+i\pi T)\tau} + (n^F(E - \mu) - 1)e^{(-E+\mu+i\pi T)\tau}
$$

and impose periodicity in the interval $\tau \in [0, \beta)$ that is extended to all real values, say $f(\tau + \beta) = f(\tau)$. In the previous expression we used the fermion and boson Boltzmann distributions

$$
n^F(E) \equiv \frac{1}{\exp(\beta E) + 1}, \qquad n^B(E) \equiv \frac{1}{\exp(\beta E) - 1}.
$$

The decomposition of $f(\tau)$ in a Fourier expansion

$$
f(\tau) = T \sum_{n=-\infty}^{\infty} c_n e^{-i\omega_n^B \tau}, \qquad c_n = \int_0^{\beta} f(\tau) e^{i\omega_n^B \tau} d\tau.
$$

A. CALCULATION OF THE FERMION DETERMINANT IN CHAPTER 3

leads to some coefficients c_n that are directly related to the sum in Eq. (3.11) and thus, one automatically finds that

$$\sum_n \frac{1}{E^2 - (i\omega_n^F + \mu)^2} = -\frac{\beta}{2E} \left[n^F(E + \mu) + n^F(E - \mu) - 1 \right],$$

which is related to $f(\tau)$.

After performing the sum of frequencies, we are left with a term $(|\vec{k}| \pm \mu_5)^2$ that requires a change of variable $\hat{\vec{k}} = \vec{k}(1 \pm \mu_5/|\vec{k}|)$. Then

$$d^3\vec{k} = \frac{d^3\hat{\vec{k}}}{\det\left(\frac{\partial \hat{k}^i}{\partial k^j}\right)} = d^3\hat{\vec{k}} \frac{1}{\left(1 \pm \frac{\mu_5}{|\vec{k}|}\right)^2} = d^3\hat{\vec{k}} \left(1 \mp \frac{\mu_5}{|\hat{\vec{k}}|}\right)^2 \tag{A.2}$$

For simplicity, let us rescale the 3-momentum as $\vec{k} = \mu_5 \vec{x}$. Then, the integral we will find is

$$\int d^3\vec{k} f(|\vec{k}| \pm \mu_5) \longleftrightarrow \int d^3\vec{x} f(|\vec{x}| \pm 1).$$

The previous change of variable allows us to write

$$\int_{R^3} d^3\vec{x} f(|\vec{x}| \pm 1) = \int_{\tilde{R}^3} f(|\vec{x}'|) d^3\vec{x}' \left(1 \mp \frac{1}{|\vec{x}'|}\right)^2,$$

where $f(|\vec{x}'|) \equiv f(x') = f(-x')$ due to the structure of Eq. (3.11). Note that the integration domain changed non-trivially. $\tilde{R}^3$ corresponds to $|\vec{x}'_\pm| \in [\pm 1, +\infty)$. We can separate the $\pm$ contributions to study them more clearly. The + integral is

$$\int d\Omega \int_{+1}^{\infty} x'^2 f(x') dx' \left(1 - \frac{1}{x'}\right)^2 = \left[\int_{R^3} - \int_{0 \le |\vec{x}'| \le 1}\right] f(|\vec{x}'|) d^3\vec{x}' \left(1 - \frac{1}{|\vec{x}'|}\right)^2.$$

The - integral is given by

$$\int d\Omega \int_{-1}^{\infty} x'^2 f(x') dx' \left(1 + \frac{1}{x'}\right)^2 = \left[\int_{R^3} + \int_{-1 \le |\vec{x}'| \le 0}\right] f(|\vec{x}'|) d^3\vec{x}' \left(1 + \frac{1}{|\vec{x}'|}\right)^2,$$

where the last integral can be rewritten as

$$\int_{-1 \le |\vec{x}'| \le 0} f(|\vec{x}'|) d^3\vec{x}' \left(1 + \frac{1}{|\vec{x}'|}\right)^2 = \int d\Omega \int_{-1}^{0} f(x') x'^2 dx' \left(1 + \frac{1}{x'}\right)^2$$

$$= \int d\Omega \int_{1}^{0} f(-x')(-x')^2(-dx') \left(1 + \frac{1}{-x'}\right)^2 = \int d\Omega \int_{0}^{1} f(x') x'^2 dx' \left(1 - \frac{1}{x'}\right)^2$$

$$= \int_{0 \le |\vec{x}'| \le 1} f(x') d^3\vec{x}' \left(1 - \frac{1}{|\vec{x}'|}\right)^2$$

We can generalize the $\pm$ integrals with the following expression:

$$\int_{\tilde{R}^3} f(|\vec{x}'|)d^3\vec{x}' \left(1 \mp \frac{1}{|\vec{x}'|}\right)^2 = \int_{R^3} f(|\vec{x}'|)d^3\vec{x}' \left(1 \mp \frac{1}{|\vec{x}'|}\right)^2$$
$$\mp \int_{0 \le |\vec{x}'| \le 1} f(x')d^3\vec{x}' \left(1 - \frac{1}{|\vec{x}'|}\right)^2.$$

In the case one has the sum of both integrals, the second term disappears and one is left with

$$\int d^3\vec{x}[f(|\vec{x}|+1) + f(|\vec{x}|-1)] = 2\int f(|\vec{x}'|)d^3\vec{x}' \left(1 + \frac{1}{|\vec{x}'|^2}\right),$$

which can be rewritten again in terms of the 3-momentum $\vec{k}$ as

$$\sum_{\pm} \int d^3\vec{k} f(|\vec{k}| \pm \mu_5) = 2\int f(|\vec{k}|)d^3\vec{k} \left(1 + \frac{\mu_5^2}{|\vec{k}|^2}\right).$$

With all these ingredients Eq. (3.11) is reduced to the calculation of two different integrals. The first type of integral is finite and reads

$$I_n(\mu) = \sum_{\pm} \int \frac{d^3\vec{k}}{(2\pi)^3 E_\pm^n} n^F(E_\pm - \mu),$$

where we used the notation $E_\pm^2 \equiv (|\vec{k}| \pm \mu_5)^2 + M^2$. In the limit $T \to 0$ the Boltzmann distribution becomes $n^F(E) \to \Theta(-E)$ and then

$$I_n(\mu) = 2\int \frac{d^3\vec{k}}{(2\pi)^3 E^n}\Theta(\mu - E)\left(1 + \frac{\mu_5^2}{|\vec{k}|^2}\right)$$
$$= \frac{1}{\pi^2}\int_0^\infty \frac{k^2 dk}{(k^2+M^2)^{n/2}}\Theta(\mu - \sqrt{k^2+M^2})\left(1 + \frac{\mu_5^2}{k^2}\right)$$
$$= \frac{1}{\pi^2}\Theta(\mu - M)\int_0^{\sqrt{\mu^2-M^2}} \frac{dk}{(k^2+M^2)^{n/2}}\left(k^2 + \mu_5^2\right).$$

Finally one finds

$$I_1(\mu) = \frac{1}{2\pi^2}\Theta(\mu - M)\left[\mu\sqrt{\mu^2-M^2} + (2\mu_5^2 - M^2)\log\left(\frac{\mu+\sqrt{\mu^2-M^2}}{M}\right)\right]. \quad \text{(A.3)}$$

The second type of integral may be divergent and in such case the final result depends on the regularization scheme. In dimensional regularization usual integration techniques lead to

$$J_n = \sum_{\pm} \int \frac{d^3\vec{k}}{(2\pi)^3 E_\pm^n}$$
$$= \frac{M^{3-n}}{4\pi^{3/2}}\left(\frac{M^2}{4\pi\mu_R^2}\right)^{-\epsilon} \frac{\Gamma\left(\frac{n-1}{2}+\epsilon\right)}{\left(\frac{n-3}{2}+\epsilon\right)\Gamma\left(\frac{n}{2}\right)}\left[1 + \frac{2\mu_5^2}{M^2}\left(\frac{n-3}{2}+(n-2)\epsilon\right)\right].$$

A. CALCULATION OF THE FERMION DETERMINANT IN CHAPTER 3

In particular we are interested in

$$J_1 = -\frac{M^2}{4\pi^2} \left[\left(1 - \frac{2\mu_5^2}{M^2}\right) \left(\frac{M^2}{4\pi\mu_R^2}\right)^{-\epsilon} \Gamma(\epsilon) + 1 - \frac{4\mu_5^2}{M^2} \right],$$

which can also be calculated by means of a 3-dimensional cut-off leading to

$$\begin{aligned}
J_1^\Lambda &= \frac{1}{2\pi^2} \left[\Lambda\sqrt{M^2 + \Lambda^2} - (M^2 - 2\mu_5^2) \log\left(\frac{\Lambda + \sqrt{M^2 + \Lambda^2}}{M}\right) \right] \\
&\approx \frac{1}{2\pi^2} \left[\Lambda^2 - (M^2 - 2\mu_5^2) \log\left(\frac{2\Lambda}{M}\right) + \frac{1}{2}M^2 \right].
\end{aligned}$$

Finally, Eq. (3.11) can be summed leading to

$$\begin{aligned}
K_1^{\mathrm{DR}}(M, \mu, \mu_5) = \frac{1}{2\pi^2} &\left[\Theta(\mu - M) \left\{ \mu\sqrt{\mu^2 - M^2} + (2\mu_5^2 - M^2) \log\left(\frac{\mu + \sqrt{\mu^2 - M^2}}{M}\right) \right\} \right. \\
&\left. - \frac{1}{2}M^2 + \frac{1}{2}(M^2 - 2\mu_5^2) \left(\frac{1}{\epsilon} - \gamma_E + 2 - \log\frac{M^2}{4\pi\mu_R^2}\right) \right],
\end{aligned} \qquad (A.4)$$

in dimensional regularization while a 3-dimensional cut-off yields

$$\begin{aligned}
K_1^\Lambda(M, \mu, \mu_5) = \frac{1}{2\pi^2} &\left[\Theta(\mu - M) \left\{ \mu\sqrt{\mu^2 - M^2} + (2\mu_5^2 - M^2) \log\left(\frac{\mu + \sqrt{\mu^2 - M^2}}{M}\right) \right\} \right. \\
&\left. - \frac{1}{2}M^2 + \frac{1}{2}(M^2 - 2\mu_5^2) \log\frac{4\Lambda^2}{M^2} - \Lambda^2 \right].
\end{aligned} \qquad (A.5)$$

Appendix B

Dalitz decays in a parity-odd medium

In the calculation of the dilepton production, the inclusion of the ρ and ω contributions could seem to be insufficient. In this Appendix we will calculate the Dalitz decays of the main resonances appearing the hadronic 'cocktail' in a parity-odd medium. In fact, the most significant discrepancy in PHENIX data is observed in the region of $M \sim 500$ MeV (see Fig. 1.5), where one expects an important contribution from all the Dalitz decays. Dalitz decays are one of the main sources of dileptons in the last stages of a HIC after hadron freezout. Although one would not expect in-medium modifications of these processes, their study could help to investigate the possibility that LPB survives at low temperatures.

The processes we will consider here are: $\eta \rightarrow \gamma e^+ e^-$, $\eta' \rightarrow \gamma e^+ e^-$ and $\omega \rightarrow \pi^0 e^+ e^-$. Let us stress that the Kroll-Wada (KW) formula [158] cannot be applied directly in this context since the masses of both scalar/pseudoscalar and vector mesons depend on the 3-momentum and the calculation has to be redone. For comparison with PHENIX, we will use the same experimental cuts and temperature as discussed in Chapter 5. NA60 has also been able to identify the individual contributions from η and ω Dalitz decays and found an enhancement, particularly for the latter[164]. The behaviour of the η decay is very similar as the one predicted by KW. However, NA60 fits the ω Dalitz decay with a form factor where the ρ meson has zero width. We skip any possible comparison with the latter as the relation of this fit with our results could be misleading.

B.1 ω Dalitz decay

In this section, we will investigate the Dalitz decay $\omega \rightarrow \pi^0 e^+ e^-$ in order to see if a parity-odd medium could strongly affect the production of dileptons. The $\omega \pi \gamma$ interaction is governed by the Lagrangian

$$\mathcal{L} = ie\frac{g_{\omega\pi\gamma}}{m_\omega}\varepsilon^{\mu\nu\rho\sigma}A_\mu\partial_\nu\pi\partial_\rho\omega_\sigma, \tag{B.1}$$

with $g_{\omega\pi\gamma} \simeq g$. The calculation of this process will be performed in two ways. The first one consists in considering the decaying meson as a 'free' state with the only in-medium modification driven by the distorted propagator of the ρ meson that produces the lepton pair. In the second approach we assume that the ω meson is also modified by the parity-odd medium together with the assumption that it has been created from a previous process that induces a Breit-Wigner distribution for the initial state.

B.1.1 Free ω

In the case that the decaying ω meson is not affected by LPB, the squared modulus of the amplitude can be written as

$$\overline{|\mathcal{M}|^2} = -\frac{1}{3} \left(\frac{8\pi g\alpha}{m_\omega M^2} \right)^2 \varepsilon^{\mu\nu\alpha\beta} q_\mu k_\beta \varepsilon^{\mu'\nu'\alpha'\beta'} q_{\mu'} k_{\beta'} g_{\nu\nu'} \sum_{\epsilon,\epsilon'} P^\epsilon_{\alpha\lambda} F^\epsilon P^{\epsilon'}_{\lambda'\alpha'} F^{*\epsilon'}$$
$$\times \left(p^\lambda p'^{\lambda'} + p^{\lambda'} p'^\lambda - \frac{M^2}{2} g^{\lambda\lambda'} \right). \qquad \text{(B.2)}$$

The definition of momenta is the following: q for ω, k for ρ, and p and p' for the two leptons. Let us remark that ϵ and ϵ' are the polarizations of the ρ meson. The dilepton production is then given by

$$\frac{dN}{d^4 x dM^2} = \int \frac{d^4 q \, d^4 p_\pi \, d^4 p \, d^4 p'}{[(2\pi)^3]^4} \delta(p^2 - m_e^2) \delta(p'^2 - m_e^2) \delta(q^2 - m_\omega^2) \delta(p_\pi^2 - m_\pi^2)$$
$$\times \int \frac{d^4 k}{2\pi} \delta(k^2 - M^2)[(2\pi)^4 \delta^4(q - k - p_\pi)(2\pi)^4 \delta^4(p + p' - k)] \overline{|\mathcal{M}|} f(q), \quad \text{(B.3)}$$

where $f(q)$ is a Boltzmann distribution for the ω meson and the form factors are the same ones as in Eq. (5.28). An in-medium thermal ω meson may be disputable but it is necessary to introduce a momentum distribution for it and this could be a reasonable first approach. The results of this approach and the next one are shown together in Fig. B.1.

B.1.2 In-medium ω

The case when the decaying ω meson is affected by LPB is more involved. First of all, the squared modulus of the amplitude for one of the ω polarizations can be written as

$$\overline{|\mathcal{M}|^2}(\epsilon_\omega) = -\frac{1}{3} \left(\frac{8\pi g\alpha}{m_\omega M^2} \right)^2 \varepsilon^{\mu\nu\alpha\beta} q_\mu k_\beta \varepsilon^{\mu'\nu'\alpha'\beta'} q_{\mu'} k_{\beta'} P^{\epsilon_\omega}_{\nu\nu'} \sum_{\epsilon,\epsilon'} P^\epsilon_{\alpha\lambda} F^\epsilon P^{\epsilon'}_{\lambda'\alpha'} F^{*\epsilon'}$$
$$\times \left(p^\lambda p'^{\lambda'} + p^{\lambda'} p'^\lambda - \frac{M^2}{2} g^{\lambda\lambda'} \right). \qquad \text{(B.4)}$$

while ϵ_ω corresponds to the ω meson. The algebraic calculation of this matrix element is rather tricky so we will use a shorthand notation through the definition

$$\overline{|\mathcal{M}|^2}(\epsilon_\omega) = \frac{2}{3}\left(\frac{4\pi g\alpha}{m_\omega M^2}\right)^2 \sum_{\epsilon,\epsilon'} F^\epsilon F^{*\epsilon'}[\epsilon_\omega,\epsilon,\epsilon'], \tag{B.5}$$

$$[\epsilon_\omega,\epsilon,\epsilon'] = \varepsilon^{\mu\nu\alpha\beta}\varepsilon^{\mu'\nu'\alpha'\beta'} q_\mu q_{\mu'} k_\beta k_{\beta'} P^{\epsilon_\omega}_{\nu\nu'} P^\epsilon_{\alpha\lambda} P^{\epsilon'}_{\lambda'\alpha'} \left(4p^\lambda p^{\lambda'} + M^2 g^{\lambda\lambda'}\right).$$

We will assume that the ω meson is created from a previous process that induces a Breit-Wigner distribution for it. In this case the mass-shell condition has to be replaced in Eq. (B.3) by

$$\delta(q^2 - m_\omega^2) \quad \Longleftrightarrow \quad \Delta(q^2,\vec{q},\epsilon_\omega) = \frac{1}{\pi}\frac{\Gamma_\omega m^2_{\omega,\epsilon_\omega}/m_\omega}{(q^2 - m^2_{\omega,\epsilon_\omega})^2 + (\Gamma_\omega m^2_{\omega,\epsilon_\omega}/m_\omega)^2}, \tag{B.6}$$

and the effective meson mass $m^2_{\omega,\epsilon_\omega}$ is given by the dispersion relation in Eq. (5.27). The different combinations for the three polarizations can be summarized as follows:

$$[+\pm\pm] = [-\mp\mp] = -\frac{1}{2}\left[\vec{p}^2 - \frac{(\vec{p}\vec{k})^2}{\vec{k}^2} - \frac{M^2}{2}\right]\left(\frac{E_q}{|\vec{q}|} \pm \frac{E_k}{|\vec{k}|}\right)^2 \left(|\vec{q}||\vec{k}| \mp \vec{q}\vec{k}\right)^2,$$

$$[+\pm\mp] = [-\pm\mp] = \left(\frac{E_k^2}{\vec{k}^2} - \frac{E_q^2}{\vec{q}^2}\right)\left[\frac{1}{2}\left(\vec{p}^2 - \frac{(\vec{p}\vec{k})^2}{\vec{k}^2}\right)\left(\vec{q}^2\vec{k}^2 - (\vec{q}\vec{k})^2\right) - \vec{p}(\vec{q}\times\vec{k})\right.$$

$$\left. \times \left(\vec{p}(\vec{q}\times\vec{k}) \mp i|\vec{k}|\left(\vec{q}\vec{p} - \frac{(\vec{p}\vec{k})(\vec{q}\vec{k})}{\vec{k}^2}\right)\right)\right],$$

$$[L++] = [L--] = \left[\vec{p}^2 - \frac{(\vec{p}\vec{k})^2}{\vec{k}^2} - \frac{M^2}{2}\right]\left[(E_q E_k - \vec{q}\vec{k})^2 + \frac{(E_q\vec{q}\vec{k} - E_k\vec{q}^2)^2}{\vec{q}^2} - M^2 M_\omega^2\right],$$

$$[L\pm\mp] = M_\omega^2\left[(\vec{p}\vec{k})^2 - \vec{p}^2\vec{k}^2 + 2\frac{\vec{p}\vec{q}}{\vec{q}^2}(\vec{k}^2\vec{p}\vec{q} - 2(\vec{p}\vec{k})(\vec{q}\vec{k})) + \frac{(\vec{q}\vec{k})^2}{\vec{q}^2\vec{k}^2}((\vec{p}\vec{k})^2 + \vec{p}^2\vec{k}^2)\right]$$

$$- \frac{\lambda(M_\omega^2, M^2, m_\pi^2)}{2}\left[\vec{p}^2 - \frac{(\vec{p}\vec{k})^2}{\vec{k}^2} - \frac{M^2}{2}\right] \pm 2i\frac{|\vec{k}|M_\omega^2}{\vec{q}^2}\vec{p}(\vec{q}\times\vec{k})\left(\vec{p}\vec{q} - \frac{(\vec{p}\vec{k})(\vec{q}\vec{k})}{\vec{k}^2}\right),$$

$$[\pm L\pm] = [\mp\mp L] = \frac{1}{|\vec{k}|}\left(E_p - E_k\frac{\vec{p}\vec{k}}{\vec{k}^2}\right)(E_k|\vec{q}| + E_q|\vec{k}|)\left(1 - \frac{\vec{q}\vec{k}}{|\vec{q}||\vec{k}|}\right)$$

$$\times \left(\vec{k}^2\vec{p}\vec{q} - (\vec{p}\vec{k})(\vec{q}\vec{k}) \mp i|\vec{k}|\vec{p}(\vec{q}\times\vec{k})\right),$$

$$[\pm L\mp] = [\mp\pm L] = \frac{1}{|\vec{k}|}\left(E_p - E_k\frac{\vec{p}\vec{k}}{\vec{k}^2}\right)(-E_k|\vec{q}| + E_q|\vec{k}|)\left(1 + \frac{\vec{q}\vec{k}}{|\vec{q}||\vec{k}|}\right)$$

$$\times \left(\vec{k}^2\vec{p}\vec{q} - (\vec{p}\vec{k})(\vec{q}\vec{k}) \pm i|\vec{k}|\vec{p}(\vec{q}\times\vec{k})\right),$$

$$[\pm LL] = \left[\frac{M^4}{2} - 2 \left(E_p - E_k \frac{\vec{p}\vec{k}}{\vec{k}^2} \right)^2 \vec{k}^2 \right] \left(\vec{q}^2 - \frac{(\vec{q}\vec{k})^2}{\vec{k}^2} \right),$$

$$[L \pm L] = [LL\pm] = [LLL] = 0, \tag{B.7}$$

being $\lambda(x, y, z)$ the Källén function and M_ω^2 the squared of the 4-momentum, which is different from the effective mass $m_{\omega,\epsilon}$ that centres the Breit-Wigner distribution when LPB affects the ω meson.
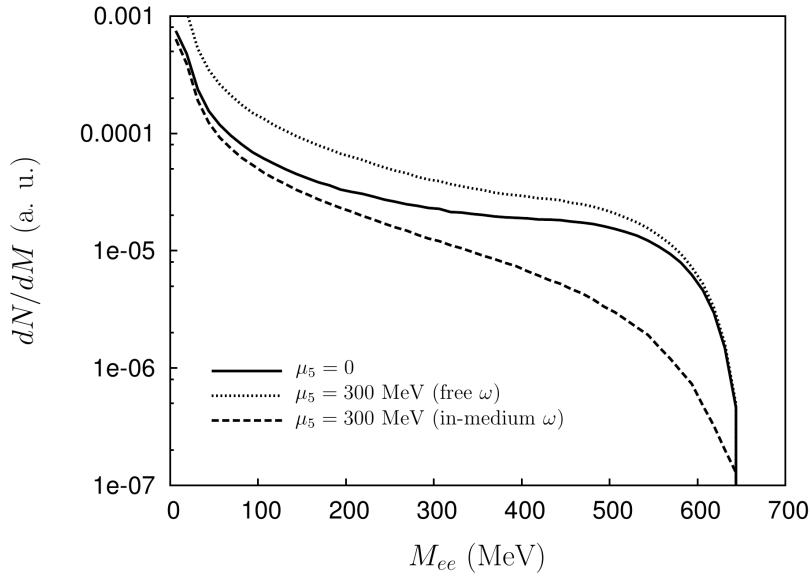
Figure B.1: The ω meson Dalitz decay is presented for parity-even matter (solid line) and for LPB with $\mu_5 = 300$ MeV in two different cases where LPB does and does not affect the ω meson (in-medium, dashed line; and free, dotted line).

In Fig. B.1 we present the results for the Dalitz decay $\omega \to \pi^0 e^+ e^-$ using the PHENIX cuts and temperature presented in Chapter 5. Note that the curve corresponding to the vacuum process is not implemented through the KW formula since we account for experimental cuts. The cases where LPB affects the Dalitz decay have been enhanced by the same factor we used in Fig. 5.4 for the ω contribution in order to fit its resonance peak. The first case where the ω meson is a free state with an intermediate ρ meson affected by LPB shows a small enhancement in the entire the region. However, this process is several orders of magnitude below the hadronic 'cocktail' and such enhancement does not substantially modify it. The second case where LPB also affects the momentum distribution and dispersion relation of the ω meson shows a slight suppression. These results suggest that even that LPB could affect the ω Dalitz decay, this effect would not be visible in the inclusive dilepton production.

B.2 η and η' Dalitz decays

We will focus now in the Dalitz decays of η and η'. As in the previous section, we separate our analysis in two parts. In the first one we assume that the only LPB effect modifies the $\eta - \eta'$ form factor through the dispersion relation of the ρ and ω mesons. In the second part we assume that the decaying mesons are also affected by LPB and therefore they are mixed due to a non-trivial μ_5 as described in Chapter 4. Here we will also investigate the coupling of 2 distorted pions to the initial state.

B.2.1 Vacuum η and η'

The chirally-invariant Lagrangian that describes the anomalous decay of light pseudoscalar mesons into a pair of photons is given by [5, 7]

$$\mathcal{L} = -\frac{3e^2}{32\pi^2 f}\text{Tr}\left(\Phi Q^2\right)\varepsilon_{\mu\nu\alpha\beta}F^{\mu\nu}F^{\alpha\beta}, \tag{B.8}$$

and we use the same notation as in Chapter 4, where we wrote explicitly Φ in (4.5). The matrix of quark charges is $Q = \text{diag}(\frac{2}{3}, -\frac{1}{3}, -\frac{1}{3})$. In fact, it is not necessary to compute the whole process. The Lorentz structure of such decay is equivalent to the one we calculated for the process $\omega \to \pi e^+ e^-$ in the previous section. In addition the overall constant is unknown and thus, our simulation is the same as the previous one with appropriate changes in the masses of the different states and the η and η' form factors.

The form factors of η and η' are the same and they can be written as [158]

$$F_\eta \equiv F_{\eta\gamma} = F_{\eta'\gamma} = \frac{\frac{m_\rho^2}{m_\rho^2 - M^2 - i\Gamma_\rho m_\rho} + \frac{1}{9}\frac{m_\omega^2}{m_\omega^2 - M^2 - i\Gamma_\omega m_\omega}}{\frac{m_\rho^2}{m_\rho^2 - i\Gamma_\rho m_\rho} + \frac{1}{9}\frac{m_\omega^2}{m_\omega^2 - i\Gamma_\omega m_\omega}}. \tag{B.9}$$

Indeed, one can check that $F_{\eta\gamma}(M = 0) = 1$ by construction.

In our simulations we include again the PHENIX cuts for the single electron momentum and dielectron rapidity as well as temperature and mass smearing previously discussed. In Fig. B.2 we show the modification of the dilepton production through this Dalitz process in the η and η' channels. A parity-odd medium with $\mu_5 = 300$ MeV slightly distorts the shape of both channels. The in-medium modification of the ρ and ω propagators only in the form factor (see Eq. (B.9)) seems not to show a clear enhancement of the dielectron production.
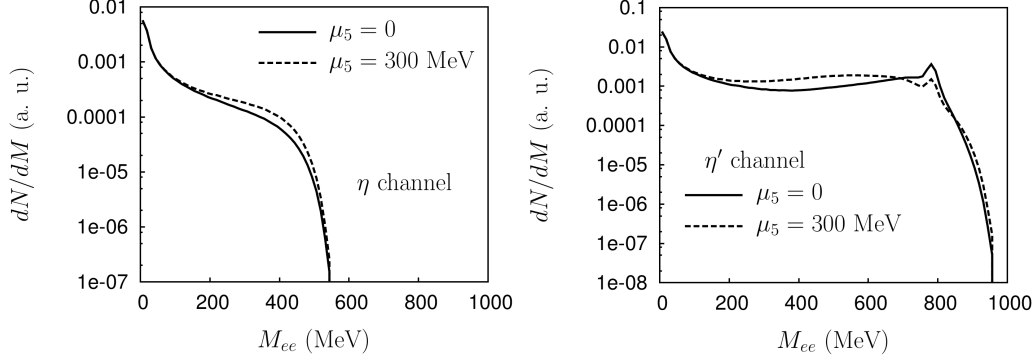
B.2.2 Direct decay of in-medium η and η'

Here we will consider that η and η' are affected by LPB and thus, they are mixed with σ leading to the eigenstates $\{\tilde{\eta}, \tilde{\sigma}, \tilde{\eta}'\}$ that we generically called X_i. After normalizing the kinetic term of the *eta* fields, the Lagrangian in Eq. (B.8) reads

$$\mathcal{L} = -\frac{e^2}{96\pi^2}\left(5\frac{\eta_q}{v_q} + \sqrt{2}\frac{\eta_s}{v_s}\right)\varepsilon_{\mu\nu\alpha\beta}F^{\mu\nu}F^{\alpha\beta} \tag{B.10}$$

Figure B.2: The η and η' Dalitz decays are presented for parity-even matter (solid line) and for LPB with $\mu_5 = 300$ MeV (dashed line). No clear dilepton excess is found.

as a function of the states η_q and η_s. We can rewrite the previous Lagrangian as a function of the proper in-medium eigenstates through Eq. (4.22), which yields

$$\mathcal{L}_i = -\frac{e^2}{96\pi^2}\left(5\frac{C_{\eta_q i}}{v_q} + \sqrt{2}\frac{C_{\eta_s i}}{v_s}\right)\varepsilon_{\mu\nu\alpha\beta}F^{\mu\nu}F^{\alpha\beta}X_i. \tag{B.11}$$

With this expression we can compute the decays $X_i \to \gamma e^+ e^-$ but we only know the form factors of the parity-defined states, not the ones related to X_i. Therefore, it is necessary to express each channel i depending on the QCD states via $X_i = \sum_j b_{ij}\eta_j$ and compute

$$i\mathcal{M}_{X_i \to \gamma ee} = \sum_j (b_{ij}\ i\mathcal{M}_{\eta_j \to \gamma ee}), \tag{B.12}$$

where $b_{i\sigma} = 0$ since σ does not couple to 2 photons. Note that b_{ij} is the inverse transformation of C_{ij} with an extra rotation since b_{ij} deals with η and η' while C_{ij} deals with η_q and η_s. The coefficients b_{ij} read

$$b_{i\eta} = N_i\frac{v_q}{v_0}\left(\cos\psi + \frac{2\sqrt{2}cv_s\sin\psi}{m_5^2 - m_{\text{eff},i}^2}\right) \quad \text{and} \quad b_{i\eta'} = N_i\frac{v_q}{v_0}\left(\sin\psi - \frac{2\sqrt{2}cv_s\cos\psi}{m_5^2 - m_{\text{eff},i}^2}\right). \tag{B.13}$$

With such decomposition, one can readily check that for the Dalitz process we have

$$\overline{|\mathcal{M}|^2}_{X_i \to \gamma ee} = \sum_{j,j'} \frac{\alpha^3 b_{ij}b_{ij'}^*}{9\pi M^4}\left|5\frac{C_{\eta_q i}}{v_q} + \sqrt{2}\frac{C_{\eta_s i}}{v_s}\right|^2 \left[g_{\lambda\lambda'}(m_{\text{eff},i}^2 - M^2)^2 + 4M^2 q_\lambda q_{\lambda'}\right]$$

$$\times \sum_{\epsilon,\epsilon'} F_\eta^\epsilon F_\eta^{\epsilon'*} P_\epsilon^{\lambda\mu} P_{\epsilon'}^{\mu'\lambda'}\left(4p_\mu p_{\mu'} + M^2 g_{\mu\mu'}\right). \tag{B.14}$$

We do not show the calculation of the phase space but let us remark the fact that the energy-dependent mass shell of the decaying particle has to be included carefully. The results of this approach are shown in Fig. B.3 where we included the contributions of

the in-medium $\tilde{\eta}$, $\tilde{\sigma}$ and $\tilde{\eta}'$ channels compared with the vacuum η. First of all, note that the η contribution in vacuum is not exactly the one shown in Fig. B.2 since this calculation is performed using the results of the sigma model studied in Chapter 4 (recall that we found a discrepancy $\simeq 10\%$ in the η mass). The number of expected η mesons is approximately the same as ρ mesons both in vacuum and in-medium (see [47]). In addition the thermalization of ρ and $\tilde{\eta}$ in the pion gas are expected to be similar. For these reason we normalized the $\tilde{\eta}$ channel in the same way as we did with the ρ meson in Chapter 5: the vacuum contribution is enhanced by an approximate factor of 1.8 that accounts for multiple regeneration into distorted pions within the fireball. Despite this factor may be controversial, our results and conclusions do not substantially depend on it. As a first approach, the normalization of the $\tilde{\eta}$, $\tilde{\sigma}$ and $\tilde{\eta}'$ channels is assumed to follow a Boltzmann distribution due to the strong coupling to pions. This assumption provides the ratios between the different channels.
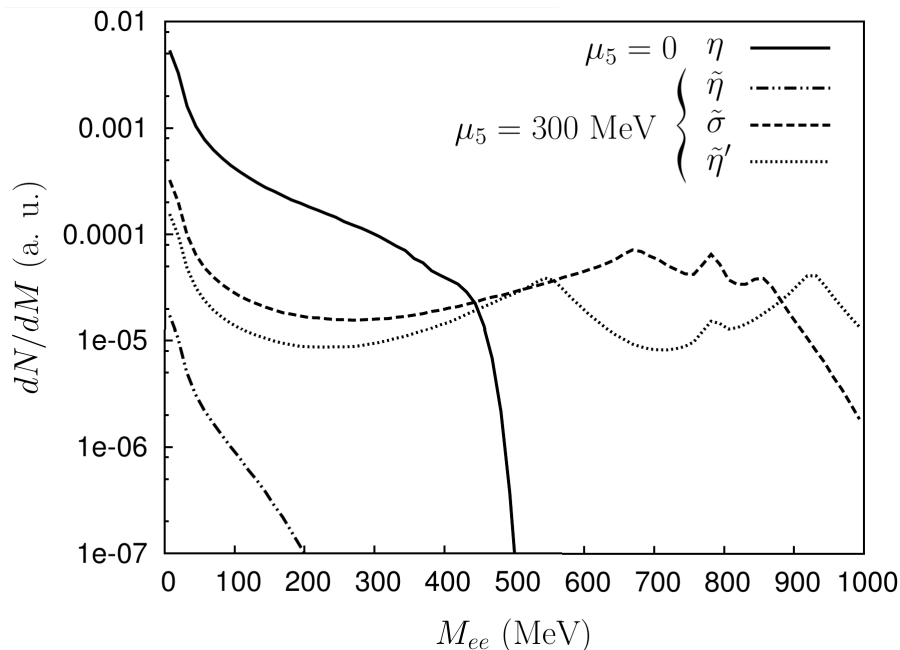
Figure B.3: The dielectron production from direct $\tilde{\eta}$ (dashed-dotted line), $\tilde{\sigma}$ (dashed line) and $\tilde{\eta}'$ (dotted line) Dalitz decays is shown in a parity-odd medium with $\mu_5 = 300$ MeV compared to the vacuum contribution of the η channel (solid line). The vertical units are taken to coincide with PHENIX experimental data [47], as well as experimental detector cuts and temperature.

The thermalization of the $\tilde{\eta}$ channel suggests that this state has a dominant contribution from the vacuum σ state. As the latter does not couple to electromagnetism, one would expect an important suppression of the dilepton production in the $\tilde{\eta}$ channel as it can be seen in Fig. B.3. The $\tilde{\sigma}$ and $\tilde{\eta}'$ channels show similar contributions that in general are subdominant compared to the PHENIX 'cocktail'. The only exception is the peak of the $\tilde{\eta}'$ right wing at $M \simeq 925$ MeV. The dilepton yield at this peak is

similar to the 'cocktail' contribution but the inclusion of the $\tilde{\eta}'$ channel would not be visible due to the low resolution of PHENIX data.

B.2.3 Indirect decay of in-medium η and η'

Due to the relatively large width of the decay $X_i \to \tilde{\pi}\tilde{\pi}$ and the possible thermal regeneration of $\tilde{\eta}$ in such 'pion' gas, the indirect Dalitz decays should also be considered. The process $\tilde{\pi}\tilde{\pi} \to X_i \to \gamma e^+ e^-$ is exactly zero in parity-even matter since the only channel that couples to a pair of pions (σ) does not couple to electromagnetism and hence it does not decay into $\gamma e^+ e^-$. In order to couple two distorted pions to the state X_i, we can use the Feynman rule for the vertex already shown in Eq. (4.25). The resulting squared element matrix is given by

$$\overline{|\mathcal{M}|^2}_{\tilde{\pi}\tilde{\pi} \to X_i \to \gamma ee} = \frac{3}{2} \frac{\alpha^3}{9\pi M^4} \left| \sum_i \left[\left(5\frac{C_{\eta_q i}}{v_q} + \sqrt{2}\frac{C_{\eta_s i}}{v_s} \right) \left(\sum_{j=\eta,\eta'} b_{ij} \right) \mathcal{M}_{\tilde{\pi}\tilde{\pi} \to X^i} D_{X_i} \right] \right|^2$$
$$\times \left[g_{\lambda\lambda'}(Q^2 - M^2)^2 + 4M^2 q_\lambda q_{\lambda'} \right] \sum_{\epsilon,\epsilon'} F_\eta^\epsilon F_\eta^{\epsilon'*} P_\epsilon^{\lambda\mu} P_{\epsilon'}^{\mu'\lambda'} \left(4p_\mu p_{\mu'} + M^2 g_{\mu\mu'} \right),$$

$$(B.15)$$

where the X_i propagator reads

$$D_{X_i} = \frac{1}{Q^2 - m_{\text{eff},X^i}^2 - i\frac{\Gamma_{X^i}}{m_{\text{eff},X^i}}Q^2}. \tag{B.16}$$

In order to simplify our numerical calculations, we take the term of the X_i width at rest. In other words, the denominator is simplified as: $Q^2 - m_{\text{eff},X^i}^2(q) - i\frac{\Gamma_{X^i}(\vec{q}=\vec{0})}{m_{\text{eff},X^i}(\vec{q}=\vec{0})}Q^2$. This approximation should not be very important since the width is dominant only at the very resonance pole. The pole $m_{\text{eff},X^i}^2(q)$ can be equally described by the 3-momentum or the energy. Let us stress that this calculation takes into account all the X_i states and their interferences.

The overall normalization is unknown but as the initial state is the same as in the ρ channel appearing in Chapter 5, we used the same constant as a first approximation (see Fig. 5.4). In Fig. B.4 we show the combined contribution of the indirect Dalitz decays of in-medium $\tilde{\eta}$, $\tilde{\sigma}$ and $\tilde{\eta}'$. For $\mu_5 = 150$ MeV, the combined distribution is almost one order of magnitude larger than for $\mu_5 = 300$ MeV. However, in both cases the dilepton production is completely subdominant. Recall that the vacuum ρ contribution is already one order of magnitude below the 'cocktail' (see Fig. 1.5). In conclusion, although this new source of dileptons is included in the 'cocktail' of hadronic processes, no visible changes would arise.
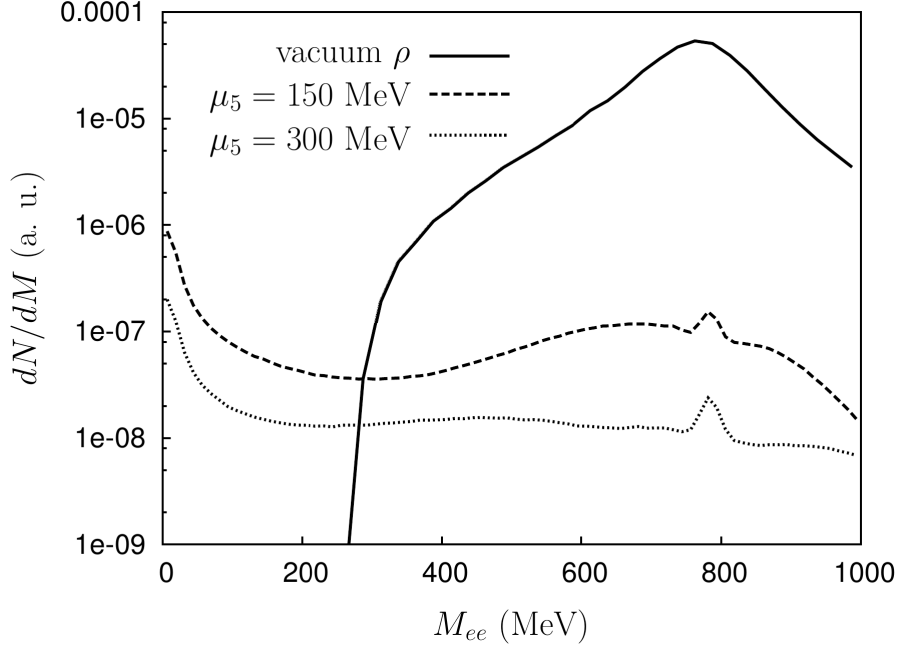
Figure B.4: The combination of the indirect $\tilde{\eta}$, $\tilde{\sigma}$ and $\tilde{\eta}'$ Dalitz decays is displayed for parity-odd matter with $\mu_5 = 150$ MeV (dashed line) and 300 MeV (dotted line). For a comparison of the scale, we also show the vacuum ρ contribution (solid line). The vertical units are taken to coincide with PHENIX experimental data [47], as well as experimental detector cuts and temperature.

B.3   Summary

In this Appendix we have calculated the in-medium modifications of the ω, η and η' Dalitz decays derived from the LPB effect. The ρ and ω propagators have been changed in the corresponding form factors according to the dispersion relation we found in Chapter 5.

In the case of the ω decay, we have analysed two different possibilities. In the first approach we considered that the initial state is unaffected by LPB and the only in-medium dependence is in the propagator of the intermediate ρ meson. In the second situation we assumed that the decaying ω meson is affected by LPB and the fact that it has been created from a previous process leading to a Breit-Wigner distribution for this state. None of these cases shows a relevant enhancement of the dilepton yield when the in-medium contributions are compared to the vacuum one.

Regarding the η and η' decays, we addressed three different approximations. In the first one, the only LPB effect is in the ρ and ω propagators that appear in the corresponding form factors. The second approach consists in computing the decays of the distorted states $\tilde{\eta}$, $\tilde{\sigma}$ and $\tilde{\eta}'$ that we discussed in Chapter 4. Finally, in the last approximation we computed the indirect decay of the previous states assuming that

they are created from two (distorted) pion scattering in the hadron gas. We saw that LPB does not severely enhance the dilepton production.

In summary, the anomalous enhancement of the dielectron production in the region of $M \sim 500$ MeV quoted by PHENIX cannot be explained by the relevant Dalitz decays that form the hadronic cocktail. In other words, although LPB could affect Dalitz decays, it would not be distinguished in the dilepton continuum below the ρ and ω resonance peak.

Bibliography

[1] M. Gell-Mann, Phys. Rev. 125 (1962) 1067.

[2] H. Fritzsch, M. Gell-Mann and H. Leutwyler, Phys. Lett. B 47 (1973) 365.

[3] D. J. Gross and F. Wilczek, Phys. Rev. D 8 (1973) 3633; S. Weinberg, Phys. Rev. Lett. 31 (1973) 494.

[4] S. Coleman, *Aspects of Symmetry: Selected Erice Lectures*, Cambridge Univ. Press (1988).

[5] M. E. Peskin and D. V. Schroeder, *An Introduction to quantum field theory*, Reading, USA: Addison-Wesley (1995) 842 p.

[6] T. Appelquist and J. Carazzone, Phys. Rev. D 11 (1975) 2856.

[7] S. Scherer, Adv. Nucl. Phys. 27 (2003) 277, arXiv:hep-ph/0210398.

[8] A. Pich, Rept. Prog. Phys. 58 (1995) 563, arXiv:hep-ph/9502366; G. Ecker, Prog. Part. Nucl. Phys. 35 (1995) 1, arXiv:hep-ph/9501357.

[9] M. Neubert, Phys. Rept. 245 (1994) 259.

[10] D. J. Gross and F. Wilczek, Phys. Rev. Lett. 30 (1973) 1343; H. D. Politzer, Phys. Rev. Lett. 30 (1973) 1346.

[11] J. C. Collins, D. E. Soper and G. F. Sterman, Adv. Ser. Direct. High Energy Phys. 5 (1988) 1, arXiv:hep-ph/0409313.

[12] K. G. Wilson, Phys. Rev. D 10 (1974) 2445.

[13] A. V. Manohar, hep-ph/9802419; M. Teper, Phys. Lett. B 397 (1997) 223, arXiv:hep-lat/9804008.

[14] G. Veneziano, Nucl. Phys. B 117 (1976) 519; E. Witten, Nucl. Phys. B 160 (1979) 57.

[15] G. 't Hooft, Nucl. Phys. B 72 (1974) 461.

[16] F. Karsch, E. Laermann and A. Peikert, Nucl. Phys. B 605 (2001) 579.

[17] K. Adcox *et al.* [PHENIX Collaboration], Nucl. Phys. A 757 (2005) 184, arXiv:nucl-ex/0410003; A. Ali Khan *et al.* [CP-PACS Collaboration], Phys. Rev. D 63 (2001) 034502, arXiv:hep-lat/0008011.

[18] F. Karsch, Nucl. Phys. Proc. Suppl. 83 (2000) 14, arXiv:hep-lat/9909006; E. Laermann, Nucl. Phys. Proc. Suppl. 63 (1998) 114, arXiv:hep-lat/9802030; and A. Ukawa, Nucl. Phys. Proc. Suppl. 53 (1997) 106, arXiv:hep-lat/9612011; H. Satz, Int. J. Mod. Phys. A 21 (2006) 672, arXiv:hep-lat/0509192; T. Schfer, arXiv:hep-ph/0509068.

[19] J. Adams *et al.* [STAR Collaboration], Nucl. Phys. A 757 (2005) 102; K. Adcox *et al.* [PHENIX Collaboration], Nucl. Phys. A 757 (2005) 184; B. B. Back *et al.* [PHOBOS Collaboration], Nucl. Phys. A 757 (2005) 28; I. Arsene *et al.* [BRAHMS Collaboration], Nucl. Phys. A 757 (2005) 1.

[20] A. Andronic, D. Blaschke, P. Braun-Munzinger, J. Cleymans, K. Fukushima, L. D. McLerran, H. Oeschler and R. D. Pisarski *et al.*, Nucl. Phys. A 837 (2010) 65, arXiv:0911.4806 [hep-ph].

[21] J. -P. Blaizot, Nucl. Phys. A 834 (2010) 515 C, arXiv:0911.5059 [hep-ph].

[22] Y. Kim and D. Yi, Adv. High Energy Phys. 2011 (2011) 259025, arXiv:1107.0155 [hep-ph].

[23] M. Gyulassy and L. McLerran, Nucl. Phys. A 750 (2004) 30.

[24] L. Adamczyk *et al.* [STAR Collaboration], Phys. Rev. Lett. 112 (2014) 032302, arXiv:1309.5681 [nucl-ex].

[25] J. Casalderrey-Solana, H. Liu, D. Mateos, K. Rajagopal and U. A. Wiedemann, arXiv:1101.0618 [hep-th].

[26] P. Kovtun, D. T. Son and A. O. Starinets, Phys. Rev. Lett. 94 (2005) 111601, arXiv:hep-th/0405231.

[27] R. A. Lacey, N. N. Ajitanand, J. M. Alexander, P. Chung, W. G. Holzmann, M. Issah, A. Taranenko and P. Danielewicz *et al.*, Phys. Rev. Lett. 98 (2007) 092301, arXiv:nucl-ex/0609025; H. J. Drescher, A. Dumitru, C. Gombeaud and J. Y. Ollitrault, Phys. Rev. C 76 (2007) 024905, arXiv:0704.3553 [nucl-th]; S. Gavin and M. Abdel-Aziz, Phys. Rev. Lett. 97 (2006) 162302, arXiv:nucl-th/0606061; A. Adare *et al.* [PHENIX Collaboration], Phys. Rev. Lett. 98 (2007) 172301, arXiv:nucl-ex/0611018.

[28] W. A. Zajc, Nucl. Phys. A 805 (2008) 283, arXiv:0802.3552 [nucl-ex].

[29] M. Alford, K. Rajagopal, T. Schfer and A. Schmitt, Rev. Mod. Phys. 80 (2008) 1455, arXiv:0709.4635 [hep-ph].

[30] N. Armesto, N. Borghini, S. Jeon, U. A. Wiedemann, S. Abreu, V. Akkelin, J. Alam and J. L. Albacete *et al.*, J. Phys. G 35 (2008) 054001, arXiv:0711.0974 [hep-ph].

[31] E. Iancu and R. Venugopalan, arXiv:hep-ph/0303204; R. Venugopalan, J. Phys. G 35 (2008) 104003, arXiv:0806.1356[hep-ph].

[32] T. Lappi and L. McLerran, Nucl. Phys. A 772 (2006) 200, arXiv:hep-ph/0602189.

[33] F. Gelis and R. Venugopalan, Acta Phys. Polon. B 37 (2006) 3253.

[34] S. A. Voloshin, A. M. Poskanzer and R. Snellings, arXiv:0809.2949 [nucl-ex].

[35] R. Snellings, New J. Phys. 13 (2011) 055008, arXiv:1102.3010 [nucl-ex].

[36] S. Voloshin and Y. Zhang, Z. Phys. C 70 (1996) 665, arXiv:hep-ph/9407282.

[37] C. Alt *et al.* [NA49 Collaboration], Phys. Rev. C 68 (2003) 034903, arXiv:nucl-ex/0303001; K. H. Ackermann *et al.* [STAR Collaboration], Phys. Rev. Lett. 86 (2001) 402, arXiv: nucl-ex/0009011; K. Aamodt *et al.* [ALICE Collaboration], Phys. Rev. Lett. 105 (2010) 252302, arXiv:1011.3914 [nucl-ex].

[38] R. Rapp and J. Wambach, Adv. Nucl. Phys. 25 (2000) 1, arXiv:hep-ph/9909229; H. van Hees and R. Rapp, Nucl. Phys. A 806 (2008) 339, arXiv:0711.3444 [hep-ph].

[39] J. Ruppert, C. Gale, T. Renk, P. Lichard and J. I. Kapusta, Phys. Rev. Lett. 100 (2008) 162301.

[40] K. Dusling, D. Teaney and I. Zahed, Phys. Rev. C75 (2007) 024908; K. Dusling and I. Zahed, Nucl. Phys. A 825 (2009) 212.

[41] G. E. Brown and M. Rho, Phys. Rev. Lett. 66 (1991) 2720; C. A. Dominguez, M. Loewe and J. C. Rojas, Z. Phys. C 59 (1993) 63.

[42] R. Rapp and J. Wambach, Eur. Phys. J. A 6 (1999) 415; M. Urban, M. Buballa, R. Rapp and J. Wambach, Nucl. Phys. A 673 (2000) 357.

[43] R. Rapp and C. Gale, Phys. Rev. C 60 (1999) 024903.

[44] G. -Q. Li, C. M. Ko and G. E. Brown, Phys. Rev. Lett. 75 (1995) 4007, arXiv:nucl-th/9504025.

[45] G. Agakichiev *et al.* [CERES Collaboration], Phys. Rev. Lett. 75 (1995) 1272; G. Agakishiev *et al.* [CERES/NA45 Collaboration], Phys. Lett. B 422 (1998) 405, arXiv:nucl-ex/9712008; G. Agakichiev et al., Eur. Phys. J. C 41 (2005) 475.

[46] R. Arnaldi *et al.* [NA60 Collaboration], Eur. Phys. J. C 61 (2009) 711, arXiv:0812.3053 [nucl-ex].

[47] A. Adare *et al.* [PHENIX Collaboration], Phys. Rev. C 81 (2010) 034911, arXiv:0912.0244 [nucl-ex].

[48] T. Matsui and H. Satz, Phys. Lett. B 178 (1986) 416.

[49] J. Lansberg, Int. J. Mod. Phys. A 21 (2006) 3857, arXiv:hep-ph/0602091.

[50] A. Adare *et al.* [PHENIX Collaboration], Phys. Rev. Lett. 98 (2007) 232301, arXiv:nucl-ex/0611020; G. Aad *et al.* [ATLAS Collaboration], Phys. Lett. B 697 (2011) 294, arXiv:1012.5419 [hep-ex]; B. Abelev *et al.* [ALICE Collaboration], Phys. Rev. Lett. 109 (2012) 072301, arXiv:1202.1383 [hep-ex].

[51] S. Chatrchyan *et al.* [CMS Collaboration], JHEP 1205 (2012) 063, arXiv:1201.5069 [nucl-ex].

[52] R. Arnaldi *et al.* [NA60 Collaboration], Phys. Lett. B 706 (2012) 263, arXiv:1004.5523 [nucl-ex].

[53] R. Reed, J. Phys. G 38 (2011) 124185, arXiv:1109.3891 [nucl-ex].

[54] D. H. Perkins, *Introduction to high energy physics*, Reading, USA: Addison-Wesley (1972) 353 p.

[55] D. Gross and F. Wilczek, Phys. Rev. Lett. 30 (1973) 1343.

[56] J. Casalderrey-Solana, E. V. Shuryak and D. Teaney, J. Phys. Conf. Ser. 27 (2005) 22 [Nucl. Phys. A 774 (2006) 577], arXiv:hep-ph/0411315.

[57] F. Wang [STAR Collaboration], J. Phys. G 30 (2004) S1299, arXiv:nucl-ex/0404010.

[58] K. Adcox *et al.* [PHENIX Collaboration], Phys. Rev. Lett. 88 (2002) 022301.

[59] C. Adler *et al.* [STAR Collaboration], Phys. Rev. Lett. 90 (2003) 082302.

[60] G. Aad *et al.* [ATLAS Collaboration], Phys. Rev. Lett. 105 (2010) 252303, arXiv:1011.6182 [hep-ex].

[61] M. M. Aggarwal *et al.* [WA98 Collaboration], Eur. Phys. J. C 23 (2002) 225, arXiv:nucl-ex/0108006; F. Antinori *et al.* [NA57 Collaboration], Phys. Lett. B 623 (2005) 17, arXiv:nucl-ex/0507012.

[62] B. I. Abelev *et al.* [STAR Collaboration], Phys. Rev. Lett. 103 (2009) 251601, arXiv:0909.1739 [nucl-ex]; Phys. Rev. C 81 (2010) 054908, arXiv:0909.1717 [nucl-ex]; S. A. Voloshin, J. Phys. Conf. Ser. 230 (2010) 012021.

[63] D. Kharzeev, R. D. Pisarski and M. H. G. Tytgat, Phys. Rev. Lett. 81 (1998) 512; D. E. Kharzeev, L. D. McLerran and H. J. Warringa, Nucl. Phys. A 803 (2008) 227; K. Fukushima, D. E. Kharzeev and H. J. Warringa, Phys. Rev. D 78 (2008)

074033 ; Nucl. Phys. A 836 (2010) 311; D. Kharzeev, Phys. Lett. B 633 (2006) 260, arXiv:hep-ph/0406125; Ann. Phys. (NY) 325 (2010) 205, arXiv:0911.3715 [hep-ph].

[64] B. Abelev et al. [ALICE Collaboration], Phys. Rev. Lett. 110, 012301 (2013) [arXiv:1207.0900 [nucl-ex]].

[65] V. D. Toneev and V. Voronyuk, Phys. Atom. Nucl. 75 (2012) 607, arXiv:1012.1508 [nucl-th].

[66] R. Rueckel, Phys. Lett. B 64 (1976) 39.

[67] J. Jalilian-Marian and V. Koch, Phys. Rev. C58 (1998) 3763.

[68] S. D. Drell and T. -M. Yan, Phys. Rev. Lett. 25 (1970) 316 [Erratum-ibid. 25 (1970) 902].

[69] C. Gale and P. Lichard, Phys. Rev. D 49 (1994) 3338, arXiv:hep-ph/9307363.

[70] K. Kajantie, J. I. Kapusta, L. D. McLerran and A. Mekjian, Phys. Rev. D 34 (1986) 2746.

[71] N. M. Kroll and W. Wada, Phys. Rev. 98 (1955) 1355.

[72] K. O. Lapidus and V. M. Emel'yanov, Phys. Part. Nucl. 40 (2009) 29; I. Tserruya, arXiv:0903.0415 [nucl-ex];

[73] G. Roche *et al.* [DLS Collaboration], Phys. Rev. Lett. 61 (1988) 1069; Phys. Lett. B 226 (1989) 228; C. Naudet *et al.*, Phys. Rev. Lett. 62 (1989) 2652.

[74] L. Xiong, Z. G. Wu, C. M. Ko and J. Q. Wu, Nucl. Phys. A 512 (1990) 772; G. Wolf, W. Cassing and U. Mosel, Nucl. Phys. A 552 (1993) 549; K. K. Gudima, A. I. Titov and V. D. Toneev, Sov. Jour. of Nucl. Phys. 55 (1992) 1715; E. L. Bratkovskaya, W. Cassing and U. Mosel, Phys. Lett. B 376 (1996) 12.

[75] R. J. Porter *et al.* [DLS Collaboration], Phys. Rev. Lett. 79 (1997) 1229, arXiv:nucl-ex/9703001.

[76] I. Frohlich *et al.* [HADES Collaboration], Eur. Phys. J. A 31 (2007) 831, arXiv:nucl-ex/0610048; G. Agakachiev *et al.* [HADES Collaboration], Phys. Rev. Lett. 98 (2007) 052302, arXiv:nucl-ex/0608031; Phys. Lett. B 663 (2008) 43, arXiv:0711.4281 [nucl-ex]; arXiv:0910.5875 [nucl-ex].

[77] K. O. Lapidus [HADES Collaboration], Phys. Atom. Nucl. 73 (2010) 985.

[78] E. L. Bratkovskaya and W. Cassing, Nucl. Phys. A 807 (2008) 214, arXiv:0712.0635 [nucl-th].

[79] M. Masera [HELIOS Collaboration], Nucl. Phys. A 590 (1995) 93C; A. L. S. Angelis *et al.* [HELIOS/3 Collaboration], Eur. Phys. J. C 13 (2000) 433.

[80] M. C. Abreu *et al.* [NA38 and NA50 Collaborations], Eur. Phys. J. C 13 (2000) 69; Nucl. Phys. A 638 (1998) 487.

[81] D. Adamova *et al.* [CERES Collaboration], Phys. Rev. Lett. 91 (2003) 042301.

[82] T. Hatsuda and S. H. Lee, Phys. Rev. C 46 (1992) 34.

[83] E. Scomparin *et al.* [NA60 Collaboration], Nucl. Phys. A 774 (2006) 67; R. Arnaldi *et al.* [NA60 Collaboration], Phys. Rev. Lett. 96 (2006) 162302, arXiv:nucl-ex/0605007.

[84] L. Adamczyk *et al.* [STAR Collaboration], arXiv:1312.7397 [hep-ex].

[85] M. C. Abreu *et al.* [NA38 Collaboration], Phys. Lett. B 423 (1998) 207; M. C. Abreu *et al.* [NA50 Collaboration], Eur. Phys. J. C 14 (2000) 443; Phys. Lett. B 499 (2001) 85.

[86] R. Arnaldi *et al.* [NA60 Collaboration], Eur. Phys. J. C 59 (2009) 607, arXiv:0810.3204 [nucl-ex].

[87] D. Weingarten, Phys. Rev. Lett. 51 (1983) 1830; C. Vafa and E. Witten, Phys. Rev. Lett. 53 (1984) 535; S. Nussinov, Phys. Rev. Lett. 52 (1984) 966; D. Espriu, M. Gross and J. F. Wheater, Phys. Lett. B 146 (1984) 67; for a review see, S. Nussinov and M. Lambert, Phys. Rept. 362 (2002) 193.

[88] A. A. Andrianov and D. Espriu, Phys. Lett. B 663 (2008) 450; A. A. Andrianov, V. A. Andrianov and D. Espriu, Phys. Lett. B 678 (2009) 416; Phys. Part. Nucl. 41 (2010) 896; PoS QFTHEP2010 054 (2010).

[89] P. Jacobs, D. Kharzeev, B. Muller, J. Nagle, K. Rajagopal and S. Vigdor, arXiv:0705.1930 [nucl-ex].

[90] J. -P. Blaizot, F. Gelis, J. -F. Liao, L. McLerran and R. Venugopalan, Nucl. Phys. A 873 (2012) 68, arXiv:1107.5296 [hep-ph].

[91] N. Brambilla, S. Eidelman, P. Foka, S. Gardner, A. S. Kronfeld, M. G. Alford, R. Alkofer and M. Butenschn *et al.*, arXiv:1404.3723 [hep-ph].

[92] D. T. Son and M. A. Stephanov, Phys. Rev. Lett. 86 (2001) 592, arXiv:hep-ph/0005225; Phys. Atom. Nucl. 64 (2001) 834 [Yad. Fiz. 64 (2001) 899], arXiv:hep-ph/0011365.

[93] T. D. Cohen, Phys. Rev. D 64 (2001) 047704, arXiv:hep-th/0101197.

[94] D. Kharzeev, A. Zhitnitsky, Nucl. Phys. A 797 (2007) 67; K. Buckley, T. Fugleberg and A. Zhitnitsky, Phys. Rev. Lett. 84 (2000) 4814, arXiv:hep-ph/9910229; D. T. Son and A. R. Zhitnitsky, Phys. Rev. D 70 (2004) 074018; D. Ahrensmeier, R. Baier and M. Dirks, Phys. Lett. B 484 (2000) 58, arXiv:hep-ph/0005051.

[95] A. A. Andrianov, V. A. Andrianov, D. Espriu and X. Planells, Phys. Lett. B 710 (2012) 230, arXiv:1201.3485 [hep-ph]; Theor. Math. Phys. 170 (2012) 17; PoS QFTHEP 2010 (2010) 053; PoS QFTHEP 2011 (2013) 025, arXiv:1310.4428 [hep-ph]; AIP Conf. Proc. 1343 (2011) 450.

[96] C. A. Baker, D. D. Doyle, P. Geltenbort, K. Green, M. G. D. van der Grinten, P. G. Harris, P. Iaydjiev and S. N. Ivanov *et al.*, Phys. Rev. Lett. 97 (2006) 131801, arXiv:hep-ex/0602020.

[97] R. D. Peccei and H. R. Quinn, Phys. Rev. Lett. 38 (1977) 1440; S. Weinberg, Phys. Rev. Lett. 40 (1978) 223; F. Wilczek, Phys. Rev. Lett. 40 (1978) 279.

[98] K. van Bibber and L. J. Rosenberg, Phys. Today 59N8 (2006) 30; S. J. Asztalos, L. J. Rosenberg, K. van Bibber, P. Sikivie and K. Zioutas, Ann. Rev. Nucl. Part. Sci. 56 (2006) 293.

[99] A. A. Andrianov, V. A. Andrianov and D. Espriu, arXiv:1211.6665 [hep-ph].

[100] A. A. Andrianov and V. A. Andrianov, Nucl. Phys. Proc. Suppl. 39BC, 257 (1995); In *Coimbra 1999, Hadron physics* 328, arXiv:hep-ph/9911383; A. A. Andrianov, V. A. Andrianov and V. L. Yudichev, Theor. Math. Phys. 108 (1996) 1069; A. A. Andrianov, V. A. Andrianov and S. S. Afonin, arXiv:hep-ph/0209260.

[101] S. S. Afonin, A. A. Andrianov, V. A. Andrianov and D. Espriu, eConf C 070910 (2007) 202, arXiv:0710.0362 [hep-ph].

[102] M. P. Lombardo, PoS CPOD 2006 (2006) 003, arXiv:hep-lat/0612017; M. A. Stephanov, PoS LAT2006 (2006) 024, arXiv:hep-lat/0701002; D. T. Son and M. A. Stephanov, Phys. Rev. Lett. 86 (2001) 592; Phys. Atom. Nucl. 64 (2001) 834; K. Splittorff, D. T. Son and M. A. Stephanov, Phys. Rev. D 64 (2001) 016003; J. B. Kogut and D. Toublan, Phys. Rev. D 64 (2001) 034007.

[103] B. -A. Li, Phys. Rev. C 61 (2000) 021903, arXiv:nucl-th/9910030.

[104] A. A. Andrianov, D. Espriu, P. Giacconi and R. Soldati, JHEP 0909 (2009) 057; A. A. Andrianov, D. Espriu, F. Mescia and A. Renau, Phys. Lett. B 684 (2010) 101; J. Alfaro, A. A. Andrianov, M. Cambiaso, P. Giacconi and R. Soldati, Int. J. Mod. Phys. A 25 (2010) 3271.

[105] E. Guendelman and D. A. Owen, Phys. Lett. B 251 (1990) 439; E. Strakhov and D. A. Owen, J. Phys. G 22 (1996) 473.

[106] A. A. Belavin, A. M. Polyakov, A. S. Shvarts and Y. S. Tyupkin, Phys. Lett. B 59 (1975) 85.

[107] F. R. Klinkhamer and N. S. Manton, Phys. Rev. D 30 (1984) 2212; V. A. Kuzmin, V. A. Rubakov and M. E. Shaposhnikov, Phys. Lett. B 155 (1985) 36.

BIBLIOGRAPHY

[108] L. D. McLerran, E. Mottola, M. E. Shaposhnikov, Phys. Rev. D 43 (1991) 2027; G. D. Moore and K. Rummukainen, Phys. Rev. D 61 (2000) 105008; E. Shuryak and I. Zahed, Phys. Rev. D 67 (2003) 014006.

[109] S. Bronoff and C. P. Korthals Altes, Phys. Lett. B 448 (1999) 85, arXiv:hep-ph/9811243.

[110] P. V. Buividovich, M. N. Chernodub, D. E. Kharzeev, T. Kalaydzhyan, E. V. Luschevskaya and M. I. Polikarpov, Phys. Rev. Lett. 105 (2010) 132001; D. Kharzeev, A. Krasnitz and R. Venugopalan, Phys. Lett. B 545 (2002) 298, arXiv:hep-ph/0109253; T. Lappi, J. Phys. G 32 (2006) S179, arXiv:hep-ph/0606090; Phys. Lett. B 643 (2006) 11, arXiv:hep-ph/0606207.

[111] A. M. Polyakov, Nucl. Phys. B 120 (1977) 429.

[112] P. V. Buividovich, M. N. Chernodub, E. V. Luschevskaya and M. I. Polikarpov, Phys. Rev. D 80 (2009) 054503; M. Abramczyk, T. Blum, G. Petropoulos and R. Zhou, PoS LAT 2009 (2009) 181, arXiv:0911.1348 [hep-lat]; P. V. Buividovich, T. Kalaydzhyan and M. I. Polikarpov, arXiv:1111.6733 [hep-lat].

[113] M. A. Shifman, Prog. Part. Nucl. Phys. 39 (1997) 1, arXiv:hep-th/9704114; I. I. Kogan, A. Kovner and M. A. Shifman, Phys. Rev. D 57 (1998) 5195, arXiv:hep-th/9712046; E. Witten, Phys. Rev. Lett. 81 (1998) 2862, arXiv:hep-th/9807109; I. E. Halperin and A. Zhitnitsky, Phys. Rev. D 58 (1998) 054016, arXiv:hep-ph/9711398; Phys. Rev. Lett. 81 (1998) 4071, arXiv:hep-ph/9803301.

[114] S. Aoki, Phys. Rev. D 30 (1984) 2653; Phys. Rev. Lett. 57 (1986) 3136; S. Aoki and A. Gocksch, Phys. Rev. D 45 (1992) 3845.

[115] J. Ambjorn, J. Greensite and C. Peterson, Nucl. Phys. B 221 (1983) 381.

[116] J. Liao, arXiv:1401.2500 [hep-ph].

[117] S. A. Voloshin, Phys. Rev. C 70 (2004) 057901, arXiv:hep-ph/0406311.

[118] A. A. Andrianov, D. Espriu and X. Planells, Eur. Phys. J. C 73 (2013) 2294; PoS QFTHEP 2013 (2014) 049, arXiv:1310.4434 [hep-ph].

[119] A. Yamamoto, Phys. Rev. D 84 (2011) 114504; Phys. Rev. Lett. 107 (2011) 031601.

[120] M. N. Chernodub and A. S. Nedelin, Phys. Rev. D 83 (2011) 105008; L.-J. Luo, S. Shi and H.-S. Zong, Mod. Phys. Lett. A 28 (2013) 1350105.

[121] I. Y. Arefeva and I. V. Volovich, Theor. Math. Phys. 174 (2013) 186 [Teor. Mat. Fiz. 174 (2013) 216], and references therein.

[122] Y. Nambu and G. Jona-Lasinio, Phys. Rev. 122 (1961) 345; Phys. Rev. 124 (1961) 246.

[123] A. A. Andrianov, D. Espriu and X. Planells, Eur. Phys. J. C 74 (2014) 2776, arXiv:1310.4416 [hep-ph].

[124] U. Vogl and W. Weise, Prog. Part. Nucl. Phys. 27 (1991) 195.

[125] S. P. Klevansky, Rev. Mod. Phys. 64 (1992) 649; T. Hatsuda and T. Kunihiro, Phys. Rept. 247 (1994) 221; M. Buballa, Phys. Rept. 407 (2005) 205.

[126] D. Ebert and K. G. Klimenko, Eur. Phys. J C 46 (2006) 771.

[127] V. Azcoiti, G. Di Carlo, E. Follana, M. Giordano and A. Vaquero, Nucl. Phys. B 875 (2013) 45.

[128] T. Inagaki, D. Kimura, H. Kohyama and A. Kvinikhidze, Phys. Rev. D 85 (2012) 076002.

[129] T. Fujihara, T. Inagaki, D. Kimura and A. Kvinikhidze, Prog. Theor. Phys. Suppl. 174 (2008) 72; Phys. Rev D 79 (2009) 096008; T. Inagaki, D. Kimura, H. Kohyama and A. Kvinikhidze, Phys. Rev. D 83 (2011) 034005.

[130] T. Inagaki, D. Kimura and A. Kvinikhidze, Phys. Rev. D 77 (2008) 116004.

[131] J. Zinn-Justin, Nucl. Phys. B 367 (1991) 105.

[132] M. Buballa, Nucl. Phys. A 611 (1996) 393.

[133] J. Gasser and H. Leutwyler, Nucl. Phys. B 250 (1985) 465.

[134] J. Beringer *et al.* [Particle Data Group], Review of Particle Physics, Phys. Rev. D 86 (2012) 010001.

[135] J. Boguta, Phys. Lett. B 120 (1983) 34; O. Kaymakcalan and J. Schechter, Phys. Rev. D 31 (1985) 1109; R. D. Pisarski, arXiv:hep-ph/9503330.

[136] A. H. Fariborz, R. Jora and J. Schechter, Phys. Rev. D 72 (2005) 034001; Phys. Rev. D 77 (2008) 034006.

[137] J. T. Lenaghan, D. H. Rischke and J. Schaffner-Bielich, Phys. Rev. D 62 (2000) 085008; D. Parganlija, F. Giacosa and D. H. Rischke, Phys. Rev. D 82 (2010) 054024.

[138] B. D. Serot and J. D. Walecka, Int. J. Mod. Phys. E 16 (1997) 15.

[139] M. Bando, T. Kugo and K. Yamawaki, Phys. Rep. 164 (1988) 217; M. Harada and K. Yamawaki, Phys. Rep. 381 (2003) 1.

[140] V. A. Rubakov, arXiv:1005.1888 [hep-ph].

[141] J. J. Sakurai, *Theory of Strong Interactions*, Ann. of Phys. (NY) 11 (1960) 1.

[142] M. Benayoun, L. DelBuono, S. Eidelman, V. N. Ivanchenko and H. B. O'Connell, Phys. Rev. D 59 (1999) 114027, arXiv:hep-ph/9902326.

[143] R. Arnaldi *et al.* [NA60 Collaboration], Phys. Rev. Lett. 102 (2009) 222301, arXiv:0812.3100 [nucl-ex].

[144] H. B. O'Connell, B. C. Pearce, A. W. Thomas and A. G. Williams, Prog. Part. Nucl. Phys. 39 (1997) 201, arXiv:hep-ph/9501251; D. Schildknecht, Acta Phys. Polon. B 37 (2006) 595, arXiv:hep-ph/0511090.

[145] F. Klingl, N. Kaiser, W. Weise, Z. Phys. A 356 (1996) 193.

[146] N. M. Kroll, T. D. Lee and B. Zumino, Phys. Rev. 157 (1967) 1376.

[147] N. Kaiser and U.-G. Meissner, Nucl. Phys. A 519 (1990) 671; E. Truhlik, J. Smejkal and F. C. Khanna, Nucl. Phys. A 689 (2001) 741.

[148] O. Dumbrajs, R. Koch, H. Pilkuhn, G. c. Oades, H. Behrens, J. j. De Swart and P. Kroll, Nucl. Phys. B 216 (1983) 277.

[149] T. Feldmann, P. Kroll and B. Stech, Phys. Rev. D 58 (1998) 114006; Y. N. Klopot, A. G. Oganesian and O. V. Teryaev, arXiv:0911.0180 [hep-ph].

[150] E. L. Feinberg, Nuovo Cim. A 34 (1976) 391; L. D. McLerran and T. Toimela, Phys. Rev. D 31 (1985) 545; C. Gale and J. I. Kapusta, Phys. Rev. D 43 (1991) 3080.

[151] H. J. Specht [NA60 Collaboration], AIP Conf. Proc. 1322 (2010) 1, arXiv:1011.0615 [nucl-ex].

[152] J. R. Nix, Phys. Rev. C 58 (1998) 2303, arXiv:nucl-th/9801029.

[153] J. Manninen, E. L. Bratkovskaya, W. Cassing and O. Linnyk, Eur. Phys. J. C 71 (2011) 1615, arXiv:1005.0500 [nucl-th].

[154] V. Ryabov, Nucl. Phys. A 774 (2006) 735, arXiv:hep-ex/0510017.

[155] U. W. Heinz and K. S. Lee, Nucl. Phys. A 544 (1992) 503.

[156] A. Adare *et al.* [PHENIX Collaboration], Phys. Rev. C 84 (2011) 044902, arXiv:1105.3467 [nucl-ex].

[157] Numerical data extracted from
https://www.phenix.bnl.gov/phenix/WWW/info/data/ppg088_data.html/fig26.txt

[158] L. G. Landsberg, Phys. Rep. 128 (1985) 301.

[159] E. L. Bratkovskaya, O. V. Teryaev and V. D. Toneev, Phys. Lett. B 348 (1995) 283.

[160] J. C. Collins and D. E. Soper, Phys. Rev. D 16 (1977) 2219.

[161] A. A. Andrianov, V. A. Andrianov, D. Espriu and X. Planells, Phys. Rev. D 90 (2014) 034024, arXiv:1402.2147 [hep-ph].

[162] A. A. Andrianov, S. S. Kolevatov and R. Soldati, JHEP 1111 (2011) 007, arXiv:1109.3440 [hep-ph]; A. A. Andrianov and S. S. Kolevatov, Theor. Math. Phys. 175 (2013) 744, arXiv:1212.5723 [hep-ph].

[163] T. Matsubara, Prog. Theor. Phys. 14 (1955) 351.

[164] R. Arnaldi *et al.* [NA60 Collaboration], Phys. Lett. B 677 (2009) 260, arXiv:0902.2547 [hep-ph].